The effect of length scale on flow properties of Micro, Nano and Macro-Emulsions

By

Mehrdad Ghahraee

A thesis

Submitted to the Victoria University of Wellington

in fulfilment of the requirements for the degree of

Doctor of Philosophy

Victoria University of Wellington

2015

Abstract

Flow properties of a complex fluid depend on not only the characterizations of the components that make up the system but also the interactions between the phases. One of the most significant factors that affect these interactions is the length scale of the dispersed phase. According to Stokes law, the root of complex fluid rheological models, the velocity of a moving particle in a fluid is a function of the viscosity of the fluid and also the size of the moving droplet. The main aim of this research is to understand the crucial elements that define and control the rheological behaviour of complex fluids and thereby provide evidence for proposed modifications of the available rheological models to include parameters that capture the deduced crucial elements. In particular, by adjusting different aspects of Stokes law. The modified models can then be applied to a wider range of complex fluid systems, including emulsions, regardless of the chemicals that form the system.

The complex fluids used in this research to develop the above are emulsions with droplets ranging over four orders of magnitude, 10 nm to 100 μm. Within a single base chemical system microemulsions, nanoemulsions and macroemulsions could be formed. The length scale and flow properties of each group were examined and the effect of length scale on rheological properties was investigated.

Critical elements there were identified include:

- Use of the appropriate viscosity value for the fluid through which the dispersed phase diffuses. It is often assumed that the viscosity of the pure continuous phase fluid can be used as the reference viscosity in the Stokes equation. In a real system the viscosity of the continuous phase can be strongly affected, and thereby defined by, the presence of the dispersed phase itself and the interfacial layer. Hence it is paramount that the appropriate reference viscosity is used. It is noted that the standard assumption is often applicable for highly diluted suspensions that are composed of rigid spheres. However, the research undertaken here demonstrates that this assumption must be reconsidered for more concentrated systems and

particularly for emulsions. We recommend that for such systems the viscosity of the pure continuous phase is replaced by the constant viscosity of the sample at a zero shear rate.

- Consideration of structural factors that also affect the viscosity. In particular it is often assumed that:

    1- the droplets/particles are spherical and non-deformable; and

    2- the dispersed phase presents as a single length scale, i.e. the system is a monodisperse system.

    The inclusion of these assumptions limits dramatically the applicability of the available models to fit and describe the real flow behaviour and thereby does not allow for predictability of behaviours. Typically models have been modified by adding experimental factors rather than explicitly incorporating the above factors into the development of a model. In this work the deviation from these rheological models are explained and correlated to the deviation from spherical structure and monodispersity.

- Defining the relative viscosity as the ratio between the sample viscosity and the reference viscosity is common practice in the application of most rheological models. The viscosity of water tends to be taken as the reference viscosity. This leads to no agreement between the well-known rheological models and the experimental data, especially when applied to analysis of microemulsion rheology. In this work, we show that by taking the viscosity of the relevant ternary surfactant solution as the reference viscosity, the existing models can be applicable to microemulsions.

This work sheds light on the relationship between the non-Newtonian behaviour of nanoemulsions and their underlying thermodynamic instability. In these systems the Newtonian behaviour is not evident till a shear rate of 100/s is reached. On the other hand the Newtonian viscosity is observed in thermodynamically stable systems, e.g. surfactant solutions and microemulsions, beyond a shear rate of 5/s or less. The Newtonian region also was observed in normal emulsions with narrow size distributions, dilute monodisperse coarse emulsions or dilute normal emulsions prepared in a Warring blender while a short chain alcohol is added to the system. By adding the short chain alcohol to the system not

only the densities of the two phases are made similar and the emulsification is eased but also the polydispersity of the final emulsion is decreased.

Finally a single model to be applicable to different types of emulsions with droplet sizes over five orders of magnitude was proposed. However the relationship is applicable to the systems with a low degree of polydispersity and once polydispersity is introduced the flow behaviour becomes complicated and the proposed model is not applicable.

Acknowledgements

Table of Contents

Introduction

An emulsion is comprised of oil and water which normally cannot be mixed. However, for many uses of emulsions it is advantageous to have properties of both of these fluids. Hence, it has long been favourable to force oil and water together in a single system. Looking at nature we find many examples of emulsions. Milk for example is a mixture of the casein protein family plus phospholipids, water and fat. The protein and lipid components, termed emulsifiers, have characteristics allowing them to bring the fat and water together in a stabilized system. Many synthetic emulsions also exist including cosmetics and pharmaceuticals. Nowadays we know more about the role that stabilizers and emulsifiers play in making an emulsion and their applicability to different systems. However, relating the chemical structure and functionality of emulsifiers to the macroscopic behaviour of emulsions remains difficult. For example the role they play in defining the flow behaviour of emulsions. This characteristic of emulsions, their response to an applied force, is routinely exploited in their use.

Emulsions are viscoelastic materials; their response is manipulated by multiple length scale features and interactions. When a force acts on viscoelastic substances it causes deformation. The extent of this deformation is studied using rheology. Since the deformation results in fluid flow, rheological data are considered to yield information on the flow properties and structural characteristics of systems. In this research surfactant micellar systems, microemulsions, nanoemulsions, emulsions and large droplet monodisperse coarse emulsions were investigated with respect to the effect of droplet size and degree of polydispersity and therefore, the length scale of interactions on their flow behaviour. Existing rheological models were used to analyse the data across the multiple systems and to evaluate therefore their scalability and also their applicability for polydisperse systems. Understanding the origin of the rheological properties of emulsions is crucial to allow tailored design of emulsions.

There are several different types of emulsions. Typically, during the emulsification process one phase, called the dispersed phase breaks up into droplets and is distributed in the other

phase, called the continuous phase. The emulsions are generally divided into three categories based on their stability and droplet size (Table 1-1):

1- microemulsions

2- nanoemulsions

3-macroemulsions.

Furthermore each of these systems can be sub-classified into three categories based on the phases they are made of:

1- Oil-in-Water (O/W);
2- Water-in-Oil (W/O); and
3- Bicontinuous.

Table 1-1 Different types of emulsions based on droplet size and stability

System	Size	Stability
Microemulsion	1-200 nm	Thermodynamically
Nanoemulsion	10-400 nm	Kinetically*
Macroemulsion	0.5-50 µm	Kinetically*

*Such a state is inherently a transition state; that is emulsions are not thermodynamically stable and over time they will phase separate to yield a lower energy state. In such a state the system is comprised of bulk water and bulk oil. By choosing the correct emulsifiers, it is possible to have a stable system for a long period of time.

In the case of microemulsions, the systems are said to be thermodynamically stable which means that they will form spontaneously. By applying the right chemicals and concentrations, generating such a system takes nothing but low-energy mixing of the components. It should be noted that microemulsions are often considered to also not be thermodynamically stable; they just have a very long life time.

In the case of nanoemulsions and macroemulsions (or more commonly those systems that are referred to as emulsions) the systems are kinetically stable. The emulsification process requires the introduction of energy often in the form of a shear force. Initially upon formation the droplets of the dispersed phase are not fully covered by the emulsifier. Over time the emulsifying agent will adsorb to the surface of the droplets creating an interfacial

thin film. This process is controlled by the concentration of the components and their chemical functionality. The characteristics of the interfacial film directly affect the surface tension of the droplets and the emulsion stability. The adsorption of emulsifying agents takes place based on well-known mass transport phenomena such as the Gibbs isotherm and the Gibbs-Marangoni effect. The former explains the adsorption and the latter the distribution of the emulsifying agents over the interfacial thin film at the oil/water interface. Both processes occur due to concentration gradients of emulsifiers in the bulk and at the interface. The adsorption process is restricted by the induced repulsive force which arises from the accumulating agents within the interfacial region. The concentration of emulsifiers at the interface also results in a repulsive force between droplets which prevents droplet coalescence from occurring.

The intrinsic thermal energy in the system hinders emulsifier adsorption at the interface. However, adsorption occurs anyway driven by the chemical nature of the emulsifiers having both polar and non-polar characteristics (Fig. 1-1). The total energy of the system is reduced when emulsifier resides at the oil/water interface. Such interfacial stabilizers are also known as surface active agents (surfactants). Surfactants are the major component of the interfacial film between the continuous and dispersed phases reducing the inherent interfacial tension between these two phases.

Surfactants, based on their charge, are categorized into three groups: non-ionic, cationic and anionic. The four surfactants used in this research; triton X-100, pluronic F127, cetyltrimethyl ammonium bromide (CTAB) and sodium dodecylsulfate (SDS), are shown in Fig. 1-1.

a) $H - (O - CH_2 - CH_2)_n - O -$ ⬡ $- C(CH_3)_2 - C(CH_3)_3$ (n=9–10)

b) $H - (O - CH_2 - CH_2)_n - (O - CH - CH_2)_y - (O - CH_2 - CH_2)_n - OH$

(n=100, y=65) CH_3

c) $H - (CH_2)_{16} - N^+(CH_3)_3 Br^-$

d) $H - (CH_2)_{11} - O - SO_3{}^- Na^+$
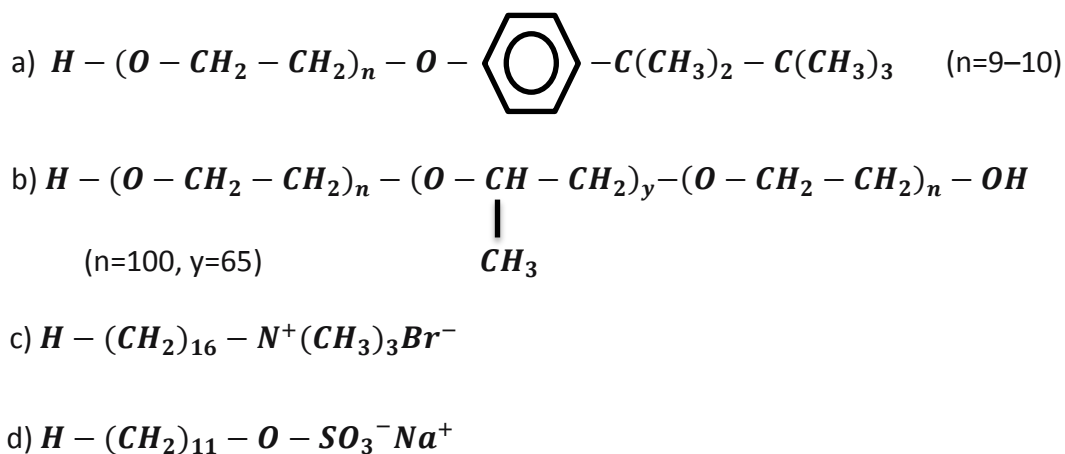
Fig. 1-1 Emulsifiers used in this research. a: Triton X-100 a non-ionic surfactant, molecular weight 647 g/mol, b: F127 a non-ionic surfactant, molecular weight ~ 12600 g/mol, c: CTAB a cationic surfactant, molecular weight 365 g/mol and d: SDSs an anionic surfactant, molecular weight 288 g/mol.

Each of these surfactants is bio-friendly they have been well studied for their ability to form emulsions (for example see [1-5]) and can be exploited in biological applications.

In addition to droplet size, especially in the case of emulsions, size distribution should also be taken into account in order to study the microstructure of a given emulsion. Emulsions, based on their size distribution, can be classified into monodisperse and polydisperse; monodisperse emulsions have a single length scale whereas polydisperse systems contain more than one length scale, e.g. bimodal or tri-modal or more. One of the parameters that affect the size distribution is the emulsification method. In this research three methods were exploited to prepare emulsions (these methods will be explained in Chapter 2):

1- a microfluidic device;

2- a Blender; and

3- a Homogenizer.

Each provides a different amount of energy that is introduced in a different way and hence produces different types of emulsions with different size distributions. There is an intrinsic difference between the first method and the last two, the first method is a continuous process whereas the other two are batch processes. These concepts will be discussed in Chapter 2.

Exploiting the above methods resulted in emulsions with droplet sizes from 0.1 μm up to 40 μm being fabricated. The generated emulsions were compared and analysed with regard to their size distribution. The first method, the continuous process, allows in-process control over the system. Hence the size can be well controlled over a very narrow range of sizes limited by the size of the channels of the microfluidic chip. In the second and third methods, batch processes, the ingredients are put together and undergo mixing while there is no in-process control. These methods normally give polydisperse systems however by manipulating the system such as through the densities of the materials, the polydispersity can be reduced. In this research two short-chain alcohols, ethanol and propanol with densities of 789.0 and 803.4 kg/m^3 at 25 °C respectively, have been exploited to decrease the density of the continuous phase and have it match that of the oil density; 750.0 and 917.0 kg/m^3 at 25 °C in the case of dodecane and soybean oil respectively.

The surfactant interfacial thin film and how it interacts with the continuous and dispersed phases define the microstructure of the system. One way to gain information on the microstructure of emulsions is via the application of a force to the fluid in a controlled way. This makes the system flow. Analysing the flow behaviour of the fluid allows information on the microstructure within the fluid to be obtained.

In the last decades the rheological responses of emulsions have attracted much attention. This is in part due to thousands of tonnes of emulsions being produced daily around the world (see [6] & [7]). Fewer studies have been undertaken in the case of microemulsions and nanoemulsions. The reason behind this is that preparing such systems is not as straightforward as the preparation of emulsions and furthermore, these systems exist only in a small region of the full phase diagram whereas in general, emulsions can be formed over wide compositional variation. Despite this a number of studies have focused on characterising the rheological response of microemulsions and nanoemulsions and the relationship between them (see [8] & [9]).

Huge numbers of different emulsions exist due to their vast range of applications. Therefore, emulsions are comprised of an abundant array of chemicals which specifically and generally determine their characteristics. Hence, analysing emulsions based specifically on their components results in a series of experimental findings which are generally reliable only for the system under investigation. On the other hand, flow is a characteristic of all fluids and hence can be used as a means of directly and indirectly probing complex fluid structure and characteristics. The reader is directed to an article by Morris et al. who have reviewed the relationships between microstructure, rheology and the flow properties of bulk materials [10].

Investigating the correlation of emulsion microstructure and emulsion flow properties may therefore lead to the development of models based on physical properties rather than chemical components which will allow great predictability of emulsion behaviour. This was one of the major focuses of the research undertaken for this thesis. In a complex fluid, the interactions between the components define the properties of the whole fluid. Since complex fluids display viscoelasticity, part of the induced energy results in deformation while the rest is stored. Using this we aim to determine the relationships between emulsion microstructure, droplet deformation and flow behaviour, for surfactant micelle systems through to coarse emulsions.

First we consider the microstructure of fluids. A simple liquid is made of molecules, the length scale of which is a few Ångstroms. The molecules move around due to their thermal energy and hit each other millions of times a second. Hence relaxation times are short enough to ensure the bulk structure is unaffected by these motions. In other words all of the applied energy is dissipated through the system via thermal fluctuations. If the components in the system are larger they can affect the structure of the bulk and the result is that a part of the energy is now stored in the system and relaxation takes longer. This is one of the most important features of the microstructures of complex fluids; deformation and relaxation effects dominate the physical properties of the system. Therefore in a complex fluid such as an emulsion, the dispersed phase which presents a vast surface area is generally in the form of spheres which collectively define the microstructure of the fluid (Fig. 1-2). In this research the droplet size is considered as the index of the microstructure

since most systems contain spherical droplets. For non-spherical systems the proposed structure will be discussed.

It is worth mentioning that the relaxation time is directly related to the length scale of the system, hence as the droplet size is enhanced going from a microemulsion to a coarse emulsion the relaxation time increases and the liquid-like material turns to a solid-like material.

100 μm
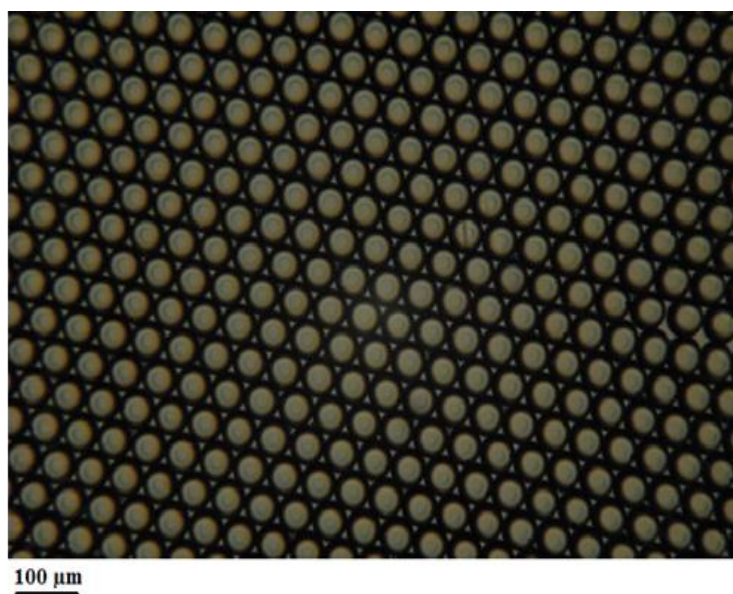
Fig. 1-2 Optical image of a monodisperse coarse emulsion containing spherical microstructures prepared using a microfluidic device.

How emulsion flow properties are associated with the underlying microstructure of the emulsion is still an ambiguous aspect of emulsion technology. The main reason for this is that there are many interactions within the system. The information obtained about the system by performing rheological experiments needs to be correlated to the interactions within the sample, however prediction is limited since the relative weighing of each interaction that should be applied is not known and may differ considerably between the different systems. This limits our ability to model systems well and predict their behaviour.

It is generally known that in emulsions, deformation of the microstructure affects the bulk properties of the system. In particular, the droplet size, droplet size distribution and

therefore polydispersity, and the interfacial film thickness are all key physical parameters that control the emulsion structural deformation process. However, deformation in general and the role of each of the key physical parameters in controlling the deformation are not well understood.

The focus in this research is to begin to determine how to correlate each of droplet size, droplet size distribution and interfacial thin film characteristics to the flow properties. To achieve this objective and by means of a microfluidic device, we start with a simple system made of a single length scale of spherical droplets, a so-called monodisperse coarse emulsion. Hence the effect of polydispersity has been omitted and the effect of droplet size and interfacial film thickness come into direct consideration. In the next step we start making bimodal emulsions by mixing a specified amount of two monodisperse emulsions and beginning to determine the polydispersity effect. In the parallel experiments, microemulsions were prepared using a Warring blender. These microemulsions were then used to prepare nanoemulsions using the low-energy two-step process [11]. Hence, within a single chemical system emulsions with droplets ranging over five orders of magnitude (1 nm to 100 μm) were formed with a range of different poydispersities including monodisperse coarse macroemulsions, low polydispersity micro-emulsions and high polydispersity emulsions.

Diffusion nuclear magnetic resonance (DNMR) was used to measure the droplet size of macroemulsions. This technique also yields information on the microstructures. Dynamic light scattering (DLS) was applied to determine the size of microemulsions and nanoemulsions. Static light scattering (SLS) was used for emulsions. Small Angle X-ray Scattering (SAXS) was exploited to probe the micellar size in the surfactant systems. All systems were investigated using rotational and oscillatory rheology experiments to measure the non-linear flow properties and deformation-relaxation behaviours, respectively.

The relationship between viscosity and droplet size is well studied with its roots stemming from the time when Brownian motion was discovered where the movement of molecules in a fluid is correlated to the viscosity of the fluid. This relationship can be expressed as per Einstein's equation:

$$d_H = \frac{K_B T}{3\pi\eta D} \qquad\qquad\qquad Eq. 1-1$$

where d_H is the hydrodynamic diameter, K_B is Boltzmann's constant, T is absolute temperature, η is the viscosity and D is the diffusion coefficient.

With the same baseline Einstein and Stokes proposed a relationship between the size of a moving object within a fluid and the viscosity of the fluid as follows:

$$F_d = 3\pi\eta d_H v \qquad\qquad Eq. 1-2$$

where F_d is the frictional force, Stokes drag, v is the particle's velocity and the other terms are as mentioned below Eq. 1-1. While this is limited, in allowing measurement of the interaction between the droplets that interferes with the Brownian motion and the external applied force, which requires for example either fluid dynamic simulation [12] or applying coupled methods such as Rheo-NMR [13] and Rheo-SAXS [14]. The first approach is computational and more suitable for engineers or mathematicians and the latter needs very expensive machines; it does allow considerable information to be obtained.

The aim of this research is to correlate length scale and flow properties by utilising instruments that can be easily found in any physical chemistry laboratory. It is possible for a vast range of systems with different structures to be explored in a straightforward manner and be directly compared and through doing this gain insight into the fundamental elements of emulsion flow behaviour and retrieve enhanced predictability. To achieve this objective the various rheological models were considered and modifications applied to better fit the data.

Consider the following rheological models: The Einstein relationship for surfactant micellar solutions, microemulsions and diluted normal emulsions [82] and the Pal relationship for concentrated and coarse emulsions [90], respectively. The first relationship is an example of a simple analytical rheological model that expresses the viscosity of a dilute dispersion and is the basis of lots of emulsion models and the second one is a practical model built based on the analytical model (the factor of 2.5 is seen in the both formulas). Taking more affecting parameters on the viscosity into account, as will be explained below, this model is more complicated than the first model and has proved to be applicable to many concentrated emulsions that are similar to the concentrated emulsions studied here.

$$\eta_r = 1 + 2.5\emptyset. \qquad\qquad Eq. 1-3$$

$$\eta_r \left(\frac{2\eta_r + 5\lambda}{2 + 5\lambda}\right)^{1/2} = \exp\left(\frac{2.5\emptyset}{1 - \left(\emptyset/\emptyset^*\right)}\right).$$ $Eq. 1 - 4$

Where η_r is the relative viscosity, the ratio between the sample viscosity and the reference viscosity, which is usually assumed to be the viscosity of the continuous phase, λ is the viscosity of the continuous phase divided by the viscosity of the dispersed phase, $\emptyset$ is the oil volume fraction, and $\emptyset^*$ is the volume fraction at the closest packing of droplets.

These models have been found to not be applicable to the microemulsions and coarse emulsions investigated in this research for the following reasons:

1- The reference viscosity being used is the viscosity of the continuous phase, which is not appropriate and it results in Eq. 1-3 not being applicable to the microemulsion systems studied in this research. In this study it is shown that the appropriate reference viscosity for microemulsion rheological models is the viscosity of the ternary water/surfactant/alcohol system from which the microemulsion is made.

2- The maximum packing is assumed by many researchers to be a constant value, is not appropriate and it results in Eq. 1-4 not being applicable for the monodisperse coarse emulsions investigated in this thesis. In this study it is shown that the maximum packing of a coarse emulsion must be considered as a function of droplet deformation. This provides information on the microstructure and structural changes that occur upon applying the shear force.

To determine the length scale of each system the appropriate size probing method is selected and modified. For microemulsions and nanoemulsions, dynamic light scattering (DLS) is applied. Eq. 1-1 is the basis for the calculation of the droplet size for this method.. The viscosity is one of the input parameters that must be entered by the user. The default value is generally set to be the viscosity of water, 1 cp, which is the continuous phase in oil-in-water complex fluids. However, the estimated droplet size obtained using DLS is incorrect unless the value of the viscosity is set to the zero-shear viscosity of the material. However the appropriate zero-shear viscosity can be read from the relevant flow curve at a very low shear rate where an increasing shear rate is applied. This constant, initial, solid-like viscosity will be discussed in Chapter 3.

In the case of coarse monodisperse emulsions, diffusion nuclear magnetic resonance (DNMR) is exploited. This is already well studied for monodisperse systems [15] and [16]. In this research the relationships are modified to be applicable to polydisperse systems as well (see Chapter 5).

To correlate the length scale and flow properties requires consideration of droplet shape as well as droplet size. For surfactant micellar solutions, microemulsions and nanoemulsions the Simha relationship is used to probe the shape over the Newtonian region, meaning the constant viscosity region at high shear rates:

$$\eta = 2.5 + 0.4075(J-1)^{1.508} \qquad\qquad\qquad Eq. 1-5$$

where J, is the ratio of the major and minor axes' rotation. The larger J, the more deviation from spherical shape is expected.

In the case of concentrated emulsions, droplet shape changes continuously upon applying shear resulting in, droplet deformation. It is for this reason that in this work a shear-dependant maximum packing, $\emptyset^*$, in Eq. 1-4 is suggested to be used instead of a constant maximum packing (see Chapter 5 for more information).

Using modified methods and relationships, it is demonstrated here how rheological models can be more applicable to a vast range of different types of emulsions with droplet sizes from 1 nm to 100 μm, droplet shapes from spherical to worm-like, with different degrees of polydispersity and different packing patterns to be explored. In order to correlate length scale and flow properties models with strong theoretical foundations have been selected. The reason for this is that most of the existing appropriate rheological models for complex fluids are case-dependant and contain experimentally determined values [17]&[18]. Furthermore, for some of these expressions different authors suggest different values for the same experimental parameter. This limits their use and applicability to a range of systems with similar physical properties and different chemical basis. The aim of this research is to correlate physical properties to flow behaviour regardless of the chemicals that are used to make the system. This means the chemical properties are considered indirectly through the structural properties that they provide to the system.

Finally, it should be mentioned that being able to produce nanoemulsions, microemulsions and macroemulsions within the same chemical system with droplets over five orders of magnitude (1 nm-100 μm) and then compare their flow properties, as done in this research, allows a formulator to design the appropriate system for the specific need. For example by going from an emulsion-based drug delivery system to a microemulsion-based one, not only may the shelf life and the appearance of the product have been improved but also the release rate enhanced. Such information is required to allow researchers and practitioners to produce tailored emulsions with predictable macroscopic properties.

Materials and methods

2-1 Materials

All emulsion systems used were oil-in-water emulsions. The exploited oils were dodecane, a hydrocarbon; poly di-methyl siloxane (PDMS), an organic silicon-based polymeric liquid; and soybean oil, a vegetable oil extracted from the seeds of the soybean. The oils were purchased from Sigma-Aldrich; their supplied specifications are given in Table 2-1.

Table 2-1 Specifications of the oils

Oil	Dodecane	PDMS	Soybean oil
Density (g/L at 25℃)	0.75	0.97	0.92
Viscosity (at 25℃)	1 cp	5 cp	50 cp
Purity	≥ 99%	≥ 99%	≥98%

Four surfactants or emulsifiers were used to study the effect of the interfacial layer in emulsions: Sodium dodecyl sulfate (SDS) allowed microemulsions (10 nm) through to coarse emulsions (~40 µm) to be formed and as such it was the main emulsifier used. SDS is a ionic surfactant with a hydrophilic-lipophilic balance (HLB) of 40 [19]. The three other surfactants were Pluronic F127, a tri-block copolymer surfactant which is non-ionic and a relatively nontoxic surfactant; Triton X-100, a non-ionic and relatively nontoxic surfactant; and N-cetyl trimethylammonium bromide (CTAB) which is a cationic surfactant. All the surfactants were purchased from Sigma-Aldrich. The chemical structures of the surfactants are given in Chapter 1, Fig 1-1. In Table 2-2 are given some of the surfactant's features.

Table 2-2 The characterisations of the surfactants used in this research

Surfactant	SDS	F127	Triton X-100	CTAB
Polarity	Ionic	Non-ionic	Non-ionic	Cationic
HLB*	~ 40	~20	~ 13.5	~ 10
Molecular Weight (g/mol)	286	12600	647	365

*The values of HLB are based on the information provided with the product by the company.

Ethanol and propanol were purchased from Sigma-Aldrich with purity of 99%.

2-2 Methods

In order to provide insight into the effect of droplet size and polydispersity on the rheological properties of emulsions, a range of emulsions were fabricated with droplet sizes ranging from 5 nm to 50 μm having narrow (monodisperse) to broad size distributions. Large monodisperse oil droplets can be generated using a microfluidic chip setup (similar to a micro mixer in terms of functioning) that works as a continuous droplet formation unit enabling in-process control over emulsion fabrication. Smaller but more polydisperse emulsions are made using a blender and a homogenizer. Nanoemulsions can be prepared by the low energy method [11]; and microemulsions via the addition of a fourth component, here a short-chain alcohol. To produce microemulsions and nanoemulsions a Warring blender was used. Each of these methods is described below.

2-2-1 Microfluidic device (preparation of coarse, monodisperse emulsions)

To mix and deliver micro and nanolitres of fluid a device with dimensions less than a millimetre needs to be used. However, as length scales decrease frictional forces arising from wall effects need to be taken into consideration. Indeed other effects also come into play and different physics governs the system as compared with normal industrial sized equipment. Hence it is not possible to simply scale down the devices used in industry and have them work in the microfluidic system. Microfluidic devices have channel dimensions only a few times larger than the droplets that are formed and wall effects such as wall wettability, define and control the behaviour of the fluids under flow. Such devices have recently attracted much attention due to the unique ability to enhance process efficiency in the field of DNA extraction [11], gold nano-particle generation ([12], [13], and [14]) and microfluidic droplet-based extraction [15].

Since microfluidic devices can be used to form controlled monodisperse droplets, such devices have opened new windows of opportunity in different areas of science and technology including bio-sensors, genetic analysis, drug screening and also as a measurement tool of fluid viscosity, density and pH [20]. A microfluidic device used in this research is shown in Fig. 2-1.
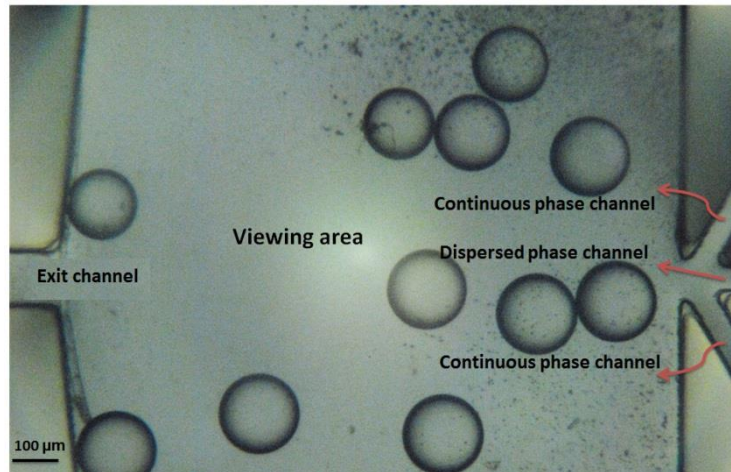
Fig. 2-1 A microfluidic chip used in this study.

2-2-1-1 Preparing monodisperse emulsions- Continuous process

Microfluidic devices are governed by rules that enable generation of monodisperse emulsions. In particular, dimensionless numbers are often used to characterize these systems. Each of these numbers, through a combination of physical parameters, depending on the terms they encompass, explains some property of the material. By controlling these numbers the length scale of the system can be controlled. In a microchip, the oil and water (single phase fluids) are delivered through micro-channels, and then meet at a junction which results in droplet formation (break-up process). Afterwards the generated complex fluid (multiphase fluid) is delivered through a micro-channel to the sample collection container. To characterize the system at each stage of the process, a specific dimensionless number(s) is (are) needed. Three numbers in particular are important to consider here:

- Reynolds number, which is the ratio between inertia and viscous forces, and is used to describe both single and multi-phase fluids;
- flow ratio between the continuous and dispersed phase, used to explain the break-up process; and
- Capillary number, which contains interfacial forces as well as viscous ones and is applied for complex fluids.

In a microfluidic device, by choosing an appropriate flow ratio and keeping the Reynolds number sufficiently low, monodisperse emulsions can be prepared. The above

dimensionless numbers are defined through a number of physical properties of the material. These properties are either intrinsic (such as density) or due to the system being exposed to external forces (such as flow rate). Additionally geometric features which are not included in these relationships may be important features to consider. In this section the importance of such geometric factors are discussed. The results presented here demonstrate that by including geometric parameters in the Reynolds and capillary numbers in a microchip, the effect of the geometry can be straightforwardly observed. From this basis, modified Reynolds and capillary numbers can be defined and applied. In this section, it is shown that the physical properties along with geometric features define the range of droplet sizes that can be achieved using a given microfluidic geometry.

In the following sections by investigating the abovementioned dimensionless numbers we demonstrate how the length scale in an emulsion system can be controlled by setting these numbers to appropriate values.

2-2-1-1-1 Fluid Dynamics of Single Phase Fluids

The Navier-Stokes equation is the most well-known relationship in the field of fluid dynamics:

$$\rho\left(\frac{\partial u}{\partial t} + (u.\nabla)u\right) = -\nabla P + \eta\nabla^2 u \qquad\qquad Eq.\,2-1$$

where u is the fluid velocity, P is the pressure, ρ is the density, and η is the fluid viscosity. The right hand side of the equation contains the pressure gradient, $(-\nabla P)$, and forces arising from the viscosity of the fluid per unit area, $\eta\nabla^2 u$. In the left hand side are terms concerning accumulation (time dependency of the system), $\rho(\frac{\partial u}{\partial t})$, and forces related to the velocity of the fluid, $\rho((u.\nabla)u)$.

The ratio of the inertial forces to the viscous forces is called the Reynolds number:

$$Re = \rho\,\frac{u/t + u^2/l}{\eta u/l^2} \qquad\qquad Eq.\,2-2$$

where u is velocity, l is the length scale, ρ is the density, η is the viscosity, and t is time. If we replace t with $\frac{l}{u}$ the following expression is obtained after omitting the constant coefficient, 2:

$$Re = \frac{\rho u l}{\eta}. \qquad\qquad Eq. 2-3$$

At low Reynolds numbers viscous forces govern the system. As we can be seen from Eq. 2-3, Reynolds number decreases with length scale, therefore for a constant velocity, as the dimensions of the device decreases, the viscosity dominates the system. This kind of flow pattern is called laminar flow which is observed at low Reynolds numbers (Re < 1). In this pattern, movement is layer by layer and the speed is assumed to be zero on the walls and reaches the maximum value in the centre (Fig. 2-2, top). On the other hand there is turbulent flow for high Reynolds numbers (Re > 2000) in which inertia dominates the system and the fluid is carried through vortices which gives a complicated but also uniform system (Fig. 2-2, bottom) which is different from the layer by layer flow (laminar flow). For Reynolds numbers between 1 and 2000 a transition state is observed which contains laminar flow next to the walls up to a specified distance and then turbulent flow in the middle. It should be mentioned that in laminar flow, zero velocity at walls is assumed which can be altered under slip condition. In this case it is possible to have plug flow at very low Reynolds numbers.
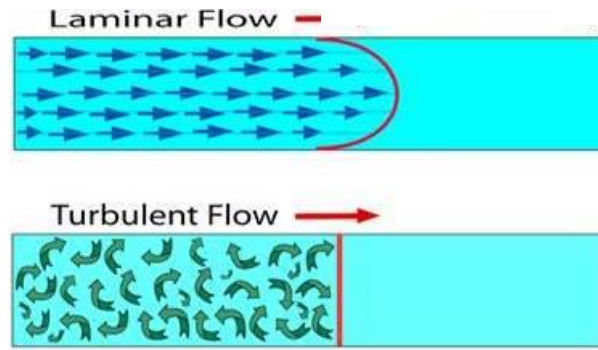
Fig. 2-2 Laminar flow with a parabolic profile (top) and turbulent flow with plug profile (bottom).

In microfluidic devices we typically deal with low Reynolds number allowing us to assume that the flow pattern is laminar. In such a case the left hand side of Eq. 2-1, which is related to inertial terms, becomes negligible resulting in a linear differential equation:

$$\eta \nabla^2 u = \nabla P. \qquad\qquad Eq. 2-4$$

The time dependent term is not included in this equation owing to the low Reynolds number for which, the motions are symmetric in time.

The velocity distribution profile for low Reynolds number is parabolic while it is plug flow for high Reynolds numbers (Fig. 2-2). It should be noted that this profile can be plug even in the low Reynolds number limit [21] provided that diffusion dominates shear forces. If this is the case, Brownian motion becomes important. Diffusion occurs along the radius transverse to the mean flow direction and so the parabolic profile becomes flat and we can see vortices in the system. In this case turbulences are based on internal thermal energy of the particles not external shear energy.

When designing a microfluidic device it is very important to consider the equations which govern the system based on the flow rates that the device is designed to deliver.

2-1-1-1-2 Fluid Dynamics of Multiphase Flows

Once two streams of single fluids meet each other they are no longer considered to be a single phase fluid (Fig. 2-3). To describe the generated multiphase flow the Reynolds number needs to be modified and an additional dimensionless number containing the forces that arise due to the presence of an interface is needed. We apply the capillary number, Ca. The capillary number is the ratio of viscous effects to surface tension effects acting on the interface.

The capillary number plays an important role in the characterisation of multi-phase systems:

$$Ca = \frac{\eta\, u}{\sigma} \qquad\qquad\qquad Eq.\, 2-5$$

where η is viscosity, u is velocity, and σ is interfacial tension.

It is worth noting that for each term in the Reynolds and capillary numbers, different parameters can be used provided that they have the same dimension. The user is therefore able to select the best match for their system. For instance to calculate the Reynolds number for a passing emulsion in a micro-channel, one may apply the droplet size or the width of the channel as the length. They are both acceptable. However when different systems are compared, dimensionless numbers made of the same parameters must be applied.

The Reynolds number relationship for a complex fluid in a microchip is discussed in the next sections.

A microfluidic chip (similar to a micro mixer in terms of functioning) works as a continuous droplet formation unit enabling in-process control over emulsion fabrication. In such a chip two immiscible phases (oil and water) are delivered through separate channels and then meet each other at a junction, break-up happens and droplets form (Fig. 2-3).
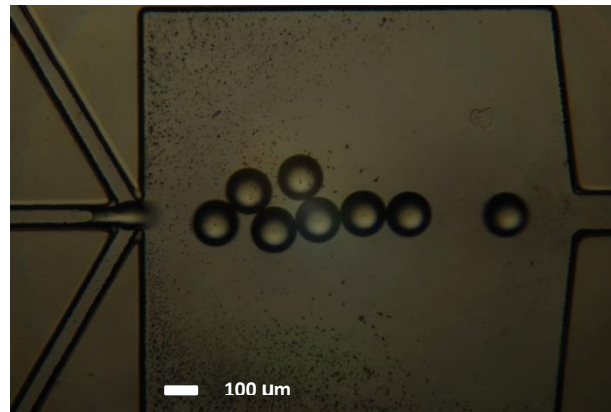

Fig. 2-3 Droplet formation in a microchip.

Christopher *et al*. have divided microfluidic methods into three groups as below [22]:

(1) break-up in co-flowing streams;

(2) break-up in cross-flowing streams; and

(3) break-up in elongational or stretching dominated flows.

This division is based on the break-up mode, which completely depends on the geometry of the device (Fig. 2-4). The geometries in Fig. 2-4 (a) and (c) allow fluids to go through parallel paths whereas in (b), which is T-shaped, fluids are delivered through perpendicular micro-channels. Normally before the break-up point a jet of fluid is observed. The type and shape of this jet is related to the chemical properties such as surfactant concentration as well as physical parameters dictated by the geometry. These aspects will be discussed in the next section.
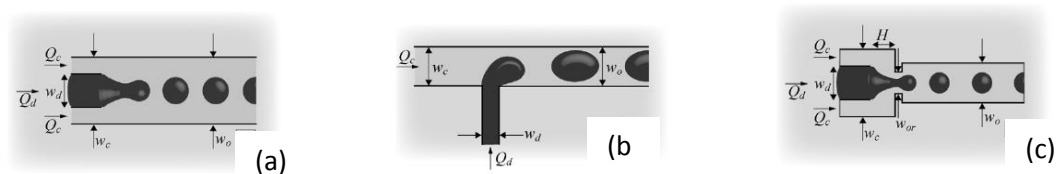

Fig. 2-4 Different breakup patterns (adapted from [22]).

The wettability of the walls of the channels near the junction determines which fluid is the dispersed phase. This is an important factor to be taken into account in microfluidic device design [22].

As mentioned previously, the velocity distribution in a micro-channel is parabolic. As such, at the junction the leading tips of the streams meet, which helps pinch-off and allows break-up to happen. As a matter of fact the stream which is going to become the dispersed phase is pulled by the other stream(s) from the tip so that the leading parabolic layer forms the jet. Besides this parabolic shape, the leading edge allows the interference of streams to occur so that mixing and mass transfer (surfactant distribution) take place efficiently; these phenomena are followed by droplet formation.

The geometry of the microfluidic device which is used in this PhD programme is based on a modified flow focusing geometry which will be discussed in Chapter 5.

2-2-2 Homogenisers and blenders (preparation of normal emulsions)

Homogenisers and blenders are equipment for non-continuous, batch process of preparation of emulsions and microemulsions, therefore the control over the system during emulsification is poor. As a result the products of these methods are normal (polydisperse) emulsions. However the degree of polydispercity can be controlled by the chemicals that make up the system.

2-2-2-1 Homogeniser (preparation of emulsions)

This device was used in order to prepare normal emulsions with relatively broad size distributions. For this purpose the sample is pre-blended using a Warring blender. This pre-blended emulsion is introduced into the homogeniser and then passed through the high pressure area that provides up to 20 atm pressure. The more times the sample is passed through the high pressure area the finer the dispersion and the lower the polydispersity. The homogenizer used in this research is shown in Fig. 2-5. This is a home-made device that has been developed at the workshop of the School of Chemical and Physical Sciences at Victoria University of Wellington.

Fig. 2-5 Home-made homogenizer used in this study.

## 2-2-2-2 Warring blender (preparation of microemulsions)

This device is a simple mixer. This machine works at two speeds, 22000 and 18000 RPM respectively. The device was used to prepare some of the normal emulsions and also all the microemulsions studied in this research. For the purpose of making microemulsions a short-chain alcohol, ethanol or propanol, was added to the oil/surfactant/water system. Such agents are called co-surfactants and are used in order to lower the density of the continuous phase and the interfacial tension. Since microemulsions are thermodynamically stable, it is not required to apply energy for the process over time if left undisturbed a microemulsion will be formed assuming the correct quantity of each ingredient was used. To speed up this process it is common for sufficient energy to be added. Furthermore, for some systems it is not possible to form single system microemulsion and in these cases additional energy is required to mix the components [8, 23]. In the case of microemulsion preparation the emulsion was left for 12 hours. For some samples the generated emulsion was found to be stable and for others a two phase system was resulted. Based on the surfactant used this two phase system included microemulsion/excess oil or microemulsion/upper emulsion (Fig. 2-6).

Fig. 2-6 Right: Representative microemulsions for CTAB, SDS, Triton X-100 Left: F127 microemulsion in coexistence with an upper emulsion phase.

2-2-3 Low energy process (preparation of nanoemulsions)

All nanoemulsions investigated in this work were produced using the low energy process. Microemulsions were prepared as described above. The microemulsions were then subjected to dilution with their corresponding continuous phase to 1/5 of their original concentration. This low energy dilution-based method was used by Wu and coworkers for nano-emulsification [24] and is shown in Fig. 2-7.
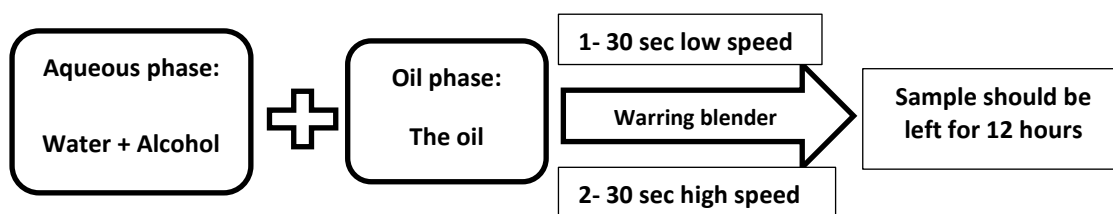
Fig. 2-7 Low energy method to prepare microemulsions.

The droplet sizes and size distributions for all samples were determined using a range of different methods appropriate for the sample being considered. These are outlined below.

2-2-4 Light scattering

For all of the different emulsion systems the presence of the suspended oil droplets scatter light. Hence the droplet size and size distribution can be probed by monitoring the scattering of light. For macro-emulsions, static light scattering (SLS) is applied since this instrument is able to detect droplet sizes between 30 nm and 100 µm whereas for

31

microemulsions and nanoemulsions dynamic light scattering (DLS) is used to determine droplet size between 1 nm and 6 μm.

2-2-5-1 Dynamic Light Scattering (DLS)

Dynamic light scattering or quasi-elastic light scattering is a method to detect the size distribution of particles in a solution or a complex fluid. Based on Rayleigh's theory (Eq. 2-6 & Eq. 2-7) particles in a fluid would scatter the emitted light due to their size. When it comes to small particles (very much smaller than the wavelength of the incident light), the intensity of the scattered light shows time-dependent fluctuations. The reason for this is that small particles constantly undergo Brownian motion. The intensity of the scattered light also reflects the number of particles in the volume unit that can have constructive or destructive impact on each other. From this information, the particle size and size distribution can be derived.

$$I = I_0 \frac{1 + \cos^2 \theta}{2R^2} \left(\frac{2\pi}{\lambda}\right)^4 \left(\frac{n^2 - 1}{n^2 + 2}\right)^2 \left(\frac{d}{2}\right)^6 \qquad\qquad Eq.\,2-6$$

$$x = \frac{2\pi r}{\lambda} \qquad\qquad Eq.\,2-7$$

where, I_0 is the intensity of unscattered light, θ is the scattering angle, R is the distance to the particle, λ is the wavelength, n is the refractive index, d is the diameter of the droplet and x is the particle's relative length scale while r is the size of the spherical particle

From DLS the hydrodynamic diameter of the droplet is determined, corresponds to the size of the diameter of an equivalent sphere with the same diffusion.

2-2-5-2 Static Light Scattering (SLS)

Static light scattering is a method to determine the molecular weight and size of particles or droplets in a complex fluid with droplet size comparable to the visible light's wave length (~ 400 nm) (i.e. the factor x as expressed in Eq. 2-7 is not significantly smaller than 1) . In this case Mie solution of Maxwell's equation can provide information on the size of the droplet. The intensity of the scattered light can be related to the molecular weight.

2-2-5 Rheology of Complex Fluids

An RA2000, stress controlled rheometer, was used to measure flow properties of all samples. Three common measurement geometries were used to determine the flow

properties of the samples: the parallel plate (PP), cone and plate (CP) and coaxial cylinder (Couette) geometries, each is discussed in some details below.

2-2-6-1 Parallel Plate (PP) geometry

In the PP geometry (Fig. 2-8), the radius, R, is bigger than the distance between the two plates, H. The angular velocity is constant in each plane parallel to the plates at a given radius and is calculated as [23]:
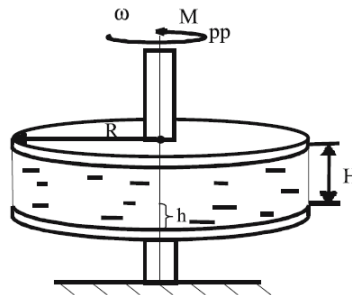
$$\omega\big|_{h,r} = r.\Omega\,\frac{h}{H} \qquad\qquad Eq.\,2-8$$

where Ω is the angular frequency. The shear rate is $\frac{\omega(h)}{h}$, substituting for $\omega\big|_{h,r}$ yields:

$$\dot\gamma = \frac{r.\Omega}{H}. \qquad\qquad Eq.\,2-9$$

From a practical perspective we measure and control the torque (M_{PP}) and angular velocity. The shear stress of a Newtonian fluid is related to the torque and the angular velocity as follows:

$$\tau = \frac{2M_{PP}}{\pi R^3}. \qquad\qquad Eq.\,2-10$$

Fig. 2-8 PP geometry, M_{PP} is the torque, ω is the angular velocity, R the radius of the plates, H the gap between the two plates and *h* is the height (adopted from [25]).

By changing the distance between the two plates and the angular velocity, the shear rate is varied. The gap between the plates should not be less than five times that of the droplet size otherwise frictional effects dominate the data [25]. The disadvantage of this method is that the shear rate depends on the radius and it changes from zero at the central axis to the maximum at the radius R.

Eq. 2-10 gives us the shear stress for a Newtonian fluid. Rabinowitsch and Weissenberg suggested a relationship (Eq. 2-11) [25] to derive the real shear stress for non-Newtonian fluids based on the measured stress and the shear stress at the rim ($\dot\gamma_R$):

$$\tau_c = \frac{\tau_{measured}}{4} \cdot \left[3 + \frac{d\ log\ \tau_{measured}}{d\ log\ \dot\gamma_R}\right] \qquad\qquad Eq.\,2-11$$

where τ_c is the corrected stress and $\tau_{measured}$ is the measured stress by the PP geometry.

2-2-6-2 Cone and Plate geometry

In the PP geometry shear rate is variable across the gap. To overcome this issue the top flat plate is replaced with a cone. This geometry is called the cone and plate geometry (CP) (Fig. 2-9). However PP geometry would be preferred when the droplet size of the sample under investigation is as large as that of the emulsions studied in this research which is typically larger than 10 μm. The reason for this is that the minimum gap size , the distance between the tip of the cone and the bottom plate, should be several times larger than the droplet size but it should not be more than 20 μm [25]. Hence for complex fluids containing microstructures with larger length scales, the CP geometry cannot be used and as such despite the variance of shear rate as a function of radius the PP geometry becomes the preferred geometry.

The shear rate for the CP geometry is defined as [25]:

$$\dot\gamma = \frac{\omega}{\tan\beta} = \frac{\omega}{\beta} \qquad\qquad Eq.\,2-12$$

where $\tan\beta = \frac{h}{R}$ and $\tan\beta \approx \beta$ when β is a small angle. Therefore the shear rate across the fluid is constant. The CP geometry therefore yields more reliable data than the PP geometry. The shear stress is again obtained from the torque (M_{cp}) as:

$$\tau = \frac{3.M_{cp}}{2.\pi.R^3}. \qquad\qquad Eq.\,2-13$$
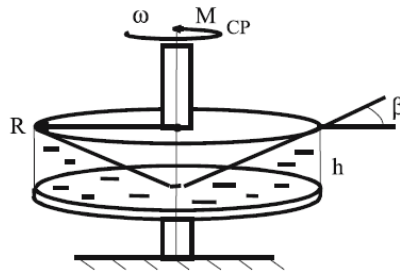
Fig. 2-9 CP geometry, M_{CP} is the torque, ω is the angular velocity, R the radius of the plate, h is the height, and β is the cone angle (adopted from [25]).

The cone angle, β, is usually between 0.5° to 4° which is small enough to ensure that $\tan\beta = \beta$.

2-2-6-3 Coaxial (Couette) geometry

Neither the PP or CP geometries are suitable for low viscosity materials, where the material is ejected from between the plates. In this case a coaxial cylinder geometry (Couette) should be used.

This geometry was used to measure rheological properties of dilute emulsions, microemulsions and nanoemulsions prepared in this research.

In this geometry, similar to the PP geometry, the shear rate varies across the gap. The shear stress and shear rate functions can be written as follow with regard to the parameters explained in Fig. 2-10.
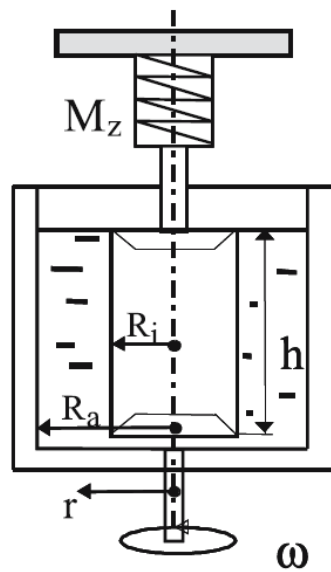
Fig. 2-10 Couette geometry, M_z is the torque, ω is the angular velocity, R_i is the radius of the inner cylinder, R_a is the radius of the outer cup, h is the height, and r is the the radial position from the origin (adopted from [25]).

$$\tau = \frac{M_z\ h\ (R_a{}^2 - R_i{}^2)}{2\pi} \qquad\qquad Eq.\,2-14$$

$$\dot{\gamma}_{app} = \frac{\omega\ R_a{}^2\ R_i{}^2}{r^2\ (R_a{}^2 - R_i{}^2)} \qquad\qquad Eq.\,2-15$$

The couette geometry dimensions were R_i 20 mm and the gap size, $R_a - R_i$, 500 μm.

Similar to the PP geometry, $\dot{\gamma}_{app}$ which is apparent shear rate needs to be corrected. For this purpose the Schurz correction method can be used:

$$\gamma = \gamma_{app} \frac{1 - \left(\frac{R_i}{R_a}\right)^2 s}{\left(1 - \left(\frac{R_i}{R_a}\right)^2\right) s} \qquad\qquad Eq.\,2-16$$

where s is $\;s = \dfrac{d \log \gamma}{d \log \tau}$

2-2-6 Nuclear magnetic resonance (NMR)

^{1}H NMR, was used to determine the volume fraction of the monodisperse coarse emulsions. A Bruker AVANCE 400 spectrometer was used. The strength of the magnetic field is 9.4 Tesla.

In Fig. 2-11 is shown a typical NMR spectrum recorded for a concentrated dodecane/F127/water coarse emulsion. The first peak is attributed to water and the second peak represents the oil. The volume fraction of the relevant component can be calculated via the standard peak integration method. It should be mentioned that the surfactant peak is not visible in the spectrum since its concentration is too small.
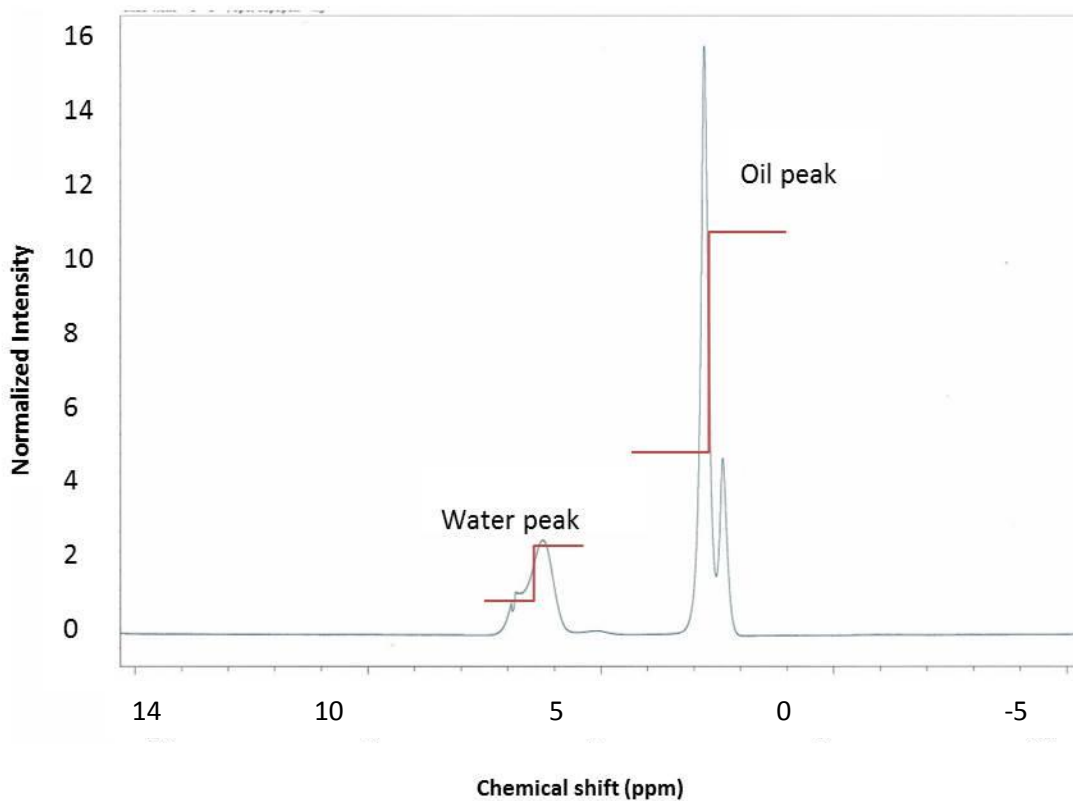
Fig. 2-11 ^{1}H NMR spectrum of dodecane/F127/water coarse emulsion system. The estimated oil volume fraction is 55%.

2-2-7-1 Diffusion NMR

Diffusion NMR, was used to probe the droplet size for coarse emulsions as well as the degree of polydispersity. In this method ^{1}H NMR is coupled with radio frequency (RF) magnetic field gradients. For this purpose a Bruker Diff 60 probe was used. The experiments took place at 20 ℃ with a maximum gradient strength of 40-50 G/cm (1.4% of the maximum gradient that the probe can provide) for monitoring oil diffusion and 10-14 G/cm for monitoring water diffusion.

2-2-7-2 The concept of molecular diffusion

Self-diffusion is a normal phenomenon taking place in all materials due to their thermal energy. In addition to that a difference in concentration within a sample makes components transfer from the concentrated environment to the dilute one. This transfer not only depends on the concentration difference but also on the diffusivity of the system. It has been expressed mathematically by Fick:

$$J = -D\nabla C. \hspace{4cm} Eq.2-17$$

where D is the transport diffusion coefficient, J is the molecular flux, and, ∇C, is the molecular concentration gradient. Based on mass conservation the change of concentration over time exactly equals the transported mass:

$$\frac{\partial C}{\partial t} = -\nabla \cdot J. \hspace{4cm} Eq.2-18$$

Combining Eq. 2-17 and 2-18, yields:

$$\frac{\partial C}{\partial t} = -\nabla \cdot J = \nabla \cdot (D\nabla C). \hspace{3cm} Eq.2-19$$

To solve this differential equation we need an initial condition, typically:

$$C(r,0) = \delta * (r - r_0). \hspace{4cm} Eq.2-20$$

where $\delta *$ is the Dirac delta function, r is the radius at time t and r_0 is the radius at time $t=0$. Using this definition we consider all possible positions for molecules relative to a molecule at the origin of the time ($t=0$).

Solving Eq. 2-19 we obtain a relationship between the concentration, the position and the time:

$$C(r,t) = \left(\frac{1}{\sqrt{4\pi Dt}}\right)^3 exp\left(\frac{-(r-r_0)\cdot(r-r_0)}{4Dt}\right). \hspace{2cm} Eq.2-21$$

From this we can calculate the diffusion coefficient. It is also possible to determine the diffusivity of a system by directly measuring the displacement which is related to the diffusion coefficient, and then applying the well-known Einstein relationship:

$$< (r - r_0) \cdot (r - r_0) > = < z^2 > = 2Dt. \qquad\qquad Eq. 2 - 22$$

where $< z^2 >$ is the mean squared displacement in the z direction.

This equation holds for two and three dimensions as well. The coefficient which is 2 in Eq. 2-22, would be 4 and 6 for two and three dimensions respectively. This relationship is at the foundation of diffusion NMR.

2-2-7-3 Diffusion Measurement Based on PGSE and PGSTE Data

The first diffusion measurements performed using the Pulse Gradient Spin Echo (PGSE) method were done by Tanner and Stejskal who published their results around 50 years ago. [26] & [27]. In NMR a constant magnetic field, B_0, is applied usually in the z direction, which ensures that all nuclei spins align either toward the *+z* or *–z* direction. There is an energy difference between these two states of spins in nuclei which is the principle of NMR spectroscopy (see[28] & [29]).

In PGSE a gradient magnetic field is applied in addition to B_0, this method includes a 90° RF pulse to move the spins from the z direction into the x-y plane, after a time, τ, a 180° RF pulse is applied which keeps the spins in the x-y plane but in the opposite direction and after another time, τ, the signal is recorded. After each RF pulse, a gradient magnetic field pulse of strength g and duration δ is applied, the time span between two gradient pulses is Δ (observation time) (Fig. 2-12).
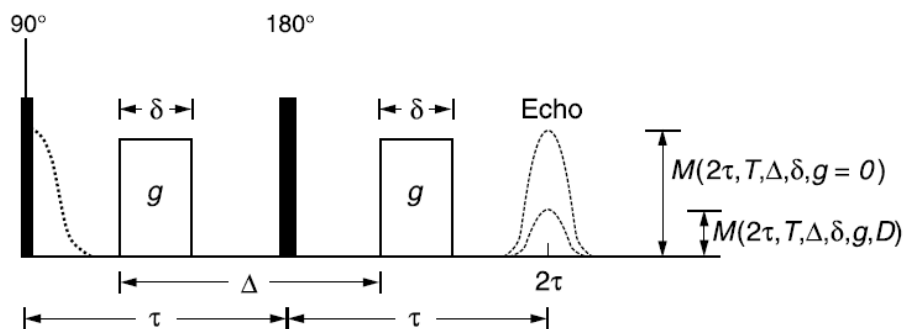
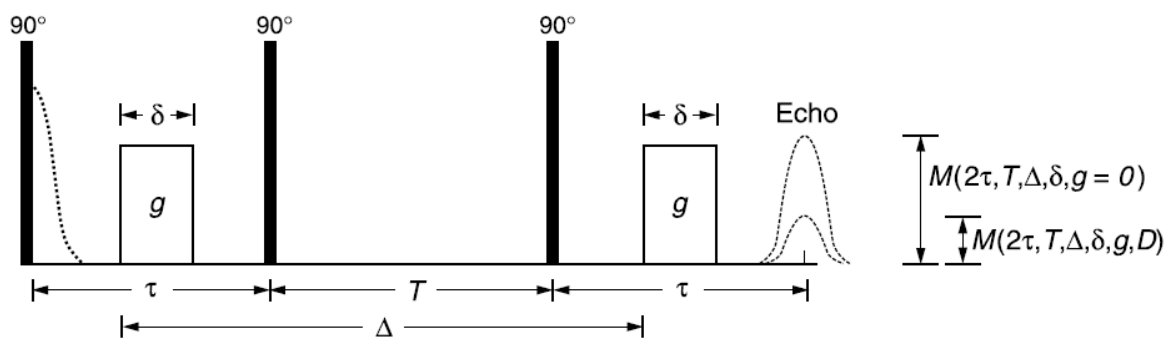**Fig. 2-12** Basic PGSE pulse sequence (adopted from [30]).

As soon as the gradient field is removed the dephased spins begin to relax and will be partially rephrased. The relaxation time associated with this is called T_2. The spins will also

return to being aligned with B_0 in the z direction, this relaxation time is called T_1, normally T_1 is larger than T_2.

When the gradient field acts on the sample it induces an inhomogeneous magnetic field. This results in the spins dephasing due to their positions. After the second gradient is applied, in principle the spins are totally refocused, but since the molecules diffuse, the refocusing is incomplete so the final signal ($M_{xy}(2\tau$, $g > 0$, Δ, δ, D)) is weaker than before the gradient field was applied ($M_{xy}(2\tau$, $g = 0$, Δ, δ)). This dying away of the signal is called signal attenuation; based on this attenuation, molecular displacement can be obtained from NMR experiments.

As stated previously in many materials, especially systems with high interfacial area, such as emulsions, $T_1 > T_2$, and dephasing and refocusing occurs due to spin relaxation as well as the gradient field effect. As such the observation time, Δ, must be shorter than T_2. In this way we can be sure that our results is more significantly affected by diffusion rather than relaxation effects.

Based on the above Tanner [31] has introduced a stimulated echo method in which the 180° RF pulse is replaced with two 90° pulses (Fig. 2-13). The spins now spend more time aligned in the z direction instead of in the x-y plane so that T_2 relaxation time is unlikely to interfere with diffusion data. This method is called the Pulse Gradient Stimulated Spin Echo (PGSTE) which is widely applied to emulsion samples.

Fig. 2-13 Basic PGSTE pulse sequence (adopted from [30]).

2-2-7-4 Attenuation

The self-diffusion coefficient is determined as follows. The first gradient pulse, induces a shift in the phase as expressed by short gradient pulse (SGP) approximation [26] :

$$\phi_1 = \gamma \int_0^{\delta} g z_1 dt = \gamma g \delta z_1. \qquad\qquad Eq.2\text{-}23$$

where z_1 is the position of the spins. This is assumed to be constant during the time of the gradient pulse, δ, of strength, g, and γ is the gyromagnetic ratio. After the time, Δ, the second pulse also produces a phase shift, in order to refocus the spins:

$$\phi_2 = \gamma \int_{\Delta}^{\Delta+\delta} g z_2 dt = \gamma g \delta z_2. \qquad\qquad Eq.2\text{-}24$$

The total phase shift is:

$$\delta(\phi) = \phi_2 - \phi_1 = \gamma g \delta (z_1 - z_2). \qquad\qquad Eq.2\text{-}25$$

The signal attenuation (the ratio between the strength of the signal before and after applying the gradient field) is related to the sum of the magnetization:

$$\frac{M}{M_0} = \sum_{j=1}^{N} \exp(i\delta(\phi_j)). \qquad\qquad Eq.2\text{-}26$$

If $P(z_2|z_1, \Delta)dz_2$ is the probability of spin distribution:

$$P(z_2 \mid z_1, \Delta) = \frac{1}{\sqrt{4\pi D\Delta}} \exp\left(\frac{-(z_1 - z_2)^2}{4D\Delta}\right). \qquad\qquad Eq.2\text{-}27$$

attenuation comes in an integral form as:

$$\frac{M}{M_0} = \int_{-\infty}^{\infty}\int_{-\infty}^{\infty} \exp(i\gamma g \delta(z_1 - z_2)) \times P(z_2 \mid z_1, \Delta) dz_1 dz_2. \qquad\qquad Eq.2\text{-}28$$

where D is the diffusion coefficient. The final form of signal attenuation as a function of diffusion is then:

$$\frac{M}{M_0} = \exp(-(\gamma g \delta)^2 D\Delta) \qquad \text{Or} \qquad \ln\left(\frac{M}{M_0}\right) = -(\gamma g \delta)^2 D\Delta. \qquad\qquad Eq.2\text{-}29$$

These equations are valid for unrestricted diffusion when we have a porous medium or droplets suspended in a continuous phase, as with emulsions. We may also have restricted diffusion in the system, where the displacement is restricted by boundaries between

phases. Since the characteristics of the oil and water are different with regard to their size and subsequently their ability to be displaced in a magnetic field, we need to perform two different series of NMR tests to measure the self-diffusion coefficients of the oil and the water separately. Water molecules move quickly due to their small size and they most likely encounter the wall of the oil droplets even at short observation times so the mean squared displacement, $<z^2>$, of the molecules is influenced by the boundaries. Oil molecules are large and move more slowly and restricted diffusion occurs over longer times. Measuring unrestricted and restricted diffusion provides us with some information on the structure of the material since the diffusion is affected by the restricting geometry of the emulsion. Hence the deviation of the unrestricted diffusion can be considered as a boundary effect.

To attain a relationship which describes restricted diffusion there are two approaches. In the first an equation is developed which includes restricting barriers. Using this approach, Murday and Cotts [32] have derived a relationship for simple geometries such as suspended spheres in a continuous media:

$$\ln\frac{M}{M_0} = \frac{2\Delta}{T_2} - 2\gamma^2 G^2 \sum_{m=1}^{\infty} ((\alpha_m^2 \, r^2 - 2))^{-1}$$

$$\times \left(\frac{2\delta}{\alpha_m^2 \, D} - \frac{2 + \exp[-\alpha_m^2 \, D(\Delta - \delta)] - 2\exp(\alpha_m^2 \, D\delta) - 2\exp(\alpha_m^2 \, D\Delta) + \exp[-\alpha_m^2 \, D(\Delta + \delta)]}{(\alpha_m^2 \, D)^2} \right) \quad Eq.\, 2-30$$

where α_m is the mth root of the Bessel equation $(1/\alpha_r)$ $J_{3/2}(\alpha_r) = J_{5/2}(\alpha_r)$, all the parameters as above. This approach has been applied to many emulsion systems and appears to be useful (for example see [33], [34]).

The second approach, has been demonstrated by Mitra $et\ al.$ [35]. Here the apparent diffusion coefficient (D_{app}) is related to the unrestricted diffusion:

$$\frac{D_{app}}{D_0} = 1 - \frac{4}{9\sqrt{\pi}} \frac{S}{V} (D_0 \Delta)^{1/2} + O(D_0 \Delta) \qquad\qquad Eq.\, 2-31$$

where S is the surface area of the droplets, V is the volume of the droplets and $O(D_0 \Delta)$ is a correction function (neglected higher order term). In this equation the surface-to-volume ratio has been taken into consideration.

In Chapter 5, the application of diffusion NMR to emulsion size probing using the pore-hopping model will be discussed. In addition to these two approaches, Callaghan $et\ al.$ [36]

have shown that using NMR-PGSTE data, it is also possible to obtain information on the pore size between droplets as well as the droplet size.

Microemulsions

The different behaviour of solids and fluids can be explained from the perspective of solids storing the total energy received under application of a force whereas ideal fluids (Newtonian fluids) dissipate the total energy received. Non-Newtonian fluids are considered as viscoelastic materials meaning they have a combination of ideal fluid and ideal solid behaviour.

Non-Newtonian behaviour basically arises due to structures that exist within the sample. Such structure gives the sample a length scale that is larger than the molecular scale. Hence, when a force acts on the system a part of the energy is consumed resulting in deformation, followed by relaxation of the microstructure. The source of the structure can be weak chemical bonds between the molecules of the ingredients (e.g. hydrogen bonds), molecular aggregations of the added ingredients (e.g. micellar solutions or droplets, e.g. emulsions) or complex networks (e.g. 2-D or 3-D gels). These states can be achieved through the addition of alcohols, surfactants, oils and/or oligomers/polymers to a Newtonian fluid.

Water is the most well-known Newtonian fluid with a viscosity of 0.001 Pa.s or 1 cp. This means that over the entire range of applied shear rates (e.g. 0.001/s to 100/s) the viscosity is constant. Ageno proposed a collective model for hydrogen bonds between water molecules that form assorted aggregates (Fig. 3-1). These structures transform into each other, however the number of existing hydrogen bridges remain unchanged upon transformation [37]. These aggregates are not stable and rapidly transform into each other, typically in less than a millisecond. Only stable relatively long-lived structures and aggregates within a sample affect the viscosity. In such cases the deformation and relaxation times are long enough to cause non-Newtonian behaviour. It is for this reason that the viscosity of water remains Newtonian despite existing as different aggregates.

Ethanol is also a Newtonian fluid; however, upon adding 30 weight-percent ethanol to water the obtained flow curve (Fig. 3-2) provides evidence that non-Newtonian behaviour occurs at low shear rate, before eventually Newtonian behaviour is observed. Ageno and Frontali measured the viscosity of the mixtures of water and alcohol [38]. They found that

the added alcohol saturates the hydrogen bonds in the system and stops the transformation of the water aggregates between the different forms, giving rise to the changed viscosity of the mixture. The viscosity of the mixture is always higher than that of the individual ingredients.
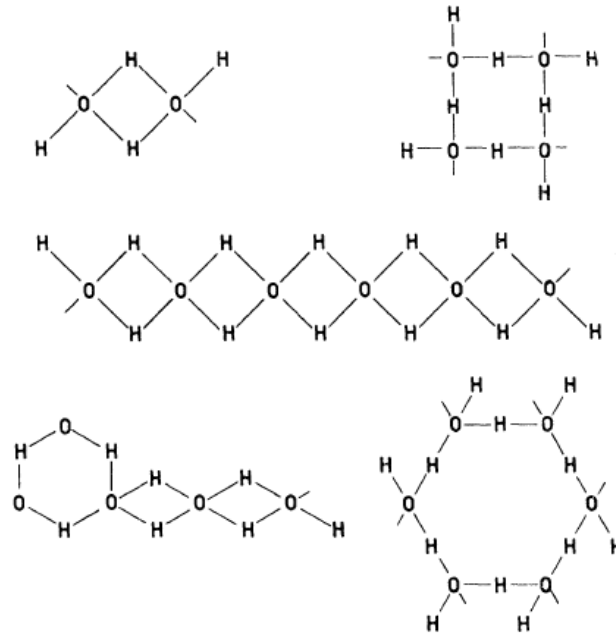
Fig. 3-1 Examples of water molecular aggregates proposed by Ageno to exist spontaneously in water (adopted from [37]).
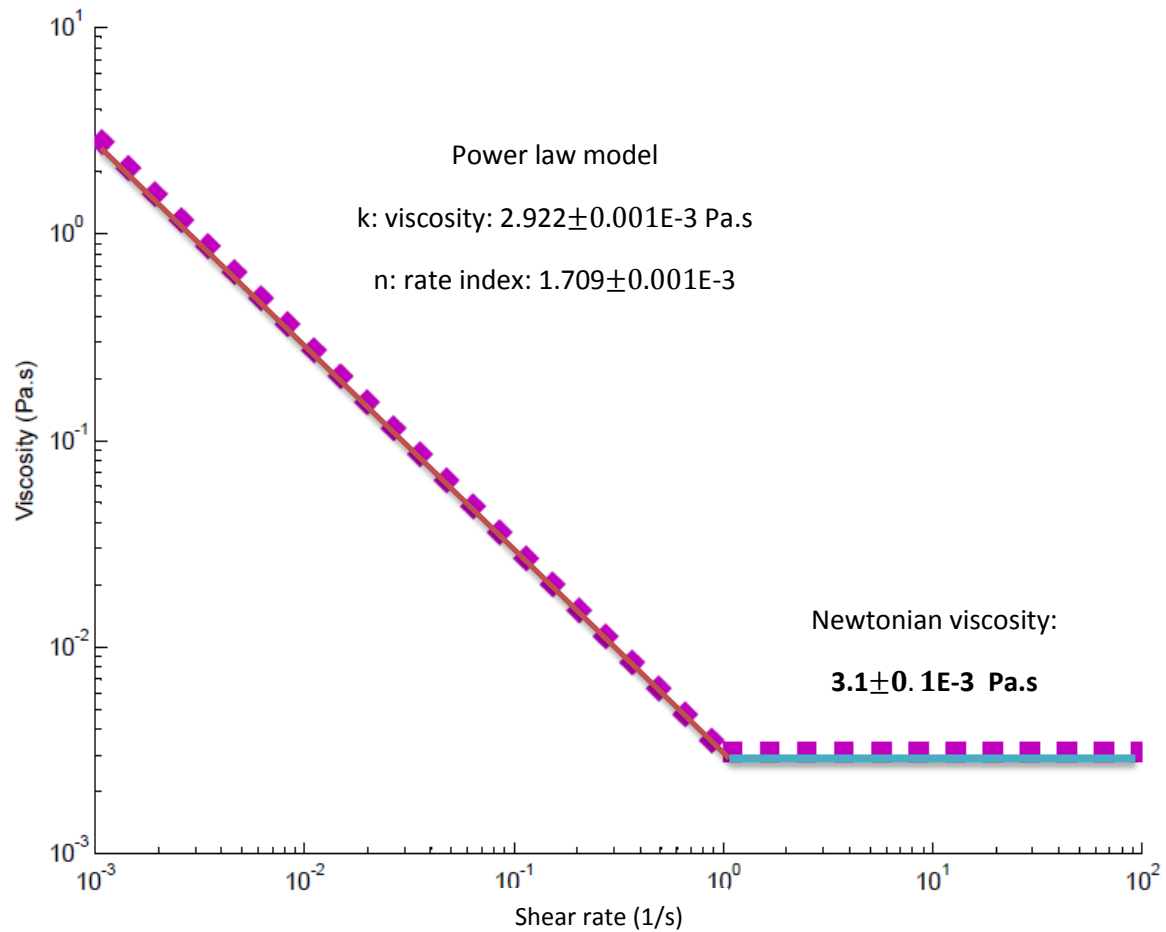
As seen in Fig. 3-2 for shear rates up to ~ 1/s the behaviour of the 30 wt % ethanol mixture is shear-thinning (or pseudoplasticity). A transition to Newtonian behaviour is then evident. The viscosity of the system over the Newtonian region (3.1 cp) is higher than that of both water (1 cp) and ethanol (1.1 cp).

Shear-thinning behaviour can be modelled using a power law relationship:

$$\tau = k.\dot{\gamma}^n \hspace{4cm} Eq.3-1$$

where τ is the shear stress, $\dot{\gamma}$ is the shear rate, k and n, are constants. The two constants k and n, can be obtained from a log-log plot of τ vs. $\dot{\gamma}$ which should be linear. For many real fluids this plot is not linear except within a reduced range of applied shear rates. For example concentrated emulsions and suspensions exhibit ideal dilatancy and pseudoplasticity (constant n) only under intermediate shear rates [39]. However performing rheometry on the ethanol/water solution displayed simple shear-thinning behaviour with a

linear decrease over three decades of shear rate (Fig. 3-2). Eq. 3-1 was used to fit the data shown in Fig 3-2. The fitting parameters are given in the figure.

Power law model

k: viscosity: 2.922$\pm$0.001E-3 Pa.s

n: rate index: 1.709$\pm$0.001E-3

Newtonian viscosity:

3.1$\pm$0.1E-3 Pa.s

Fig. 3-2 Simple shear-thinning followed by Newtonian behaviour in a 70 wt. % water/ 30 wt. % ethanol solution.

The observed shear-thinning followed by Newtonian behaviour in Fig. 3-2 can be explained by considering that ethanol forms a hydrogen-bonded network with water. This network supports a higher energy, i.e. a stronger force is needed to deform the system, and increases the relaxation times. At higher shear rates, the higher external force dominates the interaction between the aggregates within the sample resulting in Newtonian behaviour at high shear rates (beyond 1/s).

Hence non-Newtonian systems can be achieved simply by mixing two Newtonian fluids. This generic ability to manipulate the internal structure of a fluid through the use of additives will be explained further with respect to the behaviour of surfactants.

## 3-1 Addition of surfactant to water: Creation of a complex fluid

Surfactants self-assemble forming for example micelles in water. Micellar solutions are non-Newtonian fluids. This non-Newtonian behaviour is affected by the chemical structure and charge of the surfactant. The four surfactants used in this research differ in their molecular weight, structure and charge.

To explore the effect of these differences the flow properties of concentrated micellar surfactant solutions of Triton X-100, F127, SDS and CTAB have been investigated. In particular the effect of micellar shape, size and surfactant chemical functionality was probed.

3-1-1- Effect of micelle shape

Surfactants form micelles of different shapes including spherical and cylindrical depending on the molecular structure of the surfactant, the surfactant concentration, the temperature etc. The shape of micelles affects the flow properties of the sample. This effect can be observed in the non-Newtonian region of the flow curve since over this region inter-droplet forces dominate the system as compared to the Newtonian region where there are negligible droplet interactions.

10 wt. % micellar solutions of the four surfactant solutions were investigated. This concentration was selected because it corresponds to the base preparation system for all other systems explored except the coarse emulsions prepared via microfluidics (Chapter 5). Considering the relevant flow curves of these solutions, Fig. 3-3, it is revealed that the CTAB system displays two shear-thinning regions, whereas F127, Triton X-100 and SDS display initially yield stress behaviour with constant viscosity at low shear rates, followed by shear-thinning and then Newtonian behaviour. The CTAB system has the highest viscosity over the entire range of the applied shear rates. CTAB forms worm-like micelles at this concentration ([40], [41] and [42]) whereas the other three surfactants generate ellipsoidal or globular micelles [43]. This inherent difference in the shape of the micelles and therefore the interactions between the micelles accounts for the observed difference in the measured rheological response of the four systems.
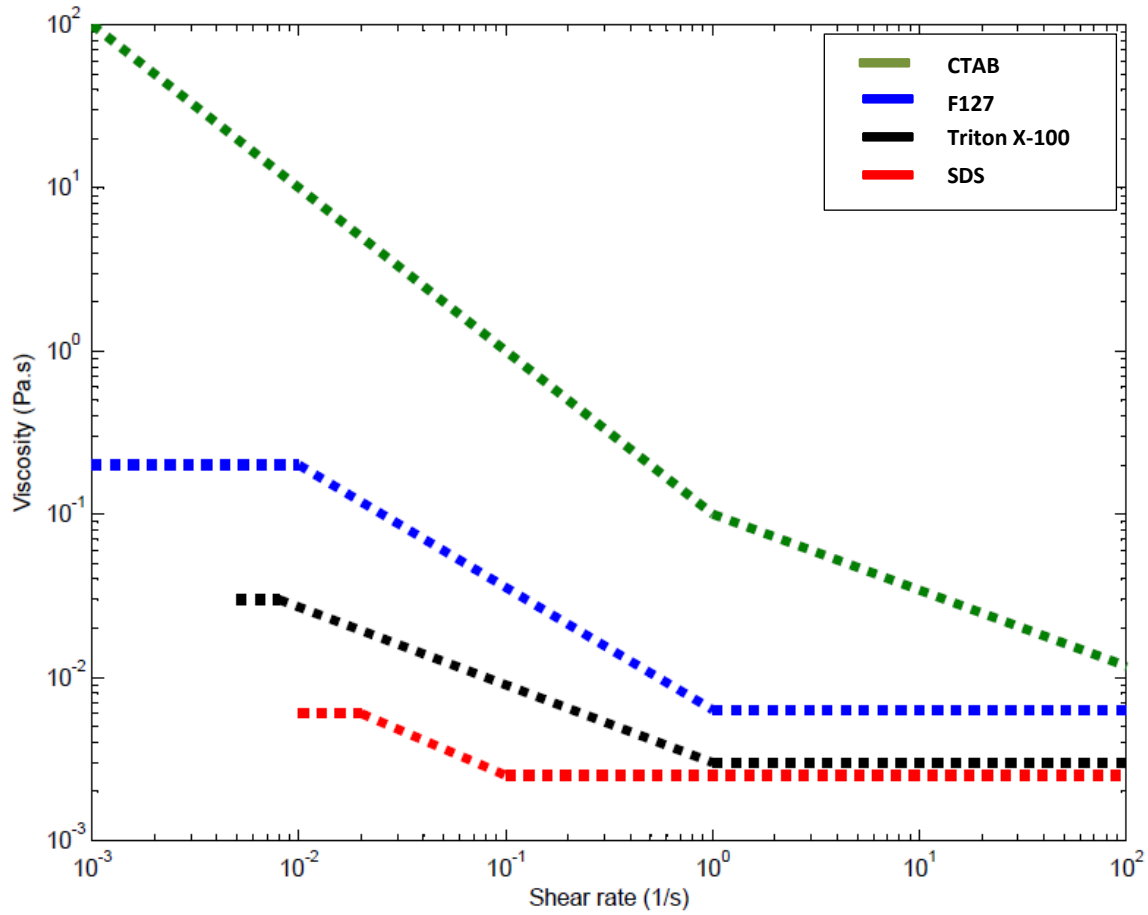
Fig. 3-3 Flow curves for four surfactant micellar solutions (10 wt. % of surfactant).

Considering the three systems that have a Newtonian flow region, Simha *et al.* have suggested [44] that the following relationship holds within the Newtonian region of the flow curve when there is a deviation from spherical morphology for the primary elements in the complex fluid:

$$\eta = 2.5 + 0.4075(J - 1)^{1.508} \qquad\qquad Eq.\,3-2$$

where J, is the ratio of the major and minor axes' rotation. The larger J, the more deviation from spherical shape is expected.

According to this formula, in the Newtonian region, when micelles are spherical, e.g. $J=1$, the viscosity tends toward 2.5 cp which is the lower limit of Eq. 1-3 where the concentration of the dispersed phase goes toward zero. The second part of the equation that expressed the deviation from spherical morphology is emprical. Based on Eq. 3-2, the 10 wt. % SDS

solution can be confidently assumed to be comprised of globular micelles (Table 3-1). Triton X-100 micelles however slightly deviate from the spherical ideal structure and F127 micelles are ellipsoidal with a larger J, 5.5.

The initial yield stress behaviour seen for these three globular systems shows that an initial force is needed to make the systems flow. This could be due to flocculation or initial packing of the micelles. Investigation of this behaviour was beyond the scope of this research. This behaviour is seen when an increasing shear sequence is applied and not for decreasing shear sequence.

Table 3-1 Proposed micellar shape for the three globular surfactant solutions based on the analysis of their Newtonian flow behaviour

| Surfactant	Newtonian Viscosity (cp)	J estimated from Eq. 3-2	Shape
SDS	2.5±0.1	1.0±0.1	
Triton X-100	3.0±0.1	2.0±0.1	
F127	6.3±0.1	5.5±0.1	

As seen in Table 3-1, as the micelle distorts from spherical and elongates, the viscosity increases. This results from the increased surface area of the micelles from the spherical SDS micelles to the rod-like F127 micelles and hence the interaction between the micelle and the continuous phase increases giving rise to the increased viscosity. In the case of CTAB, J becomes very large resulting in a worm-like morphology. The worm-like behaviour of CTAB micelles have been well studied, see for instance [4], [45] and [46]. In particular, Rojas *et al*. have shown that the worm-like structure results in a sharp rise in the viscosity of the solution [40].

The effect of micelle shape on the flow behaviour of the four surfactant systems was investigated further by performing dynamic rheological frequency sweep tests (Fig. 3-4). The dynamic data clearly highlight the effect of micelle shape on the flow properties of the surfactant solutions. Data were collected within the linear viscoelastic region with a strain value of 0.05. The dynamic data (Fig. 3-4) are in good agreement with the flow curve data (Fig. 3-3), particularly within the Newtonian region for F127, Triton X-100 and SDS. In the case of CTAB Newtonian behaviour is not observed in either experimental data sets.

The Newtonian viscosity can be determined from the dynamic frequency data extracted from the constant slope of the complex modulus vs. frequency curves in Fig. 3-4. The Newtonian viscosities based on the dynamic frequency sweep results are given in Table 3-2.

Table 3-2 Newtonian viscosities estimated from the dynamic results

Surfactant	Newtonian viscosity (cp)
SDS	2.6± 0.2
Triton X-100	3.2± 0.2
F127	6.5± 0.2
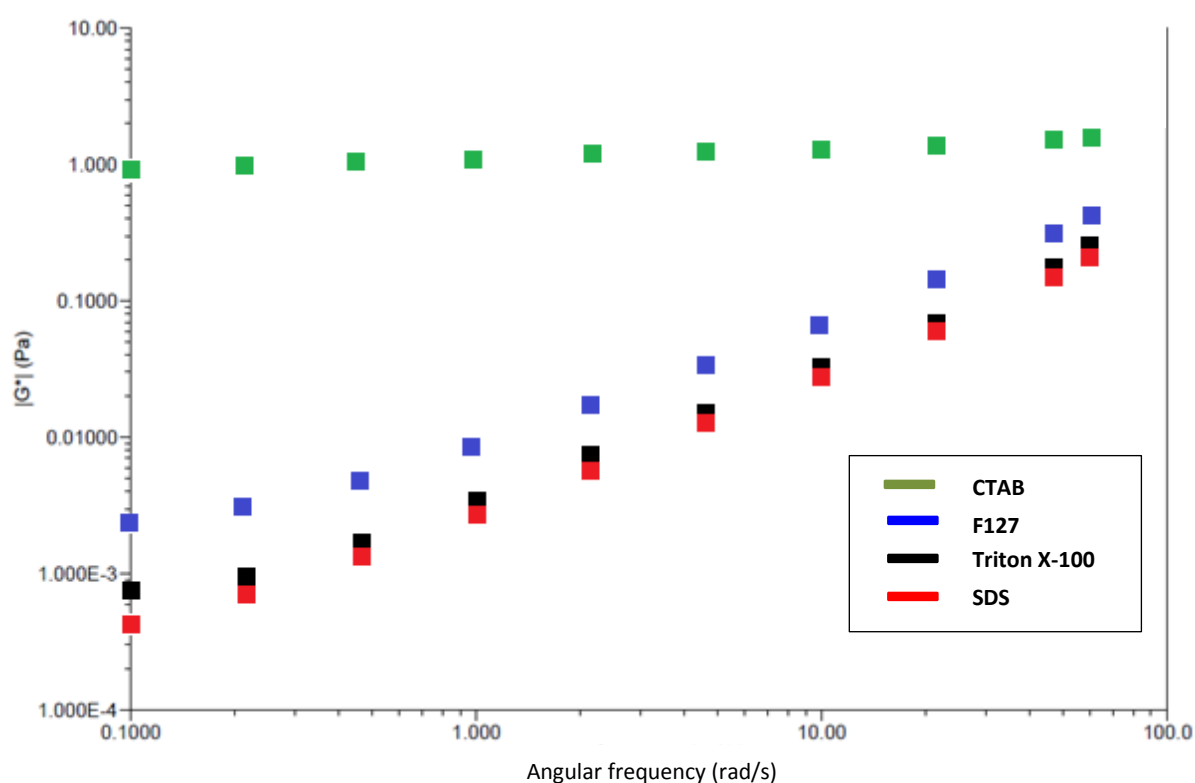
Fig. 3-4 Frequency sweep dynamic rheological data for the four surfactant micellar solutions (10 wt. %) at a strain value of 0.05.

As seen in Fig. 3-4, the CTAB micelle solution does not display Newtonian behaviour for angular frequencies up to 100 rad/s. This conforms with the behaviour observed in the CTAB micelle solution flow curve data where the maximum applied shear rate, 100/s, is insufficient for the CTAB micelle solution to reach a plateau. However, extending the applied shear rate to 10000/s results in a plateau in the viscosity at 1000/s of 4 cp (Fig. 3-5). To induce Newtonian behaviour a shear rate four orders of magnitude higher than that

required in the spherical SDS micelle system is required for the worm-like micelles formed in the CTAB system, due to the significant intermicellar interactions that are present in this system. To see the effect of the pattern of applying shear rate, the experiments were performed firstly with increasing and secondly with decreasing shear rates. A comparison between the results of the two, demonstrates that there is a hysteresis loop, over the second shear-thinning zone (Fig. 3-6). This can be explained by considering the fact that the morphology of the system is not spherical hence the pattern of applying shear rate affects the packing of the micelles. When a decreasing shear rate is applied, the micelles locate in the network and start interacting with each other. This reduces the Newtonian region and results in a rise in the viscosity within the second shear-thinning zone. For the low shear rate shear-thinning region both curves match showing that at low shear rates the shear-thinning behaviour does not depend on the pattern of the application of shear (Fig. 3-6).
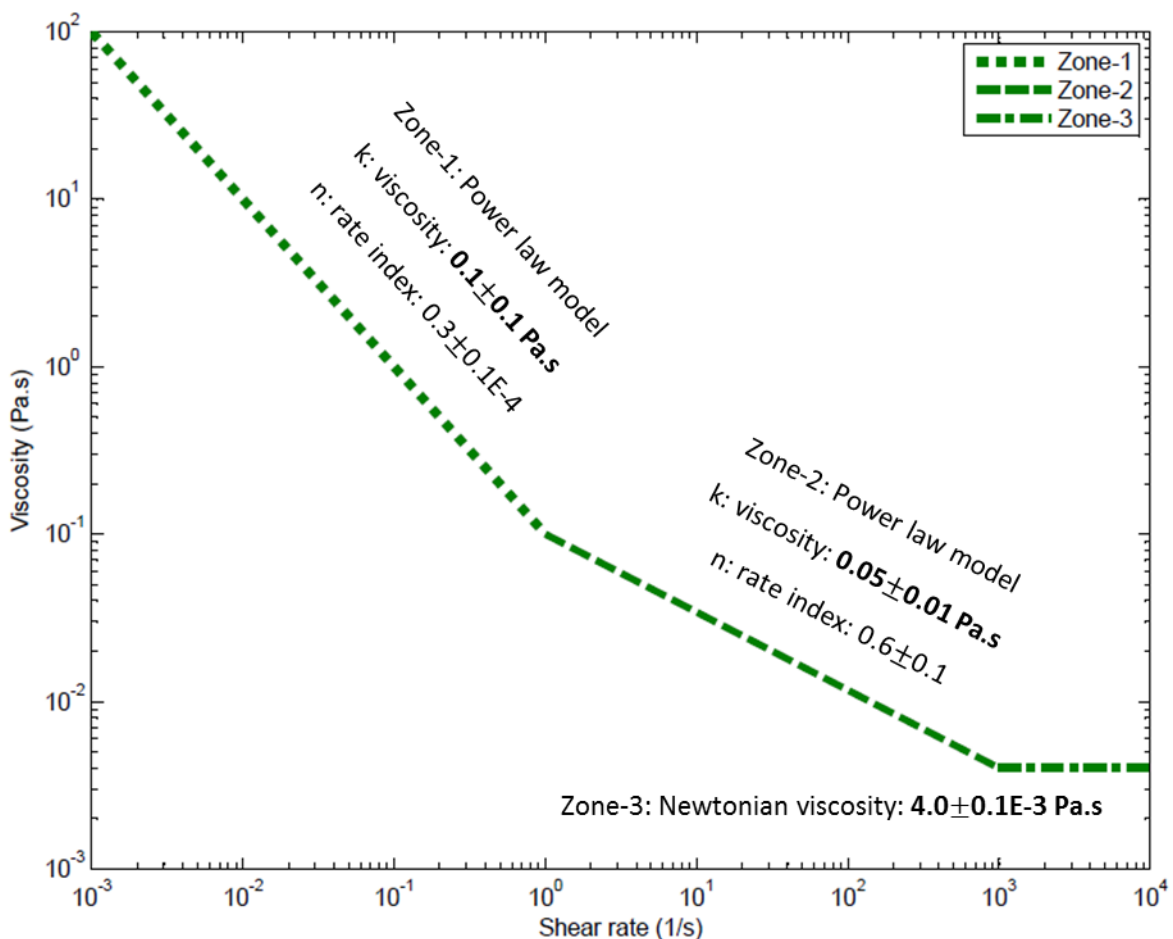
Fig. 3-5 Flow curve of CTAB micellar solution (10 wt. %). In zone-3, Newtonian behaviour is observed.
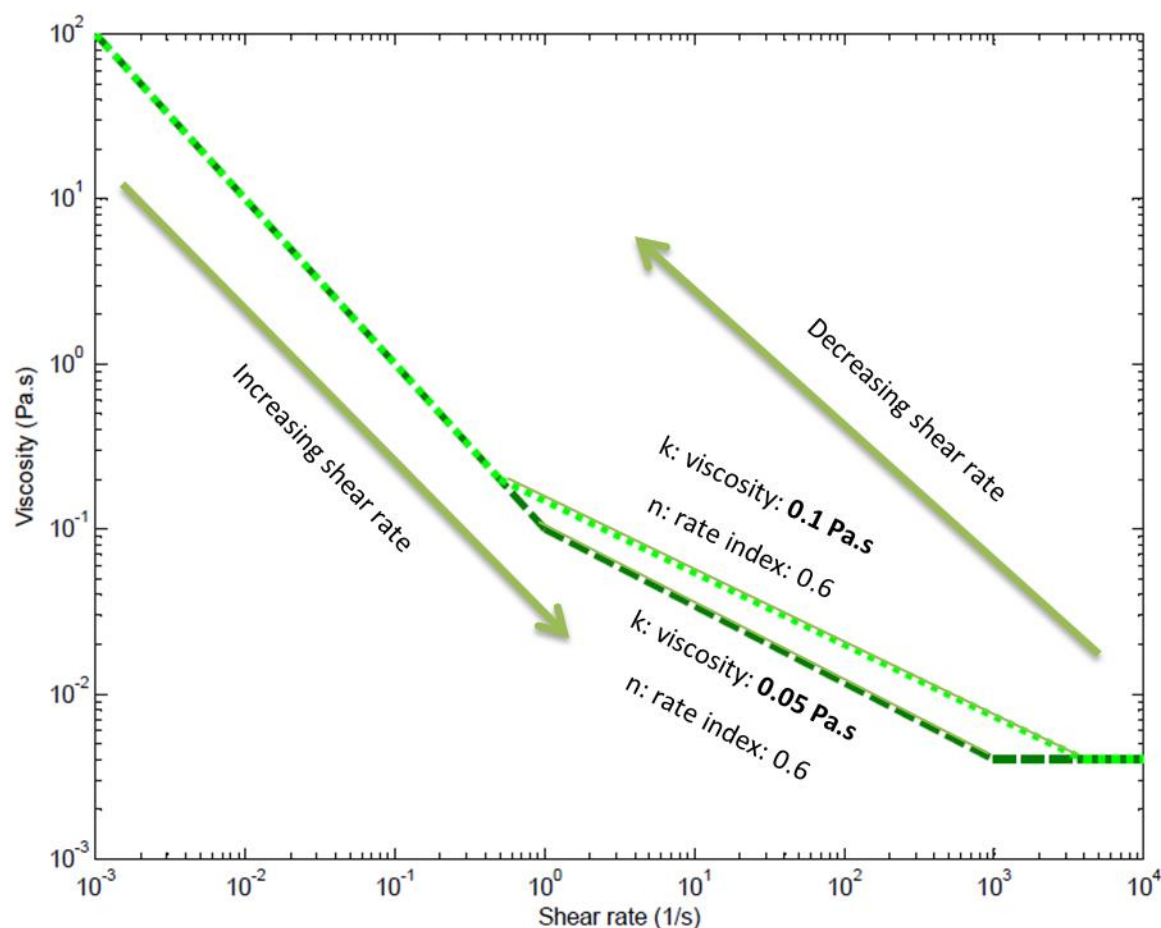
Fig. 3-6 Flow curve of CTAB micellar solution (10 wt. %); data obtained upon increasing and decreasing shear rates. The viscosity over the second shear-thinning region, around the hysteresis loop, has doubled (from 0.05 to 0.1 Pa.s) while the rate index has remained unchanged within uncertainty.

The relatively low viscosity of the CTAB micelle solution within the Newtonian region, 4 cp, indicates that the worm-like structure of the micelles has changed under shear. Based on Eq. 3-2, a J factor of 3.4 ± 0.1 is obtained for this system. This demonstrates that at very high shear rates the previously long worm-like micelles undergo a transition to ellipsoids. Therefore, by the application of an external force the microstructure of the surfactant solutions can be significantly changed.

We note that, it does not need to be an external force in order to manipulate the morphology, small changes in the chemical composition can achieve the same result. For example, the worm-like structure is broken down due to the addition of ethanol to the CTAB solution (Fig. 3-7). The relevant concentration is now 30 wt. % ethanol (while the CTAB concentration is now 7 wt. %), which in Fig. 3-2 was shown to be a non-Newtonian solution.

The CTAB/water/ethanol solution differs from both the ethanol/water and CTAB/water systems showing that the microstructure of all three non-Newtonian systems differ.
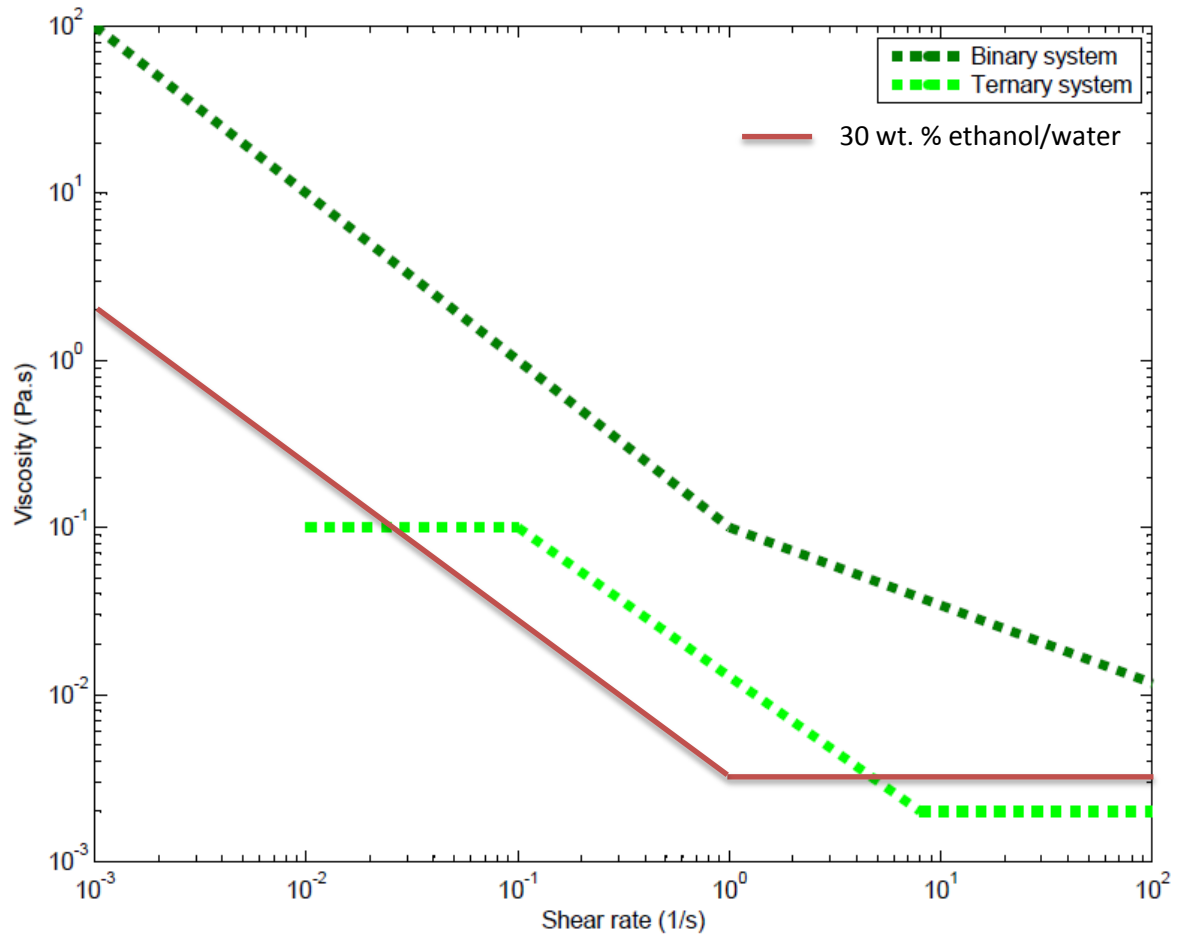
Fig. 3-7 Flow curves of ethanol/water solution, binary CTAB/water micellar solution and ternary CTAB/ethanol/water system. The worm-like morphology is broken down due to the addition of 30 wt. % ethanol.

3-1-2-Effect of size

The size of the micelles directly affects the viscosity of the sample as captured in Einstein's relationship (Eq. 1-1).

$$d_H = \frac{K_B T}{3\pi\eta D}. \qquad\qquad Eq. 1-1 \ (Recalled)$$

Hence, at constant temperature the following relationship holds:

$$\eta \ \alpha \ \frac{1}{d_H D}. \qquad\qquad Eq. 3-3$$

When the viscosity increases (decreases) the right-hand side of Eq. 3-3 increases (decreases) as well, this means the term $d_H D$ decreases (increases).

To measure the micellar size of the surfactant solutions small angle X-ray scattering (SAXS) and dynamic light scattering (DLS) were exploited (see Appendix A). The sizes are summarised in Table 3-3.

Table 3-3 Size of the micelles in the binary systems

Surfactant Solution	Micellar size (nm) - binary systems (droplet diameter)
SDS	3.7±0.5
CTAB	8.7±0.5
Triton X-100	16.5±0.5
F127	18.7*±0.5

*Dynamic light scattering

Dynamic light scattering (DLS) was used to probe the size of the F127 micelles as no clear peak was evident in the SAXS data. DLS requires the two different phases to have different refractive indexes in order for the scattering from the droplets to be detectable. Unreliable DLS results were obtained for the SDS, CTAB and Triton X-100 systems since the indexes were not sufficiently different. Due to the large size of the F127 tri-block polymer, DLS could be used successfully for this system (Fig. 3-8).
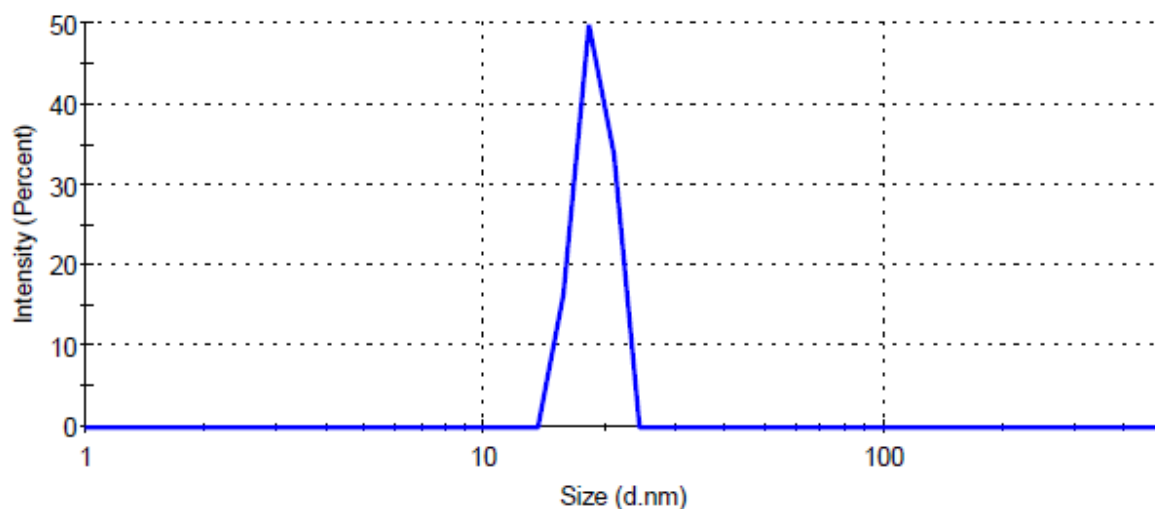
Fig. 3-8 Micellar size distribution of F127 micellar solution (10 wt. %) measured using dynamic light scattering.

Adding ethanol to the above four binary surfactant solutions, results in decreasing interfacial tension and the formation of swollen micelles. This increases the solubility of the system. Such a system can solubilize oil and produce microemulsions (see the next section). It should be mentioned that after the addition of each additive to the system the concentration of the materials that the system is made with, changes. For example adding 30 wt. % ethanol to a 10 wt. % surfactant/water solution results in the concentration of the surfactant in the new generated surfactant/water/ethanol solution to be 7 wt. %. Therefore in any of the following case where the effect of adding an additive on system properties is investigated, the decrease in the concentration of the materials that already exist in the formulation must also be considered to be part of the reason for any observed differences. As explained previously the research method to generate complex fluids in this work is through a multiple step procedure where the ingredients are added to the system one by one and studying the system after the addition of each component. The viscosity of each system is considered to be the reference viscosity in order to calculate the viscosity of the next system. It means the reference viscosity is the viscosity of the new system at a zero concentration of the additive, hence it is appropriate to consider the initial concentration (the concentration in the reference system) and not the final reduced concentration in calculations. We further note that it is not possible to explore all the systems investigated here in a 'single' chemical system without varying the amount of each component.

Although the effect of adding alcohol to micellar solutions has long been extensively investigated ([47],[48] and [18]) it is still not fully understood. The reason for this is that the added alcohol partly dissolves in the micelles, contributes to the interfacial layer and also dissolves in the continuous phase. Depending on the partition coefficient of the alcohol in each phase and the interface, the size, shape and packing of the micelles are all altered. It is very difficult to determine the partition coefficient of the alcohol in each phase. Therefore, usually experimental or semi-experimental models need to be applied. To shed light on this, considerable research has been performed. For instance, Leung and co-workers have studied the effect of a range of short-chain alcohols on the dynamic properties of SDS solutions and concluded that the chain length and characteristics of the alcohol play a

significant part in defining the effect of each of the above factors [49]. The reader is also referred to Zana's review article on surfactant- alcohol system [50].

In this research, by applying ethanol as the short chain alcohol, we have minimized the chance of solubilizing the alcohol into the micelles so that the change in flow behaviour can mostly be explained through interpreting the effect of enhanced hydrophilicity of the continuous phase due to the addition of ethanol [51]. In such systems the short chain alcohol plays the role of cosurfactant and by decreasing the interfacial tension and altering the curvature of the system significantly affects the microstructure of the system. Aramaki *et al*. [52] have mentioned the relevant papers in this regard (for example see [53]).

The concentration of the surfactant and the short-chain alcohol, cosurfactant, and also the ratio between them are important in determining the microstructure of the system. The reader is referred to the following references to get more information on the effect of concentration on the microstructure:[4], [54] and [55] respectively.

Porte *et al*. [54], based on the theoretical work of Israelachvili [56], have proposed the structural change in micellar solutions from spheres to small disks to cylinders to branched cylinders to bilayers to multiphasic domains by increasing the concentration of the surfactant and alcohol.

The micellar size of a ternary system is normally larger than that of the corresponding binary system. The reason is that ethanol increases the hydrophilicity of the continuous phase resulting in the accumulation of the surfactant molecules into micelles. This does not apply to the cationic surfactant investigated here, CTAB. The reason is that in the CTAB binary solution, the micelles are worm-like and the addition of ethanol increases the curvature of the interfacial film resulting in a structural transition from worm-like to spherical micelles. The transition between spherical and worm-like micelles has been of interest for about 50 years [39]. The thermodynamics of such a transition has been explained (for example see [56]), however the fundamental drivers for the transition are not fully understood. Lin *et al*. studied this transition by cryo-TEM and rheological data [4] and have shown that this transition is strongly dependent on the ratio between the area of the cross section of the head group and chain of the surfactant, $\frac{a_h}{a_c}$; as this ratio increases the transition is driven to the spherical side. The added ethanol to the binary solution of CTAB is adsorbed to the head

groups, resulting in the transition from worm-like to spherical micelles. This transition can be observed qualitatively by looking at the flow curves of the two systems (Fig. 3-7).

On the other hand for the other three surfactants, an increase in viscosity is seen due to the addition of ethanol rather than a reduction. This is most likely due to the increase in size of the micelles as well as a change in shape. In the ternary systems, the deviation from globular morphology is more significant. For example, in the case of SDS the viscosity has increased from 2.5 to 4.3 cp and the size of the micelles as measured using SAXS increases from 3.7 to 10 nm. For this system, the globular microstructure of the micelles, based on Eq. 3-2, has deformed into ellipsoidal with a J factor of 3.7. This demonstrates that ethanol molecules are attached to the aliphatic part of the surfactant resulting in making ellipsoids out of spherical micelles. The micellar sizes of the four ternary systems are given in Table 3-4. The effect of aggregate size increase on the viscosity of the surfactant solutions is demonstrated in Fig. 3-9, 3-10 and 3-11 by demonstrating static and dynamic rheological results. As seen in Fig. 3-9 to 3-11, Fig. 3-7, Table 3-3 and Table 3-4 the change in each system's relevant Newtonian viscosity is directly correlated to the change in droplet size and shape; i.e. the greater the available droplet surface interacting with the continues phase, the higher the Newtonian viscosity.

Table 3-4 Size of micelles for the ternary systems

Surfactant Solution	Micellar size (nm) in ternary systems (droplet diameter)
SDS	10.0±0.5
CTAB	5.7 *±0.5
Triton X-100	No information**
F127	27.0±0.5

*This value is obtained by SAXS and confirmed by DLS (see Appendix-B).

**SAXS does not give a reasonable size for this system due to the large size of the micelles. DLS fails to detect the micellar size due to the similarity of refractive indexes of the phases.
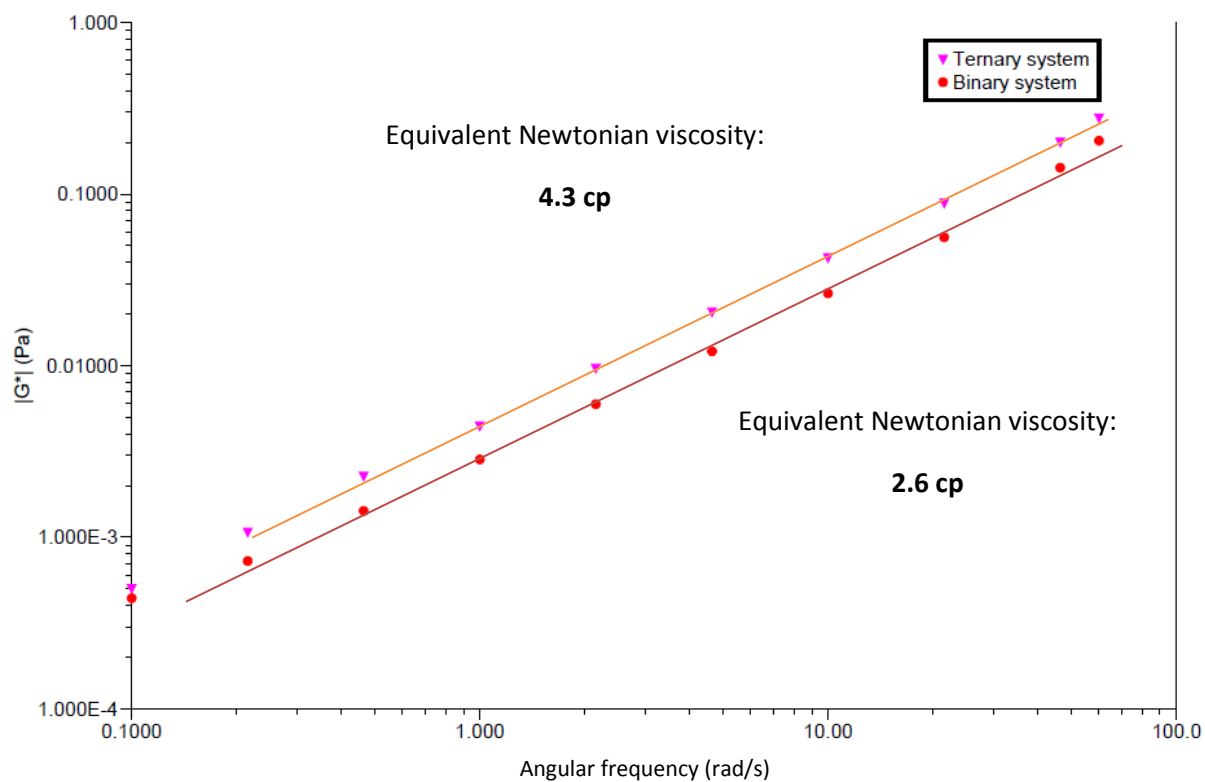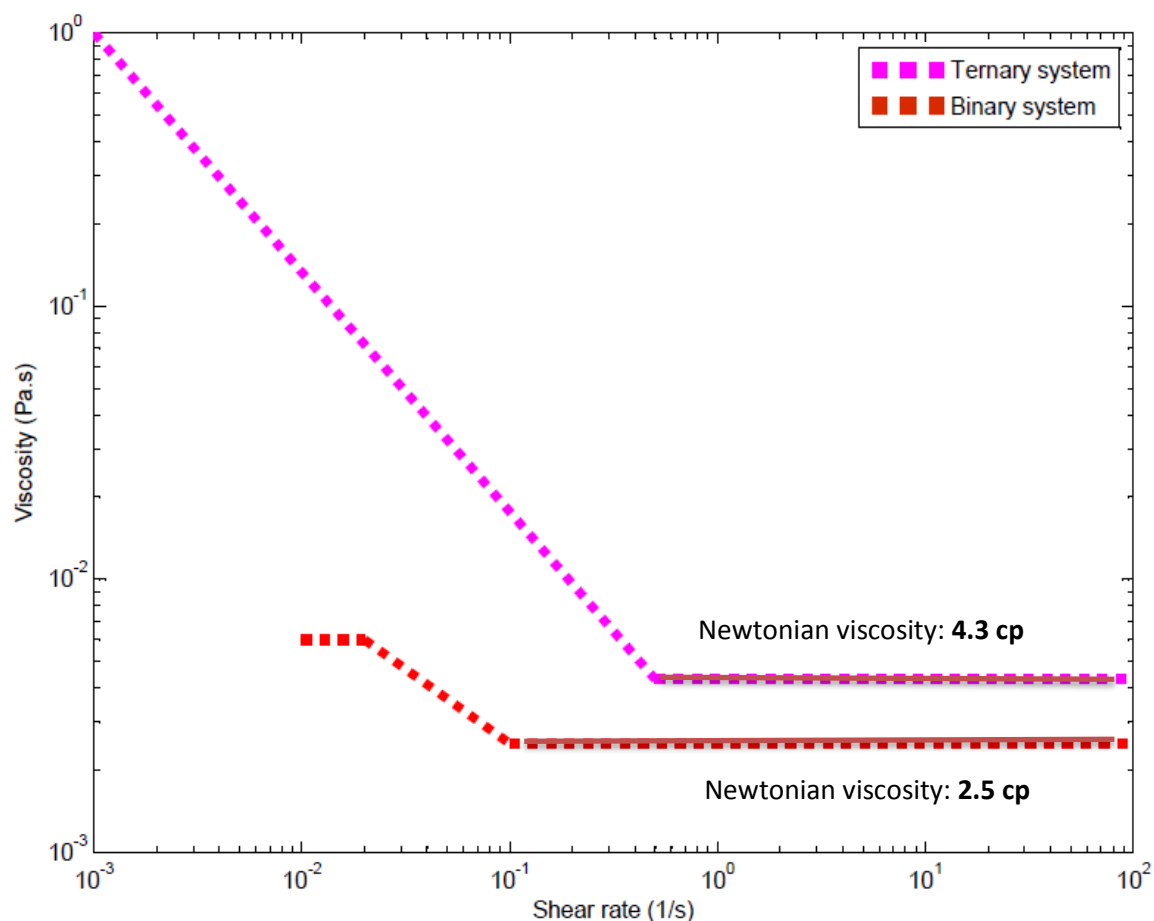
Fig. 3-9 Flow curves (top figure) and viscoelastic modulus at strain=0.05 (bottom figure) for SDS, binary and ternary solutions.
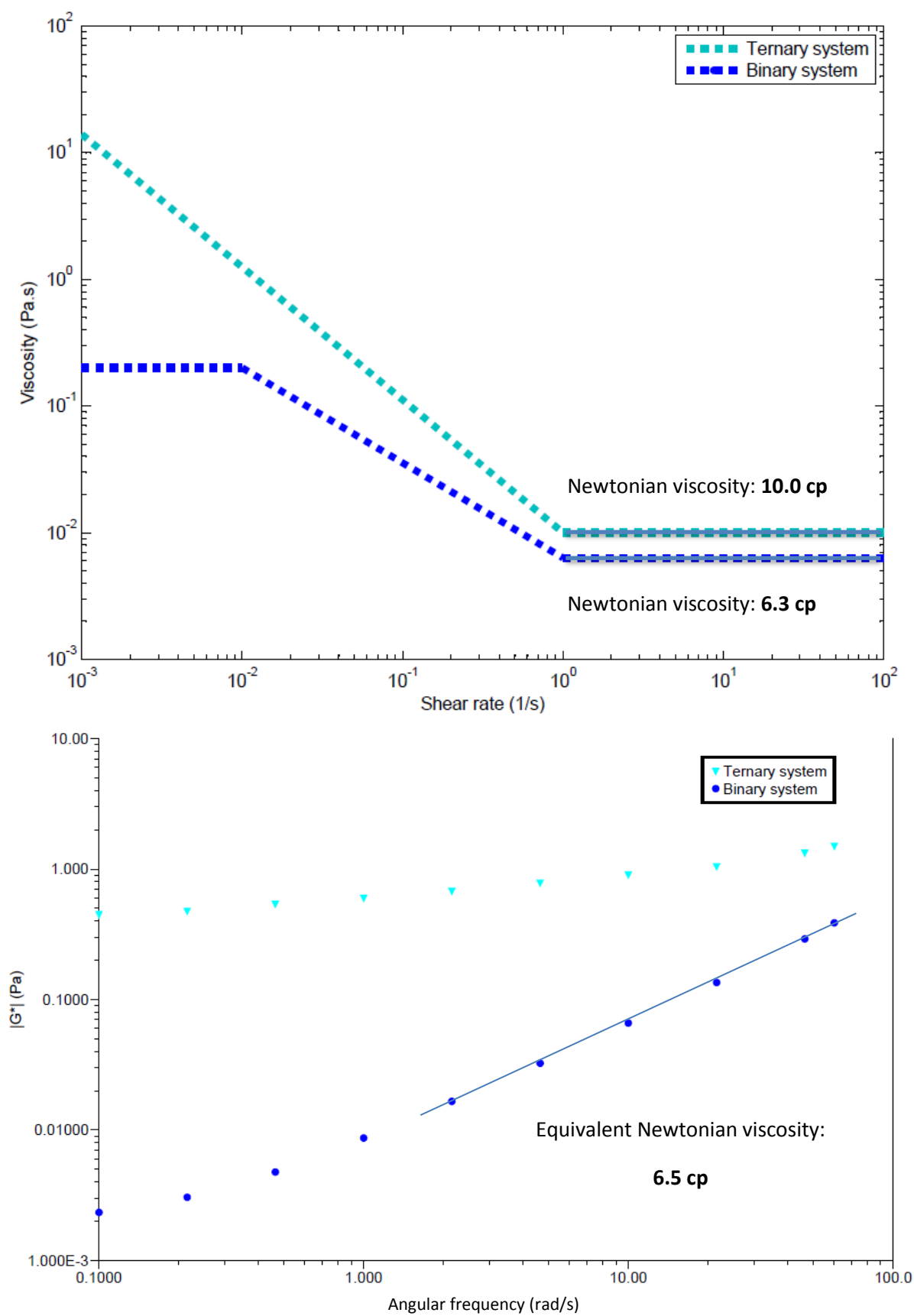
Fig. 3-10 Flow curves (top figure) and viscoelastic modulus at strain=0.05 (bottom figure) for F127, binary and ternary solutions.
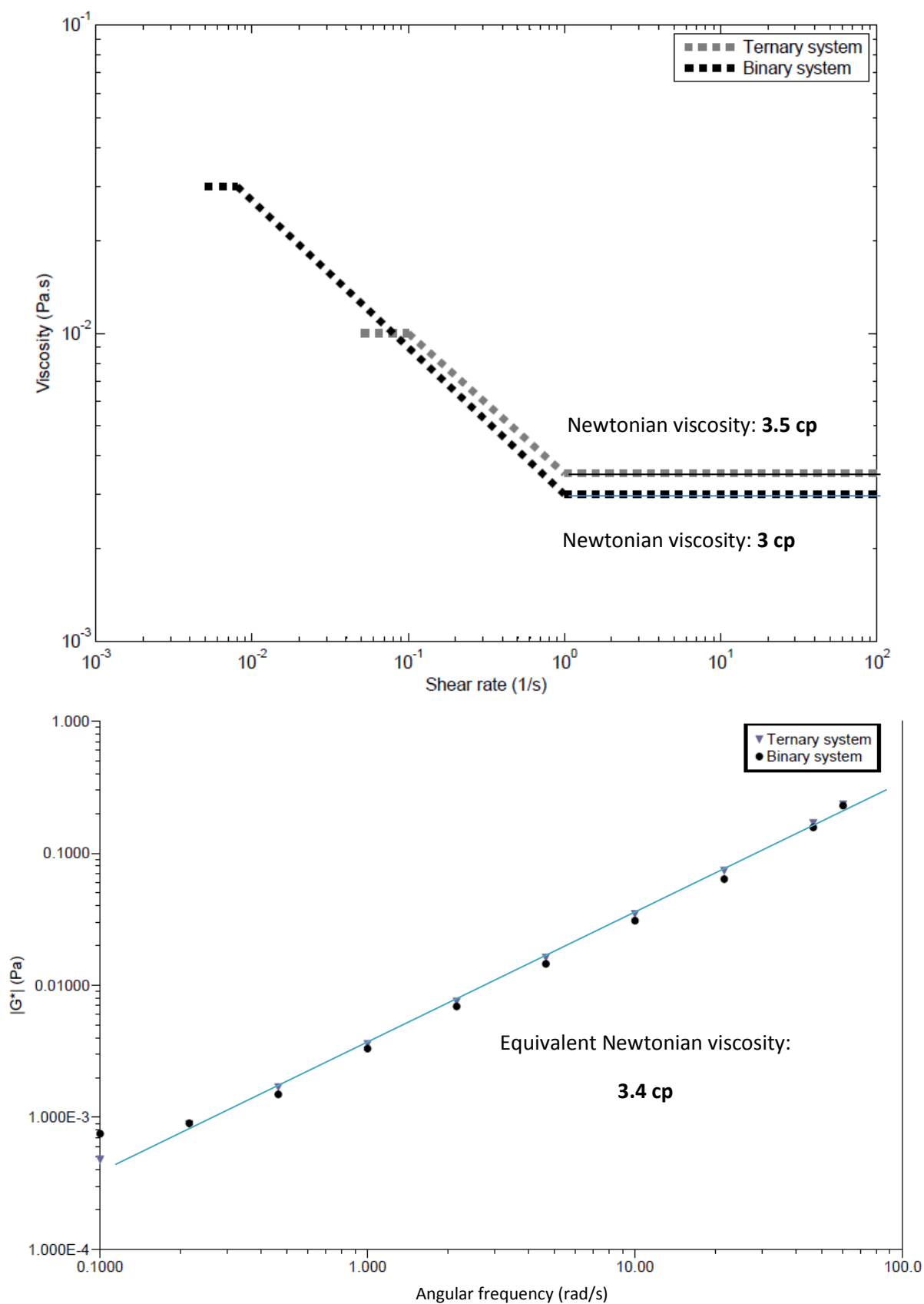
Fig. 3-11 Flow curves (top figure) and viscoelastic modulus at strain=0.05 (bottom figure) for Triton X-100, binary and ternary solutions.

3-1-3 Effect of the surfactant

The morphology of surfactant systems depends on the surfactant properties such as molecular weight, charge and hydrophilic-lipophilic balance (HLB). In this research by choosing two nonionic surfactants of low and high molecular weight, one cationic and one anionic surfactant a range of different surfactant characteristics and the effects of these properties on flow properties have been studied. The addition of ethanol to t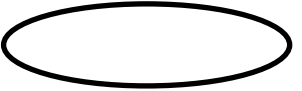he two nonionic surfactants does not have an effect on the Newtonian transition point (Fig. 3-10 and 3-11). The shear-thinning-Newtonian transition occurs at a shear rate of about 1/s. For the anionic surfactant (SDS) this transition point has been increased by about five times upon the addition of 30 wt. % ethanol (from about 0.1/s to 0.5/s) (Fig. 3-9). For the cationic surfactant (CTAB) as discussed earlier, upon adding the ethanol the Newtonian region has become visible beyond a shear rate of 8/s, which is a reduction of more than two orders of magnitude compared with the binary system (Fig. 3-7 and 3-6). This finding is confirmed by dynamic rheological data where for the binary worm-like micellar solution of CTAB no Newtonian behaviour was detected whereas the 30 wt. % ethanol ternary solution shows Newtonian behaviour at relatively high angular frequencies (Fig. 3-12). As Einstein and Simha have mentioned, the viscosity of macromolecules is independent to their size over the Newtonian region; however it does depend on their shape (see [57]). The degree of this dependence is defined by the surfactant features. For example both F127 and Triton X-100 are nonionic surfactants that make ellipsoidal micelles, however F127 due to its polymeric nature displays a higher viscosity (Fig. 3-10 and 3-11). The shape as determined using Eq. 3-2 and confirmed by literature where other methods have been used (see [54] and [58]) and size determined by SAXS and DLS of each system is given in Table 3-5.

Table 3-5 Size and shape of micelles in binary and ternary systems

Surfactant Solution	Micellar size* (nm) in binary systems	Micellar size* (nm) in ternary systems
SDS	3.7±0.1	10.0±0.1
CTAB	8.7±0.1	5.7±0.1
Triton X-100	16.5 ±0.1	No information*
F127	19 ±0.1	27.0±0.1

* The size is the size of the equivalent sphere (hydrodynamic size) ** Neither DLS or SAXS give reliable data, the shape is estimated from the Newtonian viscosity as predicted by Eq. 3-2.
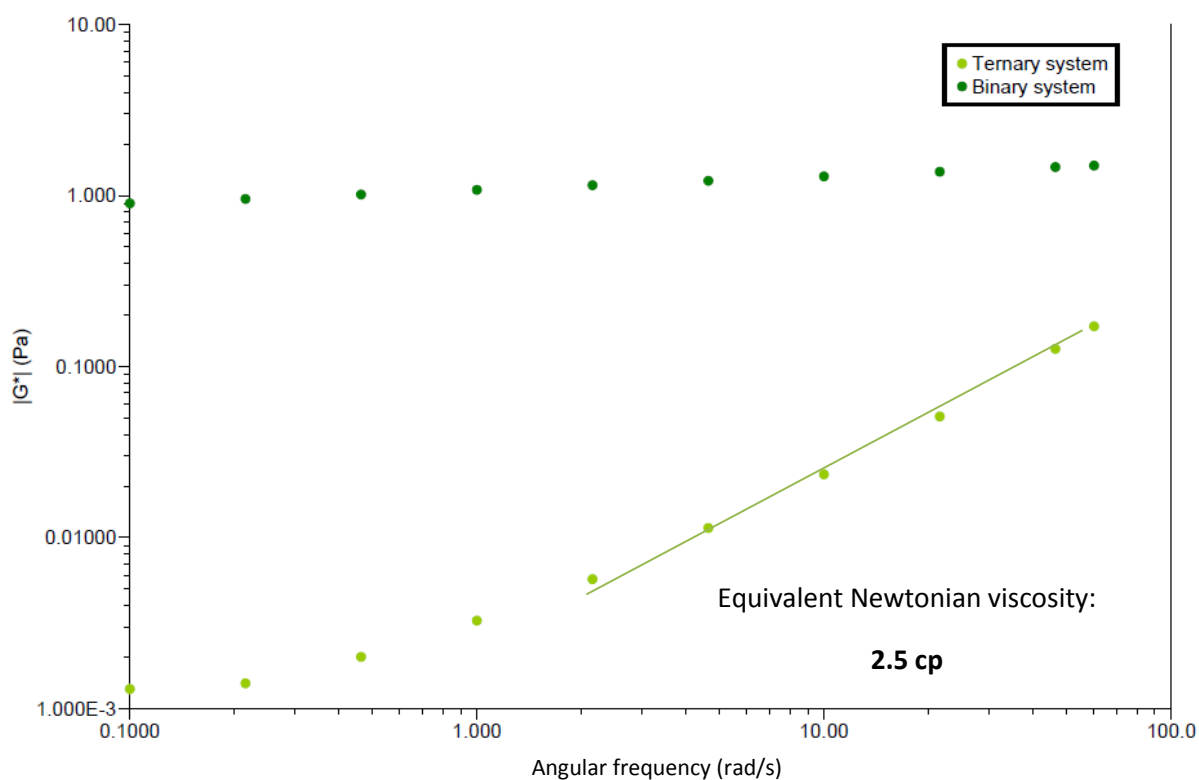
Fig. 3-12 Viscoelastic modulus, at strain=0.05, of CTAB, binary and ternary solutions; 10 wt. % CTAB, 30 wt. % ethanol.

3-1-4 Discussion

As seen in Table 3-5, by comparing the binary and ternary solutions of each surfactant one can determine that:

1- The anionic system, SDS, undergoes a morphological change from spherical to ellipsoidal micelles upon adding ethanol to a final concentration of 30 wt. %. While the cationic system, CTAB, the micelles become globular compared with the worm like micelles formed in the binary system.

2- The polymeric nonionic system, F127, changes to more elongated ellipsoids.

3- The simple nonionic surfactant, Triton X-100 is the least altered by the introduction of ethanol with the system remaining ellipsoidal only with a slightly larger J.

The above findings show that the addition of ethanol to binary solutions of ionic surfactants results in significant changes to micelle morphology in comparison to the non-ionic surfactants. This can be elaborated by considering the effect of charge density on structure transition in surfactant solutions. The charge density on a sphere is lower than that on an ellipsoid (see Fig. 3-13). This means the higher the curvature the lower the charge density.
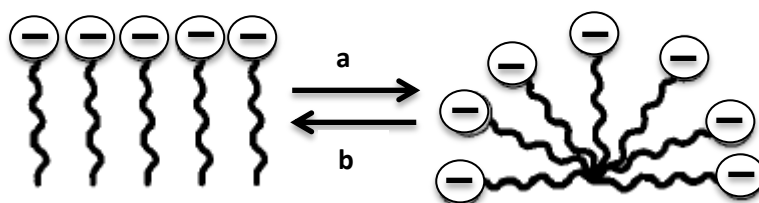
Fig. 3-13 Change in the curvature upon a) decreasing and b) increasing the charge density (reproduced from [59].

The addition of ethanol to the four surfactant solutions results in increasing the negative charge density since ethanol makes water molecules to releases OH^-, hydroxide (see [60]). Hence ethanol gives negative charge to the system. This negative charge significantly increases the charge density in the case of SDS, anionic surfactant, slightly increases the charge density in the case of non-ionic surfactants, F127 and triton X-100, and significantly decreases the charge density in the case of cationic surfactant, CTAB. This explains the enhanced curvature in the CTAB/ethanol/water ternary solution and the decreased curvature in the case of the other three surfactant systems. Guo and Colby studied the

structure transition in non-ionic polymeric surfactant upon the addition of different additives, showing the addition of alcohol to the binary surfactant solution results in a decrease in the curvature of the system [61]. However, the effect of adding a short-chain alcohol to nonionic, anionic and cationic surfactants under the same conditions within a single study has not been investigated so far. The advantage of studying these surfactant solutions together, as done in this research, is that the applicability of charge density theory can be examined straightforwardly.

By comparing the viscoelastic modulus of the CTAB binary system in Fig. 3-12 and that of the F127 ternary system, Fig. 3-10, one can realize the behaviour is similar. This confirms the finding of previous researchers who state that the rheological behaviour of worm-like micelles is similar to that of a solution of flexible polymers [4]. Hence both the binary CTAB micelles and the ternary F127 micelles are long flexible rod aggregates.

Based on the flow curves of the binary and ternary surfactant solutions investigated in this research, it is concluded that the flow curves of surfactant solutions are composed of different regions:

1- Constant viscosity at low shear rates;

2- Shear-thinning behaviour at medium shear rates; and

3- Newtonian viscosity at high shear rates.

The constant viscosity at the beginning is due to a yield stress behaviour and might be observed in most or all non-Newtonian systems, if a sufficiently small increasing shear rate is applied to the system. After which flow occurs.

Based on the above, the following multi-element model is proposed for the viscosity of a surfactant solution over the entire range of shear rate:

$$\eta = \eta_0 \qquad\qquad \dot{\gamma} < \dot{\gamma}_1 \qquad\qquad Eq.\,3-4$$

$$\eta = \frac{A_{ss}}{\dot{\gamma}^{n_{ss}}} \qquad\qquad \dot{\gamma}_1 \ < \dot{\gamma} < \dot{\gamma}_2 \qquad\qquad Eq.\,3-5$$

$$\eta = \eta_{Newtonian} \qquad\qquad \dot{\gamma} > \dot{\gamma}_2 \qquad\qquad Eq.\,3-6$$

where $n_{ss} = n_{surfactant\ solution} = \frac{\eta_{Newtonian} - \eta_0}{\dot\gamma_2 - \dot\gamma_1}$, A_{ss} is the viscosity at a shear rate of 1/s times the shear rate, which equals unity here, to the power of n_{ss}. This gives the value of the viscosity at shear rate of 1/s. Hence the middle part of the model can be rewritten as follows:

$$\eta = \frac{\eta_{@\dot\gamma=1*(1/s)^{n_{ss}}}}{\dot\gamma^{n_{ss}}} \qquad \dot\gamma_1 \ < \ \dot\gamma < \dot\gamma_2 \qquad\qquad Eq.\,3-7$$

For these systems, where the Newtonian plateau has been reached by a shear rate of 1/s, the relationship takes the simple form of:

$$\eta = \frac{\eta_{Newtonian}}{\dot\gamma^{n_{ss}}} \qquad \dot\gamma_1 \ < \ \dot\gamma < \dot\gamma_2 \qquad\qquad Eq.\,3-8$$

The term $\boldsymbol{n_{ss}}$ is determined not only by the nature of the surfactant but also the interactions between the interfacial layer and the engaged phases. The values of the zero-shear viscosity, $\boldsymbol{n_{ss}}$ and Newtonian viscosity for SDS, F127 and Triton X-100 are given in Table 3-6 and 3-7.

Table 3-6 Model details of the binary surfactant solutions

Surfactant	Zero-shear viscosity (cp)	n_{ss} for the binary system	Newtonian viscosity
SDS	6±1	0.43±0.01	2.5±0.1
F127	120±1	0.75±0.01	6.3±0.1
Triton X-100	13±1	0.50±0.01	3.0±0.1

Table 3-7 Model details of the ternary surfactant solutions

Surfactant	Zero-shear viscosity (cp)	n_{ss} for the binary system	Newtonian viscosity
SDS	1000±1	0.89±0.01	4.3±0.1
F127	10500±1	1.07±0.01	10.0±0.1
Triton X-100	10±1	0.40±0.01	3.5±0.1

*Zero-shear viscosity for the systems that do not show constant viscosity at low shear rates is considered to be the viscosity at a shear rate of 10^{-3}.

n_{ss}, given in Table 3-6 and 3-7 is the rate of transfer from zero-shear viscosity to the Newtonian viscosity. The more significant difference between the values of these two viscosities results in a larger n_{ss}. n_{ss} of 30 wt. % ternary surfactant solutions of SDS and F127 are higher than that of their corresponding binary systems. The reason is that the zero-shear viscosity of the ternary solutions are significantly higher than those of binary systems (1000 cp and 10500 cp vs 6 cp and 120 cp for SDS and F127, respectively). On the other hand Triton X-100 solution displays a decrease in n_{ss} upon the addition of ethanol to the binary surfactant solution. This is due to the zero-shear viscosity of the binary system being higher than that of the 30 wt. % ethanol ternary solution.

In the case of the CTAB binary solution two shear-thinning regions exist (see Fig. 3-6). Hence the proposed model requires two shear-thinning regions with two n_{ss} terms, the value of n_{ss} attributed to each shear-thinning region can be extracted from the rate indexes given in Fig. 3-6 which are 1.0±0.1 and 0.4±0.1 for the first and second shear-thinning regions respectively.

3-2 Flow properties of microemulsions

By adding oil to a ternary surfactant/ethanol/water system a new complex fluid is formed; a microemulsion. In this research about 20 wt. % dodecane was added to a ternary solution of ~55 wt. % binary surfactant solution and ~ 25 wt. % ethanol or propanol. The binary surfactant solution contains 10 wt. % surfactant. However after the microemulsion is produced some excess oil separates. Hence the concentrations in the final products need to be recalculated. This can be done based on a variety of methods that will be fully discussed below.

Since the micelles in the ternary system are swollen and ready to solubilize oil, the microstructure of the microemulsion is not expected to be significantly different to that of the ternary system. Consequently, the general flow behaviour of microemulsions is similar to that of the ternary systems. In this section the relationship between the size, shape and chemical functionality of the surfactant and the corresponding flow properties of microemulsions is studied.

The most common rheological models for microemulsions are discussed and related to the obtained data and the applicability of each model to such systems is considered. The most

appropriate model for each system, with regard to its microstructure was selected and developed to represent the flow behaviour of the system more accurately. It should be noted that almost all rheological models for microemulsions are applied to the Newtonian region of the flow curve only.

In this research the concentration of alcohol within each of the different microemulsions, has been adjusted to give stable and reproducible data since maintaining the same alcohol concentration in all four systems did not produce stable microemulsions.

We show here that the value used for the reference viscosity term is crucial and must be separately determined to allow application of the literature models in the analysis of the experimental data.

3-2-1 Effect of droplet shape

To generate a microemulsion, dodecane was solubilized (between 5 and 15 wt. %) within the micelles of each of the four ternary surfactant/alcohol solution. Hence a size increase is expected due to the addition of the oil which is confirmed by DLS (Table 3-8). This results in the viscosity increasing over the Newtonian region [62]. In Table 3-8, both the surfactant ternary system and microemulsion droplet sizes are given.

The droplets in the microemulsions prepared using the two ionic surfactants have the same size in the microemulsions. The viscosity curves of these two systems confirm that they display the same Newtonian viscosity which implies the droplets are also the same shape; however the transition to the microemulsion Newtonian region is found at a higher shear rate in the SDS (5/s) system than for CTAB (0.5/s) (Fig. 3-14). The values for the relevant ternary aggregates are 0.5/s for the SDS system (Fig. 3-9) and 10/s for the CTAB system (Fig. 3-7).

Comparing the minimum shear rate at which the Newtonian region is observed in SDS (5/s) and CTAB (0.5) microemulsion systems with their corresponding ternary aggregates (0.1/s and 10/s, respectively) shows that this value has decreased 50 times for SDS and increased 50 times for CTAB. The reason is the different charge of the surfactants and its synergist effect with ethanol being present in the system. In a ternary surfactant aggregate ethanol molecules are mostly hydrogen bonded to water molecules; this makes a network that inter-connects the droplets. Given the more OH^- that is released in water/ethanol system

as compared to the pure water, the interaction between this network and the surfactant would be adsorption for the cationic CTAB and repulsion for the anionic SDS. Therefore it is more difficult to overcome droplet interactions in the CTAB ternary solution as compared with the SDS/ethanol/water system hence for the CTAB system the Newtonian region is evident at higher shear rates. By adding dodecane a microemulsion is generated in which ethanol molecules would mostly go to the interfacial layer. This migration results in a decrease in the ethanol concentration in the media, adding dodecane itself decreases the percentage of ethanol in the system as well. This causes a decrease in repulsive force between the SDS system droplets and a decrease in the attractive force between CTAB droplets. Hence an increase and a decrease in the minimum shear rate at which Newtonian behaviour is observed occurs for SDS and CTAB ternary systems as compared with their corresponding microemulsion systems, respectively. It should be noted that due to the adsorption of ethanol to the interface the thickness of the surfactant layer increases resulting in an increase in the Newtonian viscosities of both microemulsion systems (~ 5 cp for both systems) as compared with their relative ternary solutions (4.3 cp and 2.3 cp for SDS and CTAB systems, respectively).

Table 3-8 Comparison of aggregate size in the ternary and microemulsion systems

Surfactant Solution	Micellar size (nm) in ternary systems	Microemulsion droplet size (nm)
SDS	10±0.5	12±0.5
CTAB	5.7 ±0.5	12±0.5
Triton X-100	---	33±0.5
F127	27±0.5	36.5±0.5
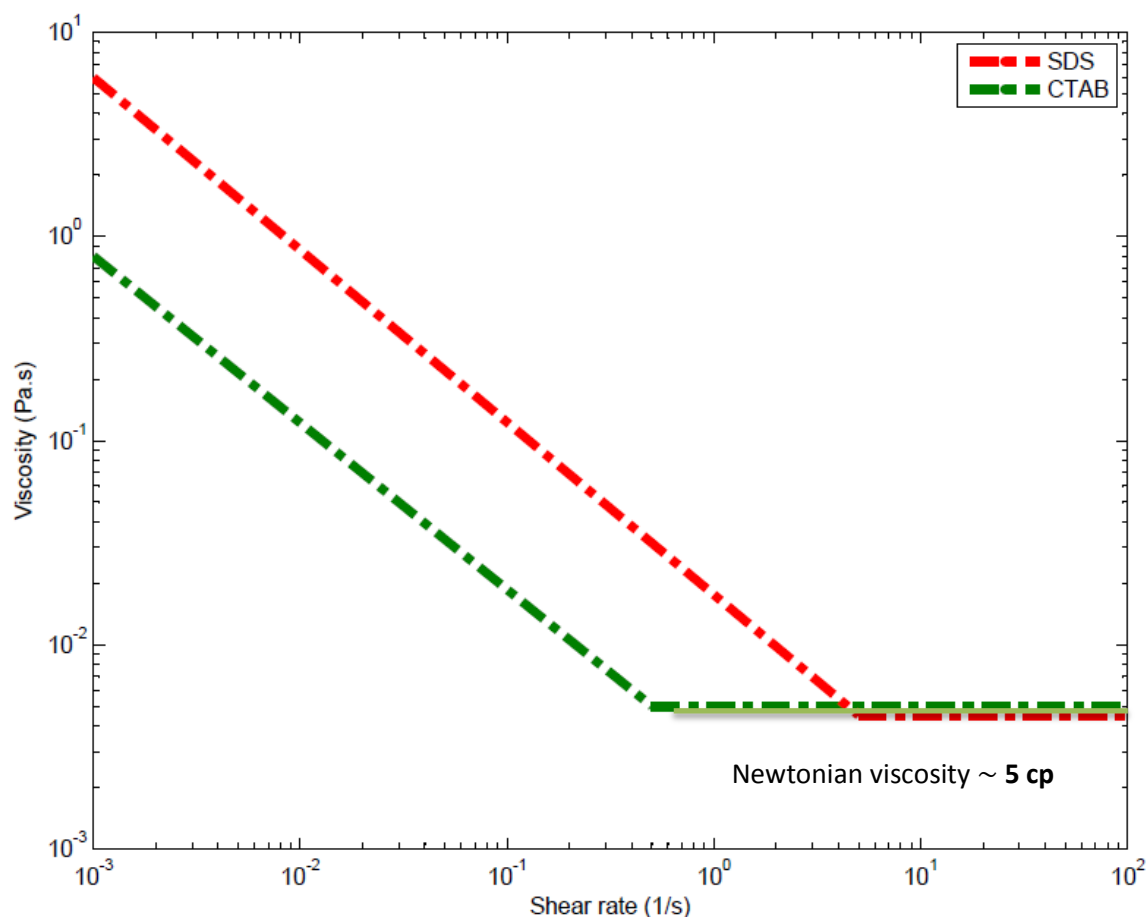
Fig. 3-14 Flow curves of microemulsions of SDS and CTAB.

For both flow curves the data were obtained using a decreasing shear rate sequence, therefore the initial constant viscosity is not observed (reliable data could not be obtained when an increasing shear rate sequence was applied). The slope of the straight line, representing the shear-thinning region, in the two microemulsions is also similar (Fig. 3-14). This slope, *n*, as explained in the previous section of this chapter is the rate of transfer from the high viscose state of the material (at low shear rates) to the Newtonian viscosity (at high shear rates). One explanation for these slopes being similar in the microemulsions prepared using the ionic surfactants could be that there is a relationship between the ionic strength or the charge density of the system and the corresponding flow behaviour.

On the other hand in the non-ionic systems, although the droplet sizes are similar, different Newtonian viscosities, beyond 0.2/s and 0.5/s of applied shear rate for the F127 and Triton X-100 systems respectively, are observed due to shape differences (Fig. 3-15). Both

increasing and decreasing applied shear rates could be used for the Triton X-100 and F127-based systems. A constant initial viscosity is only seen for the Triton X-100 microemulsion. However, better quality data are obtained for an decreasing shear rate sequence. The slope of the shear-thinning region of the F127 microemulsion is higher than that in the Triton X-100 system. This is most likely due to the effect of the molecular weight difference and consequently the thickness of the surfactant layer on the flow properties.
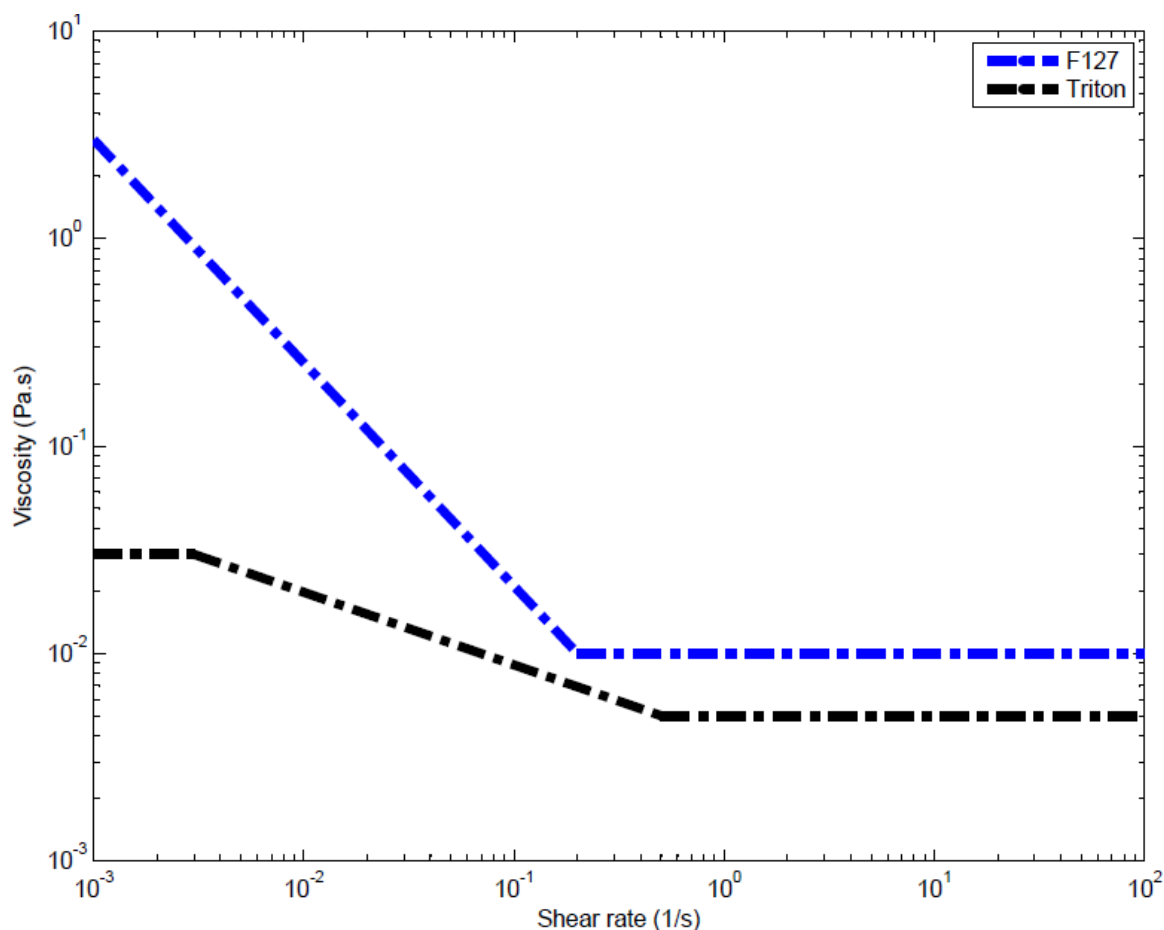
Fig. 3-15 Flow curves of microemulsions of F127 and Triton X-100 show different Newtonian viscosities in spite of their similar droplet sizes (36.5 and 33 nm respectively).
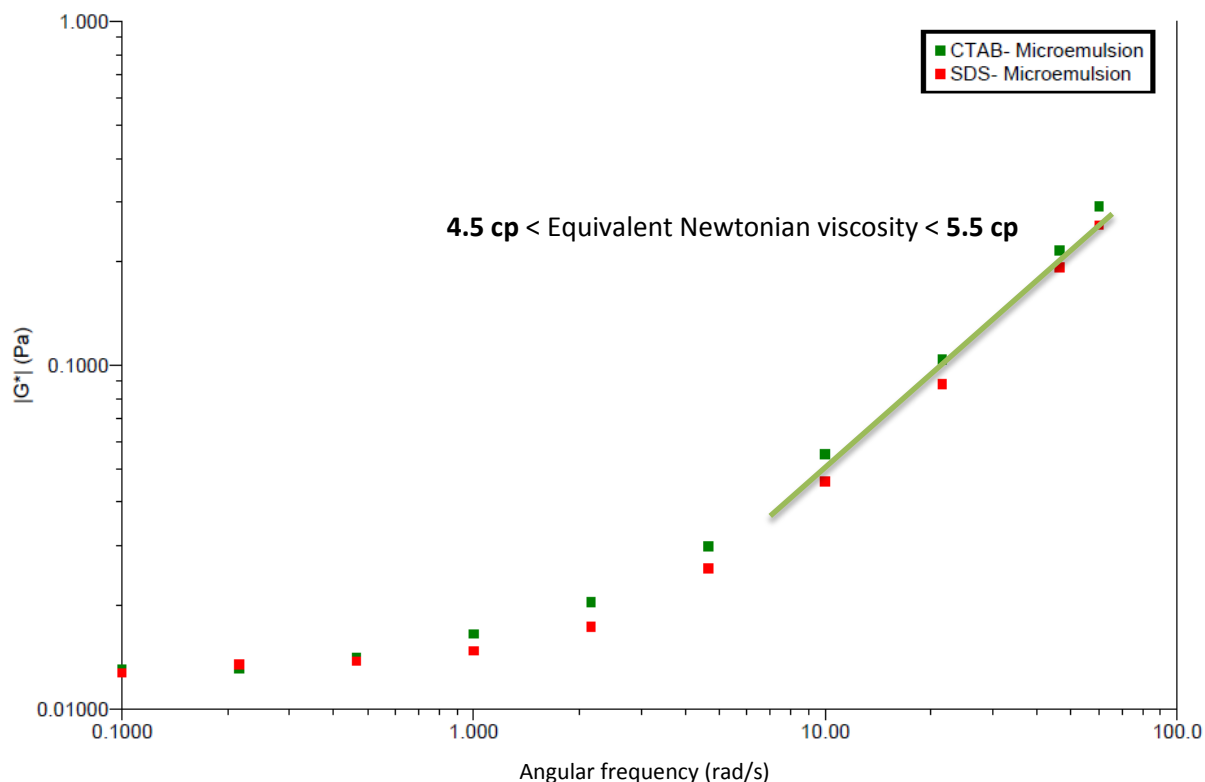
Fig. 3-16 Frequency sweep experiments at a strain of 0.05 for CTAB and SDS microemulsion systems.

As seen in Fig. 3-16, the equivalent Newtonian viscosity of approximately 5 cp for both SDS and CTAB microemulsions is obtained. The relevant viscosity of CTAB is slightly higher than that of SDS which is confirmed in the flow curve data (Fig. 3-14).

As seen in Fig. 3-17, the dynamic frequency sweep data confirm that the Newtonian viscosity of the F127 microemulsion system is more than twice that of the Triton X-100 system. One can conclude that the viscosity is a function of not only the droplet size but also the droplet shape.

Static and dynamic rheological data as seen in Fig 3-14 to Fig 3-17 both indicate that the Newtonian viscosity of approximately 5 cp is gained for the three microemulsions made of SDS, CTAB and Triton X-100, however the Newtonian viscosity of F127-based system is more than twice that obtained for the three other systems, approximately 13 cp as compared to 5 cp.
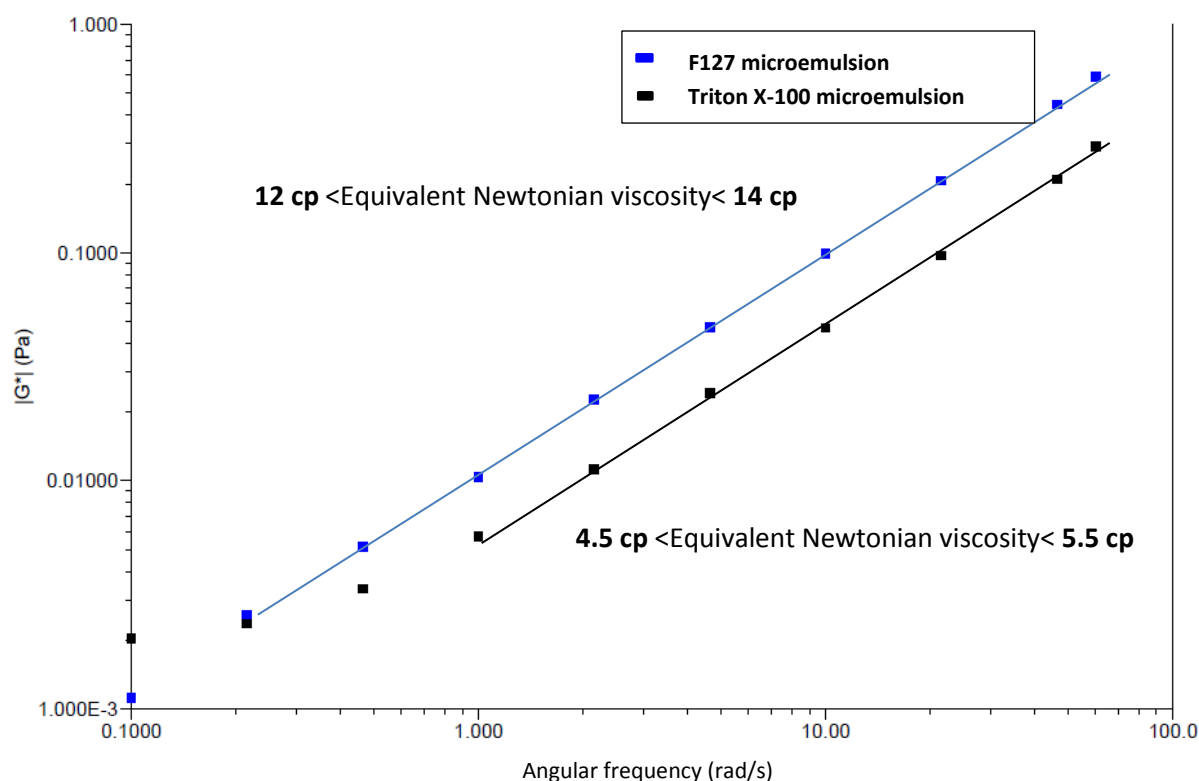
Fig. 3-17 Frequency sweep experiment for F127 and Triton X-100 microemulsion systems at a strain of 0.05/s.

Considering the sizes of the four microemulsions, Table 3-8, and the corresponding flow curves, it is evident that for the ionic surfactants, SDS and CTAB, regardless of being positively charged vs. negatively charged, have the same droplet size and the same Newtonian viscosity. However while the Triton X-100 microemulsion also has approximately the same Newtonian viscosity as the ionic microemulsions, its droplets are about three times larger. In the case of the F127 microemulsion, the droplet size is close to that of Triton X-100 but the Newtonian viscosity is higher than that of the Triton X-100 systems (~13 cp vs. ~5 cp) indicating that ionic strength/charge density has an effect on the interactions in the system and therefore the Newtonian viscosity. The higher Newtonian viscosity in the F127 system is most likely due to the flexible polymeric nature of this emulsifier that forms a thicker interfacial layer and therefor higher viscosity.

Based on the above discussion the effect of the droplet size cannot be considered individually in order to investigate microemulsion rheology. This factor needs to be taken into account along with the ionic strength and also the nature, especially molecular weight, of the surfactant.

These factors together can be observed in the effect of droplet shape on the Newtonian viscosity. Using Eq. 3-2 the *J* factors obtained for Triton X-100 and F127 microemulsions, with similar droplet sizes but different Newtonian viscosities were calculated and are 4.1 cp and 9.6 cp, respectively. This means that despite these two microemulsions having similar measured hydrodynamic droplet sizes, F127 droplets elongate along their major axis more than twice that of Triton X-100 droplets. Hence the droplets in F127 microemulsion system provide more surface area compared with Triton X-100 and therefore higher Newtonian viscosity. This phenomena along with the above mentioned higher thickness of F127 are two important affecting parameters on the viscosity however to indicate the weight of each parameter is complicated and beyond the scope of this thesis.

3-2-2 Effect of droplet size

The formation of a microemulsion through the addition of oil results in the size of the discrete droplets increasing (Table 3-8). One can easily calculate the size ratio between the ternary solution and microemulsion droplets for each of the surfactant systems (Table 3-9).

Table 3-9 Size ratio between microemulsion and ternary aggregates

Surfactant Solution	Size ratio between microemulsion/ ternary system*
SDS	1.2
CTAB	2.1
F127	1.3

* The size of the aggregates in the Triton X-100 ternary system could not be determined; hence this surfactant is not included. A method to estimate the size for this system will be introduced shortly.

Considering the relevant flow curve, one can extract the Newtonian viscosity ratio between the ternary solution and the microemulsion (Fig. 3-18 to 3-21). The viscosity ratios are given in Table 3-10.
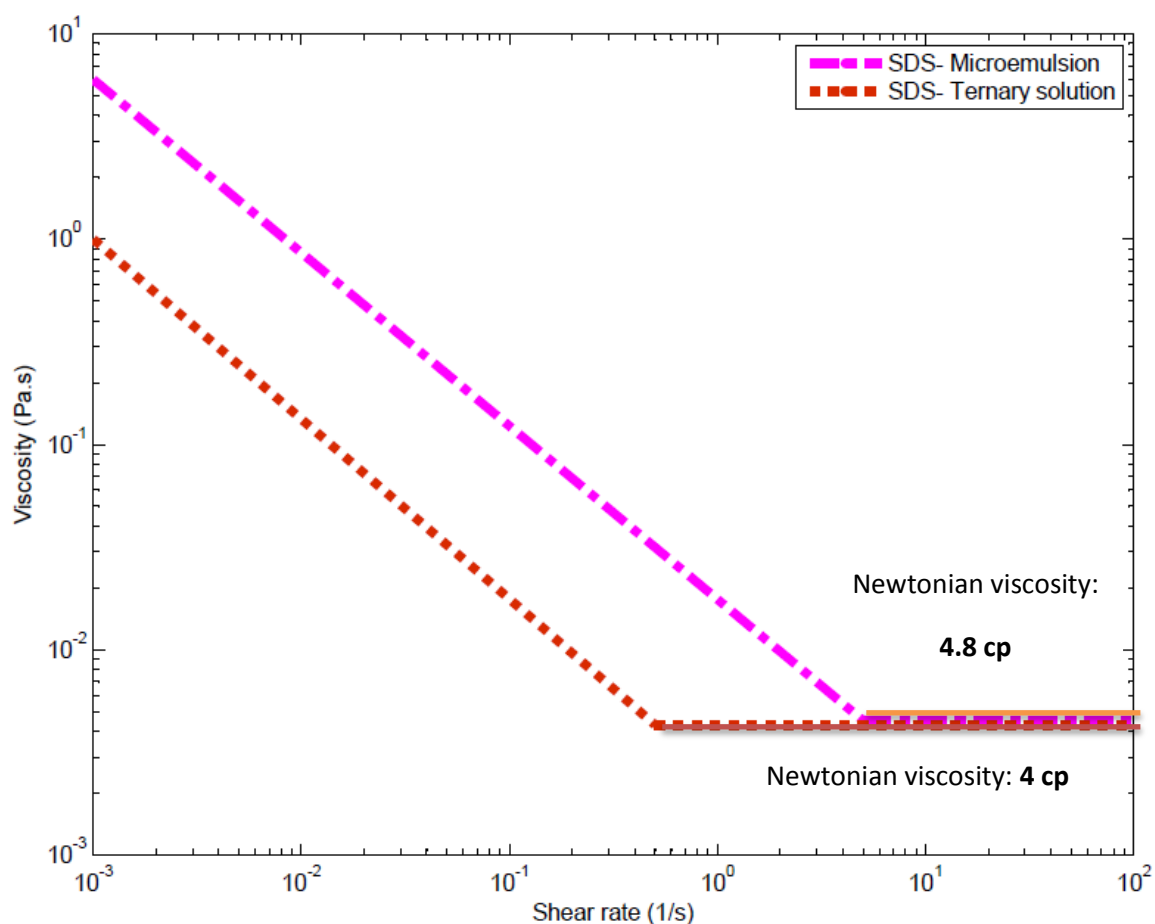
Fig. 3-18 Flow curves of SDS microemulsion and ternary solutions.

As seen in Fig. 3-18 the Newtonian viscosity for the SDS system has increased upon the addition of dodecane; the viscosity of the microemulsion solution is higher than that of the ternary solution. This is true for all four systems. The Newtonian plateau in the SDS system is achieved at a higher shear rate in the microemulsion (5/s) as compared to the ternary system (0.5/s). For the other three systems the reverse is true, the transition is lowered upon formation of the microemulsion.

Table 3-10 Relative viscosity ratio between the Newtonian viscosities of microemulsion and ternary solutions

Surfactant Solution	Viscosity ratio between microemulsion/ternary system
SDS	4.8/4.0 = 1.2$\pm$0.1
CTAB	4.9/2.3 = 2.1 $\pm$0.1
Triton X-100	4.8/3.6 = 1.3$\pm$0.1
F127	13.0/10.0 = 1.3$\pm$0.1
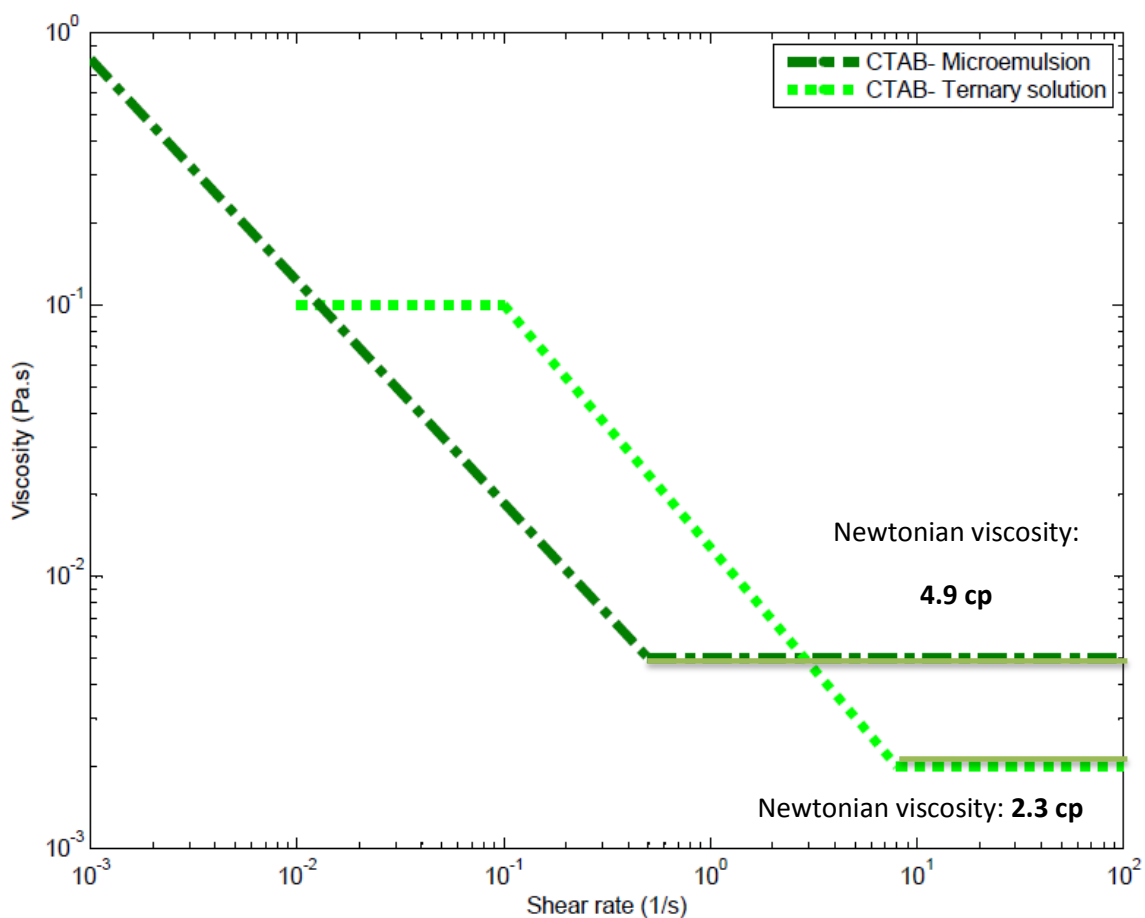
Fig. 3-19 Flow curves of CTAB microemulsion and ternary solutions.

From the data given in Tables 3-9 and 3-10 one can conclude that there is a direct relationship between Newtonian viscosity and the size of the aggregates in the ternary and microemulsion solutions as follows:

$$\frac{\eta_{Microemulsion}}{\eta_{Ternary\ solution}} = \frac{d_{Microemulsion}}{d_{Ternary\ solution}}.$$

This relationship is based on observation and can be explained by considering that the relationship between the droplet size and viscosity in micellar solutions and also microemulsions is direct as previously explained.

For the Triton X-100 ternary system, size information is not available as neither SAXS nor DLS measurements gave reproducible data; however by applying Eq. 3-9, the micellar size of the ternary system can be estimated to be 25 nm.
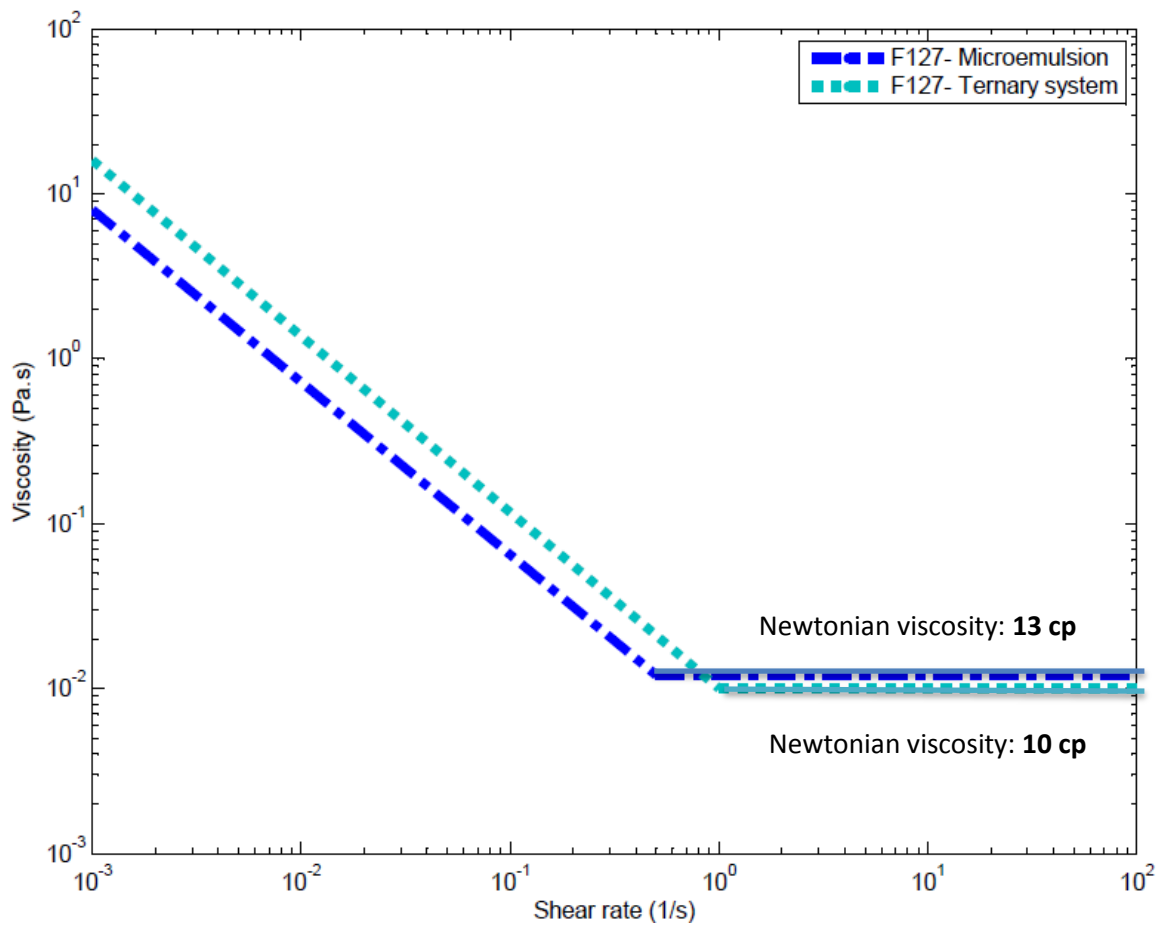
Fig. 3-20 Flow curves of F127 microemulsion and ternary solutions.
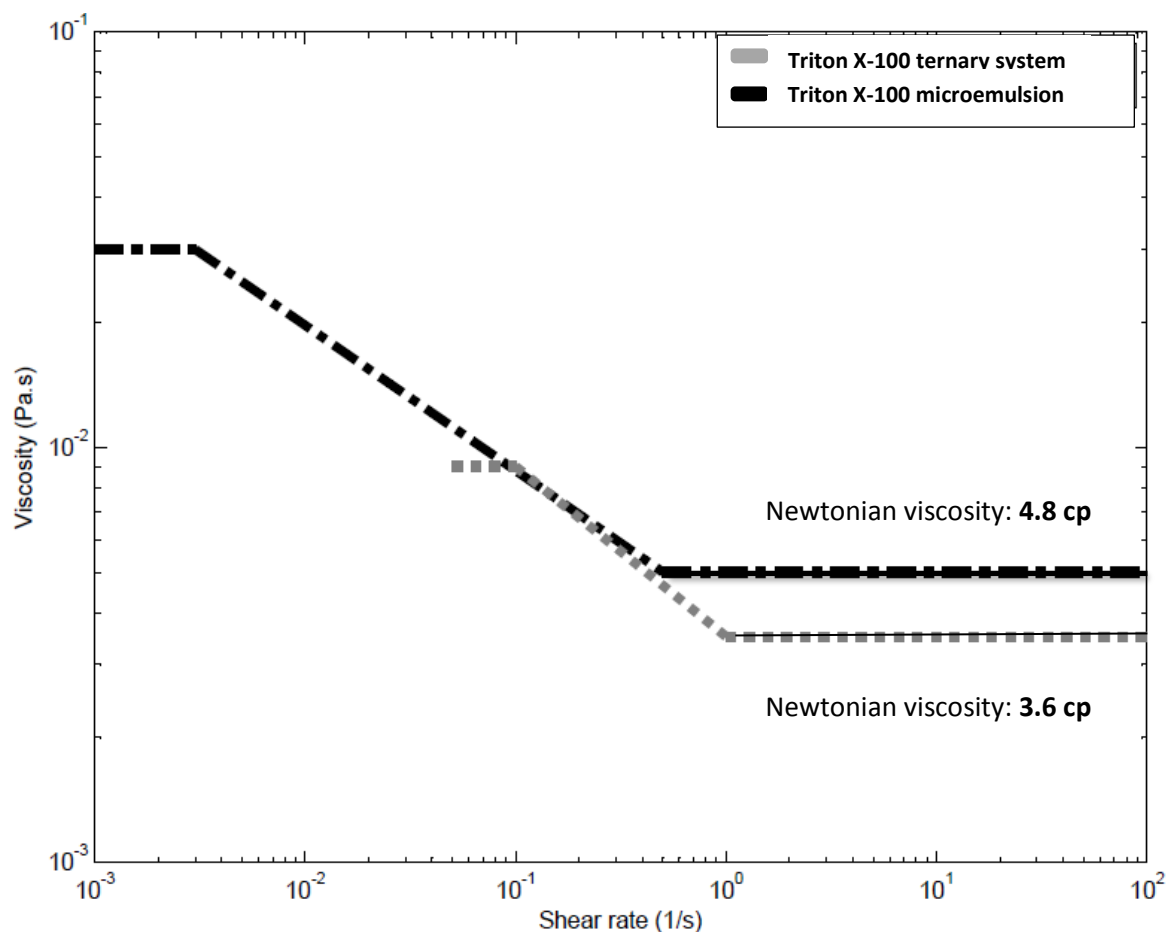
Fig. 3-21 Flow curves of Triton X-100 microemulsion and ternary solutions.

According to Fig. 3-19 and 3-20 for the non-ionic surfactants (F127 and Triton X-100), the Newtonian region in the relevant microemulsions is observed at lower shear rate than in the equivalent ternary systems. The shear-thinning-Newtonian transition point has moved from 1/s to 0.5/s in both systems. Since Newtonian behaviour arises due to the droplets not strongly interacting with each other, the ethanol plays a significant role in inter-connecting the ingredients, one reason for this shift might be due to the decrease in the total concentration of the ethanol in the system with the addition of dodecane to make the microemulsion. The amount of oil that is taken up is different in each system as mentioned previously, and hence the final total concentration of ethanol is also different in each system. The oil concentration in each microemulsion system will be estimated in the following section.

It should be noted that in Fig. 3-20 and 3-21 the flow data were recorded against decreasing and increasing shear rates, respectively. Once again this is to ensure that the most reproducible data are reported. This is evident by the appearance of the initial solid-like behaviour in the Triton X-100 data. As with nearly all soft mater systems, the internal structure and interactions respond differently on increasing and decreasing applied shear rate and often for seemingly no reason reproducible data can only be obtained in one direction.

In the case of CTAB (Fig. 3-19), the Newtonian viscosity is increased and shifted to lower shear rate upon the addition of the oil, however the viscosity of the microemulsion over the shear-thinning region is lower than for that of the ternary aggregates. Additionally, the solid-like behaviour of the ternary aggregate is observed between shear rates of 0.01/s and 0.1/s when an increasing shear rate is exploited, at shear rates below 0.01 no reliable data were able to be obtained. The structural change from spherical to ellipsoidal in changing from the ternary surfactant solution to the relevant microemulsion of CTAB should be noted in order to elaborate on the different regions of the flow curve.

Attwood [63] has proposed the following relationship that relates the relative viscosity of a solution in the Newtonian region, given in Table 3-10, to the volume fraction and the droplet size:

$$\eta_r = \exp\left[\frac{a\varnothing}{1-k\varnothing}\right] \qquad\qquad Eq.\ 3-10$$

where a equals 2.5 for spheres and k is the hydrodynamic interaction coefficient that can be calculated using the following empirical expression as the same author proposed:

$$k = 1.079 + \exp\left(\frac{0.01008}{d_m}\right) \qquad\qquad Eq.\ 3-11$$

where d_m is the average diameter of the aggregates in micrometres.

Based on Eq. 3-10 and 3-11 the volume fraction of the four microemulsions can be estimated and are given in Table 3-11.

Table 3-11 Estimated oil volume fraction of the microemulsions

Microemulsion	Volume fraction (%)
SDS	6.0±0.1
CTAB	14.0±0.1
Triton X-100	9.0±0.1
F127	9.0±0.1

Because of the preparation method (see Section 3-2), the oil volume fraction of each of the microemulsions cannot be directly known and must be determined via experimental measurement. The observed trend of all take up, Table 3-11, agrees with the quantitative observation during microemulsion formulation.

It is noted that the reference viscosity that is used to calculate the relative viscosity and hence the volume fraction in Eq. 1-3 for these systems must be the viscosity of the relevant ternary solution. This is a missing point in many rheological studies of microemulsions. Researchers assume that the relevant reference viscosity is the viscosity of the continuous phase (see [64], [65] & [66] for instance). However this has resulted in proposing assorted experimental values for the same parameters depending on the system under investigation.

Using the values of the volume fractions in Table 3-11, one can check the ability of the Einstein and modified Einstein relationships (Eq. 1-3 and 3-12 [67]) to predict the relative viscosities of the solutions:

$$\eta_r = 1 + 2.5\emptyset. \qquad\qquad Eq.\,1-3\,(Recalled)$$

where $\emptyset$ is the volume fraction of the sample.

$$\eta_r = 1 + 2.5\emptyset + 10.05\emptyset^2 \qquad\qquad Eq.\,3-12$$

10.05 is the third Virial coefficient. The calculated relative viscosities are given in Table 3-12 in comparison with the experimental values given in Table 3-10. This comparison shows that the obtained relative viscosities are in good agreement except for the CTAB system. We believe the different behaviour of CTAB is because of the structural change, from spherical to ellipsoidal, that occurs due to the addition of oil [68]. Hence the viscosity of the ternary

system is not appropriate for the CTAB system. For the other three systems the ternary solution viscosity is appropriate to use as the reference viscosity.

For none of the systems is the reference viscosity the viscosity of water. For example for the samples investigated here, with the relative viscosities calculated from Eq. 3-12 as given in Table 3-12, if the viscosity of the continuous phase was used rather than that of the ternary solution, considering the viscosity of water is 1 cp, the estimated viscosities of the corresponding microemulsions would be as given in Table 3-13. A seen in Table 3-13, there is no agreement between the experimental and calculated data indicating it is not appropriate to use the viscosity of water as the reference viscosity.

Table 3-12 Relative viscosity of the microemulsion systems based on the Einstein and modified Einstein equations

Microemulsion	η_r based on Eq. 1-3	η_r based on Eq. 3-12
SDS	1.15±0.01	1.19±0.01
CTAB	1.35±0.01	1.55±0.01
Triton X-100	1.22±0.01	1.31±0.01
F127	1.22±0.01	1.31±0.01

Table 3-13 Newtonian viscosity of the microemulsion systems given the reference viscosity being 1 cp as compared to the experimental data

Microemulsion	Newtonian viscosity as extracted from flow curves (Fig. 18 to 21)	Newtonian viscosity if reference material is water
SDS	4.8±0.1	1.2±0.1
CTAB	4.9±0.1	1.5±0.1
Triton X-100	4.8±0.1	1.3±0.1
F127	13.0±0.1	1.3±0.1

Furthermore, for instance if the reference viscosity used is that of water, 1 cp, the estimated volume fraction calculated from Eq. 1-3 for SDS, CTAB and Triton X-100 systems would be $\emptyset = 0.52$. This is physically impossible since the initial amount of the applied oil was 20 weight percent!

3-2-3 Effect of packing

Krieger-Dougherty [69] proposed the following empirical relationship with regard to the maximum packing of microemulsion droplets:

$$\eta_r = (1 - \frac{\emptyset}{\emptyset_m})^{-2.5\emptyset_m} \qquad\qquad Eq. 3-13$$

where $\emptyset$ is the volume fraction and $\emptyset_m$ is the maximum packing. For compact cubic and a random arrangement of spheres, the appropriate value of $\emptyset_m$ is 0.75 and 0.65 respectively [67]. For other lattice packings $\emptyset_m$ would take different values such as $\frac{\pi}{6}$ for a cubic lattice, $\frac{\pi}{3\sqrt{3}}$ for a hexagonal lattice and $\frac{\pi\sqrt{3}}{16}$ for a tetrahedral lattice.

A modified form of Eq. 3-13, where the coefficient 2.5 in the power is replaced with the intrinsic viscosity, was proposed by Mueller et al. (Eq. 3-14) [69]. As discussed before 2.5 is the relative viscosity of a very dilute dispersion with spherical morphology. Hence by replacing this value with the intrinsic viscosity a more accurate expression is obtained:

$$\eta_r = (1 - \frac{\emptyset}{\emptyset_m})^{-(\eta)\emptyset_m} \qquad\qquad Eq. 3-14$$

where η is the intrinsic viscosity of the sample. These equations were used to calculate $\emptyset_m$ for each of the four microemulsion systems. The results are summarised in Table 3-14.

Table 3-14 Estimated relative viscosities and maximum packing for the microemulsion systems*

Microemulsion	Relative Viscosity	Maximum packing
SDS	1.19±0.01	$0.3 < \emptyset_m < 0.4$
CTAB	2.10±0.01	$0.6 < \emptyset_m < 0.7$
Triton X-100	1.31±0.01	$0.3 < \emptyset_m < 0.4$
F127	1.31±0.01	$0.3 < \emptyset_m < 0.4$

*The calculations are based on Eq. 3-14 for CTAB and based on Eq. 3-13 for the other 3 microemulsion systems.

As seen in Table. 3-14, by adjusting the maximum packing factor in Eq. 3-13 and 3-14, the value of the relative viscosities are in good agreement with the experimental data as given in Table 3-10.

Eq. 3-13 does not work for CTAB. The estimated oil volume fraction of this system is 0.14 (Table 3-11) and the relative viscosity is 2.1 (Table 3-10); using these numbers, there is no value for $\emptyset_m$ to satisfy Eq. 3-13. Therefore the modified form, Eq. 3-14, has been applied. The reason for this is that Eq. 3-13 is ideally applied to systems composed of spherical or close to spherical aggregates.

This analysis shows that equations 3-13 and 3-14 can be applied to microemulsions that have a microstructure similar to that of the corresponding reference system, such as the ternary solution, taking into consideration the maximum packing.

As seen in Table 3-14 the appropriate maximum packing for SDS, Triton X-100 and F127 suggests a tetrahedral lattice. This would need to be confirmed by methods that allow the structure to be more directly probed which is beyond the scope of this thesis. It should be taken into account that the deviation from globular morphology and also the polydispersity in the aggregate size affect the maximum packing. Hence it is not feasible to determine the morphology by only considering the value of the maximum packing; however it can be used to give an indication of the structural morphology.

In the CTAB system the aggregates go through considerable structural change upon addition of the oil and the size distribution is also changed and hence Eq. 3-14 must be applied. The obtained maximum packing for CTAB is higher than that of the other systems. This is due to the system being more ordered. This is because of the synergist effect of several factors including the charge of the surfactant, the interaction between droplets and the continuous phase.

3-2-4 Effect of Cosurfactant

Ethanol plays the role of cosurfactant in our microemulsions. Changing the cosurfactant to propanol may alter the droplet size and also the amount of oil that can be solubilized in the system. This is because of the different hydrophobicity of ethanol versus propanol. This gives a way of probing the effect of droplet size and dispersed phase volume fraction more closely.

In Table 3-15 are given the droplet sizes of microemulsions made using propanol, the values of the corresponding ethanol systems are repeated for ease of comparison. By considering

the viscosity curves and relevant viscoelastic moduli (Fig. 3-22 to 3-25) one can gain information on the oil uptake of the microemulsions which is summarised in Table 3-16.

Table 3-15 Aggregate size of ethanol and propanol microemulsions

Surfactant	Ethanol as Cosurfactant-droplet size (nm)	Propanol as Cosurfactant-droplet size (nm)*
SDS	12$\pm$0.5	14$\pm$0.5
CTAB	12$\pm$0.5	14$\pm$0.5
Triton X-100	33$\pm$0.5	35$\pm$0.5
F127	36.5$\pm$0.5	36$\pm$0.5

*Droplet size and size distribution in propanol microemulsions are given in Appendix-D based on DLS results.

Table 3-16 Estimated oil volume fraction- ethanol versus propanol

Surfactant	Ethanol as Cosurfactant-Oil uptake (%)	Propanol as Cosurfactant-Oil uptake (%)
SDS	6$\pm$0.5	8$\pm$0.5
CTAB	14$\pm$0.5	16$\pm$0.5
Triton X-100	9$\pm$0.5	11$\pm$0.5
F127	9$\pm$0.5	7$\pm$0.5

*The calculations are based on Eq. 3-14 for CTAB and based on Eq. 3-13 for the other 3 microemulsion systems.
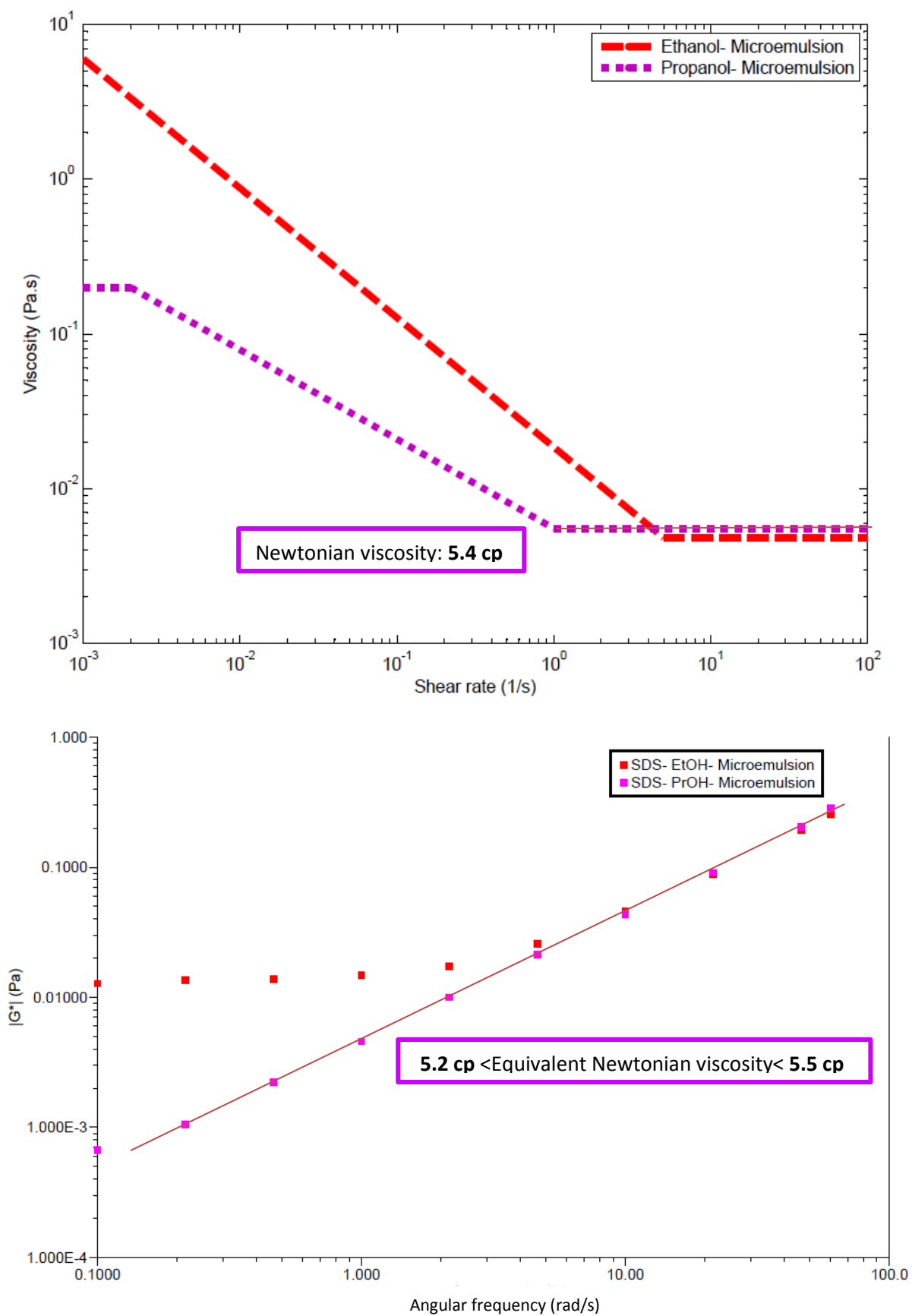
Fig. 3-22 SDS, ethanol and propanol microemulsions. Top: flow curves and bottom: viscoelastic moduli.
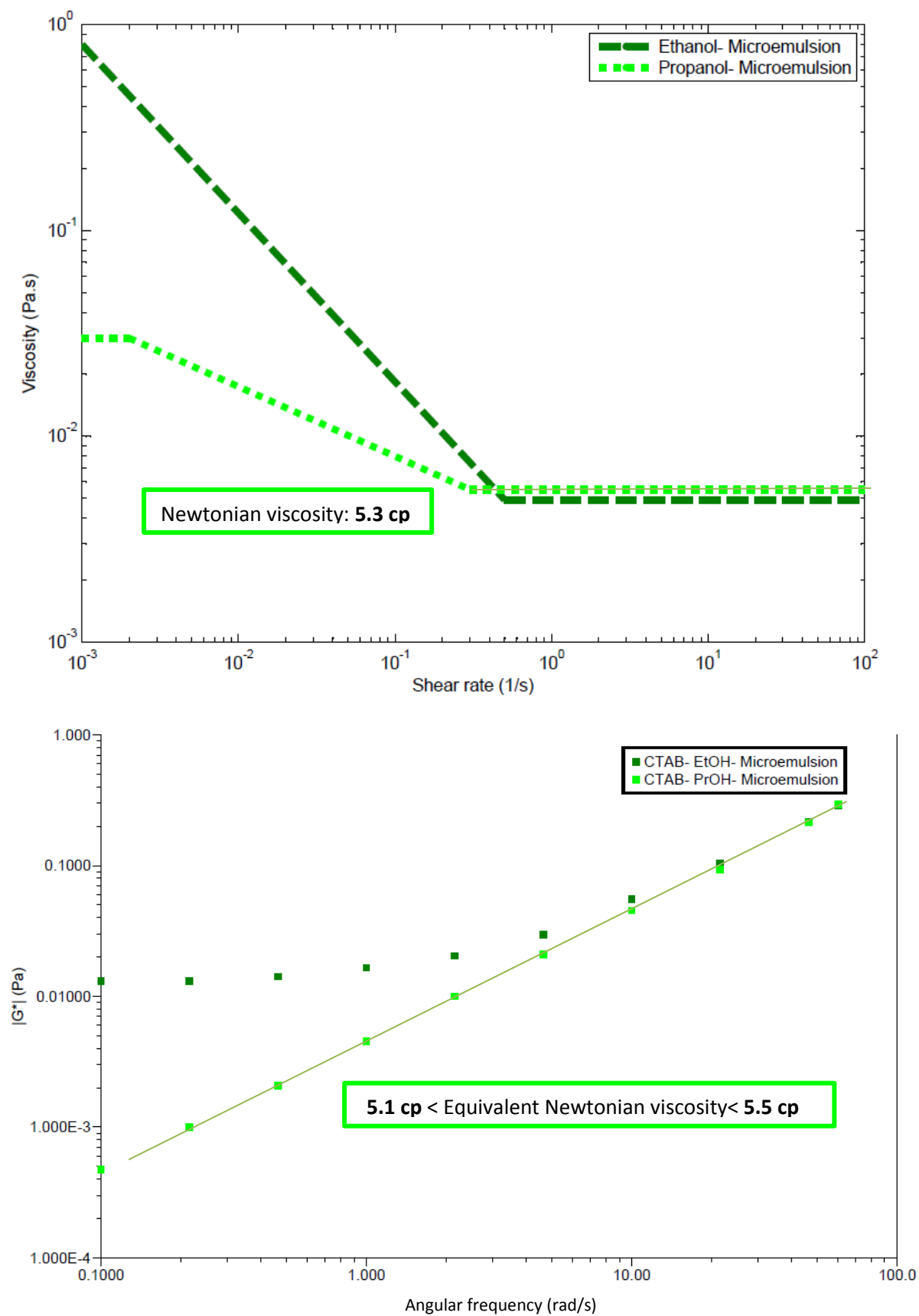
Fig. 3-23 CTAB, ethanol and propanol microemulsions. Top: flow curves and bottom: viscoelastic moduli.

Newtonian viscosity: **5.4 cp**

5.2 cp <Equivalent Newtonian viscosity< **5.5 cp**
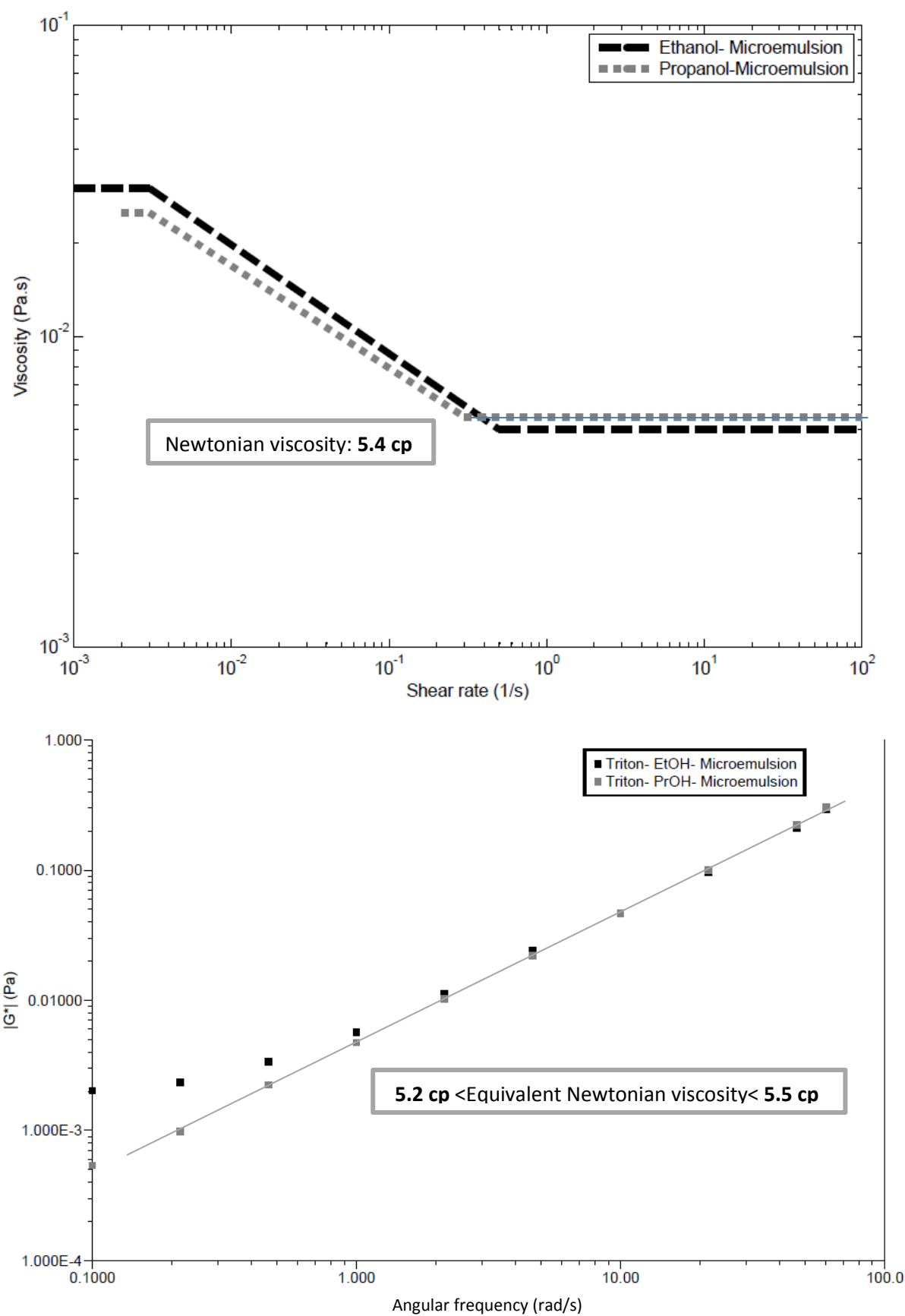
Fig. 3-24 Triton X-100, ethanol and propanol microemulsions. Top: flow curves and bottom: viscoelastic moduli.
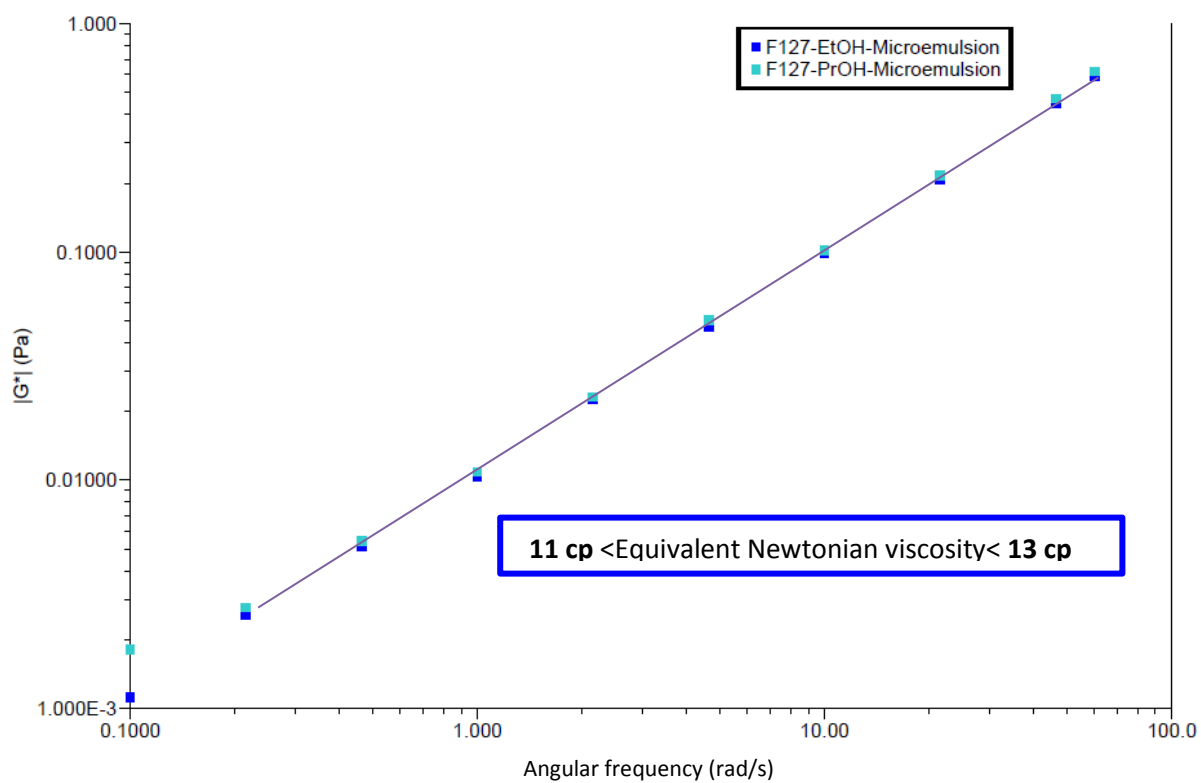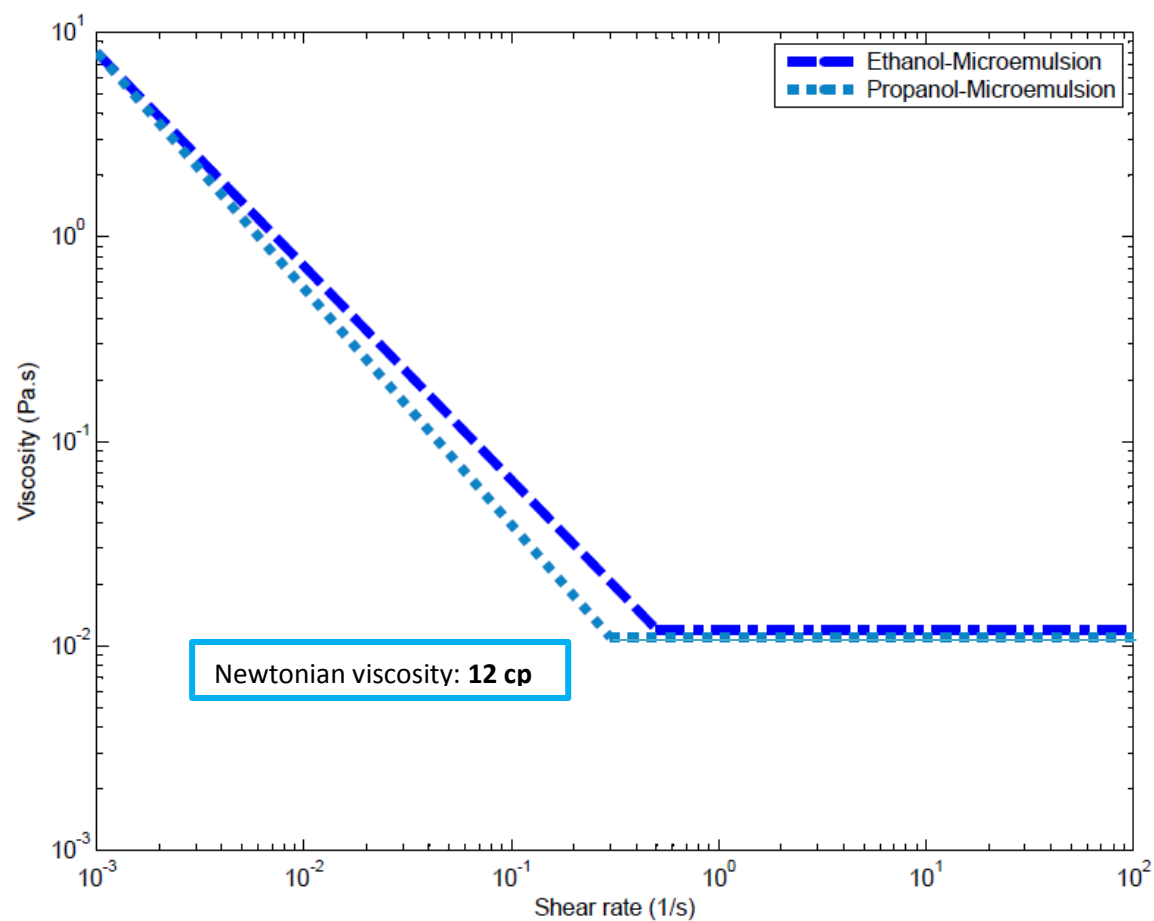
Fig. 3-25 F127, ethanol and propanol microemulsions. Top: flow curves and bottom: viscoelastic moduli.

As seen in Fig. 3-22 to 3-25, for those systems for which the yield stress behaviour, initial constant viscosity, is evident the data were collected with increasing shear rate. When decreasing shear rate is used, this low shear rate constant viscosity is not seen. This is consistent for all systems. There is no apparent correlation between which systems respond better to increasing or decreasing shear rate.

According to Fig. 3-22 to 3-24, the ethanol microemulsion systems show higher Newtonian viscosities as compared to the corresponding propanol microemulsions which is due to the larger droplet size and the higher oil volume fraction. For these three surfactants SDS, CTAB and Triton X-100, the Newtonian region of the propanol systems occurs at lower shear rates than for the ethanol systems indicating that the inter-droplet interactions are overcome at lower shear rates in propanol systems. This is related to the higher polarity of ethanol as compared to propanol and the ability of ethanol to bond to water molecules more strongly via hydrogen bonds. The data show that the trend with respect to the solid-like viscosity and the viscosity of the shear-thinning region of the ethanol systems are higher than those of propanol systems. In this region in contrast with what was concluded for the Newtonian region the larger the droplet, the less force is required to make the system deform. The reason is for smaller droplets the packing is more dense and ordered resulting in higher viscosity [70].

For the F127 system, Fig. 3-25, the only system in which the droplet size has, within uncertainty, remained unchanged upon replacing ethanol with propanol (36.5±0.5 nm to 36±0.5 nm) and the amount of oil uptake has decreased (9% to7%), the Newtonian viscosity has slightly decreased from 13 cp for the ethanol microemulsion to 12 cp for propanol microemulsion. This indicates that over the Newtonian region droplet size controls the viscosity. In this system, similar to the other three systems, the Newtonian region of the propanol microemulsion starts at a lower shear rate, indicating this transition is independent of the droplet size and oil volume fraction and is dictated by the intrinsic features of ethanol/water and propanol/water mixtures (see Section 3-1).

Dynamic frequency sweep data confirm the Newtonian viscosities obtained from the flow curves and also highlight the effect of the surfactant used where for anionic SDS and cationic CTAB, Fig. 3-22 and 3-23, the propanol microemulsions show Newtonian behaviour over the whole range of applied angular frequency, 0.1 rad/s to 100 rad/s, as compared to their relevant ethanol microemulsions that demonstrate Newtonian behaviour only beyond

an angular frequency of 10 rad/s. For non-ionic Triton X-100 both ethanol and propanol systems show Newtonian behaviour beyond 1 rad/s of angular frequency and in the case of non-ionic F127, where the droplet size of the ethanol and propanol systems are almost the same, similar Newtonian behaviour is observed for the two systems over the whole angular frequency range.

As seen in Table 3-15 and 3-16 the droplet size and oil up take have increased for SDS, CTAB and Triton X-100 indicating that the propanol partly contributes to the droplets (the interfacial layer and/or the core). This results in an increase in the droplet size and consequently an enhanced oil uptake.

In the case of F127, for some reason, the cosurfactant does not seem to contribute to the droplets. This might be due to the large molecular structure of F127, which is non-polar in most parts and repels the polar cosurfactant. Hence the propanol remains in the continuous phase. The decrease in the concentration of the cosurfactant at the interface results in an increase in the interfacial tension and consequently a decrease in the oil uptake.

3-2-5 Discussion

The viscosity of microemulsions depends on the droplet size, shape and packing pattern. Anionic and cationic surfactants, SDS and CTAB, give droplet sizes of about 12 nm; in these two systems not only the size but also the shape of the droplets match. Hence they display similar Newtonian viscosity. Non-ionic surfactants, Triton X-100 and F127, produce larger droplets, 33 and 36 nm. Although the sizes are similar they possess different droplet shape resulting in completely different Newtonian viscosities.

When microemulsions are compared to the relevant ternary solutions, the data obtained in this research showed that there is a direct relationship between the Newtonian viscosity ratio and the droplet size ratio (Eq. 3-9). This indicates that loading oil into the swollen micelles of the ternary surfactant solutions to prepare microemulsions, results in an equivalent change (increase) in both the droplet size and the Newtonian viscosity (this is an interesting finding and requires more investigation). However over the non-Newtonian region the behaviour in the microemulsion vs. its corresponding ternary surfactant system varies differently for different surfactants.

The effect of packing on rheology can be seen in the CTAB-based microemulsion where the significant structural change, from spherical to ellipsoidal, due to the addition of the oil, increases the maximum packing and significantly alters the flow behaviour.

The oil uptake is about 9% for the microemulsions made of non-ionic surfactants and ethanol. This amount is enhanced for CTAB and decreased for SDS. This indicates that there might be an inverse relationship between the oil uptake and the hydrophilic/lipophilic balance (HLB) of the surfactant. This can be explained by considering that the higher HLB, the more water solubility is anticipated and consequently less oil uptake (see HLB of the surfactants in Chapter 2, Table 2-2).

The oil uptake is strongly dependent on the chemical composition of the system and as soon as one ingredient, such as the short-chain alcohol is changed, the oil volume fraction is altered.

For rheological models to be applicable to microemulsions, the appropriate reference viscosity should be used which does not equate to the viscosity of the solvent or the continuous phase but rather the viscosity of the relevant ternary system, assuming that the shape of the aggregates has not significantly changed.

The above data and analysis results in the following three-component empirical model being proposed for microemulsions, similar to that for the surfactant solutions discussed previously, as follows:

$$\eta = \eta_0 \qquad\qquad \dot{\gamma} < \dot{\gamma}_1 \qquad\qquad Eq.\,3-4\;(Recalled)$$

$$\eta = \frac{A_{me}}{\dot{\gamma}^{n_{me}}} \qquad\qquad \dot{\gamma}_1 \; < \dot{\gamma} < \dot{\gamma}_2 \qquad\qquad Eq.\,3-15$$

$$\eta = \eta_{Newtonian} \qquad\qquad \dot{\gamma} > \dot{\gamma}_2 \qquad\qquad Eq.\,3-6\;(Recalled)$$

where $n_{me} = n_{microemulsion} = \dfrac{\eta_{Newtonian} - \eta_0}{\dot{\gamma}_2 - \dot{\gamma}_1}$

As discussed for surfactant solutions for the systems that have reached their Newtonian plateau by a shear rate of 1/s, the shear-thinning part of the model can be rewritten as:

$$\eta = \frac{\eta_{Newtonian}}{\dot{\gamma}^{n_{me}}} \qquad\qquad \dot{\gamma}_1 \; < \dot{\gamma} < 1 \qquad\qquad Eq.\,3-16$$

In such systems the value of *A* is the same as the value of the Newtonian viscosity, for the systems with Newtonian viscosity not occurring at 1/s *A* can be calculated as below:

$$at \ \dot\gamma = \dot\gamma_2: \ \eta_{Newtonian} \ = \frac{A}{\dot\gamma_2{}^{n_{me}}} \rightarrow A = \ \eta_{Newtonian} \ * \ \dot\gamma_2{}^{n_{me}}$$

The values of the A for the microemulsions made with ethanol and propanol are given in Table 3-17. The value of A can be assigned to the time scale of the system and therefore shows the time dependency of the system. The explanation for this is that the units of A as can be determined from Eq. 3-15 is $Pa.s^{n+1}$, this factor is called consistency coefficient and is representative of non-Newtonian behaviour of the system [71] since the rheometer that has provided the rheological data measures the viscosity at each shear rate by dividing shear stress by the shear rate, as if the behaviour is Newtonian at that point, and n=1 describes Newtonian behaviour the units of A becomes $Pa.s^2$ or in other words local Newtonian viscosity (with the units of $Pa.s$) times by the time scale of the system. Hence, the value of A is equited to a time that also shows the deviation from Newtonian viscosity.

Table 3-17 *A* of ethanol microemulsions and propanol microemulsion

Surfactant	*A* in ethanol-based system	*A* in propanol-based system
SDS	(19.5±0.1)E-3	(5.4±0.1)E-3
CTAB	(2.7±0.1)E-3	(3.5±0.1)E-3
Triton X-100	(3.7±0.1)E-3	(3.6±0.1)E-3
F127	(6.2±0.1)E-3	(3.0±0.1)E-3

As seen in Table 3-17 all systems have a representative time scale below 20 ms, indicating these samples are not time-dependant, in Section 5-2 it will be shown that for time dependant systems this parameter is more than 2 s. The highest A is for the SDS microemulsion system made with ethanol. This is due to the synergist effect of the surfactant and ethanol as explained in Section 3-2-1.

In Table 3-18 are given the values of n_{me} for ethanol microemulsions and n_{ss} of the ternary systems. n is an indicator of the rate of change from initial solid-like behaviour to the final Newtonian plateau. During this transformation the inter-connection between droplets breaks down; hence the packing of the droplets undergoes a transition until the droplet interactions tend towards zero and the flow curve reaches a plateau.

Table 3-18 n_{me} of ethanol microemulsions and n_{ss} of ternary aggregates

Surfactant	n_{me}	n_{ss}
SDS	0.84±0.01	0.89±0.01
CTAB	0.85±0.01	0.83±0.01
Triton X-100	0.38 ±0.01	0.39 ±0.01
F127	1.07±0.01	1.07 ±0.01

Considering the values of n_{me} and n_{ss} given in Table 3-18, demonstrates that the values for the ternary and microemulsion solutions of each system are similar. This explicitly demonstrates why we proposed that the reference system for a microemulsion should be the relevant ternary aggregate. The term *n* is most likely to be determined by the properties of the continuous phase and not the dispersed (oil) phase. The transformation from a ternary surfactant aggregate to its corresponding microemulsion by adding oil, results in an increase in the ethanol concentration in the continuous phase. As explained in Section 3-2-1, this decreases repulsive forces in the SDS-based system and attractive forces in the CTAB-based system. Hence the rate of shear-thinning to Newtonian behaviour, *n*, is decreased in SDS-based system (from 0.89 to 0.84) and increased in CTAB-based system (0.83 to 0.85). In the case of the nonionic surfactants the values of n_{SS} and n_{ME} have remained constant within uncertainty indicating the value of *n* is independent of the addition of the oil to the ternary aggregate.

In Table 3-19 are given the values of n_{me} for ethanol microemulsions and n_{me} for propanol microemulsions. The data in Table 3-19 show that the value of n_{me} upon replacing the short-chain alcohol (from ethanol to propanol) is significantly altered CTAB and SDS microemulsions. However n_{me} for the Triton X-100 and F127 ethanol and propanol microemulsions remain similar. This indicates that for non-ionic surfactants the effect of the hydrocarbon chain of the short-chain alcohol is minimal.

Table 3-19 n_{me} of ethanol and propanol microemulsions

Surfactant	n_{me} of ethanol system	n_{me} of propanol system
SDS	0.84±0.01	0.58±0.01
CTAB	0.85±0.01	0.35±0.01
Triton X-100	0.38 ±0.01	0.33±0.01
F127	1.07±0.01	1.14±0.01

It should be noted that the cosurfactant partly contributes to the continuous phase and partly to the interfacial layer, see Section 3-1-2 for more explanation. The more the cosurfactant contributes to the interfacial film the lower the interfacial tension becomes resulting in a decrease in the drag force within the system and consequently an easier transition to the Newtonian state upon applying an imposed shear rate. This means that such a system has a higher *n.* When the cosurfactant mostly contributes to the continuous phase, which hydrodynamically interconnects the droplets, the droplet interactions are enhanced and therefore the slope of the shear-thinning region decreases. Hence the higher *n* shows the lower contribution of the surfactant to the continuous phase. As seen in Table 3-19, for all the four systems except for F127 replacing ethanol with propanol has resulted in a lower n_{ME}. The reason is that propanol has a longer hydrocarbon chain and larger size than ethanol. Therefore the contribution of propanol to the interfacial layer is less than that of ethanol. In the case of F127, however the large non-ionic nature of the surfactant makes the interfacial layer more favourable for the Cosurfactant. In this case the n_{ME} of propanol system is higher than ethanol system, which might be due to the large structure of the surfactant that allows propanol molecules to contribute more to the interfacial layer.

3-3 Conclusion

Flow behaviour of microemulsions and their mother surfactant solutions were investigated. For all systems, three regions in the flow cure could be detected:

1- Initial solid-like behaviour

2- Shear thinning region

3- Newtonian region

The solid-like behaviour is seen only when the applied shear sequence is low to high.

The slope of the shear-thinning region, n_{ME}, is between 0.3 and 1.14 for all the microemulsions studied here. It was found that this factor is significantly affected by synergist impact of the surfactant and the short chain-alcohol, e.g. surfactant charge, charge density and the length of the alcohol hydrocarbon chain.

The Newtonian viscosity was found to be related to the droplet size inversely. The droplet size was between 12 and 15 nm for the ionic microemulsion systems and between 33 and 37 nm for non-ionic systems. Furthermore the following relationship found to be held:

$$\frac{\eta_{Newtonian}}{Droplet\ size} = constant.$$

In microemulsions made with ethanol, the Newtonian viscosity appears to be independent on the oil uptake where η_{∞} was obtained experimentally to be about 5 cp for microemulsions made with SDS, 6 % oil uptake, CTAB, 14 % oil uptake, and Triton X-100, 9 % oil uptake and 13 cp, 9 % oil uptake, for the microemulsion made with F127. However, it was evident that the oil uptake is similar for non-ionic surfactants; highest for the cationic surfactant, CTAB; and lowest for the anionic surfactant SDS. This is due to the ionic strength of the system along with the HLB (see Table 2-2) of the surfactant; e.g. the higher HLB the lower oil uptake.

Newtonian viscosity was found to be considerably affected by the droplet shape. Non-ionic microemulsions made with F127 and Triton X-100 with similar droplet size and oil uptake show different Newtonian viscosities (13 and 5 cp, respectively) due to F127 forming more elongated micelles (*J* factor 9.6 for F127 system and 4.1 for Triton X-100 system).

Although the microemulsion systems investigated are dilute (with a maximum oil concentration of 14 %), calculating the maximum packing using the Krieger-Dougherty modified relationship, Eq. 3-14, allows information on the microstructure to be gained. Based on this relationship a tetrahedral morphology is suggested for SDS, Triton X-100 and F127 microemulsions made with ethanol and a cubic morphology for the dodecane/CTAB/ethanol/water microemulsion (see Table 3-14).

Flow properties were altered upon changing the Cosurfactant from ethanol to propanol. To study this, the partition coefficient of the surfactant, in the continuous phase and the

interfacial layer should be taken into account. This is determined by the length of the hydrocarbon in the cosurfactant.

In all cases to calculate the relative viscosity of a microemulsion the viscosity of the corresponding ternary aggregate, measured in Section 3-1, was used otherwise the applied models would not fit the experimental data.

Nanoemulsions

Nanoemulsions are metastable systems, in contrast to microemulsions (which are generally considered to be thermodynamically stable) despite often having over-lapping droplet size ranges. Energy needs to be consumed in order to generate a nanoemulsion while microemulsions form spontaneously. In this research, nanoemulsions were prepared through a two-step low-energy method [11] from an initial microemulsion solution [72], the preparation method is explained in Chapter 2. The flow properties of the generated systems prepared using this method are reported here. For the CTAB and Triton X-100 systems, the flow curves indicate that the initial microemulsions have merely undergone dilution, whereas for both the F127 and SDS systems nanoemulsions have been obtained that show fundamentally different flow behaviour than the corresponding microemulsions. This microemulsion to nanoemulsion transition upon dilution is studied and explained well by Solans and co-worker [73] where they have shown that a dodecane/SDS/pantanal or hexanol/water microemulsions can transform into nanoemulsions upon dilution due to the migration of the cosurfactant partly to the continuous phase. This therefore results in an increase in the interfacial tension and thermodynamic stability is lost.

Wulff-Perez *et al*. have demonstrated that nanoemulsions show non-Newtonian behaviour which is dependent on their oil concentration during preparation of the nanoemulsions [74]. The microemulsions were diluted to one fifth of their original oil concentrations. The corresponding oil concentrations in the diluted nanoemulsion systems are given in Table 4-1.

**Table 4-1** Oil weight fraction of the diluted microemulsions

Microemulsion	Weight percentage
SDS	1.2±0.1%
CTAB	2.8±0.1%
Triton X-100	1.8±0.1%
F127	1.8±0.1%

Given that the oil volume fractions in the diluted systems are one fifth of that in the microemulsions, the viscosity is expected to be lower than that of the microemulsions and to tend towards 2.5 cp; the limit discussed in Chapter 3 indicating that the morphology has become more globular.

By considering the flow curves and dynamic rheological data attributed to the four systems, summarised in Table 4-2 (Fig. 4-1 to 4-4), it is immediately evident that for the CTAB and Triton X-100 systems the typical flow behaviour is shear-thinning behaviour followed by a Newtonian region which is typical for our microemulsions as discussed in Chapter 3. The Newtonian viscosity of these systems was calculated using the models discussed in Chapter 3, with the reference viscosity used being that of the relevant ternary system as was shown previously to be appropriate.

In contrast, the diluted microemulsion solutions of F127 and SDS show non-Newtonian behaviour over the whole range of applied shear rates, e.g. 0.001/s – 100/s. Furthermore both solutions were blueish, as nanoemulsions are expected to look. Both of these changes indicate that nanoemulsions have been formed upon dilution of the concentrated microemulsions. Their non-Newtonian behaviour at high shear rates is due to thermodynamic instability. The Gibbs energy is positive and the droplets move faster due to dilution and possible morphology changes and exhibit lower viscosity; therefore the external shear force cannot dominate the system to be driven into Newtonian behaviour.

The two-step low energy method for nanoemulsion formation only works when the original microemulsion is in a particular phase state (see [69] for more information in this regard). This condition is evidently only met for the F127 and SDS microemulsions and not the Triton X-100 and CTAB microemulsions. The full microemulsion regions of the respective phase diagrams were not explored in this research.
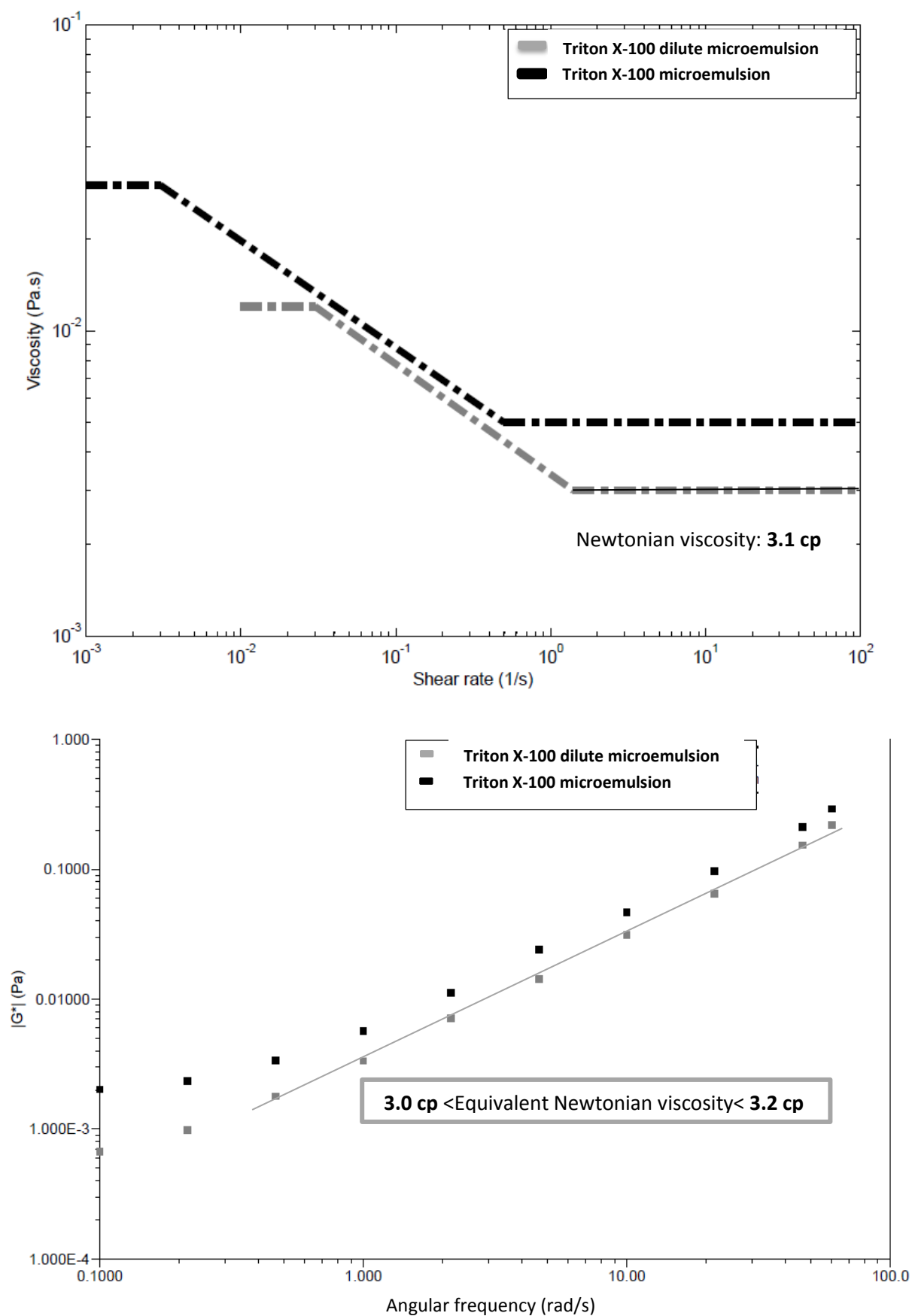
Fig. 4-1 Static and dynamic rheological results for triton X-100 microemulsion and the corresponding diluted microemulsion.

Newtonian viscosity: **2.1 cp**

2.0 cp < Equivalent Newtonian viscosity< **2.2 cp**
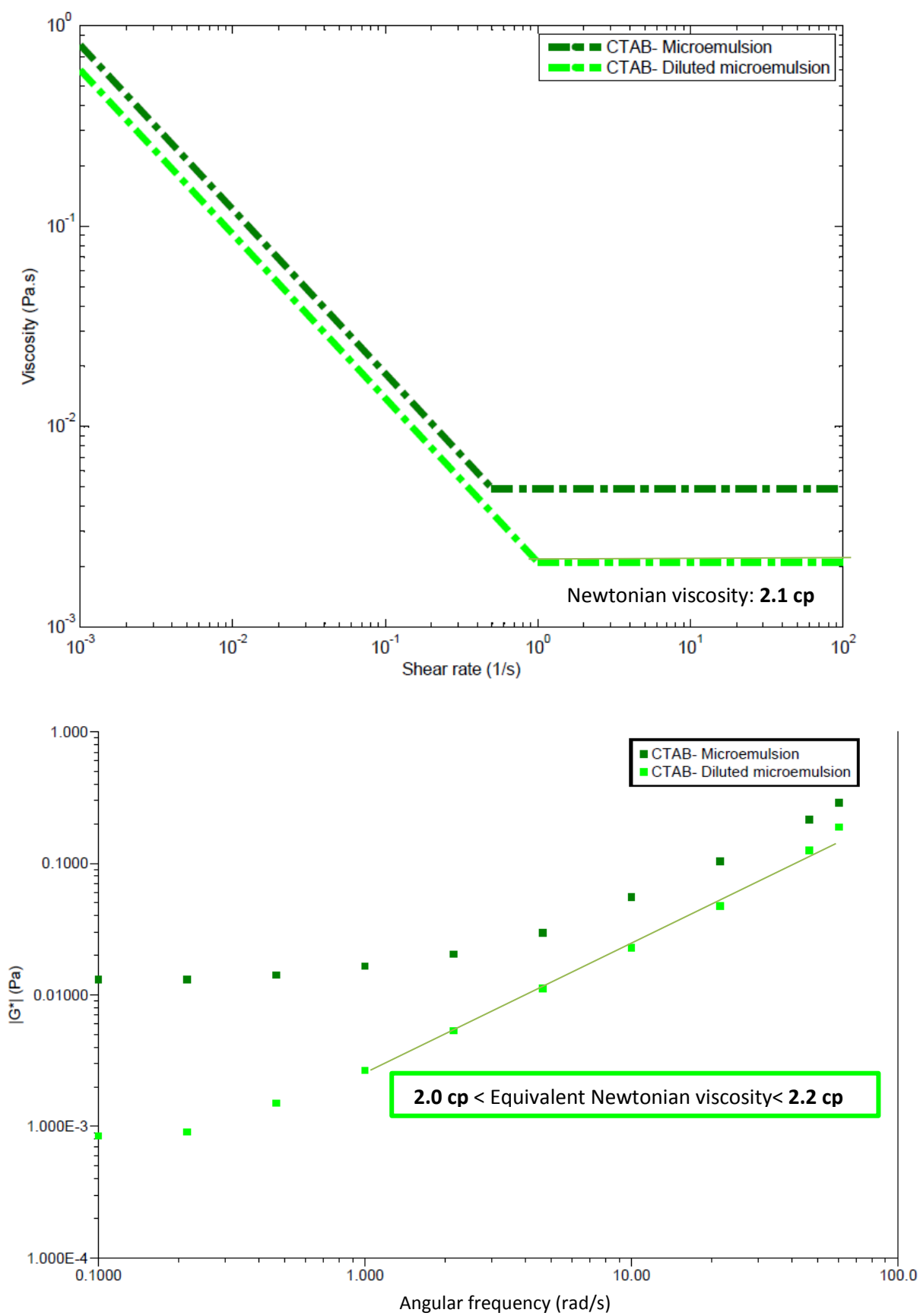
Fig. 4-2 Static and dynamic rheological results for CTAB microemulsion and the corresponding diluted microemulsion.
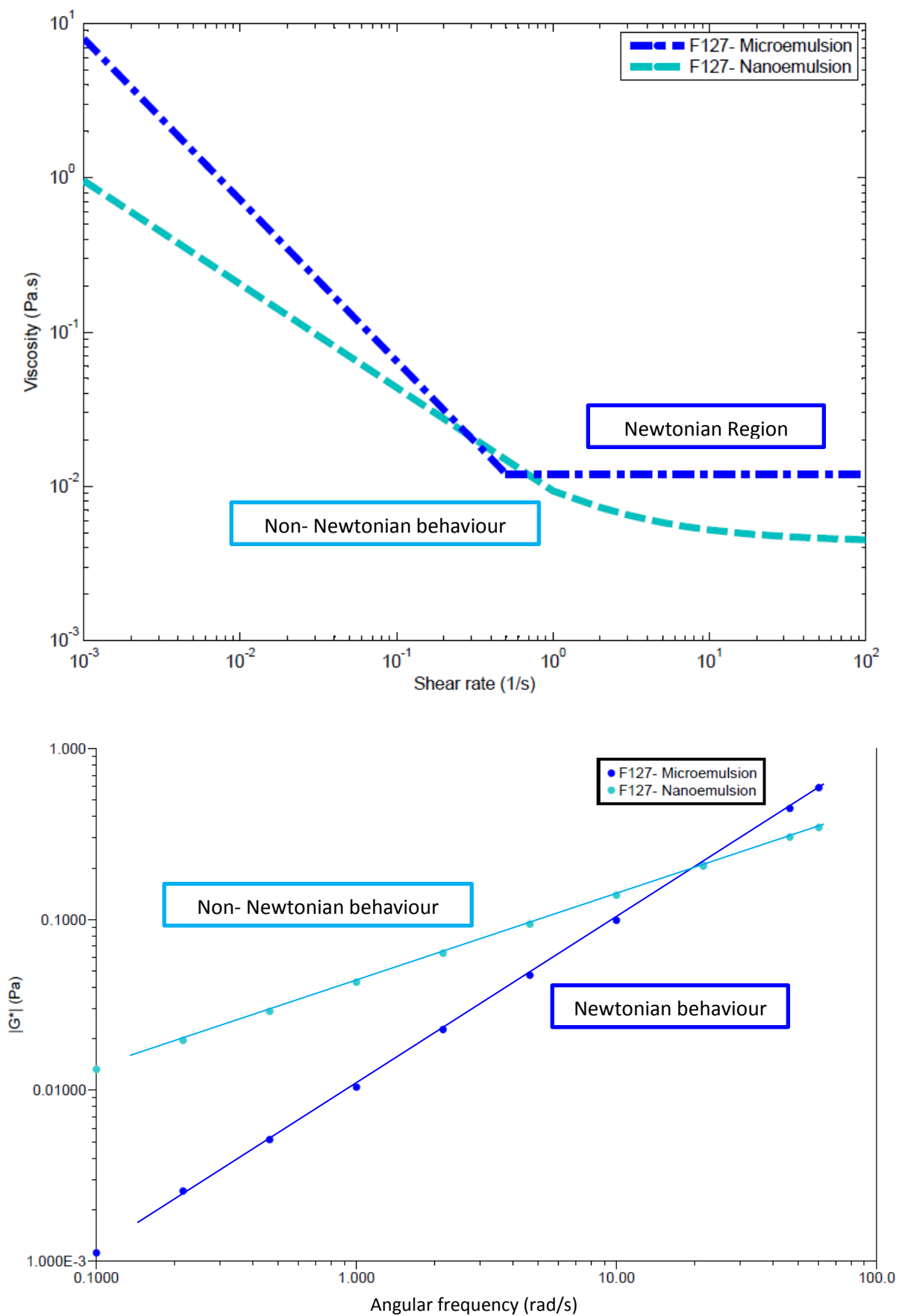
Fig. 4-3 Static and dynamic rheological results for F127 microemulsion and the corresponding nanoemulsion.

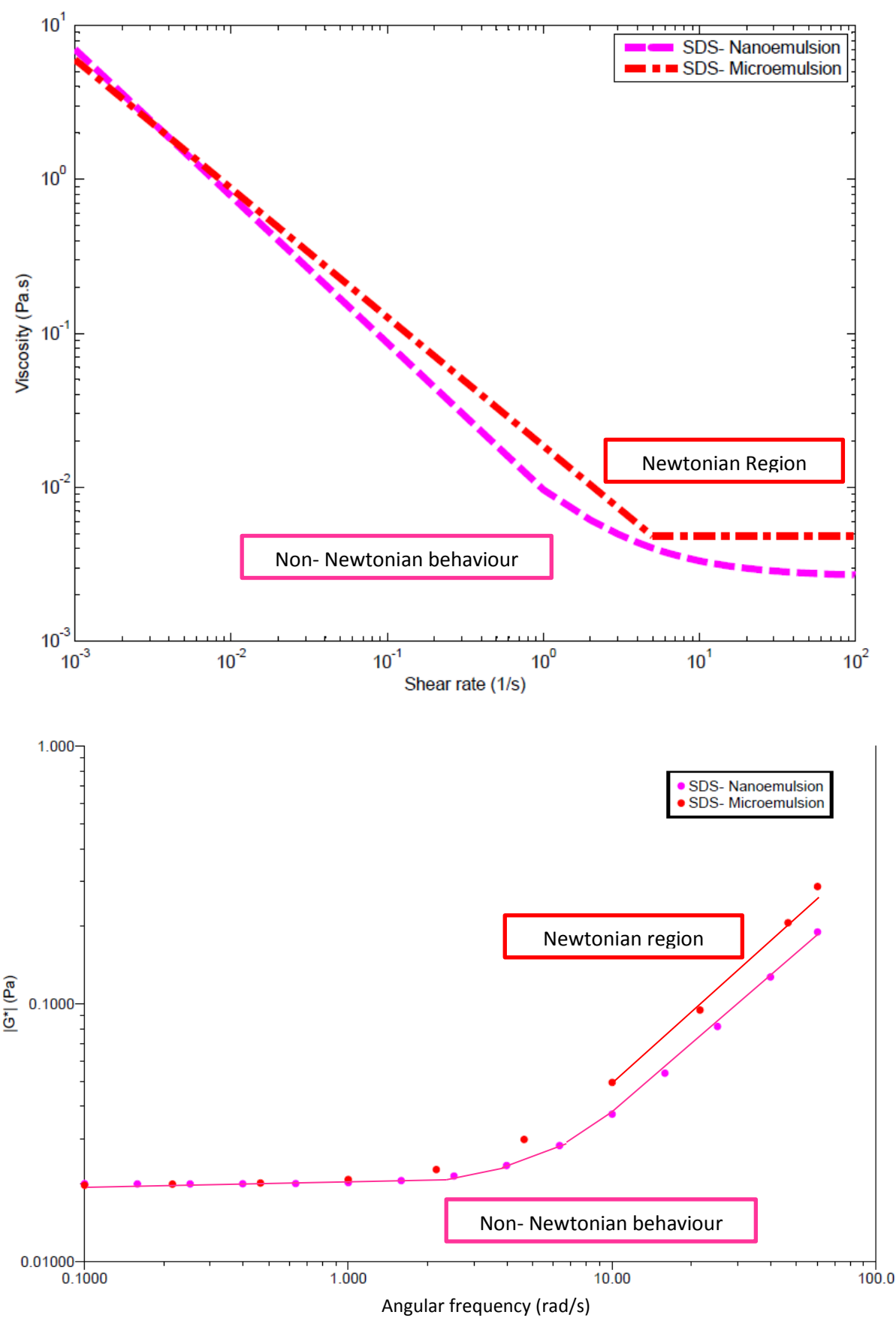**Fig. 4-4** Static and dynamic rheological results for SDS microemulsion and the corresponding nanoemulsion.

In the case of the CTAB and Triton X-100 systems where mere dilution of the microemulsion has occurred (Fig. 4-1 and 4-2), the flow behaviour can be modelled using the proposed model for microemulsions as discussed in Chapter 3. For the Triton X-100 system all three parts of the flow curve are evident therefore the three-term model needs to be applied. For the CTAB system in contrast since the viscosity is recorded versus a decreasing shear rate, only the last two terms of the model are required. In Table 4-2 the attributed parameters for these systems are reported.

Table 4-2 Comparison between concentrated and diluted microemulsions

System	η_0	n_{me}	η_∞
Triton X-100, 9 wt. % oil	0.030±0.001	0.37±0.01	0.0048±0.0001
Triton, 1.8 wt. % oil	0.012±0.001	0.38±0.01	0.0031±0.0001
CTAB, 14 wt. % oil	---	0.82±0.01	0.0049±0.0001
CTAB, 2.8 wt. % oil	---	0.82±0.01	0.0021±0.0001

The zero and infinite viscosities of the concentrated systems are higher than those of the diluted ones due to the reduced oil volume fraction as expected; however the slope of shear-thinning region has not change upon dilution. This demonstrates that this slope is independent of the volume fraction and size and shape of the system and is determined principally by the inherent makeup of the system, e.g. the chemicals which form the microemulsions.

The relationship between the viscosity and the shear rate for the F127 and SDS nanoemulsions can be considered by fitting the following empirical formula to the data which is basically a combination of the power law model and an infinite viscosity. The fits are included in Fig. 4-3 and 4-4, respectively.

$$\eta = \eta_\infty + \frac{A}{\dot{\gamma}^{n_{ne}}} \qquad\qquad Eq.\,4-1$$

Table 4-3 Values of the parameters in Eq. 4-1 for SDS and F127 nanoemulsions

Nanoemulsion	n_{ne}	A	η_∞ (cp)
SDS	1.00 ± 0.01	0.011 ± 0.001	2.6 ± 0.1
F127	0.76 ± 0.01	0.005 ± 0.001	4.3 ± 0.1

The parameters for both systems are given in Table 4-3. n_{ne} is representative of the rate of transition toward the Newtonian region. For the SDS system this rate is higher than for the F127 system due to the lower molecular weight of SDS allowing it to flow more easily. *A* is the time scale of the system. This value is the difference between the viscosity at the shear rate of 1/s and the infinite viscosity (solve Eq. 4-1 for $\dot{\gamma}$=1). Therefore there is a direct relationship between n_{ne} and *A*. However η_∞ is dictated by droplet size as will be discussed in the next section.

4-1 Effect of size and shape

The observed changes in the rheological response for all four systems cannot be explained by dilution alone, droplet size and shape are also important. The droplet sizes of the concentrated and diluted systems measured using DLS are given in Table 4-4.

Table 4-4 Estimated droplet size of concentrated and diluted systems

Surfactant	Microemulsion droplet size (nm)	Diluted Microemulsion droplet size (nm)
CTAB	12 ± 0.5	10 ± 0.5 (microemulsion)
Triton X-100	33 ± 0.5	30 ± 0.5 (microemulsion)
SDS	12 ± 0.5	11.5 ± 0.5 (nanoemulsion)
F127	36.5 ± 0.5	35 ± 0.5 (nanoemulsion)

The droplet sizes reported in Table 4-4 are hydrodynamic diameters, which inherently depend on the shape of the droplet. Hence, although the droplet volume is constant upon dilution, the hydrodynamic size has decreased in all cases due to the transition from a more ellipsoidal to a more spherical morphology with a diminishing effect in the order CTAB, Triton X-100, SDS and F127. Considering the Newtonian viscosities of the concentrated and

diluted microemulsions of the CTAB and Triton X-100 systems respectively, one can calculate the J factor [57]. The following relationships correlate the ratio between the hydrodynamic diameter of an ellipsoid and a sphere to the relevant J factor of the ellipsoidal structure (Eq. 4-2 and 4-3) [57].

$$\frac{d_H}{d_0} = \frac{\sqrt{1-J^2}}{J^{\frac{2}{3}} \ln\frac{1+\sqrt{1-J^2}}{J}} \qquad \text{if } J < 1 \qquad\qquad Eq.\,4-2$$

$$\frac{d_H}{d_0} = \frac{\sqrt{J^2-1}}{J^{\frac{2}{3}} \tan^{-1}\sqrt{J^2-1}} \qquad \text{if } J > 1 \qquad\qquad Eq.\,4-3$$

where d_H is the length scale of the ellipsoid (the diameter of a sphere diffusing with the same speed as the ellipsoid) and d_0 is the diameter of a sphere of the same volume as the ellipsoid. Let d_{H_1} be the hydrodynamic diameter of the concentrated microemulsion and d_{H_2} the hydrodynamic diameter of the diluted system. The ratio between the hydrodynamic diameters can then be calculated as:

$$\frac{d_{H_1}}{d_{H_2}} = \frac{\left.\sqrt{J_1^{\,2} - 1}\middle/ J_1^{\frac{2}{3}} \tan^{-1}\sqrt{J_1^{\,2} - 1}\right.}{\left.\sqrt{J_2^{\,2} - 1}\middle/ J_2^{\frac{2}{3}} \tan^{-1}\sqrt{J_2^{\,2} - 1}\right.} \qquad\qquad Eq.\,4-4$$

where J_1 and J_2 are attributed to the concentrated and diluted systems, respectively.

The values of J and d_H/d_o are given in Table 4-5 for the CTAB and Triton X-100 systems.

Considering the values given in Table 4-5, the droplet sizes (Table 4-4) and Eq. 4-4 one can see that Triton X-100 and CTAB microemulsions undergo an ellipsoidal to globular transition upon dilution.

Table 4-5 The values of J and d_H/d_o for Triton X-100 and CTAB concentrated and diluted microemulsions

| System	J	d_H/d_o
Triton X-100- Con.	4.17±0.01	1.18±0.01
Triton X-100- Dil.	2.29±0.01	1.06±0.01
CTAB-Con.	4.26±0.01	1.20±0.01
CTAB-Dil.	2.00±0.01	1.00±0.01

As seen in Table 4-4, the characteristic droplet length scale for the SDS and F127 systems (which form nanoemulsions upon dilution from microemulsions) has decreased significantly less than in the case for the CTAB and Triton X-100 systems that represent diluted microemulsions, to calculate this the difference between the averaged droplet size before and after dilution were divided by the original droplet size of the relative microemulsion. This gives 17%, 9%, 4% and 4% for CTAB, Triton, SDS and F127 systems respectively. The chemical and structural properties of the systems allow SDS and F127 to undergo microemulsion-nanoemulsion transition. Fig. 4-5 to 4-8 show the differences between the size of concentrated and diluted microemulsions, data obtained from DLS experiments.
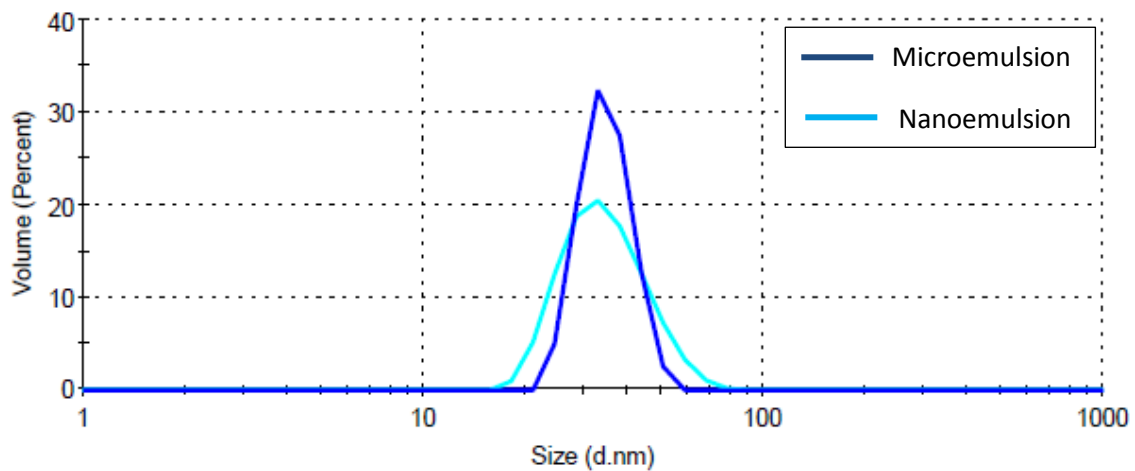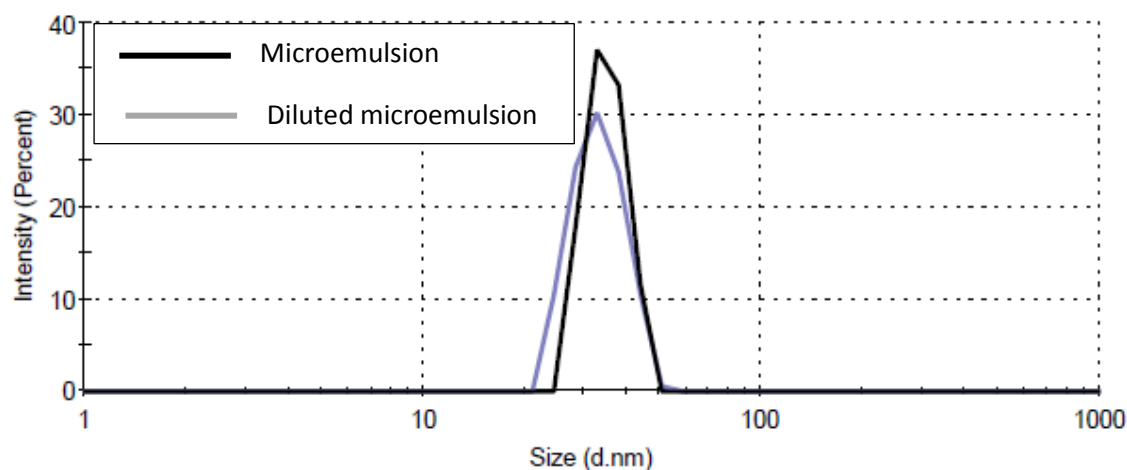

Fig. 4-5 Size distribution of F127 microemulsion and the corresponding nanoemulsion.
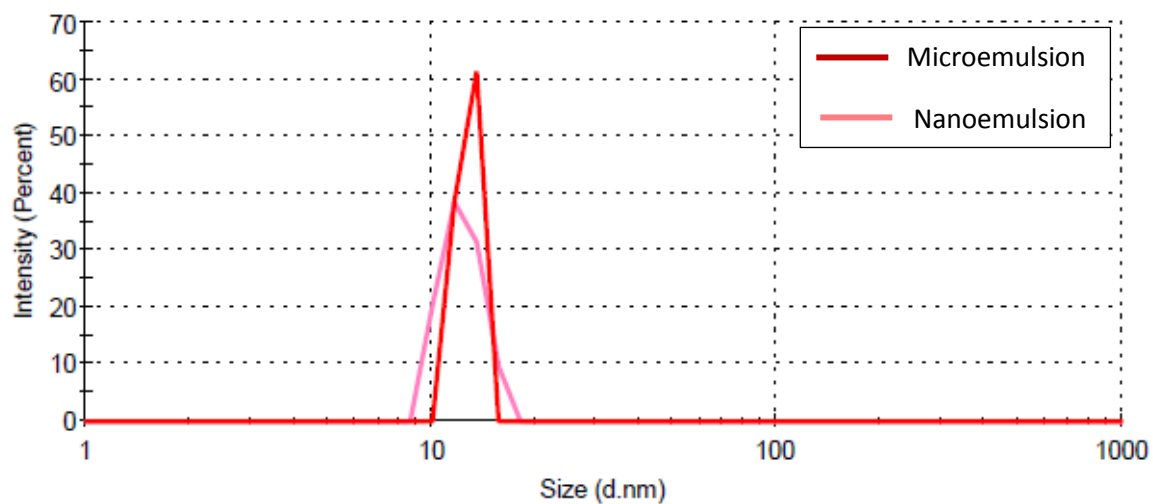
Fig. 4-6 Size distribution of SDS microemulsion and the corresponding nanoemulsion.
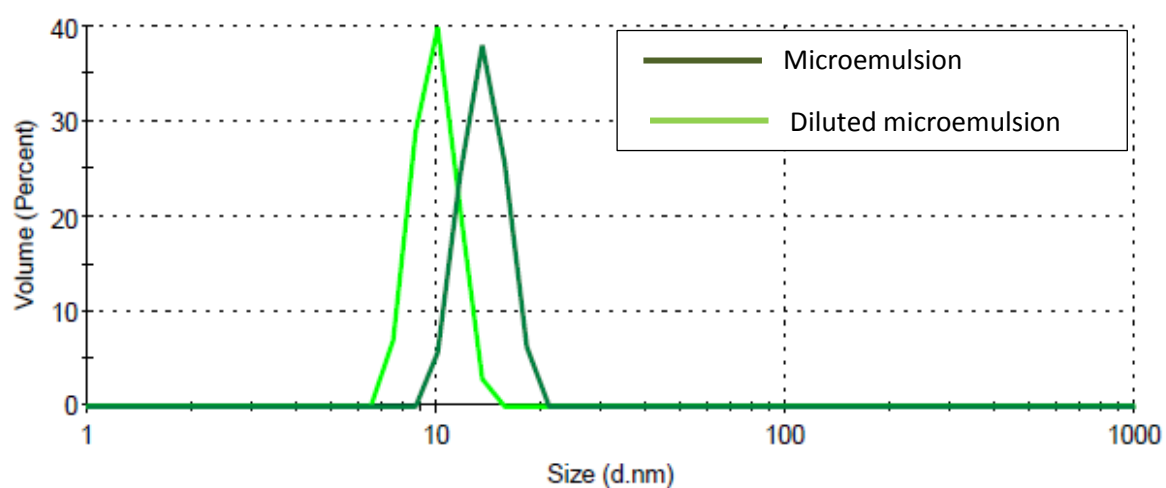
Fig. 4-7 Size distribution of CTAB microemulsion and the corresponding diluted microemulsion.

Fig. 4-8 Size distribution of Triton X-100 microemulsion and the corresponding diluted microemulsion.

As seen in Fig. 4-5 to 4-8 the polydispersity in the dilute systems is increased as compared to the corresponding mother microemulsions. The reason is that, as previously explained, upon dilution the concentration of the cosurfactant at the interface decreases resulting in the curvature being altered. In the case of SDS and F127 (Fig. 4-5 and 4-6), the size distribution of the dilute system is broadened around the average droplet size of the mother microemulsion. In the case of SDS the broadening is not considerable and the size distribution of the both microemulsion and nanoemulsion are similar within uncertainity however the maximum intensity decreased in the nanoemulsion as compared to the microemulsion confirming the polydispersity of this system is higher than that of the microemulsion (see Fig. 4-6). In these systems the thermodynamic stability has transformed to a kinetic stability due to the enhanced polydispersity. In the case of CTAB and Triton X-100 the microemulsion-nanoemulsion transition has not occurred. The increase in polydispersity is slightly less (Fig. 4-7 and 4-8) with a new thermodynamic stability being achieved in the dilute microemulsions pronounced. The size distributions in such systems are centred around a smaller value as compared to their mother systems. It should be noted that any process that stops the cosurfactant from leaving the interfacial layer can stop the microemulsion-nanoemulsion transition as well. For example in the case of CTAB the positive charge of the surfactant forms a dipole interaction with the short-chain alcohol, cosurfactant, which may be the reason for the system not undergoing a microemulsion-nanoemulsion transition.

4-2 Discussion

By diluting a microemulsion, the system may either undergo a microemulsion-nanoemulsion transition or be merely diluted. Which occurs depends on the underlying phase behaviour and interactions inherent in the system. A phase transition occurs in the case of the larger non-ionic (F127) and anionic surfactants (SDS). Nanoemulsions show non-Newtonian behaviour even at high shear rates. The infinite viscosity of the SDS nanoemulsion (2.6 cp) is lower than that of the F127 nanoemulsion (4.3 cp). This is reasonable given the difference in the chemical structures of the two surfactants, the total dispersed phase volume fraction (1.2 vs. 1.8 wt. %) and the droplet size (11.5 nm vs. 35 nm) of the two nanoemulsion systems. The viscosity of the SDS nanoemulsion at low shear rates is however higher than that of the F127 nanoemulsion; this is due to the added ethanol used to prepare the nanoemulsion. This increase in viscosity upon the addition of ethanol to an SDS/water solution was discussed previously, see Chapter 3.

The cationic surfactant (CTAB) and the small non-ionic surfactant (Triton X-100) systems in contrast do not experience the microemulsion-nanoemulsion transition. Like our other microemulsions, these systems display Newtonian behaviour at high shear rates.

The hydrodynamic droplet size of the microemulsions decreases upon dilution. This is due to the corresponding shape change (from ellipsoidal to spherical) (Fig. 4-1 and 4-2, Table 4-4 and 4-5).

The droplet size of nanoemulsions is similar to that of their relevant microemulsions; however the size distribution, polydispersity, is enhanced.

As the thermodynamic stability terminated within a sample (e.g. microemulsion to nanoemulsion transition) the flow curve follows a more complicated pattern. In this case, for F127 and SDS nanoemulsions, Eq. 4-1, which is derived from the Sisko model, can be applied to determine the viscosity vs. shear rate.

In conclusion, the effect of thermodynamic instability can be observed in the flow curve. In Section 5-2 the rheological behaviour of emulsions will be discussed so that the reader will see that the flow curve of nanoemulsions follow the same model as emulsions.

4-3 Conclusion

Flow properties of nanoemulsions, produced through microemulsion-nanoemulsion transition using the low energy method were investigated.

Using this method ensured that the nanoemulsion systems studied were chemically similar to their mother microemulsions, with only slightly altered length scale and lower dispersed phase concentration due to the dilution. The nanoemulsions form due to the change in the system free energy resulting from the dilution and not due to input of external energy (normally preparing nanoemulsions requires large amounts of energy being imposed on the system). It was found that the flow behaviours of these nanoemulsions are not comparable with those of microemulsions.

It was found however that the same model used to fit the microemulsion rheology data is also applicable to the nanoemulsions behaviour. The difference between the nanoemulsions and their corresponding microemulsions was that the nanoemulsions do not have a Newtonian region within the range of applied shear rate, 0.001/s to 100/s, while the microemulsions systems display Newtonian behaviour. This shows that the thermodynamic stability of microemulsions make their flow behaviour simpler than the corresponding kinetically stable nanoemulsions.

The reduced stability in nanoemulsion systems can be further observed in their slightly higher polydispersity as compared with the corresponding microemulsions.

Considering and comparing the flow behaviour of the nanoemulsions and their mother microemulsions enabled us to explore the relationship between the effect of diluting microemulsions, stability and length scale all in a single work which has not been done previously.

Emulsions

Emulsions have variety of applications in different industries. Rheological measurement can be used as a tool in order to design a system for a specific need. Size and size distribution are very important factors that affect emulsion flow behaviours.

## 5-1 Coarse monodisperse emulsion preparation- continuous process

As discussed in Chapter 1 & 2, to generate monodisperse coarse emulsions a microfluidic divice was exploited. The general physics governing such a system, e.i. single phase and multi-phase fluid mechanics, was explained in Chapter 1 however the relationships needs to include geometry parameters in order to perfectly match a given geometry [74].

5-1-1 Geometry-dependent Capillary and Reynolds numbers

As discussed in Chapter 2, coarse monodisperse emulsion droplets are generated in a microfluidic chip after the two phases meet, typically form a jet and finally breaks into droplets through the break-up process. The concept of forming the jet before the break-up point depends on the shear rate and the surface tension (the ratio of them is represented by the capillary number (Eq. 2-5). Furthermore in a flow-focusing device the orifice is also important to consider. Anna *et al*. have rewritten the capillary number given in Eq. 2-5 such that it now contains geometry characteristics:

$$Ca = \frac{\mu_0 \gamma a}{\sigma_{EQ}} = \frac{\mu_0 a \, \Delta u}{\sigma_{EQ} \Delta Z} = \frac{\mu_0 a \, Q_c}{\sigma_{EQ} h \Delta Z} \left(\frac{1}{W_{OR}} - \frac{1}{2W_{UP}} \right) \qquad\qquad Eq. 5-1$$

where μ_0 is the viscosity of the outer phase, σ_{EQ} is the equilibrium surface tension, γ is the shear rate, Q_c is the volume flux of the continuous phase, h is the depth of the channel, and other parameters are as labelled in Fig. 5-1. This relationship is derived for a flow-focussing parallel stream device (Fig. 5-1).
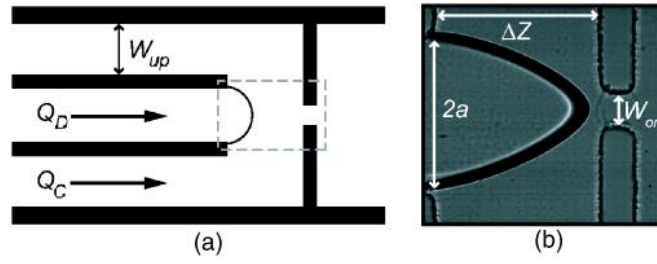
Fig. 5-1 Microfluidic flow-focusing geometry. (a) Continuous phase is delivered through the side channels and the dispersed phase through the central channel. (b) Mixing zone in the microchip. W_{up} = 280 µm, a = 90 µm, ΔZ = 180 µm, and W_{or} = 34 µm (adopted from [75]).

It can be seen from Eq. 5-1 that Anna *et al.* have replaced the velocity term with shear rate times the radius of the inner channel. This radius is the distance in which the flow velocity changes from zero at the wall up to the maximum at the centre. They also replaced the shear rate with the velocity gradient divided by the distance (ΔZ). The stream experiences a change in its speed related to the area through which it passes and if the volume flux is used instead of velocity, the final form of the capillary number will be achieved.

$$Q = A.u \qquad\qquad Eq.5-2$$

where Q is the volume flux, u is velocity and A is the area.

Anna *et al.* also defined the Reynolds number for the continuous and dispersed phases as:

$$Re_C = \frac{\rho u_{UP} W_{UP}}{\eta_o} = \frac{\rho_o Q_C}{h\eta_o} \qquad\qquad Eq.5-3$$

$$Re_D = \frac{\rho_i Q_D}{h\eta_i} = \frac{(\rho_i/\rho_o)}{\emptyset\lambda} Re_C \qquad\qquad Eq.5-4$$

where $\emptyset = \frac{Q_C}{Q_D}$ is the flow rate ratio, λ is the viscosity ratio and h is the depth of the channel. ρ_o and ρ_i are the densities of the outer and inner liquid respectively. η_o and η_i are the viscosities of the outer and inner liquid respectively. Q_C and Q_D are the volume flux of the continuous and dispersed phases respectively. u_{UP} is the velocity of the upstream (single phase fluid) and W_{UP} is the width of the channel which carries the continuous phase.

110

5-1-1-1 Modified flow focusing geometry

In a microfluidic device two phases are pumped using syringes and are delivered to micro-channels through plastic tubes. To do that programmable syringe pumps are applied and the flow rate (volume flux) is set. It is for this reason that flux is used instead of velocity in Eq. 5-1 to 5-4.

In the microchip which has been used in this research (Fig. 2-3) two side streams (continuous phase) meet the central flow (dispersed phase) at 60° and then the flow passes through an orifice, the width of which is comparable to the channels entering the open terrace in which droplets form and go through to the exit channel.

Xu *et al*. have studied monodisperse droplet formation using the same device [76]. The angle between the streams imposes a shear rate to the system so that the capillary number increases and break-up occurs more easily. However, since the break-up is affected by many parameters at the same time, such as the flow-rate ratio, the viscosity ratio and the interfacial tension (the concentration of the surfactant), the process is complicated and typically leads to the requirement of experimental models specific to the system. For example Anna *et al*. have shown four different break-up processes for a given flow focusing geometry that can be achieved by varying experimental parameters (Fig. 5-2). As the capillary number increases, the droplet formation mode changes from geometry controlled to thread formation and then dripping followed by jetting.
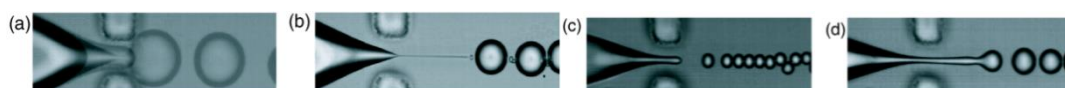
Fig. 5-2 Different droplet formation modes in a flow focusing microfluidic device: (a) Geometry-controlled (b) thread formation (c) dripping, and (d) jetting (adapted from [75]).

Before discussing the different droplet formation modes, it is assumed that all other parameters are held constant. Hence, at low capillary number droplet formation is fully controlled by the geometry itself so Eq. 5-1 holds and the droplet diameter is comparable to the orifice width. As the capillary number increases, the tip of the central stream is drawn beyond the orifice and the droplets form. The stream then retracts and this phenomenon

occurs periodically. This mode may yield polydisperse droplets due to the long droplet formation period which results in the formation of satellites along with the primary droplets. As the capillary number continues to increase, the break-up point returns back to be near the orifice, the formation period gets shorter and droplets form more steadily. At higher capillary numbers, due to high velocity, there is not enough time for mass transfer between two phases to take place. As a result, the break-up point shifts beyond the orifice and because of inefficient mixing droplet size may be comparable to the orifice width even though the break-up point is away from the orifice and these droplets appear not to be monodisperse [75].

Based on the above discussion, by increasing the capillary number one can shift the droplet formation mode from geometry-controlled to hydro-dynamically-controlled.

Xu *et al*. have tried to overcome the dependency between droplet size and the geometry [76] and as can be seen in Fig. 5-3 the droplet formation mode is comparable to those shown in Fig. 5-2 and thread formation, dripping and jetting can be observed. It should be mentioned that the flow ratio under which these experiments have been performed by Xu *et al*. [76], is higher than that used by Anna *et al*., ~225 and ~40, respectively [75].
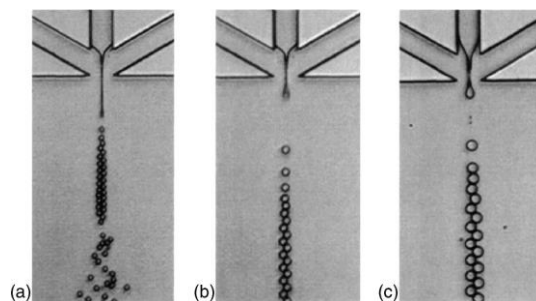
Fig. 5-3 Different droplet formation mode (adopted from [76]).

On the other hand, Monahan [77] has shown a series of geometry-controlled droplet break-up modes in his Master's thesis work for flow ratios up to 10, showing that by decreasing the flow ratio droplets of a diameter comparable to the channel width or height can be generated (Fig. 5-4).
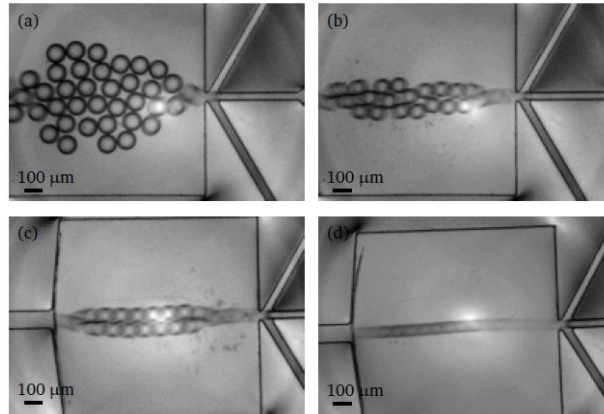
Fig. 5-4 Droplet break-up for flow rates, Ø of: (a) Ø = 2.5 (b) Ø = 5 (c) Ø = 7.5 (d) Ø = 10; as the continuous phase flow rate increases, the dispersed phase is thinned and produces a narrower stream (adapted from [77]).

Another important factor in droplet break-up is the concentration of the surfactant which affects the capillary number by changing the interfacial tension, σ. Taylor began investigating droplet deformation and break-up [78]. These studies were then applied to a microfluidic device in the case of elongation and tip-streaming (jet formation) and eventually break-up. Bruijn [79] has demonstrated that break-up is enhanced when the concentration of the surfactant increases. This is due to the decrease of interfacial tension. Hu *et al.* [80] have shown that the concentration gradient of the surfactant affects the break-up mode causing tip-streaming phenomenon to occur.

We should emphasize that the viscosity of complex fluids such as emulsions, strongly affects the droplet formation and break-up process [81]. It should be noted that as soon as two phases meet a viscoelastic complex fluid forms, the flow properties of which are completely different as compared to the individual components. One of the most important factors used to define the flow properties of complex fluids is the droplet size which can be altered by manipulating the three factors that make up the capillary number:

- the viscosity term which can be changed via the oil component of the emulsion. For example, a nearly four-fold change can be achieved by switching from normal dodecane (η = 1.34 mPa.s at 20 ℃) to polydimethylsiloxane (PDMS) (η = 5 mPa.s at 20 ℃);

- the interfacial tension term which can be changed by changing the emulsifier or the concentration of the emulsifier. The interfacial tension for each of the systems was measured (see Appendix B). Pluronic F127 and SDS were used at different concentrations as emulsifiers. The interfacial tension, σ, of a dodecane/5% aqueous solution of F127 is 4.8 mN/m while it is reduced to 3.2 mN/m in dodecane/1% aqueous solution of SDS as compared to 25 mN/m in dodecane/pure water. σ in PDMS/4% aqueous solution of F127 is 6.5 mN/m and 9.6 mN/m in PDMS/1% aqueous solution of SDS and 35 mN/m in PDMS/pure water, as measured by interfacial tensiometry; and

- the velocity term can be changed using the flow rates of the two phases (oil and water) in the microfluidic device.

5-1-1-2 Size probing: Pore Hopping Analysis

Studying an oil-in-water emulsion system, Callaghan *et al.* [36] have demonstrated that the signal attenuation recorded from PGSTE experiments, as explained in Chapter 2, is related to the water pore separation length, *b*, between oil droplets in an oil in water emulsion from which the microstructure can be estimated. It should be noted that the system under investigation is assumed to be spherical and loosely packed [36], e.g. concentrated emulsions. If one defines the reciprocal space vector, *q*, as equal to γgδ/2π, then the attenuation will be:

$$M(q,\Delta) = |M_0(q)|^2 \exp\left(-\frac{6D_{eff}\Delta}{b^2 + 3\,\xi^{\,2}}\left(1 - exp(-2\pi^2 q^2\,\xi^{\,2})\frac{sin(2\pi qb)}{2\pi qb}\right)\right) \quad Eq.\,5-5$$

where:

$$|M_0(q)|^2 = \left|\frac{3(2\pi qa\,\cos(2\pi qa) - \,\sin(2\pi qa))}{(2\pi qa)^3}\right|^2 \qquad\qquad Eq.\,5-6$$

where *b* is the mean pore water spacing and ξ is the standard deviation based on a Gaussian distribution, D_{eff} is the long-range diffusion coefficient for Brownian motion through the permeable structure and $|M_0(q)|^2$ is the form factor of the pores, considered as spheres with a diameter of *a*.

Romoscanu *et al.* [82] have fitted NMR data to this model for an oil-in-water emulsion with droplet size around 35 μm, and showed that this method has a high ability to predict the

emulsion structure. This model was established for glassy spherical beads with rigid surfaces, hence the dynamics of the interface are not taken into account, resulting in deviation of the model at high q-value [77]. Romoscanu *et al*. [82] claimed that the oil droplet size and structure information can be extracted from the extrema of the model.

5-1-1-3 Results and Discussion

Diffusion–NMR data, and specially PGSTE as applied to emulsions can provide information on the microstructures of emulsions. Diffusion-NMR was performed on five monodisperse emulsions with droplet sizes given in Table 5-1. Signal attenuation was recorded vs. q (see Chapter 2 for more information on the method). The diffraction curves were then fitted to Eq. 5-5 in order to extract the minimum (Fig. 5-5). Looking at Eq. 5-6 one would determine that $|M_0(q)|^2$ does not take minus values and the minimum occurs when this term goes toward zero. The q at which $|M_0(q)|^2$ equals zero is called q_{min} and is written as Eq. 5-7 [15]:

$$a = \frac{0.75}{q_{min}} \qquad\qquad Eq.\,5-7$$

where a is the droplet radius.

The droplet sizes calculated using Eq. 5-7 are given in Table 5-1:

Table 5-1. Details of the five systems studied, estimated droplet size as calculated through Eq. 5-7

System	Oil	Surfactant	Surfactant concentration (wt. %)	Droplet size (µm)
1*	Dodecane	F127	5%	40
2*	Dodecane	F127	5%	36
3	Dodecane	SDS	1%	32
4	PDMS	F127	4%	32
5	PDMS	SDS	1%	30

* The only difference between System 1 and 2 is that the flow rate of the continuous phase is 8 mL/hr and 12 mL/hr respectively. This will be discussed in this chapter.
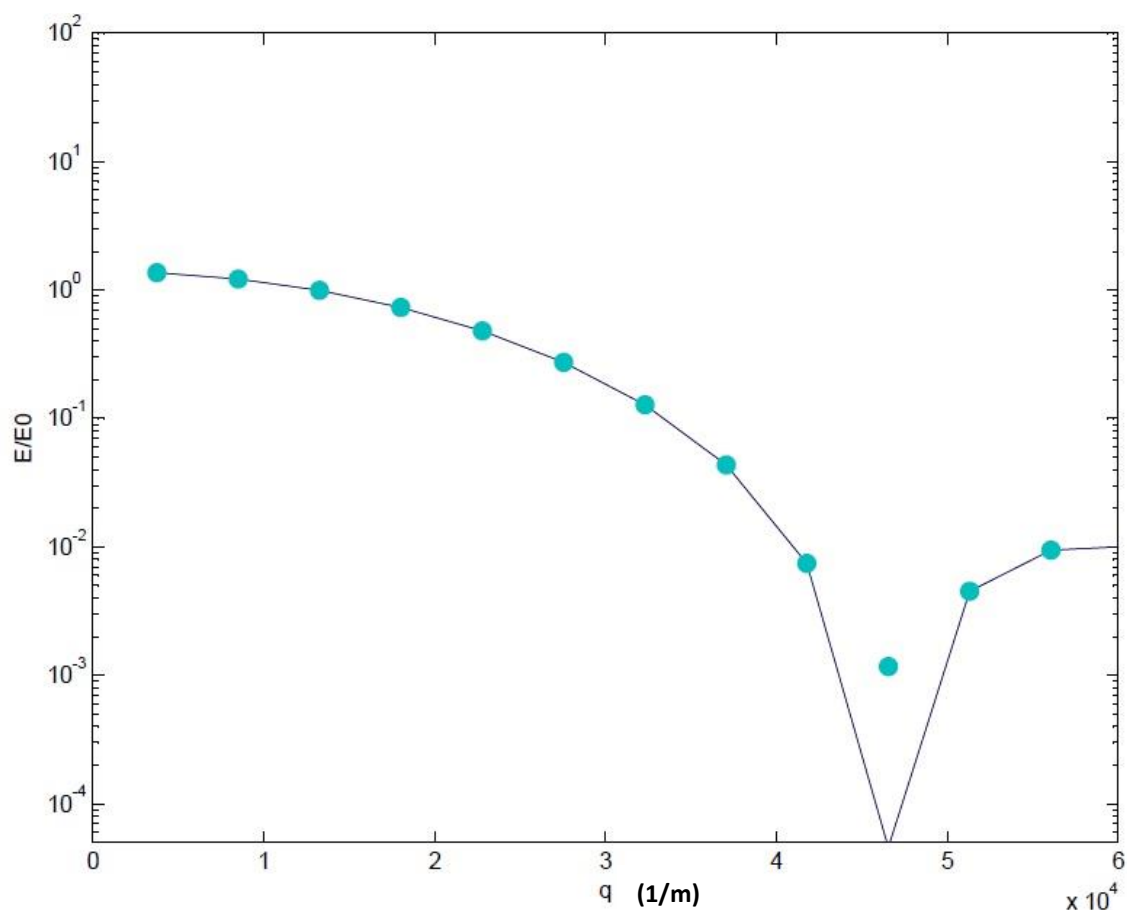
Fig. 5-5 Diffusion NMR data for the PDMS/F127/water emulsion, System 4 fit with Eq. 5-5**.**

To simplify the calculations the term that is multiplied by the form factor, $|M_0(q)|^2$ in Eq. 5-5, is replaced with a coefficient B which is representative of packing and polydispersity (Eq. 5-8) The corresponding B factor of each system is given in Table 5-2.

$$M(q, \Delta) = B|M_0(q)|^2. \qquad\qquad Eq.\, 5-8$$

Table 5-2. Droplet size and B factor of the emulsions

| Emulsion	B
System 1- Dodecane/F127	1.000±0.025*
System 2- Dodecane/F127	1.000±0.028
System 3- Dodecane/SDS	1.000±0.031
System 4- PDMS/F127	1.000±0.031
System 5- PDMS/SDS	1.000±0.033

*The uncertainties are calculated based on the uncertainty in the droplet size, e.g. 1/40=0.025.

The obtained values of B as reported in Table 5-2 are very close to one for all the systems confirming these systems are monodisperse. In Fig. 5-5 are shown the diffusion NMR data for System 4 as an example of the data obtained for the five systems. By fitting the data to Eq. 5-8, B can be calculated as a fitting parameter. In Fig. 5-5 the minimum occurs at q 47000/m, and the droplet radius is calculated through Eq. 5-7. The droplet size in this system is 32 ± 1 μm.

Eq. 5-8 can be modified [77] in order to probe the effect of polydispersity (Eq. 5-9).

$$M(bimodal) = x_1 B|M_{01}(q)|^2 + (1 - x_1)B|M_{02}(q)|^2. \qquad Eq.\ 5-9$$

For the purpose of testing this, a bimodal system made of 50% PDMS/F127/water and 50% PDMS/SDS/water was prepared and investigated using the diffusion-NMR technique. The relevant data are shown in Fig. 5-6.
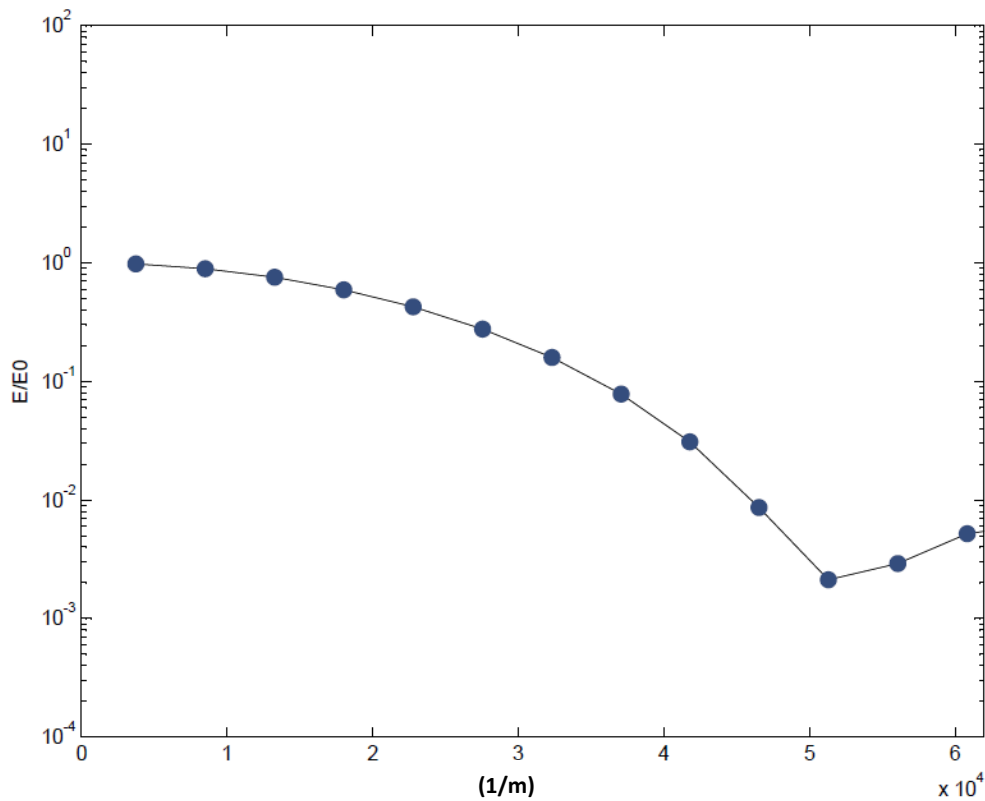
Fig. 5-6 Diffusion NMR data for a bimodal system made of 50% PDMS/F127/water and 50% PDMS/SDS/water fit using Eq. 5-9.

As seen in Fig. 5-6, once polydispersity is introduced into the system, despite the fact that the two droplet sizes used are similar, we start to lose the minimum in the curve. However the value of a q of about 51000/m is still evident which is relevant to a droplet size of 30 μm, indicating the smaller droplet size is more likely to be detected using this method. This is consistent with the smaller droplets dominating the restricted diffusion data.

Performing the same experiment also on a mixed system but now of higher polydispersity, 47.5 wt. % of the PDMS/F127/water, 47.5 wt. % PDMS/SDS/water and 5 wt. % PDMS/SDS/water emulsion with droplets of about 20 μm* (which is 2/3 of the droplet size of the majority of the droplets) shows the continued loss of coherency in the data evidenced by the loss of the minimum (Fig. 5-7).

For Eq. 5-8 to be applicable to such polydisperse systems, it must be further modified [77]. Hence, we proposed the following relationship.

$$M(Polydisperse) = B \sum_i x_i |M_{0i}(q)|^2 \qquad\qquad Eq.\,5-10$$

We note that the factor B is attributed to the whole system. Considering the parameters that make this factor (see Eq. 5-5) shows that the only structural parameter included in B in this form of the equation is b, the mean pore water spacing, that is an averaged value for the entire system. However, since the majority of each system under investigation in this research possesses a B with a value around the unity (see Table 5-2), this factor would be omitted from the relationship. This means that the most important factor here is the volume fraction of the monodisperse individuals, x_i, that make up the polydisperse system.

----

* These droplets are the result of the flow rate of the pump not being set to the proper values. In this case small droplets form as a by-product (about 10% of the total droplet population).
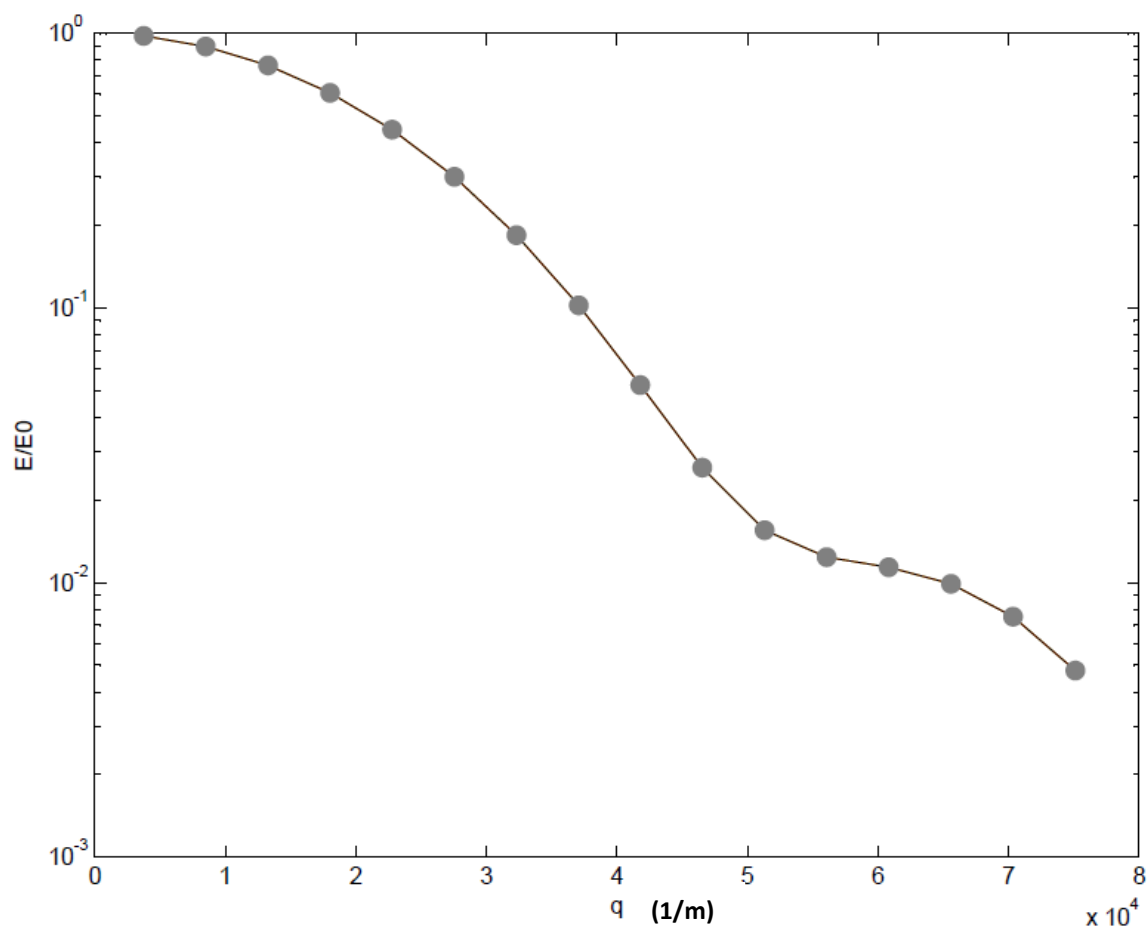
Fig. 5-7 Diffusion NMR data for a polydisperse system fit to Eq. 5-10. Systems: PDMS/F127/water mixed with PDMS/SDS/water.

In Table 5-3 are given the Reynolds and capillary numbers for the five systems (see Table 5-1 for sample information) investigated. The capillary number is dependent on the physical and geometrical characteristics as expected [83].

Table 5-3. Measured capillary numbers for different systems with relevant droplet sizes

System	η_{oil} (mPa.s)	σ (mN/m)	Q_c^* (mL/hr)	Q_d^{**} (mL/hr)	$A_{channel}$ (μm^2)	Re	Ca
1	1.34	4.8	8.0	1.00	50×100	44.4	0.124
2	1.34	4.8	12.0	1.00	50×100	66.6	0.186
3	1.34	3.2	6.5	0.10	50×60	36.1	0.252
4	5	6.5	6.0	0.04	50×100	33.3	0.256
5	5	9.6	6.0	0.10	50×60	33.3	0.289

* Flow rate of the continuous phase.

** Flow rate of the dispersed phase.

Interfacial tension, which was measured by the pendent drop method using a tensiometer apparatus, was used in order to calculate the capillary numbers given in Table 5-3 (see Appendix B for more information). Evaluation of the values in Table. 5-3, shows that the Reynolds numbers of the continuous phase is always between 1 and 100 indicating the fluid flow is not completely laminar. The Reynolds number of the dispersed phase is much lower since the flow rate of the dispersed phase is lower than that of the continuous phase (see Table 5-3) and there is a direct relationship between the Reynolds number and the flow rate. This means the oil flow is more laminar. The flow rate of the continuous phase vs. the corresponding Reynolds number is plotted and shown in Fig. 5-8.
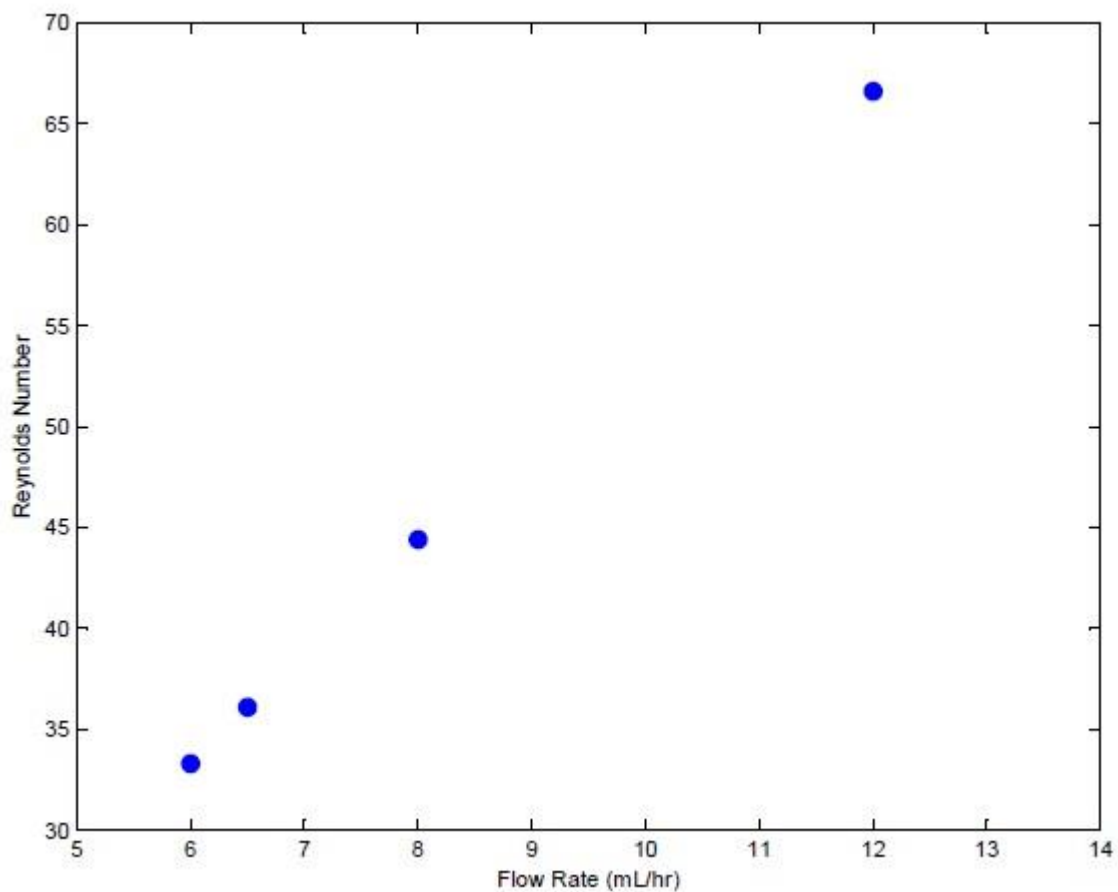
Fig. 5.8 The linear relationship between the Reynolds number and the flow rate of the continuous phase.

Further, it is evident that there is an inverse relationship between the capillary number and the relevant droplet size in each system regardless of the material which has been used to make the system. The relevant data are shown in Fig. 5-9.
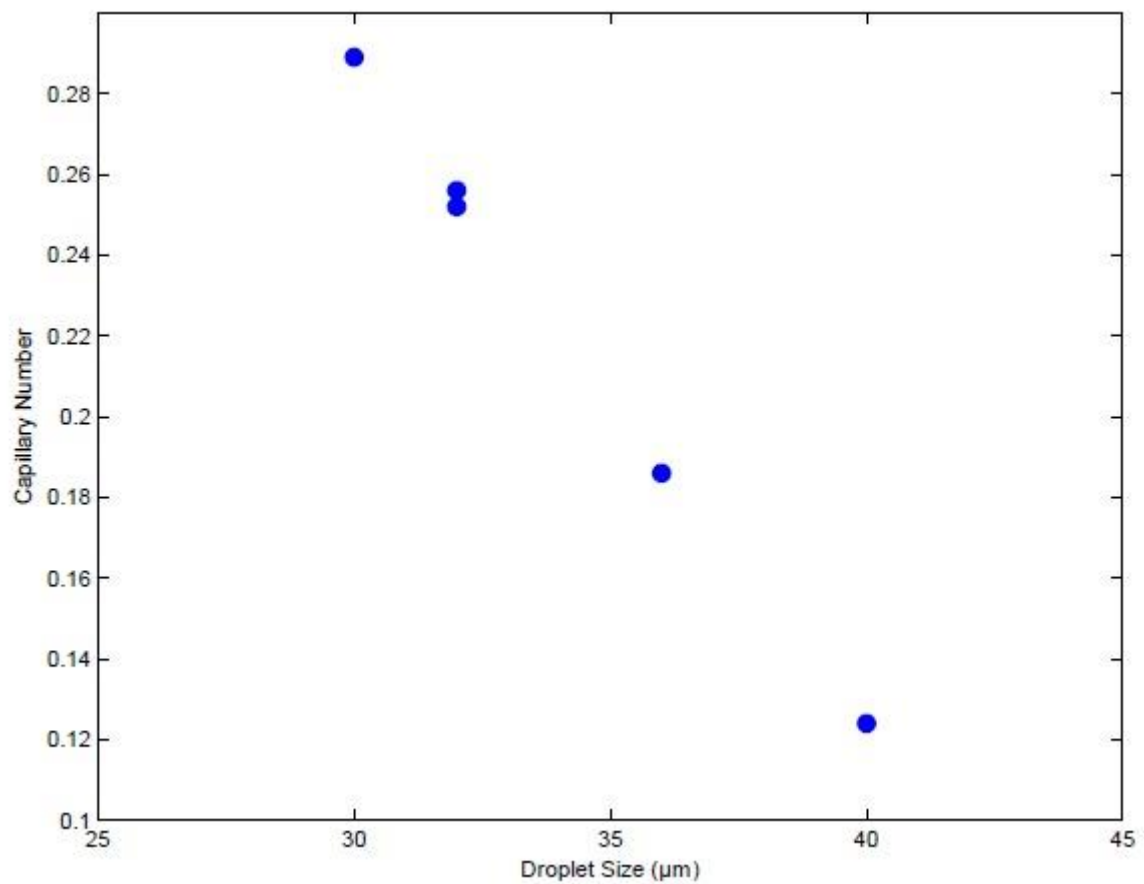
Fig. 5-9 Capillary number as an inverse function of droplet size.

As seen in Fig. 5-10, the stream of formed droplets after the break-up point is multi-branched for Systems 1 and 2. As the flow rate increases from System 1 to 2 the stream narrows. On the other hand, multi-branched streams do not occur for Systems 3, 4, and 5, due to the high flow ratio between the continuous phase and the oil phase in these systems (Fig. 5-11) [76] & [65].
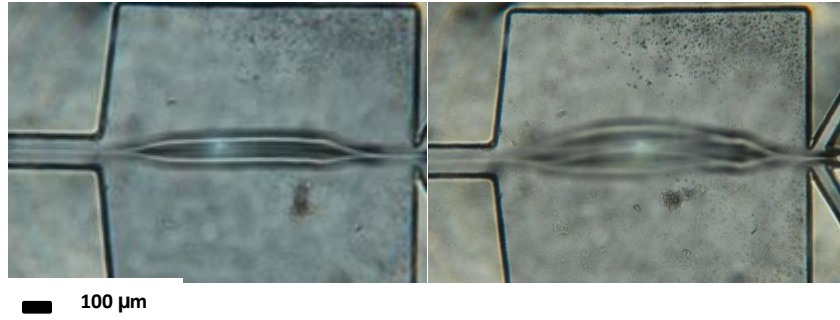
Fig. 5-10 Droplet streams for Systems 1 and 2 showing multi-branching. The flow rate of the continuous phase is 8 mL/hr (*right*) for System 1 and 12 mL/hr (*left*) for System 2. The flow rate of the oil phase is 1 mL/hr in both systems. As the flow ratio increases the stream narrows.
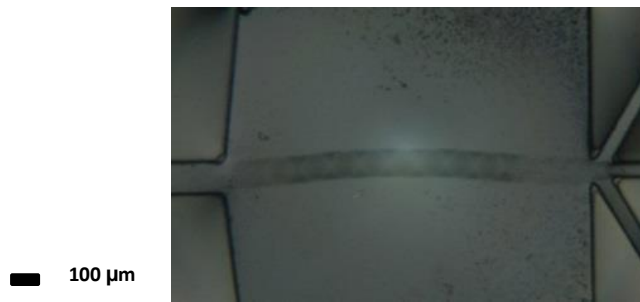
Fig. 5-11 Representative droplet stream for Systems 3, 4 and 5.

As seen in Fig. 5-8 and 5-9 there is a direct relationship between the flow rate of the continuous phase and the Reynolds number and an inverse relationship between the capillary number and droplet size. This means that by knowing the physical properties of the input fluids encapsulated in the Reynolds number and capillary number, an idea regarding the droplet size of the final product can be gained. This analysis does not however take into account that two different microchips (with different cross sections, Table 5-3) were used to prepare the emulsions.

Considering the data obtained in conjunction with the geometric parameters of the microchips used to prepare the monodisperse we proposed a new modified form of the capillary number relationship as follows:

$$Ca(modified) = Ca * \frac{a}{h} = \frac{\eta\, u}{\sigma} * \frac{a}{h} \qquad\qquad Eq.\,5-11$$

122

According to the above discussion and by including geometric parameter considerations in the Reynolds number, we were able to propose a modified form of the Reynolds number as well. (Eq. 5-12).

$$Re(modified) = Re * \frac{a}{h} \qquad\qquad Eq. 5 - 12$$

where a is the width of the micro-channel and h is the depth.

The modified capillary and Reynolds numbers are given in Table 5-4. When the data are now reconsidered in light of the geometrical characteristics of the microchips, a distinction between the two geometries can now be readily seen. The modified values are plotted in Fig. 5-12 and 5-13 along with the unmodified values.

Table 5-4 Modified Reynolds and capillary numbers for the emulsions

System	Materials	Ca (modified)	Re (modified)
1	Dodecane/F127	0.062	22
2	Dodecane/F127	0.093	33
3	Dodecane/SDS	0.210	30
4	PDMS/F127	0.128	16.5
5	PDMS/SDS	0.240	27.5
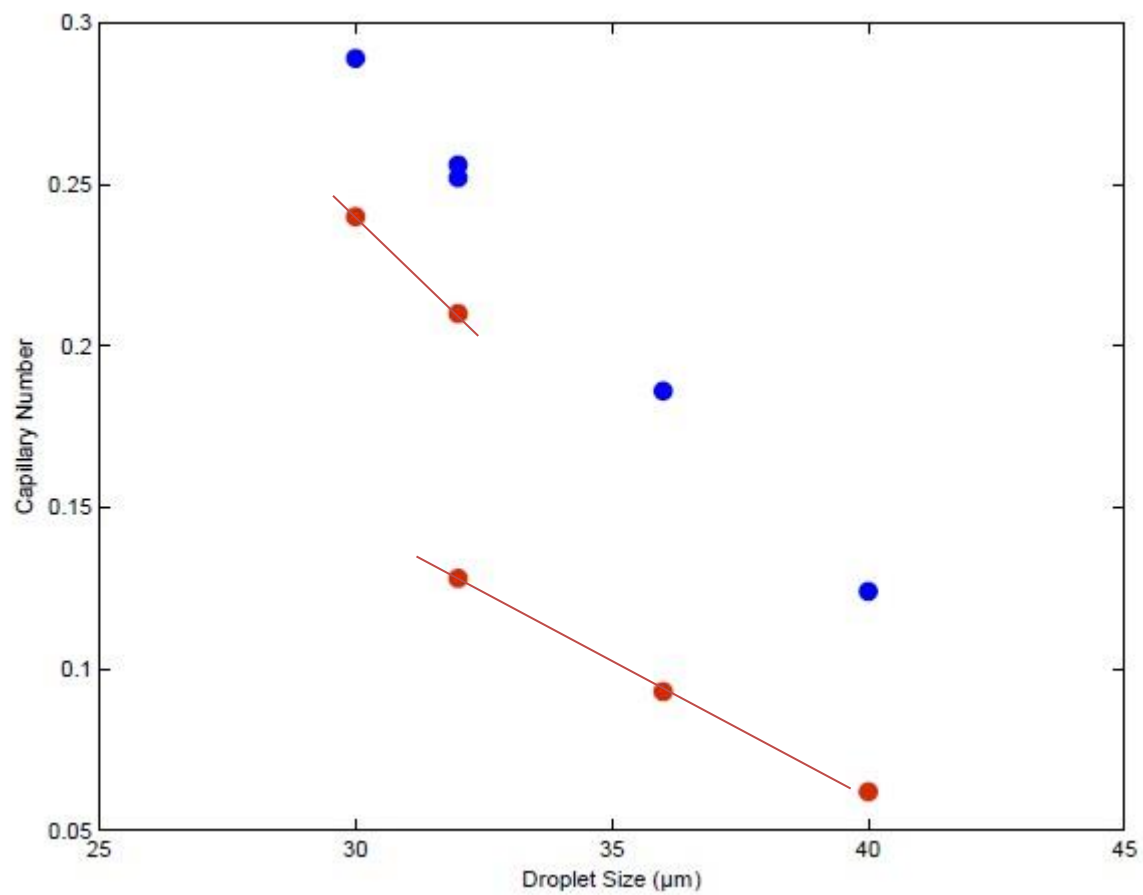
Fig. 5-12 Modified and unmodified capillary number as a function of droplet size . Red data points represent modified Reynolds number.
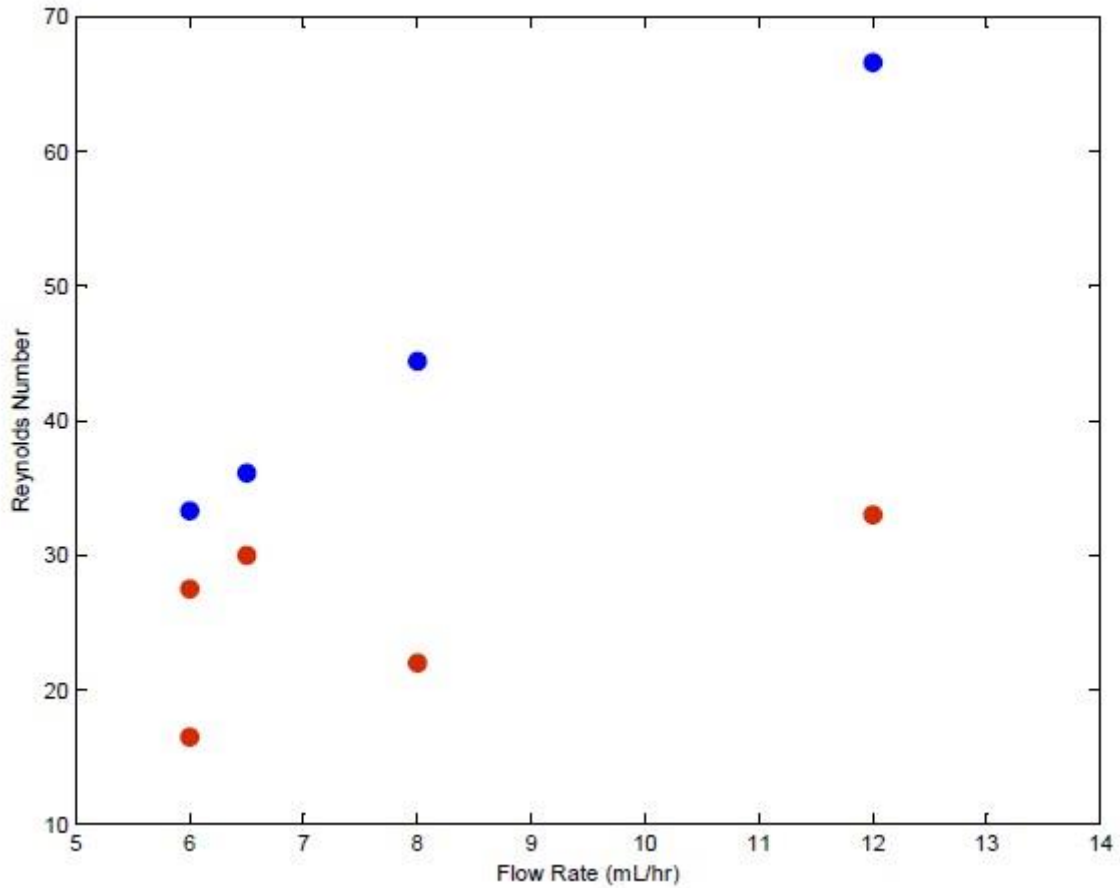
Fig. 5-13 Modified and unmodified Reynolds number as a function of flow rate . Red data points represent modified Reynolds number.

In Fig. 5-12 the first three red data points are attributed to the microchip with the cross section 50×100 μm^2 (the surfactant used was F127) whereas the last two data points are related to the other microchip with cross section 50×60 μm^2 (the surfactant used was SDS).

From this we can therefore conclude that the capillary number of a complex fluid in a microchip can be correlated to the range of achievable droplet sizes using that given microchip. By applying the modified capillary number, Eq. 5-11, in which geometric parameters are included, the effect of geometry on the capillary number and consequently on droplet size is determined. For the given geometries (two microchips with similar width and different depth of channels) used in this study the relationship between the capillary number and the droplet size is inversely linear with two different slopes; each slope is attributed to one geometry (Fig 5-12). And the slope of the line is defined by the applied

geometry (the depth of the channel). The deeper the micro-channel is the higher the slope of the line (see Fig. 5-12). The reason for this is that in a deeper channel the restriction imposed by the walls of the channels is decreased as compared to the narrower channel so that a wider range of droplet sizes can be generated, indicating that the slope of the function is enhanced.

By increasing the flow ratio between the continuous phase flow rate and the dispersed phase flow rate practically (this means increasing the continuous phase flow rate since the flow rate of the dispersed phase was fixed in this study), the branches of the stream after the break-up point are decreased, a higher capillary number is achieved and smaller droplets are generated. Therefore, to prepare smaller droplets which are less affected by wall effects, a higher capillary number is required. This backs up the finding of Xu *et al.*, who showed that by increasing the capillary number one can shift the droplet formation mode from geometry-controlled to hydro-dynamically-controlled [76].

The direct linear relationship between Re and flow rates shows that the higher the flow rate the higher the Reynolds number meaning that the flow pattern shifts towards turbulent flow. To generate monodisperse emulsions laminar flow is preferred where the velocity profile is always parabolic and the system is controllable whereas turbulent flow complicates the system and is difficult to control.

Hence in conclusion, determining the relationship between the capillary number, geometric parameters and the droplet size for a given microchip, paves the way to understanding which oils, surfactant and surfactant concentration are likely to give proposed predictable droplet size. It should however be taken into account that the geometrical parameters are very important in the determination of the droplet size of the final product.

5-2 Normal emulsion preparation- batch process

As explained in Chapter 2 normal emulsions can be prepared in blenders and homogenizers. Droplet size and size distribution can be controlled to some level by the ingredients that make up the system. For example, findings in this research reveal that making the density of the continuous and dispersed phases close to equal can be exploited in order to produce nearly monodisperse emulsions (Fig. 5-14). For this purpose a short-chain alcohol; ethanol or propanol, was added to the water/surfactant/dodecane system before mixing. This

results in a decrease in the interfacial tension and polydispersity. It should be mentioned that without using an added alcohol the blender does not provide sufficient energy to give kinetic stability to the system and the final product quickly separates. If on the other hand, the homogenizer is used in the absence of alcohol a stable emulsion is formed but with a very broad size distribution (Fig. 5-15). Hence the increased energy delivered when using the homogeniser is able to deal with the higher interfacial tension in the absence of alcohol.
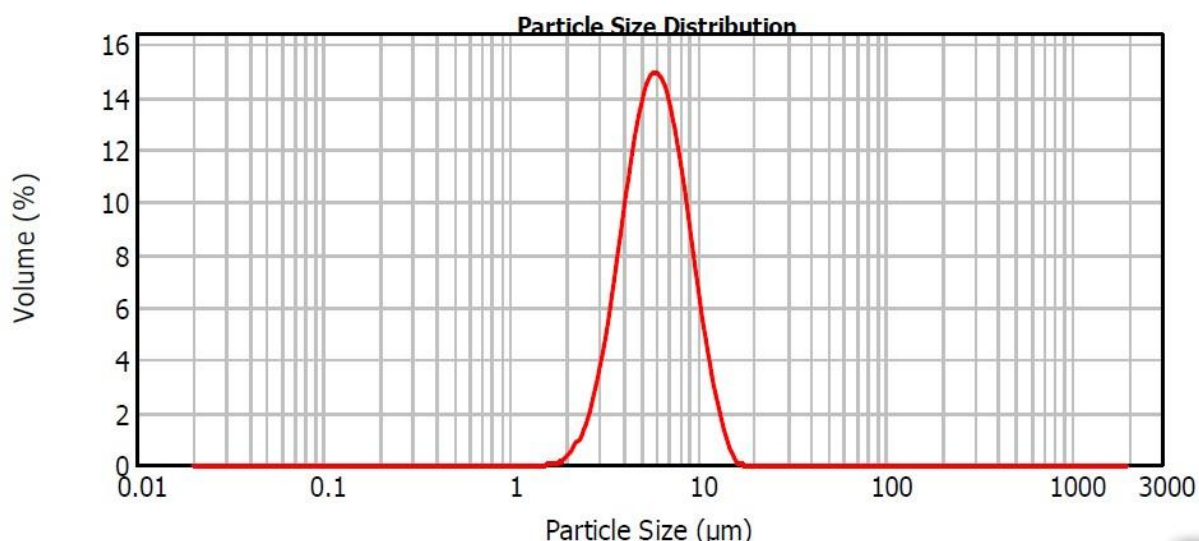
Fig. 5-14 Dodecane/F127/water/ethanol prepared in the blender with the same preparation method as explained for microemulsions in Chapter 2.
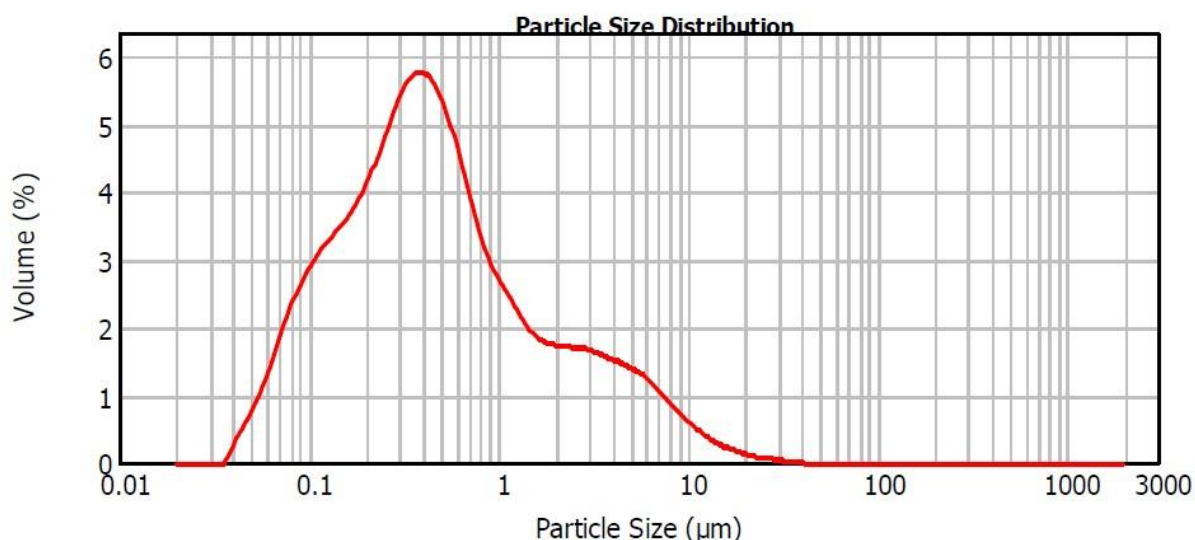

Fig. 5-15 Dodecane/SDS/water emulsion prepared using the homogenizer, 5 passes at 20 atm.

A relatively narrow size distribution could be obtained using the blender when coupled with the smaller emulsifiers, using soybean oil and an added short-chain alcohol, thereby allowing emulsions to be prepared with a near monodisperse size distribution in the low micrometre range. This then allows for a more ready comparison with the monodisperse coarse emulsions and the micro and nanoemulsions that have been fabricated in this research programme. The relevant data are given in Table 5-5 and shown in Fig. 5-16 and 5-17.

It should be mentioned that using dodecane or PDMS for this experiment resulted in the final product phase separating; hence soybean oil with one order of magnitude higher viscosity (50 cp vs. 5 cp for PDMS and 1 cp for dodecane) was selected which evidently worked appropriately in order to generate stable emulsion systems with a favourable size distribution. Ideally a single chemical system would have been used to prepare systems with droplets from 1 nm to 40 µm with monodisperse or polydisperse size distributions. However, this was not practically possible. Hence these systems were manipulated as minimally as possible to allow the most straightforward comparisons of the obtained data.

Table 5-5 Size distribution of coarse soybean oil emulsions generated in the blender

System	Size (µm)
Soybean oil/CTAB/ water/ethanol	2< droplet diameter <22
Soybean oil/Triton X-100/water/ethanol	1< droplet diameter < 5
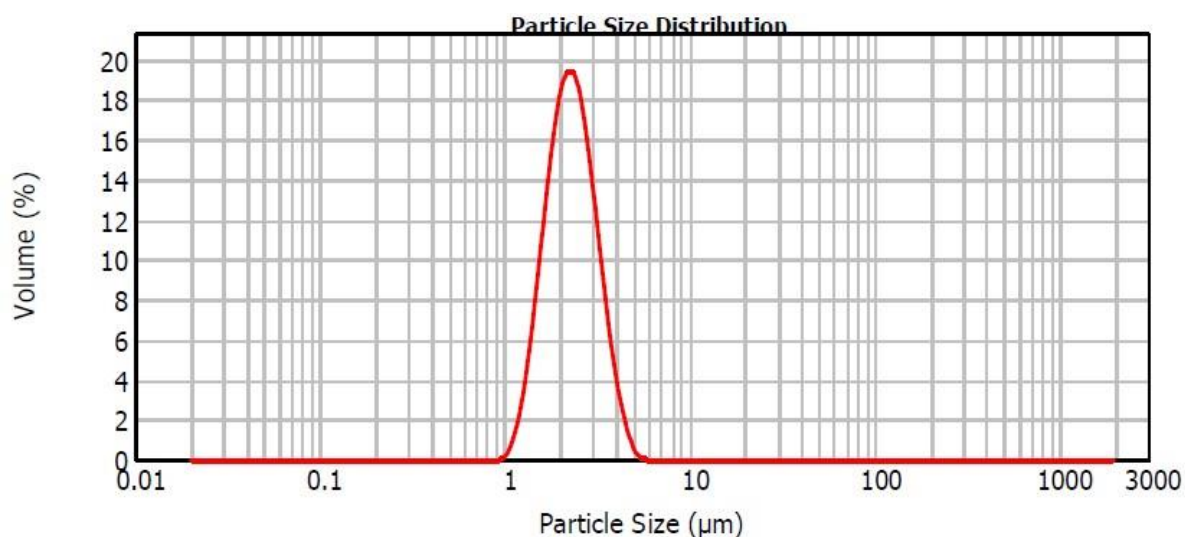
Fig. 5-16 Soybean oil/Triton X-100/water/ethanol emulsion prepared in the blender with the same preparation method as explained for microemulsions in Chapter 2.
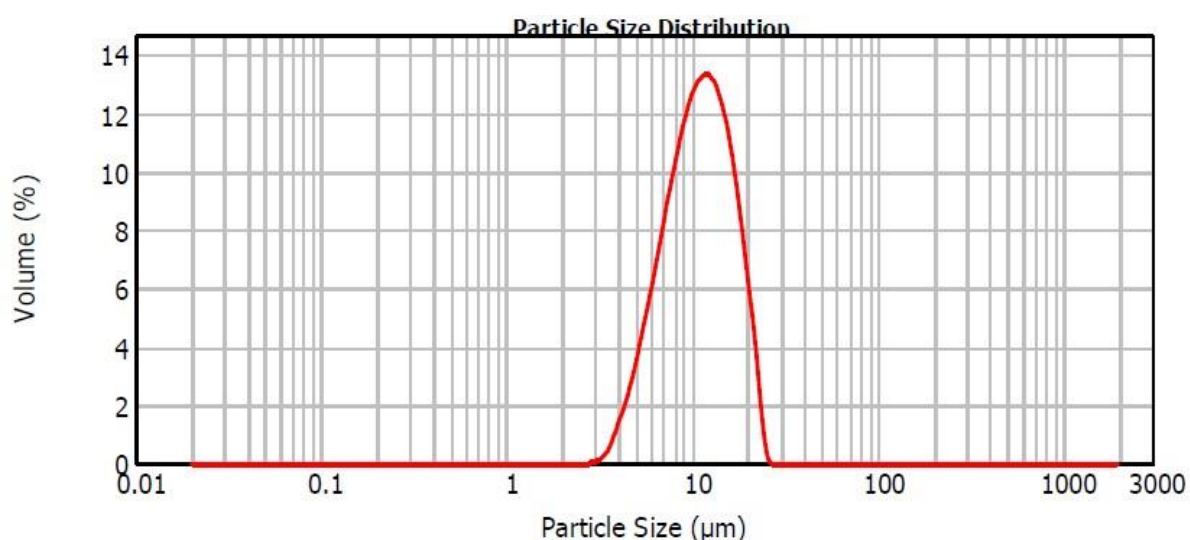
Fig. 5-17 Soybean oil/ CTAB/water/ethanol emulsion prepared in the blender with the same preparation method as explained for microemulsions in Chapter 2.

5-3 Flow properties of emulsions and coarse emulsions

In this section the physical factors that influence the rheology of emulsions and coarse emulsions are discussed and investigated. As explained previously microfluidic chips, a Warring blender or a homogenizer were used to prepare coarse emulsions and emulsions, with droplet size ranging from 1 to 40 µm.

In the case of coarse emulsions, the prepared droplets are delivered through a micro-tube to a container that contains the continuous phase. Due to the large droplet size and the density difference between the oil (dodecane or PDMS) and water the sample phase separates undergoing rapid creaming. It was not possible for these systems to separately control the volume fraction of oil due to the droplet size and density differential hence the isolated cream was used for all rheological tests and straightforwardly except in one case, detailed in Section 5-2-1. Therefore the final samples in this case were monodisperse, concentrated coarse emulsion with a large droplet size; between 30 and 40 µm. These concentrated coarse emulsions will be discussed in section 5-2.

The product of the Warring blender, noting that some short-chain alcohol has been added to the system, as explained in Chapter 1, is a dilute emulsion with a relatively low degree of polydispersity, 2.5±2 µm. A highly polydisperse dilute emulsion is formed when an homogenizer is used with droplet sizes between 200 nm and 40 µm. The dilute emulsions are discussed in the next section.

5-3-1 Dilute emulsions

In a dilute emulsion (< 20 % dispersed phase), droplet interactions can be neglected. From this point of view, an emulsion can be studied as a suspension. The observed behaviour of emulsions however encompasses, but is not restricted to, that of solid suspensions. Hence in general, emulsions cannot be modelled by applying suspension relationships. This is due to differences in droplet interactions and droplet deformations. For a dilute emulsion the well-known Einstein equation for the viscosity of suspensions [84] can and is often applied:

$$\eta(\emptyset) = \eta_0 (1 + 2.5\emptyset) \qquad\qquad Eq. 5-13$$

where $\eta(\emptyset)$ is the viscosity as a function of the volume fraction ($\emptyset$) and η_0 is the zero point viscosity. Eq. 5-13 is basically Eq. 1-3, written in another format. By rewriting this equation in terms of the reduced viscosity (η_r), with regard to the fact that $\eta - \eta_0 = \eta(\emptyset)$, Eq. 1-3 is reached:

$$\eta_r = \frac{\eta - \eta_0}{\eta_0} = 1 + 2.5\emptyset. \qquad\qquad Eq. 1-3 \ (Recalled)$$

Taylor derived the following relationship, by including the elasticity of the interfacial layer:

$$\eta_r = 1 + 2.5 \frac{2\eta_0 + 5\eta_{dr}}{5(\eta_0 + \eta_{dr})}\emptyset = 1 + \frac{1 + 2.5\lambda}{1 + \lambda}\emptyset. \qquad\qquad Eq. 5-14$$

where $\lambda = \eta_{dr}/\eta_0$ is the ratio of the viscosities of the two liquids. Therefore the relevant viscosity is expected to be very close to the viscosity of the continuous phase.

The appropriate method to determine the reference viscosity, η_0, was introduced in Chapter 3 pertaining to investigation of flow properties of microemulsions.

Considerable research is being undertaken in which the similarity between suspensions and emulsions is exploited with the goal of developing a model to describe the behaviour of both. An example of this is the work performed by Mason *et al*. who focused specifically on the similarities between the two types of systems [85] (Fig. 5-18).
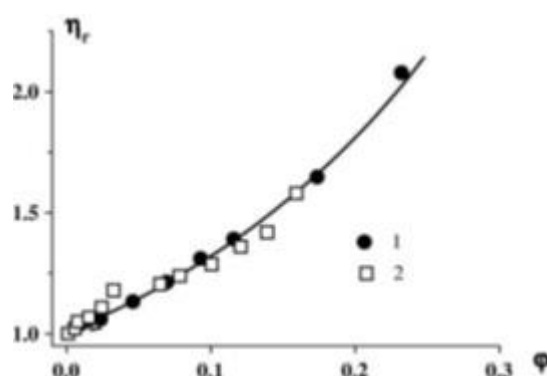
Fig. 5-18 Relative viscosity of Emulsion 1 (PDMS/SDS/water), droplet size 200 nm and Emulsion 2 (PDMS/SDS/water), droplet size 550 nm. The solid line is attributed to the relative viscosity of a suspension of hard spheres calculated through a numerical simulation based on the work of Ladd *et al.* [86] (adapted from [85]).

The similarity between the emulsions and the modelled suspensions is explained by considering the surfactant layer which forms around the droplets. If the thickness of this layer is comparable to the diameter of the droplet the interactions between droplets will be affected by this interfacial film; this results in the same behaviour as that observed for solid particles being seen for liquid droplets. Howe *et al*. have shown that this idea applies at low Reynolds number, low shear rate and for Newtonian fluids [87].

Soybean oil/water/CTAB/ethanol emulsions, droplet size 12$\pm$10 µm, were prepared using a Warring blender. The concentration of the oil in these emulsions was 20$\pm$2 wt. %. The emulsions can therefore be considered to be dilute coarse emulsions. The droplet size distribution of this system is shown in Section 5-1. The relevant representative flow curve is shown in Fig. 5-19.

131

For comparison, a dodecane/F127/water monodisperse coarse emulsion (40 wt. % oil and droplet size ~30 µm as measured using NMR and DNMR, see Chapter 2) generated in the microfluidic device was also diluted in order to produce two new emulsions with concentrations of 20 wt. % and 1 wt. %. To prepare these two dilute systems a small amount of the coarse concentrated monodisperse emulsion was diluted and put into the rheometer as quickly as possible to avoid the possibility of any creaming occurring. Since the PP geometry used has a very small gap size (50 µm), comparable to the droplet diameter, phase separation via creaming of the samples was greatly slowed down sufficient to allow reproducible rheology data to be obtained. The flow behaviour of these emulsions is presented in Fig. 5-20.
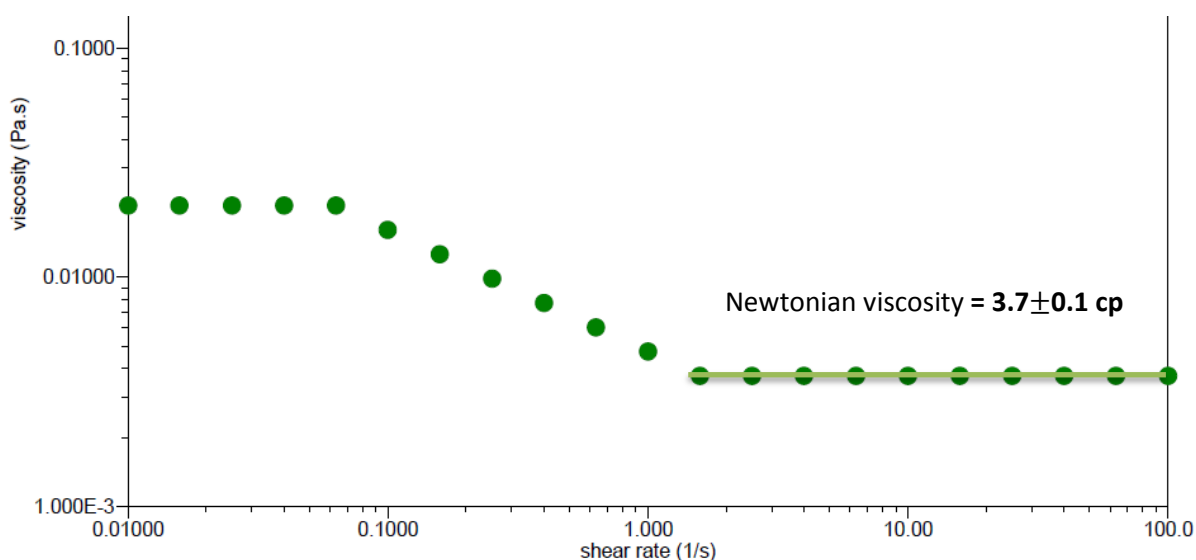
Fig. 5-19 Flow curves of soybean oil/CTAB/ethanol/water emulsion system made in Warring blender. The oil concentration is 20 wt. % and the droplet size is 12 µm.
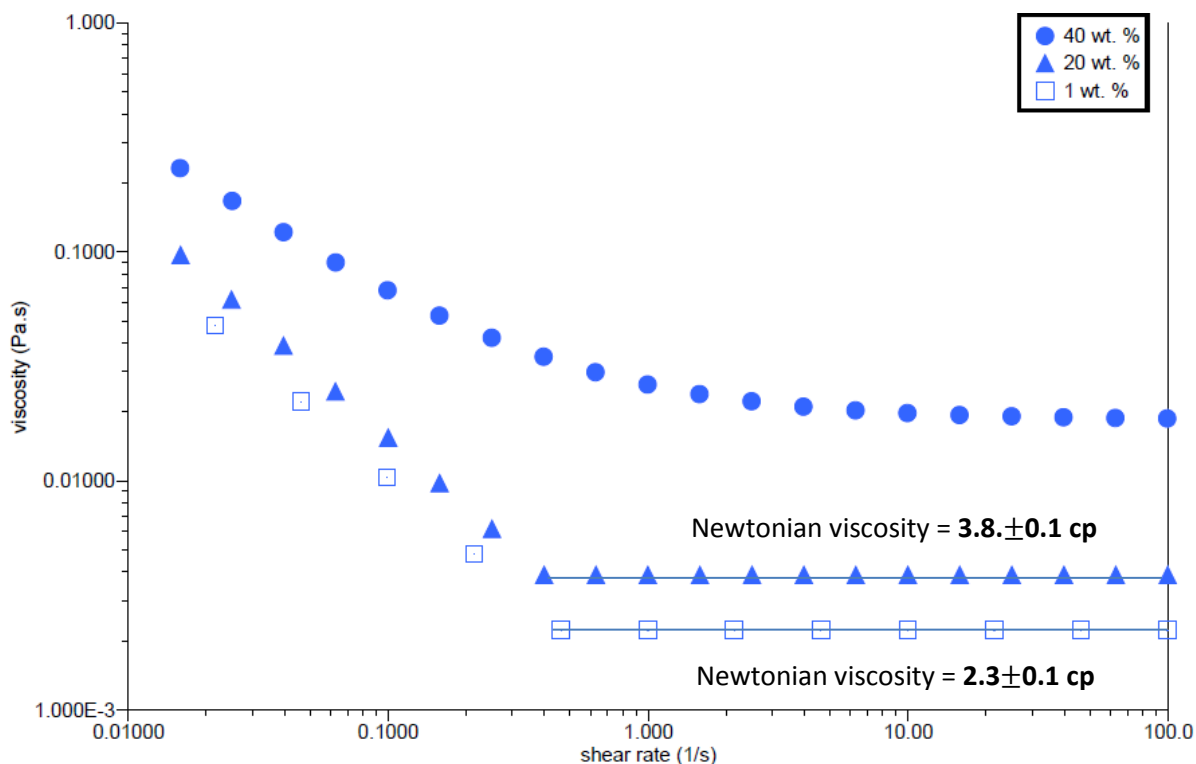
Fig. 5-20 Flow curves of dodecane/F127/water coarse emulsions, droplet size ~ 30 μm, at three different concentration of dispersed phase: 40, 20 and 1 wt. %.

In considering the data presented in Fig. 5-19 and 5-20, it is noted that the viscosity of soybean oil is 50 times that of dodecane; on this basis it is expected that the soybean oil emulsions will be more comparable to suspensions generally and that Eq. 1-3 and 5-14 will be able to be applied to this system more straightforwardly as compared to the dodecane system where the viscosity of the dispersed and continuous phases are similar and close to 1 cp.

The term $\frac{1+2.5\lambda}{1+\lambda}$ in Eq. 5-14 tends toward 2.5 for a high value of λ; in the case of soybean oil this terms is equal to 2.47$\pm$0.01. From Chapter 3, we have the viscosity of the ternary CTAB/ethanol/water solution (10 wt. % CTAB) being 2.5$\pm$0.2 cp. Using this value, Eq. 5-14 gives 3.7$\pm$0.3 cp as the viscosity of the soybean oil emulsion. This is in good agreement with the Newtonian viscosity obtained from the flow curve. Due to the high viscosity of the dispersed phase in this system, the yield stress behaviour at low shear rates, i.e. the initial constant viscosity, is evident for shear rates below 0.1/s. Whereas in the dodecane systems this yield stress behaviour is not evident within the displayed range of shear rates, 0.01 to

100/s. As seen in Fig. 5-20, the Newtonian viscosities of the 20 wt. % and 1 wt. % coarse dodecane/F127 emulsions are 3.9 and 2.3 cp, respectively with an uncertainty of 0.1.

The first thing to note here is that although the 20 wt. % systems shown in Fig. 5-19 and 5-20 are comprised of different chemicals with different surfactant concentrations and different droplet sizes, the oil concentration is the same, and they have close to the same Newtonian viscosities (3.7 and 3.8 cp). This is a very good example of the Newtonian viscosity of dilute emulsions being almost independent of the dominant length scale of the system.

Comparing the Newtonian viscosities of the 20 wt. % and 1 wt. % dodecane systems, the ratio is 3.8/2.3=1.6. Applying Eq. 5-13 and 5-14 to obtain this ratio gives 1.5. This shows that the simplicity of the system in a dilute emulsion (up to approximately 20% oil) allows us to apply simple relationships such as Eq. 5-13 and 5-14 that demonstrate only a slight deviation from the experimental data.

The non-Newtonian region of the flow curves in Fig. 5-20 shows similarity between the 20 wt. % and 1 wt. % systems. This is because of the non-Newtonian behaviour is significantly affected by the length scale and droplet interactions and since these systems have the same droplet size, are made from the same chemicals and have low droplet interactions, due to being dilute, the non-Newtonian regions are similar despite the oil concentrations being 20 times different. In contrast, the flow behaviour of the more concentrated coarse emulsion as shown in Fig. 5-20, shown specifically to demonstrate that once the system becomes more concentrated droplet interactions and droplet deformation significantly change the flow behaviour and the dilute emulsion models are no longer applicable. The flow curves of the dilute emulsions are similar to those of surfactant solutions and microemulsions as presented in Chapter 3. The Newtonian viscosity in the case of the systems shown in Fig. 5-19 and 5-20 is observed beyond a shear rate of 2/s for the soybean oil system and 0.5/s for dodecane system. In the next section the flow behaviour of concentrated emulsions is discussed which deviates significantly from this baseline behaviour.

5-3-1-1 Effect of droplet size: dilute emulsions

The effect of droplet size on emulsion rheology is directly dependent on the concentration of droplets in the system. In Fig. 5-21 are shown the flow curves of soybean oil/CTAB and soybean oil/Triton X-100 dilute emulsions (both 20 wt. % oil concentration) see Table 5-5. The droplet size distribution of the Triton X-100-based system is centred around 2 µm while that of the CTAB-based system is centred around 12 µm. Although the latter is 6 times larger, the flow behaviours match at high shear rates. This reflects that as the concentration of the oil decreases the dependency of flow properties on droplet size decreases as well.

The relationship between the viscosity and droplet size is inverse in concentrated emulsions (as will be discussed in Section 5-3-2-3) and direct in sub-micron complex fluids. Diluted emulsions are placed between these two limits where the viscosity is independent of the droplet size. However, at low shear rates the common trend for emulsions is observed, i.e. the viscosity of the Triton X-100 system with smaller droplet size is higher than that of the CTAB system with larger droplet size.
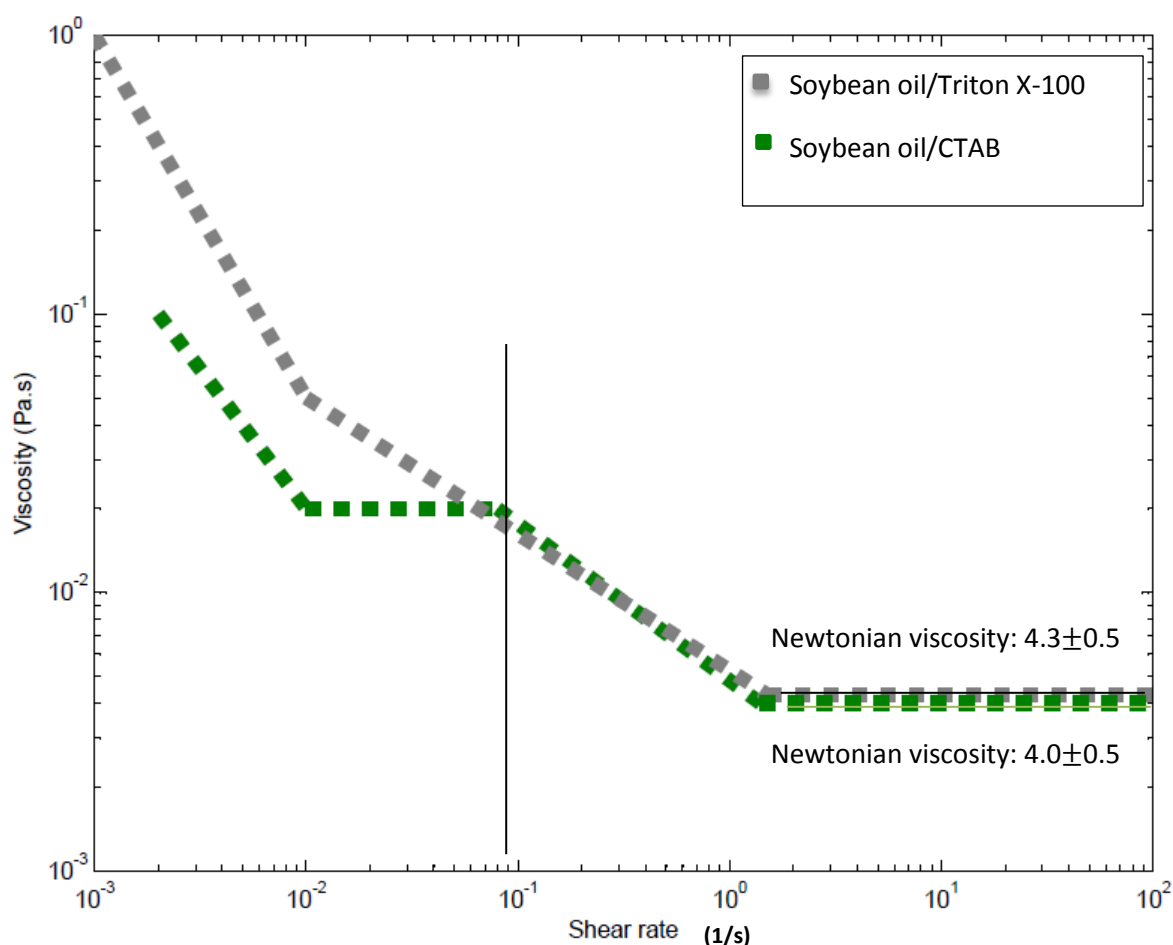

Fig. 5-21 Flow curves of soybean oil emulsions; oil concentration in both systems 20 wt. %.

The flow curves at high shear rates follow the same trend as microemulsion flow curves; see Chapter 3. At low shear rate the behaviour is more complicated as compared to microemulsion and surfactant solutions. For example the CTAB-based system has two Newtonian regions of constant viscosity. This system displays two shear-thinning regions followed by a Newtonian region. The transition from Newtonian to shear-thinning is not common in emulsion rheological behaviour. The reason is that Newtonian behaviour represents no inter-droplet forces and it is unlikely for a system that has already reached this state to undergo a transition to a non-Newtonian state on further increasing shear rate. Hence this observed transition may be due to the original emulsion being unstable and transforming to a new emulsion system upon applying shear. Similar to surfactant solutions and microemulsions, Newtonian behaviour is observed in both systems beyond a shear rate of 1/s.

5-3-2 Concentrated emulsions

When the concentration of the dispersed phase is increased in an emulsion sample, droplet-droplet interactions can no longer be ignored. Furthermore, it is not reasonable in concentrated coarse emulsions to assume that the droplets are spherical and remain un-deformed under shear forces, especially in the case of systems investigated in this research given the similar viscosities of the continuous and dispersed phases.

In this section we firstly discuss theoretical models based on a power series, and models developed from dilute emulsions, before considering the latest models that are all based on the deformation and relaxation of droplets and interfacial films. In each case our results are displayed and fitted to the models.

The term concentrated emulsions describes the group of emulsions that lie between dilute and high-concentration emulsions ($0.2 < \emptyset < 0.75$ where $\emptyset$ is the volume fraction). Here hydrodynamic interactions between droplets must be taken into account. Hence if the viscosity is described by a power series [84] it is necessary to find the second virial coefficient (A_2, the coefficient of $\emptyset^2$) which accounts for the hydrodynamic interactions [88]. Describing the viscosity as a power series is that the relative viscosity described in Eq. 1-3 modifies by adding terms containing the volume fraction , $\emptyset$, of higher powers times its relevant coefficient.

The monodisperse coarse emulsions used in this research have the oil volume fractions given in Table 5-6 as determined from our NMR data (see Chapter 2). The volume fractions range from ~40 to 55 % and hence the emulsions are considered to be concentrated emulsions.

Table 5-6 Oil volume fraction of the coarse emulsions

Emulsion	Oil volume fraction*
Dodecane/F127	0.55±0.01
Dodecane/SDS	0.42±0.01
PDMS/F127	0.50±0.01
PDMS/SDS	0.45±0.01

*The oil volume fractions were measured using NMR spectroscopy.

Yaron *et al*. [89] have developed a modified version of the power series applied to dilute emulsions considering energy dissipation through a globular system with a parabolic velocity profile. This model is analytical and derived from flow equations:

$$\eta_r = 1 + \frac{5.5(4\emptyset^{7/3} + 1 - \frac{84}{11}\emptyset^{2/3} + \frac{4}{k_1}\left(1 - \emptyset^{7/3}\right))}{10\left(1 - \emptyset^{10/3}\right) - 25\varphi\left(1 - \emptyset^{4/3}\right) + \frac{10}{k_1}(1 - \emptyset)(1 - \emptyset^{7/3})}\emptyset \qquad Eq.\,5-15$$

where k_1 is a constant obtained from solving the Stokes equation. This factor reflects the surfactant absorption at the interfacial barrier; for more information see Ref. [81]. As seen, Eq. 5-15 is a function of the emulsion volume fraction and k_1. Using the oil volume fractions given in Table 5-6, the relative viscosities of the four concentrated coarse emulsion systems can be estimated using Eq. 5-15. These expressions as a function of k_1 are given in Table 5-7. By plotting η_r, as presented in Table 5-7, vs. k_1, the stable value of the corresponding relative viscosity is determined (Fig. 5-22).

Table 5-7 Predicted relative viscosities of the coarse concentrated emulsions

Emulsion	η_r
Dodecane/F127	$\eta_r = 1 + \dfrac{9.10 - 9.48 k_1}{3.38 + 1.08 k_1}$
Dodecane/SDS	$\eta_r = 1 + \dfrac{8.02 - 6.36 k_1}{5.03 + 2.25 k_1}$
PDMS/F127	$\eta_r = 1 + \dfrac{8.81 - 8.29 k_1}{4.00 + 1.47 k_1}$
PDMS/SDS	$\eta_r = 1 + \dfrac{8.37 - 7.09 k_1}{4.65 + 1.93 k_1}$
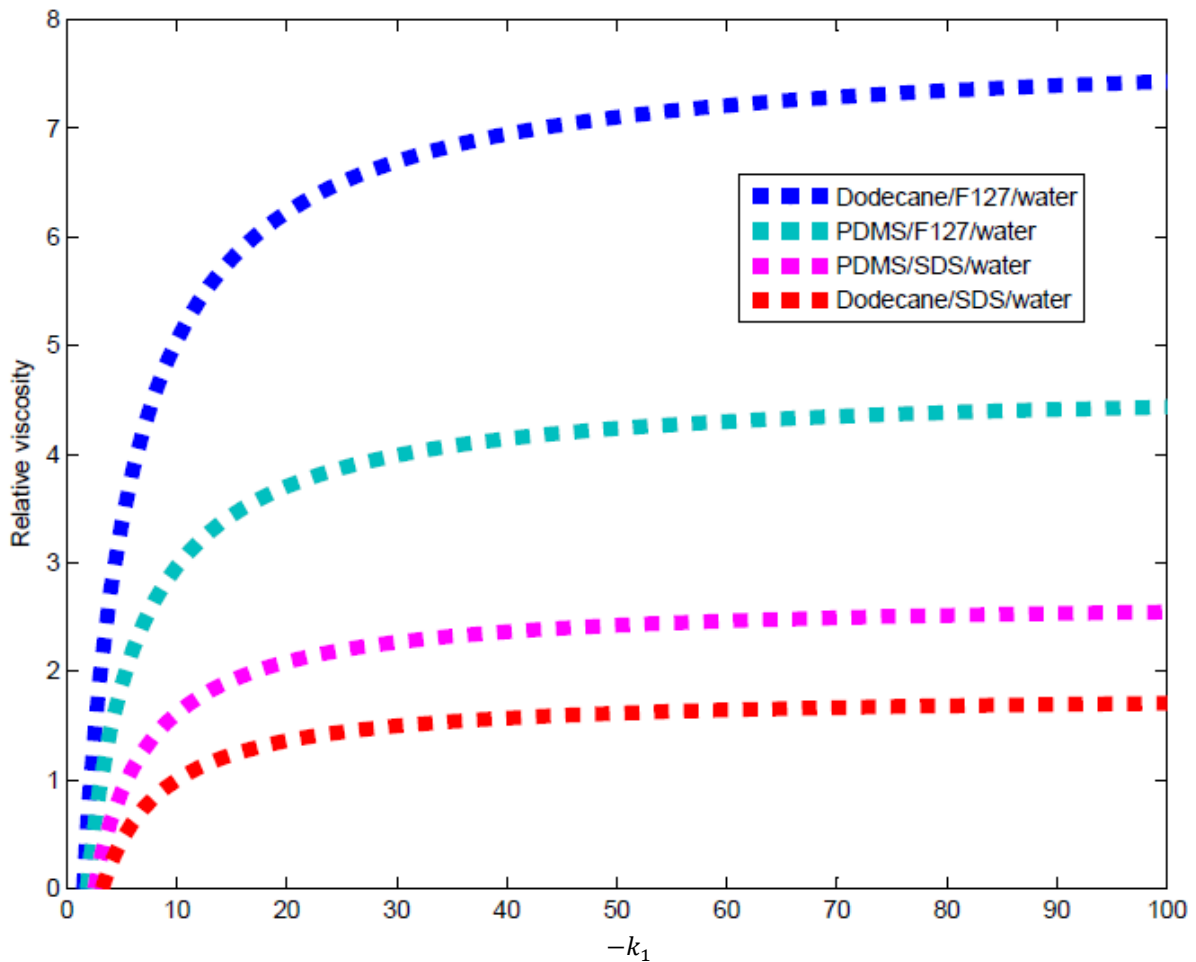
Fig. 5-22 Estimated relative viscosity of the four concentrated coarse emulsions as a function of $-k_1$.

The reason that the viscosity reaches a plateau as seen for all four systems in Fig. 5-22 is that the intrinsic adsorption encapsulated in k_1 reaches equilibrium at high values of k_1,

which is why each curve in Fig. 5-22 goes toward a plateau. The equilibrium values of η_r, based on the value of the plateau that each curve in Fig. 5-22 reaches, are reported in Table 5-8.

Table 5-8 Relative viscosities of the concentrated coarse emulsions based on Eq. 5-15, extracted from Fig. 5-22, the value of the plateau of each curve

Emulsion	Oil volume fraction	η_r
PDMS/F127	0.50± ±0.01	4.4±0.3
Dodecane/F127	0.55±0.01	7.4±0.5
PDMS/SDS	0.45± ±0.01	2.6±0.2
Dodecane/SDS	0.42± ±0.01	1.7 ±0.2

Considering Eq. 5-15 it is evident that the relative viscosity calculated using this relationship is volume fraction dependent but independent of the chemical functionality, density of the oil used, and the packing and interfacial layer effects. This places severe limitations on its use in analysing the systems investigated here. Below, the calculated data are compared with the experimental data obtained.

In Fig. 5-23 are shown representative flow curves of the four concentrated coarse emulsion systems investigated here. Two important points must be considered in comparing the experimental data and the estimated relative viscosities given in Table 5-8.
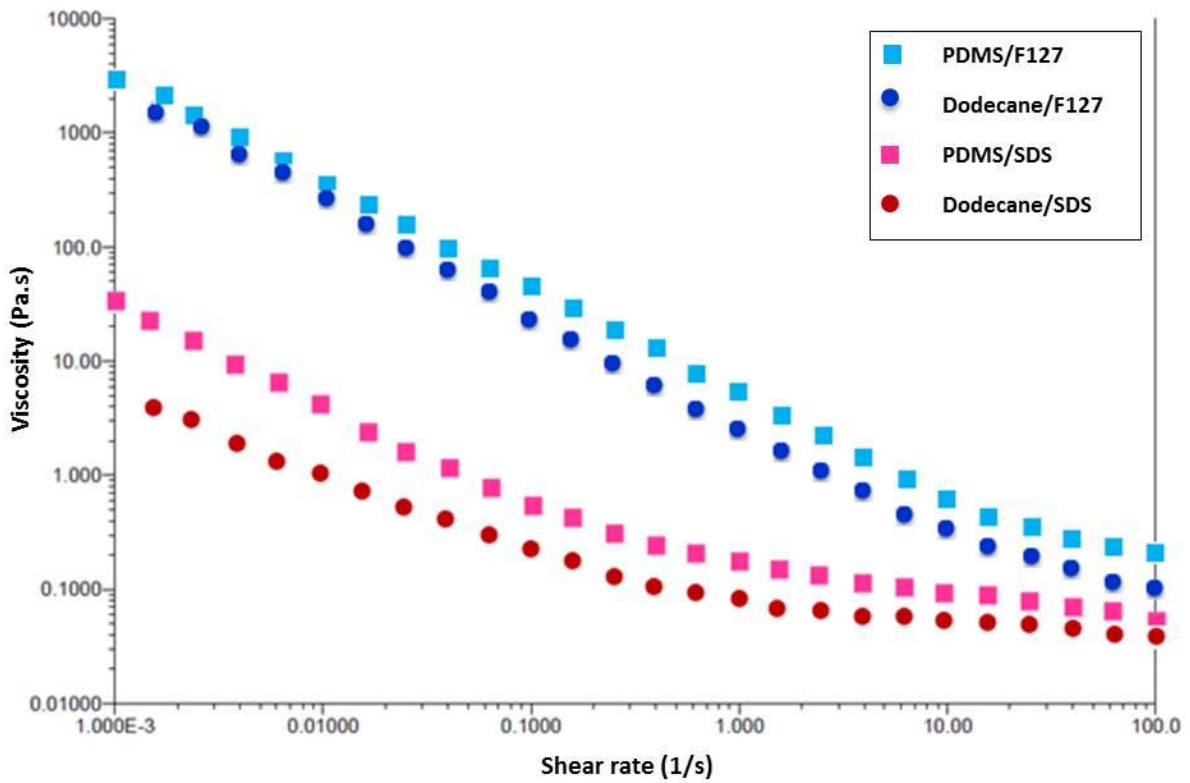
Fig. 5-23 Flow curves of the four monodisperse concentrated coarse emulsions as a function of decreasing shear rate.

1- The viscosity calculated using Eq. 5-15 is constant. Viscosity is only constant for Newtonian systems or in the high shear rate region of some non-Newtonian systems. From the data presented in Fig. 5-23 the viscosity of the systems investigated decreases on increasing shear rate only reaching near constancy above 100/s. Hence, a model is required to describe the observed behaviour over the full range of shear rate investigated.

2- Considering the viscosity trends shown in Fig. 5-23, one can see that the relative viscosity would be expected to decrease from PDMS/F127 to dodecane/F127 to PDMS/SDS to dodecane/SDS. This does not match the trend in the calculated data (Table 5-8) indicating that in our monodisperse concentrated coarse emulsions other factors apart from the volume fraction play significant roles.

Choi *et al*. [90], taking into consideration the oil viscosity derived the following equation :

$$\eta_r = 1 + \frac{2[5\lambda - 5(\lambda - 1)\emptyset^{\frac{7}{3}}]\emptyset}{4(\lambda + 1) - 5(5\lambda + 2)\emptyset + 42\lambda\emptyset^{\frac{5}{3}} - 5(5\lambda - 2)\emptyset^{\frac{7}{3}} + 4(\lambda - 1)\emptyset^{\frac{10}{3}}} \qquad Eq. 5 - 16$$

140

where λ is the viscosity of the continuous phase divided by the viscosity of the dispersed phase and $\emptyset$ is the oil volume fraction. Using the estimated oil volume fractions of the concentrated coarse emulsions, Eq. 5-16 was used to determine the relative viscosity of the four systems (Table 5-9). Significant differences are evident between the values estimated by Eq. 5-15 and 5-16 (Table 5-8 vs. 5-9).

Table 5-9 Relative viscosities of the emulsions based on Eq. 5-16

Emulsion	η_r
PDMS/F127	15.9±0.5
Dodecane/F127	11.2±0.5
PDMS/SDS	10.8±0.5
Dodecane/SDS	4.6±0.5

The observed trend in the calculated relative viscosity values now matches the pattern seen in the experimental data (Fig. 5-23). This means this model is more suitable as compared to Eq. 5-15 due to including more viscosity affecting parameters. However, the equation, Eq. 5-16, continues to assume constancy of viscosity (i.e. Newtonian systems).

Pal *et al*. [91] have shown that Eq. 5-16 holds for oil-in-water emulsions for concentrations up to 0.6 volume fraction. They also have developed a model [92] that can be used to predict emulsion viscosity for a wide range of concentrations using the factor $\emptyset^*$ which is the volume fraction at the closest packing of droplets. In this model both the packing of the droplets and the viscosity ratio of the oil and water are taken into account.

$$\eta_r \left(\frac{2\eta_r + 5\lambda}{2 + 5\lambda} \right)^{1/2} = \exp\left(\frac{2.5\emptyset}{1 - \left(\emptyset/\emptyset^* \right)} \right). \qquad\qquad Eq.\, 1-4\ (Recalled)$$

This relationship is now a function of shear rate as the close packing factor is a function of shear rate. This means that at each shear rate the packing pattern is different, which is a more reasonable assumption. When the volume fraction of the system gets close to the close packing limit the relative viscosity is significantly enhanced since the denominator in

Eq. 1-4 tends to zero. The close packing factor, $\emptyset^*$, is affected by droplet deformation; and the deformation is a function of shear rate, therefore, $\emptyset^*$ is a function of shear rate.

The flow curves shown in Fig. 5-23 were obtained upon decreasing shear rate from 100/s. By applying instead an increasing shear rate solid-like behaviour, constant viscosity or a so-called yield stress is seen at very low shear rates for all four concentrated coarse emulsion systems. This is the force required to make the system flow (Fig. 5-24).
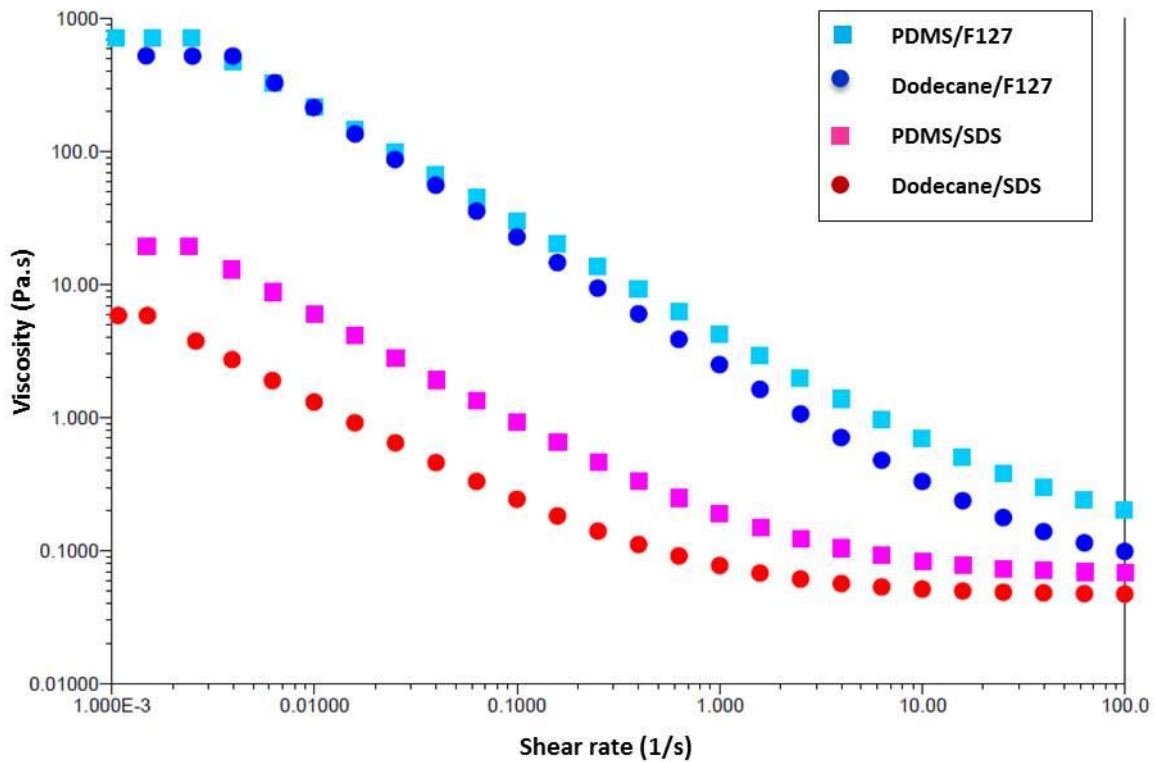
Fig. 5-24 Flow curves of the four coarse monodisperse emulsions as a function of increasing shear rate.

Many studies (for example see [6] and [91]) in the field of emulsion rheology have shown that viscosity strongly depends on the structure of the sample and as soon as the emulsion structure is changed under shear a large change in the rheological properties of the system is observed. Pal *et al*. [91] have demonstrated this behaviour in concentrated emulsions (Fig. 5-25). For concentrated emulsions the viscosity curves drop drastically after initially showing Newtonian-like behaviour at low stresses. This shift occurs over a small range of stresses and is related to the rupture point in the sample.
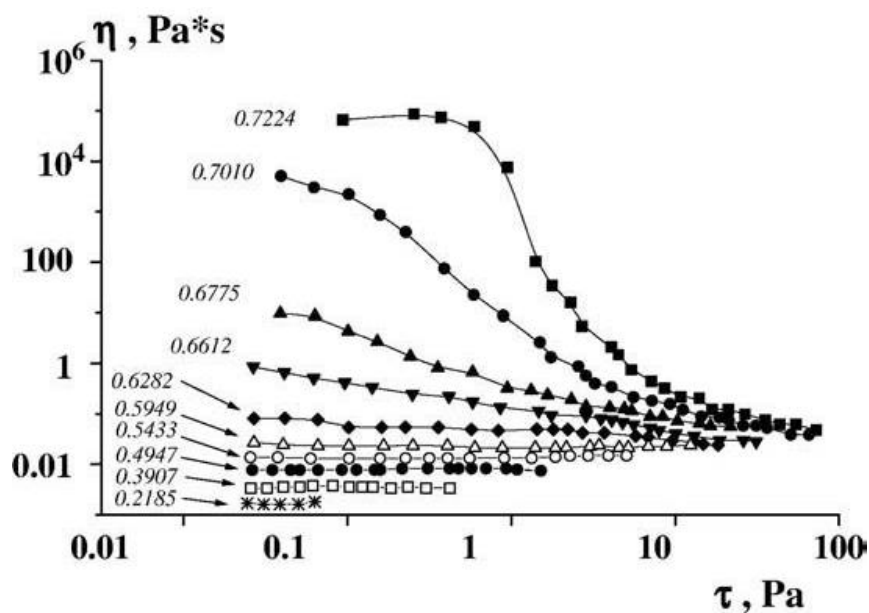
Fig. 5-25 Flow curves of an oil-in-water EMD oil/Triton X-100/water with droplet size of 4.6 μm (reproduced from [91]).

Lapasin [93] showed the same behaviour for concentrated emulsions. It should be mentioned that the test samples were polydisperse and the close packed concentration limit for polydisperse emulsions may be higher or lower than that for monodisperse ones depending on the exact distribution and inter-droplet interactions ([7] & [6] & [77]).

With this in mind, the data shown in Fig. 5-24 has been re-drawn as viscosity vs shear stress (Fig. 5-26). The structural changes occurring in the four concentrated coarse emulsions are now more clearly evident.
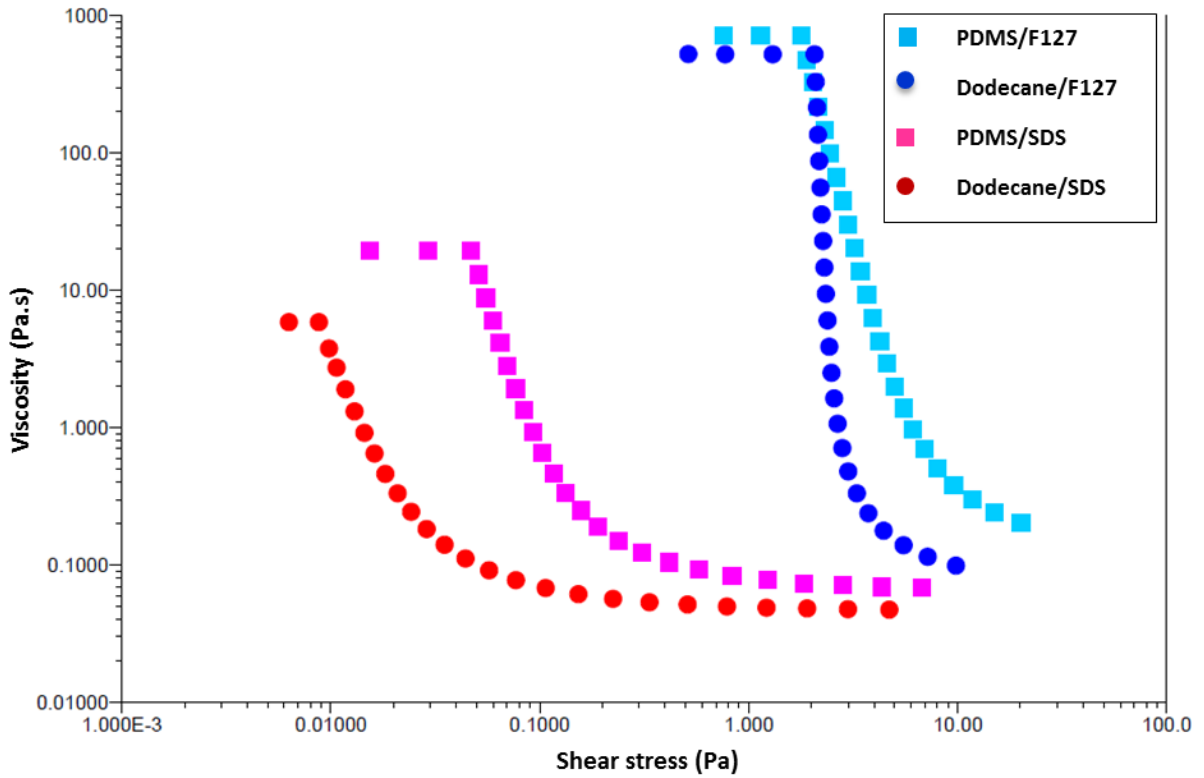
Fig. 5-26 Viscosity vs. shear stress in the four concentrated coarse emulsions.

Deformation of the droplets can affect their maximum packing. Delaney *et al*. have studied the maximum packing of ellipsoidal systems using computational simulation [94]. They found that $\emptyset^*$ of such a system is higher than that of the corresponding spherical structure up to a specific aspect ratio.

Using Eq. 1-4 and with respect to the experimental flow curve data, $\emptyset^*$ can be plotted as a function of shear rate (Fig 5-27). As seen the closest packing curves tend to a plateau at high shear rate.
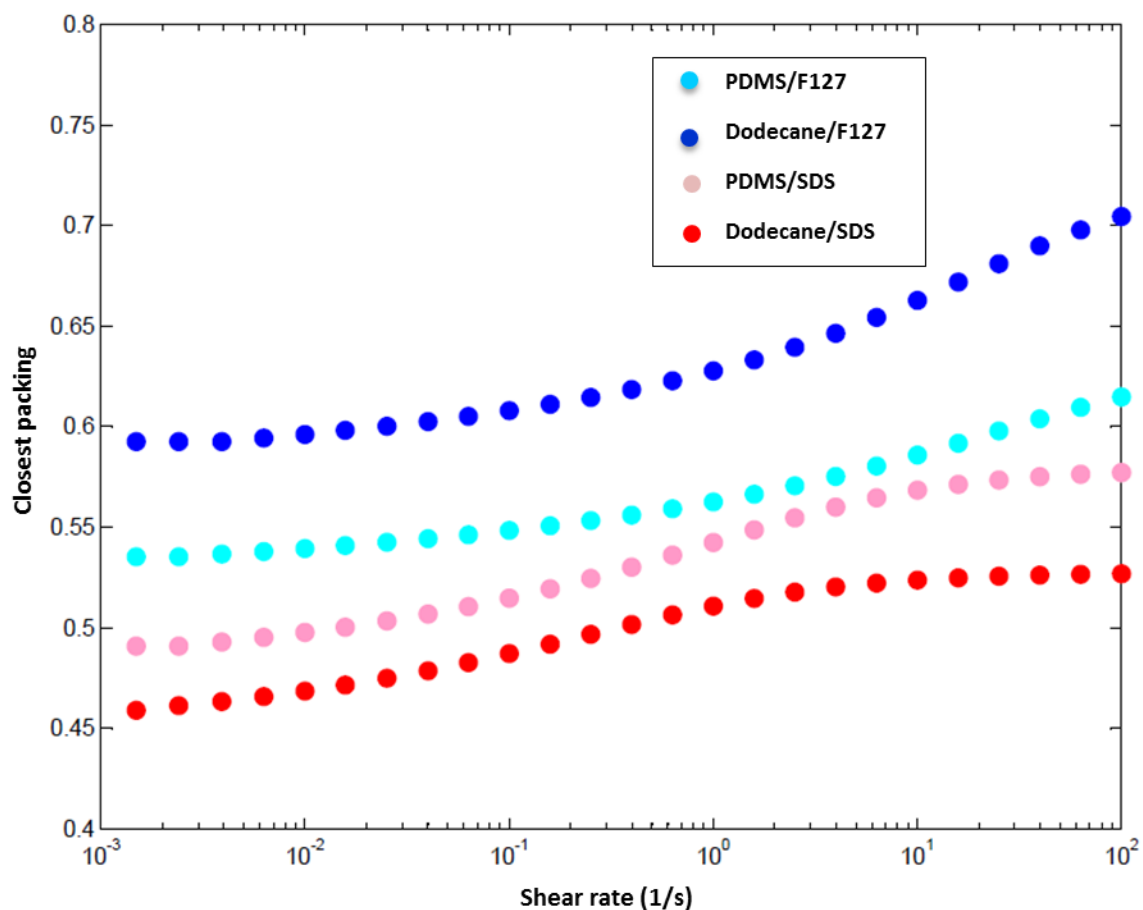
Fig. 5-27 Closest packing of the four monodisperse coarse emulsions as a function of increasing shear rate.

By modelling the flow curves shown in Fig. 5-24 using the following relationship, the value of the infinite viscosity can be estimated.

$$\eta = \eta_\infty + \frac{A}{\dot{\gamma}^n}$$ *Eq. 5-17*

The infinite viscosities of the emulsions are given in Table 5-10 in accordance with Eq. 5-17. Consequently one can calculate the relevant maximum packing at infinite viscosity (Table 5-10).

Table 5-10 Infinite viscosities based on Eq. 5-17 and the corresponding maximum packing attributed to each infinite viscosity

Emulsion	η_∞ (Pa.s)	$\emptyset^*$ (%)	A	N
PDMS/F127	0.12±0.01	63±1	4.7±0.1	0.93±0.01
Dodecane/F127	0.066±0.001	73±1	2.5±0.1	1.00±0.01
PDMS/SDS	0.065±0.001	58±1	0.08±0.01	0.86±0.01
Dodecane/SDS	0.047±0.001	53±1	0.03±0.01	0.78±0.01

We note that the droplet size and size distribution are not taken into consideration in the above described analysis. That is, the systems are assumed to be monodisperse which matches well with our four investigated systems. Polydispersity effects will be discussed in the next sections.

5-3-2-1 Effect of interfacial tension

Coussot *et al*. have studied pasty materials of various internal structures in a Couette geometry [95]. These materials show thixotropic behaviour resulting in an increase in the elastic modulus of the solid region as the resting time is increased. Oldyard [96] around 60 years ago investigated the effect of interfacial tension on droplet interaction and interfacial layer relaxation which results in viscoelasticity in emulsions. This study was followed later by Li *et al*. [97], they applied numerical methods to determine the effect of surfactants and surface tension on droplet deformation and rheological properties for a moving sphere in a Stokes-fluid.

Having considered the effect of surface tension in determining emulsion rheology, Oldyard states that non-linear viscoelastic behaviour seen in these systems is related to droplet deformation and relaxation time of the interfacial film.

A droplet under shear is considered as an ellipsoid, with an elongation factor, D, defined as:

$$D = \frac{R_{max} - R_{min}}{R_{max} + R_{min}}. \qquad\qquad Eq. 5-18$$

After removing the shear, the droplet which has already attained a specific amount of deformation, D_0, returns to its original state, for small deformation this behaviour can be expressed using the Maxwell model:

$$D = D_0 exp\left(-{t}/{\theta}\right)$$ $\qquad\qquad Eq.5-19$

where θ is a characteristic relaxation time related to the capillary number:

$$\theta = Ca\ \frac{(3+2\lambda)(16+19\lambda)}{80(\lambda+1)}.$$ $\qquad\qquad Eq.5-20$

In this research by using a simple 2-D model with regard to the droplet deformation we have been able to scale the viscoelastic modulus with the interfacial tension as follows:

$$G = \frac{\sigma C}{A}$$ $\qquad\qquad Eq.5-21$

where G is the viscoelastic modulus, σ is the interfacial tension, and C and A are the circumference and area of the droplets respectively. Since this is a 2-D model, circumference and area have been used instead of the area and volume. The reader is referred to [8] in which the author has applied the same basis to model the viscoelastic behaviour of highly concentrated emulsions.

5-3-2-2 Mathematical Modelling

To model the elastic modulus of the monodisperse concentrated coarse emulsions, a method has been developed based on experimental data collected using an RA200 rheometer using a parallel plate geometry. In this method the gap size between the two plates was decreased in order ensure that the droplets are totally trapped by the walls of the geometry representing the dimensional limit for each system and that a single layer of droplets exists between the parallel plates. In this way the maximum deformation is imposed on the droplets and the movement of the top plate of the geometry is completely correlated to the deformation of the droplets. It is worth mentioning that for such an experiment the droplets need to be sufficiently robust to undergo high strain without breaking. This is only possible when there is a thick and strong interfacial layer around the droplets. Therefore, for this part of the research, after checking all systems produced, the only system that could be used was the PDMS/F127 coarse emulsion. This is because of the relatively robust interfacial layer that F127 forms around the oil droplets; additionally the viscosity of PDMS is five times higher than that of dodecane. The parallel plate geometry is shown in Chapter 2, Fig. 2-8. The velocity profile across the material under shear between the two plates is shown in Fig. 5-28.

$V = V_0$

$V = 0$
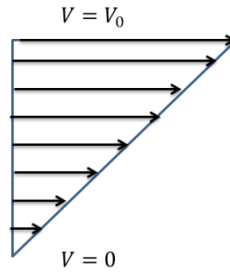
Fig. 5-28 Velocity profile in a fluid confined in a parallel plate geometry.

In the parallel plate geometry the shear rate is a function of angular velocity and the radius of the plate as previously discussed in Chapter 2 (see Eq. 2-8 to 2-10). In Fig 5-29 a representation of a droplet under shear is shown.
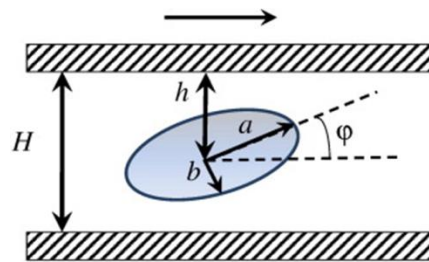
Fig. 5-29 A droplet trapped between the two plates of a parallel plate geometry with a, b and φ being the major and minor axes of the ellipsoid and orientation angle respectively (adopted from [69]).

The assumptions that are applied include:

1. The droplet is totally trapped between the two plates undergoing deformation due to the movement of the top plate;

2. The top point of the droplet moves with a speed equal to the rate of the top plate displacement and the bottom point is stationary ($D \approx H$; where D is the droplet size and H is the gap size);

3. The orientation angle is from $0°$ (at the origin of time) up to a specific value that needs to be attained, this is one of the purposes of the modelling;

4. Beyond the abovementioned specific orientation angle droplets flow;

5. No time dependant behaviour is observed;

6. There are no droplet-droplet interactions.

Based on the above assumptions and with regard to the steady state flow experiment information gained from RA 2000 software, e.g. the displacement of the moving plate and also the gap size the minor and major axis of the deformed droplet as a function of shear rate and consequently the droplet deformation can be calculated. Droplet deformation vs. capillary number is shown in Fig. 5-30. As is seen the turning point of the curve occurs at a capillary number of approximately 10^{-5}, by considering the derivative of the function the value of $(1.2 \pm 0.1) * 10^{-5}$ was obtained for the turning point. This value is equivalent to a strain of ~ 1 with an orientation angle of about 45°, based on the experiment information shown in Fig. 5-31.
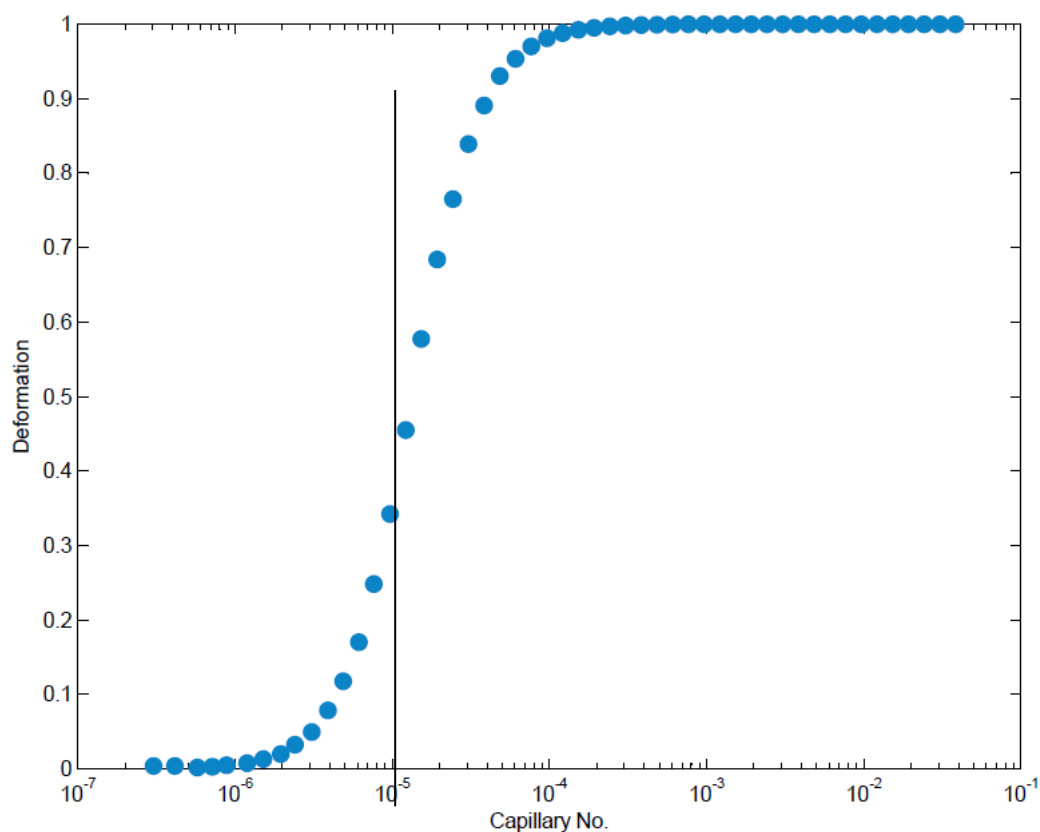
Fig. 5-30 Droplet deformation as a function of capillary number.

149

$$Strain = \frac{Displacement}{H}$$
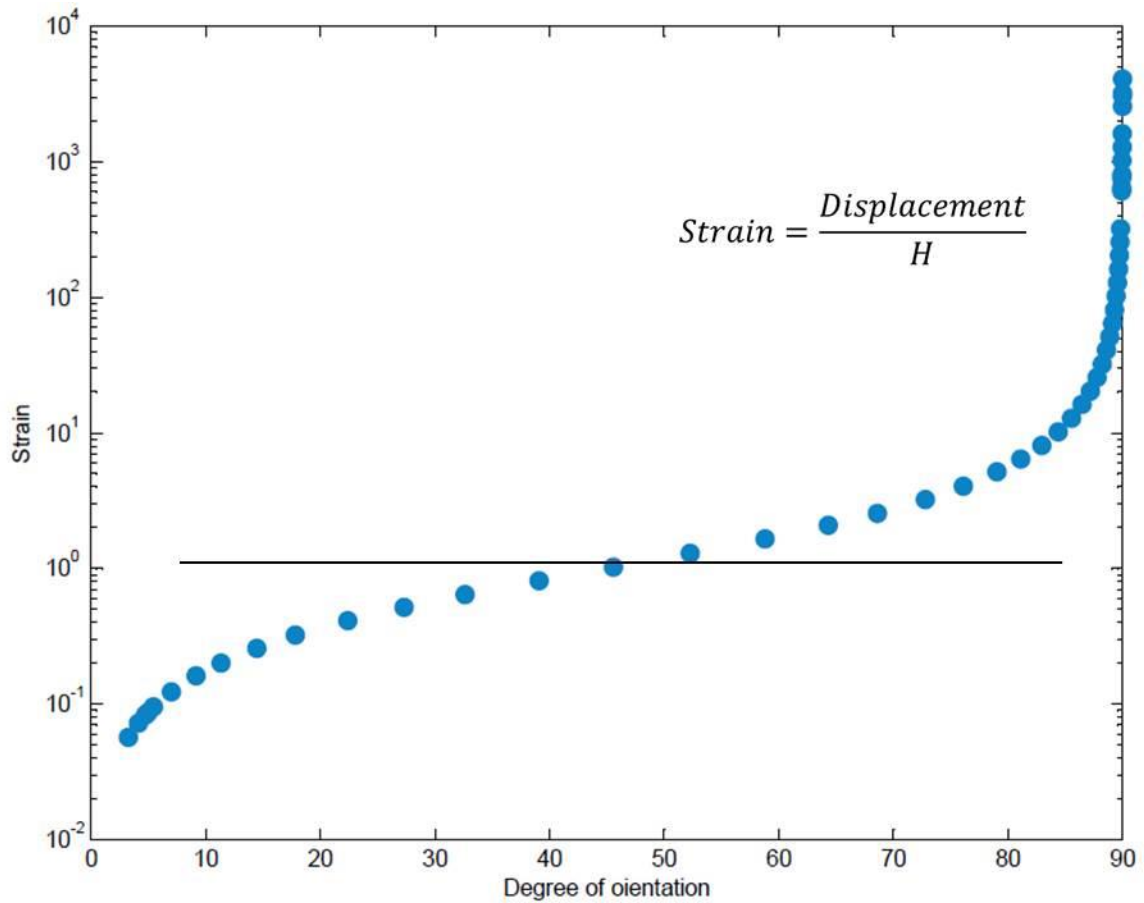
Fig. 5-31 Droplet strain as a function of degree of orientation.

In Fig. 5-31, one can observe that the turning point of this curve is at 45°. Strain, as can be seen in its expression, is the tangent of the orientation angle. Therefore, when the strain is 1 the orientation angle would be 45°.

Performing a strain sweep test, demonstrates that at a strain of 1 the structure of the sample is altered (Fig. 5-32) as expected from the above. As seen in Fig. 5-32 at a strain of ~1 the cross over point is reached followed by a non-linear viscoelastic region. Finally, by applying Eq. 5-21 one can determine the value of the sample's complex viscoelastic modulus over the LVR (Fig. 5-32). This modulus should be constant when there is no droplet deformation; Eq. 5-21 gives a value of 322±6 Pa as the viscoelastic modulus. By fitting the complex modulus to Eq. 5-21 a good match over the LVR is observed (Fig. 5-32).

150
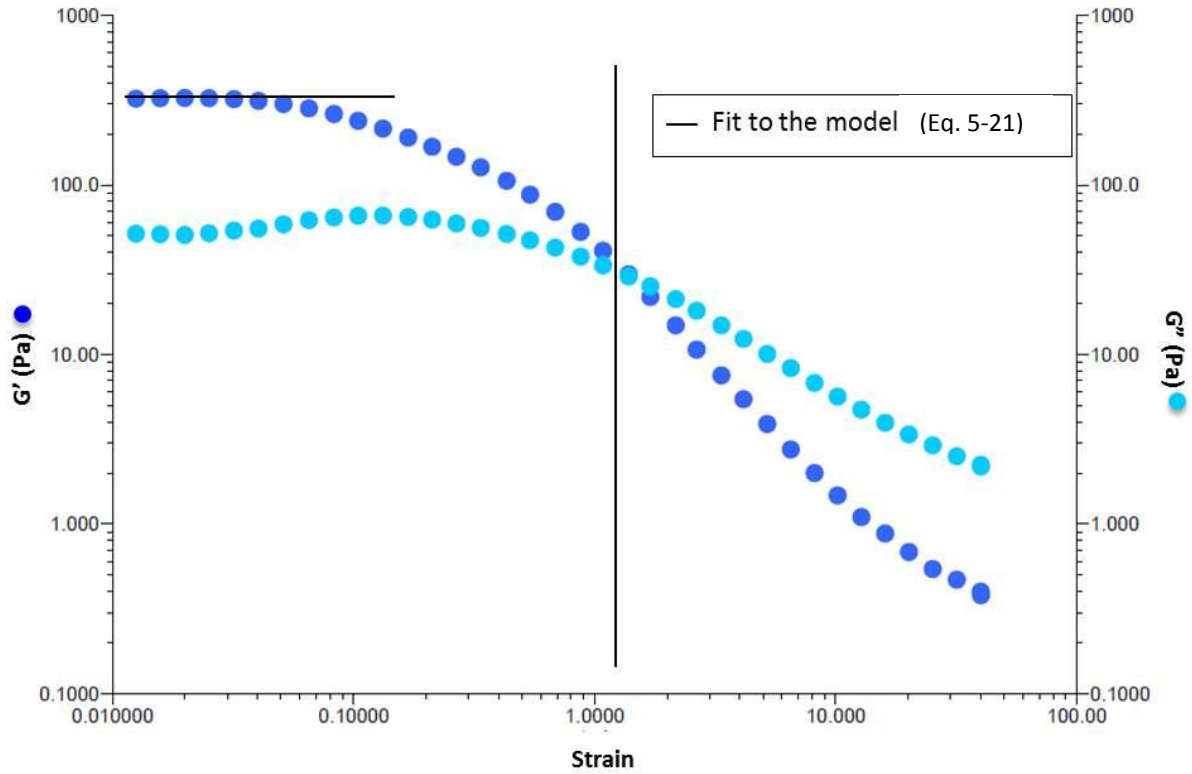
Fig. 5-32 Strain sweep test on PDMS/F127/water emulsion.

5-3-2-3 Effect of droplet size: Monodisperse concentrated coarse emulsions

The viscosity of dilute emulsions obeys Einstein's law which holds as long as droplet interactions can be ignored. Pal [91] has shown that droplet size is important only when the volume fraction is increased ($\phi > 0.6$) for oil-in-water emulsions. The viscosity of concentrated emulsions made of smaller droplets is higher than for emulsions composed of large droplets. In this study Pal also showed that shear-thinning behaviour is pronounced when the droplet size decreases.

Princen *et al*. [98] derived an equation to relate the static shear modulus to the particle size, volume fraction, and interfacial tension in high concentration emulsions:

$$G = 1.769 \, \frac{\sigma}{R_{32}} \, \emptyset^{1/3} \, (\emptyset^* - \emptyset) \qquad\qquad Eq.\,5-22$$

where σ is the interfacial tension, R_{32} is the surface-volume mean droplet radius, $\emptyset^*$ is the closest packing and $\emptyset$ is the volume fraction. This relationship holds for polydisperse emulsions (as can be seen in the factor, R_{32},), the relationship for monodisperse emulsions was also expressed by the same author earlier in 1983 [99]:

151

$$G = 0.525 \frac{\sigma}{R} \emptyset^{1/2} \qquad\qquad\qquad Eq. 5-23$$

where R is the radius of the monodisperse droplets. This equation also holds for high-concentration emulsions.

These equations relate the elastic modulus and the particle size of a size distribution in high-concentration emulsions. While many studies have been undertaken, in which the equations are modified, there remains much work to do to understand the underlying fundamental factors.

Princen also demonstrated that in concentrated systems, a higher yield stress and visco-elasticity is observed as droplet size decreases. These results were supported by Pal [100] who studied the effect of droplet size on the rheology of emulsions. Comparing two close-packed emulsions (∅ = 0.745) of two different sizes (fine and coarse), he showed that emulsions made of fine droplets have a yield stress and are also more viscose.

The same results are observed for the four monodisperse concentrated coarse emulsions under investigation in this research, where even a small increase in droplet size results in a decrease in the viscosity (Fig. 5-33 and Fig. 5-34).
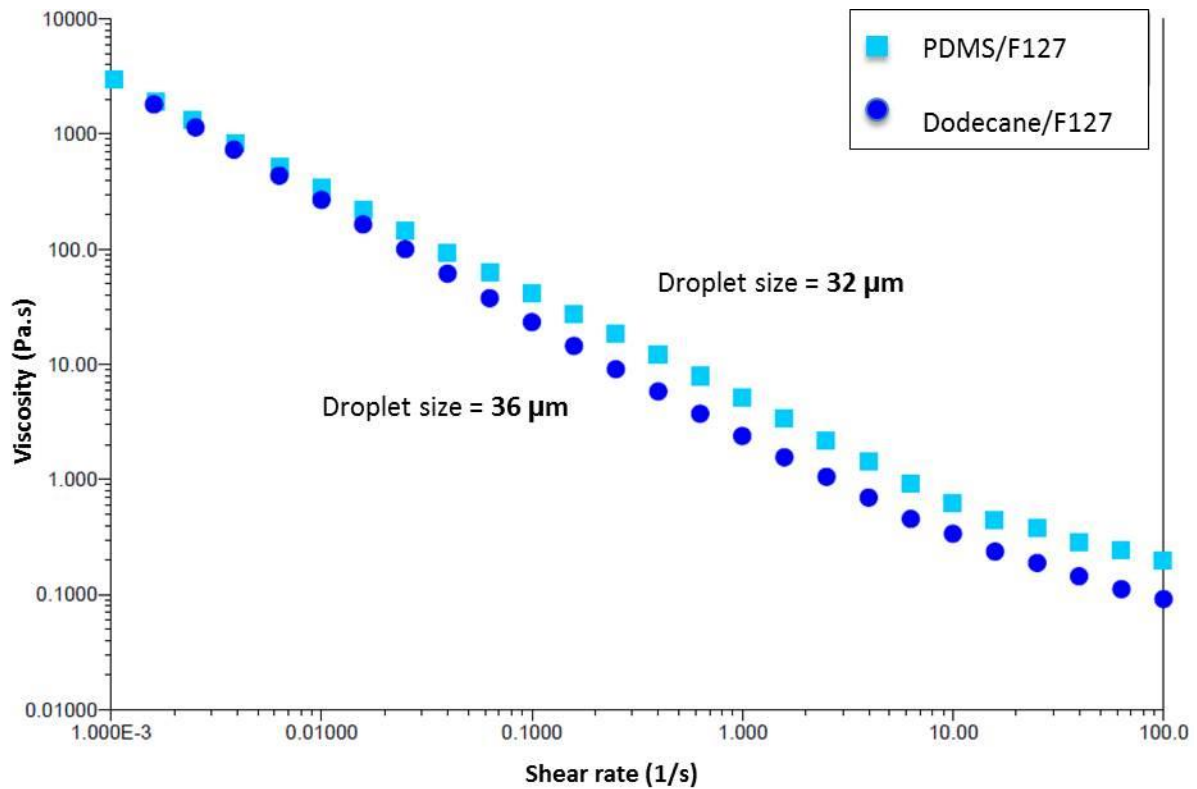
Fig. 5-33 Flow curves of the F127 based concentrated monodisperse coarse emulsions (decreasing shear).

152
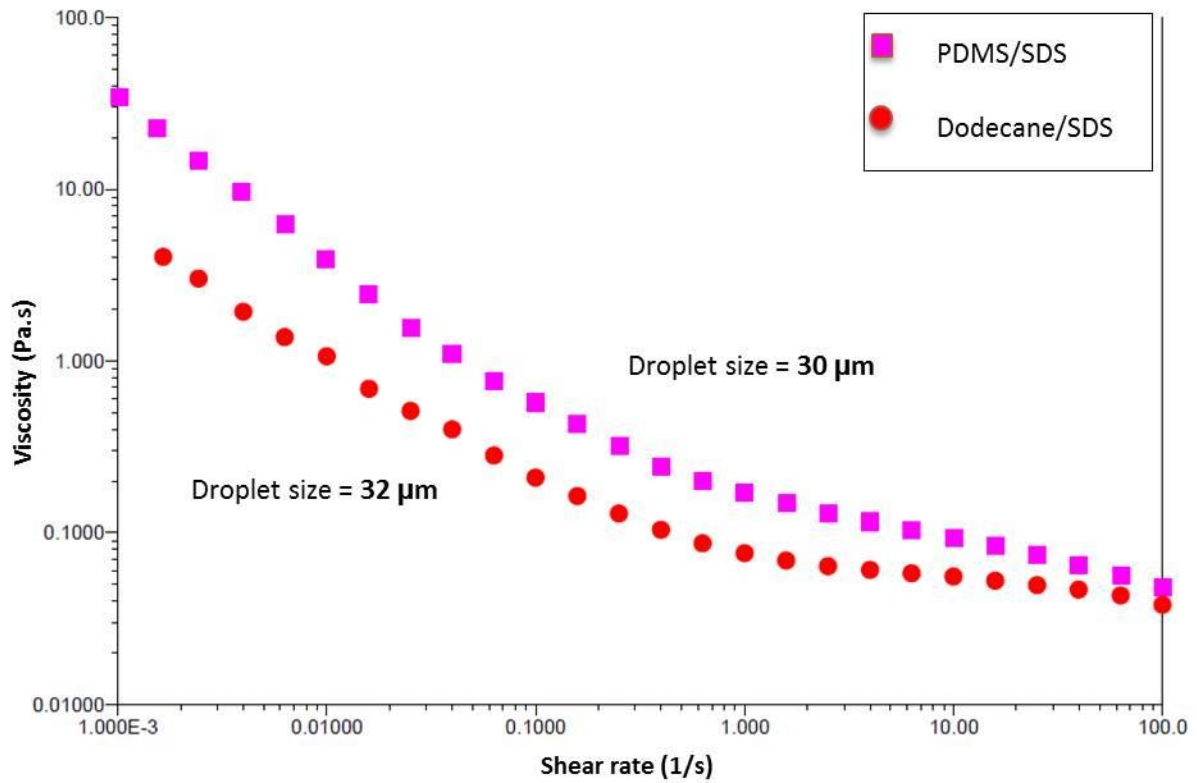
Fig. 5-34 Flow curves of the SDS based concentrated monodisperse coarse emulsions (decreasing shear).

Since Eq. 5-23 is for highly concentrated emulsions and our systems are concentrated emulsions, we propose a modified form of it as below:

$$G = F \frac{\sigma}{R} \phi^{1/2} \qquad\qquad Eq.\ 5\text{-}24$$

where *F* is the fitting parameter and has been chosen to give the best fit. The values of *F* for the coarse monodisperse emulsions are given in Table 5-11.
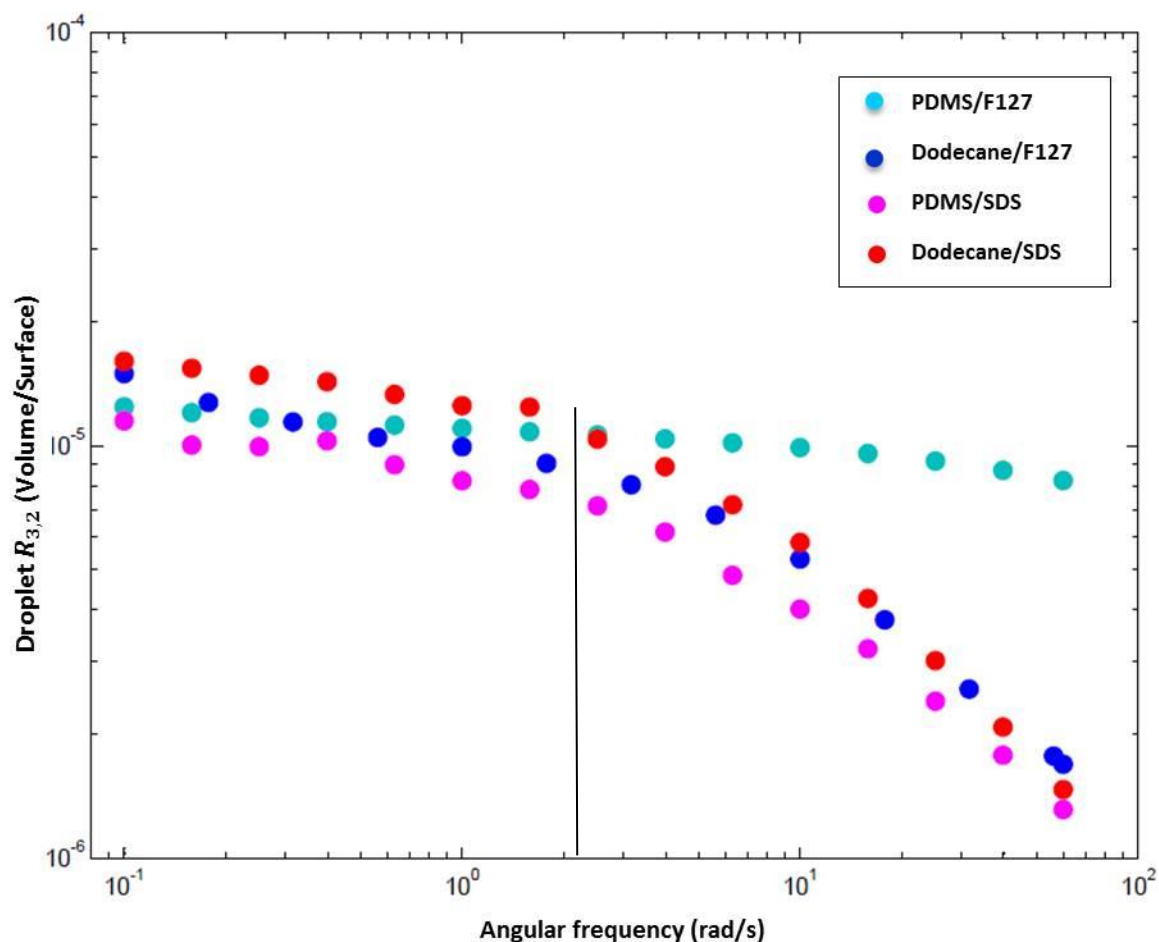
Fig. 5-35 Changing droplet size vs. angular frequency for four monodisperse coarse emulsions, strain=0.05.

In this research, by applying Eq. 5-24 the droplet deformation as a function of the angular frequency was recorded. The relevant data are shown in Fig. 5-35. As seen in Fig. 5-35, PDMS/F127/water coarse emulsions display the lowest change in droplet size over the applied range of frequency. As previously stated, this is due to the interfacial layer in this system being thick due to the large polymeric F127 and also the viscosity of the dispersed phase is five times that of the continuous phase. This makes this system robust and results in this coarse emulsion undergoing the lowest deformation. For the other three systems, a low deformation region, up to an angular frequency of 2 rad/s, followed by a relatively high deformation region is observed.

Table 5-11 Values of *F* used in Eq. 5-24 for the monodisperse coarse emulsions

Coarse emulsion	Oil volume fraction	$\log(F)$
PDMS/F127	0.50±0.01	-1.53±0.01
Dodecane/F127	0.55±0.01	-3.37±0.01
PDMS/SDS	0.45±0.01	-3.40±0.01
Dodecane/SDS	0.42±0.01	-2.76±0.01

As mentioned previously, *F* is the fitting parameter however considering the values of *F* given in Table 5-11 and the deformation curves, Fig 5-35, it is evident that there is an inverse relationship between *F* and deformation. The PDMS/F127 system has the lowest deformation, the lowest droplet size change upon applying angular frequency and the highest value of *F* for the four systems. Apart from the rate of deformation, the volume fraction also has an effect on *F*. For the three systems with the same deformation trend, dodecane/F127, PDMS/SDS and dodecane/SDS, there is a direct relationship between the value of *F* and volume fraction.

The viscoelastic modulus of the samples themselves can be written as a function of the angular frequency using a two-element Maxwell model. Each element of the model contains a spring and a dash-pot connected together (Fig. 5-36).
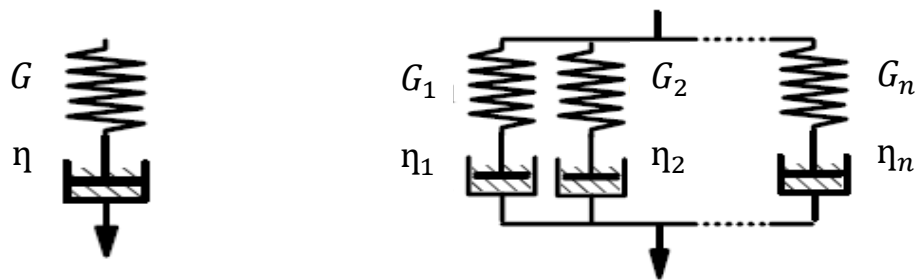
Fig. 5-36 Single-element (left) and multi-element (right) Maxwell model.

The viscose and elastic moduli of a viscoelastic material modelled using the Maxwell model, for a single-element and n-element Maxwell model respectively, can be written as follows:

$$G' = \frac{\eta \lambda \omega^2}{1+\lambda^2 \omega^2} \qquad and \qquad G'' = \frac{\eta \omega}{1+\lambda^2 \omega^2} \qquad\qquad Eq. 5-25$$

$$G' = \sum_n \frac{\eta_n \lambda_n \omega^2}{1 + \omega^2 \lambda_n^2} \qquad and \qquad G'' = \sum_n \frac{\eta_n \omega}{1 + \omega^2 \lambda_n^2} \qquad\qquad Eq. 5-26$$

Using the above relationships for a two-element Maxwell model, one can fit the frequency sweep data for the four systems as shown in Fig. 5-37. The relevant G and τ of each system are given in Table. 5-12.
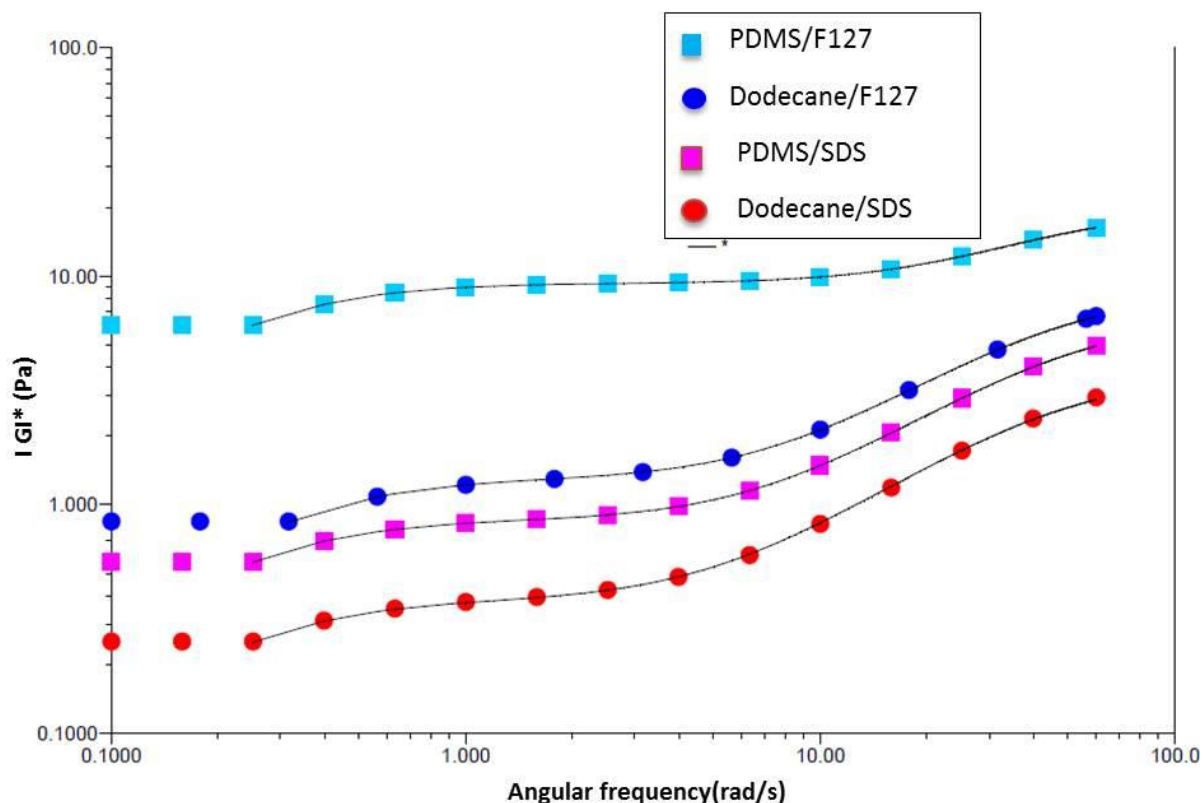
Fig. 5-37 Changing complex modulus as a function of angular frequency for the four monodisperse coarse emulsions; strain 0.05, fitted with a two-element Maxwell model.

Table 5-12 Relevant parameters for the oscillatory rheology data for the four monodisperse concentrated coarse emulsions fit to a two-item Maxwell model

System	G_1 (Pa)	τ_1 (s)	G_2 (Pa)	τ_2 (s)
PDMS/F127	10.41 ± 0.01	0.021 ± 0.001	9.22 ± 0.01	3.46 ± 0.01
Dodecane/F127	7.27 ± 0.01	0.021 ± 0.001	1.23 ± 0.01	2.75 ± 0.01
PDMS/SDS	5.69 ± 0.01	0.019 ± 0.001	0.82 ± 0.01	3.46 ± 0.01
Dodecane/SDS	3.52 ± 0.01	0.019 ± 0.001	0.36 ± 0.01	3.46 ± 0.01

As seen in Fig. 5-35 the droplet volume/surface size ($R_{3,2}$) curve of the emulsions displays two patterns of decrease as a function of frequency. The shift occurs at an angular frequency of 2-3 rad/s. This means there are two types of viscoelastic behaviour due to the structure change that occurs upon applying a higher frequency at a fixed strain. This

matches with monodisperse emulsions being modelled by a two-element Maxwell model. For F127/PDMS however a close to single decay is observed with the system displaying two values of G that are very similar at different time scales (0.02 and 3.5 s) (Table. 5-12).

5-3-3 Effect of polydispersity

The viscosity of emulsions is affected by polydispersity in the droplet distribution. As a rule of thumb [76], the viscosity decreases inversely with increasing polydispersity. For the systems under investigation, the more polydisperse the sample, the more disordered the structure of the system; thus it may be easier to deform under shear forces which means it is less viscose.

The size ratio (ratio of big particles to small ones) is important. Farris [101], studying mixtures of monodispersed droplets, has shown that the viscosity decreases more strongly when the size ratio reaches 10. Viscosity depends on the fine droplets suspended in the sample. The fine droplets and the continuous phase form a pseudo-continuous medium, decreasing the interaction between large droplets followed by a reduction in the viscosity. Haffman [102] has demonstrated this reduction reaches a minimum and afterward an increase in the viscosity will be observed due to the interactions between the fine droplets coming into play.

Droplet size distribution strongly affects the viscoelasticity of concentrated and high-concentration emulsions. Actually below the close packing volume, one expects monodisperse emulsions to not have an elastic modulus, but in reality this modulus can be seen even below the close-packed point. Lequeux [103] has explained this phenomenon by taking into account the attraction between droplets due to depletion and bridging. These effects should be seen at higher concentration in polydisperse systems since the close packing volume is higher and the interaction between the droplets is less (at least at a range of concentrations).

Finally it should be mentioned that under a specific strain, polydisperse emulsions would reach the rupture point more easily than monodisperse emulsions owing to their less ordered structure; Saiki *et al*. [104] have shown this quantitatively.

In this research a polydisperse coarse emulsion system of PDMS/SDS was studied and its flow curve was compared to the monodisperse system made of the same chemicals (Fig. 5-38 & 39). The polydispersity results from the syringe pump not generating droplets steadily;

hence about 20 percent of the droplets have a different droplet diameter (from 20 to 30 µm) to the major droplet size of the system (30 µm), the flow curves attributed to mono and polydisperse systems are given in Fig. 5-39.

━━ 30 µm
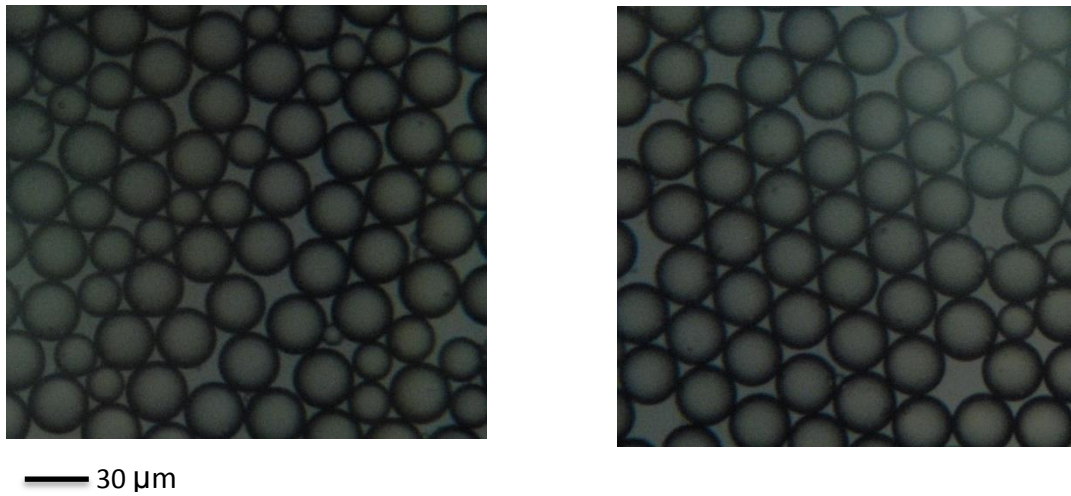
Fig. 5-38 Polydisperse (left) and monodisperse (right) emulsions of PDMS/SDS.
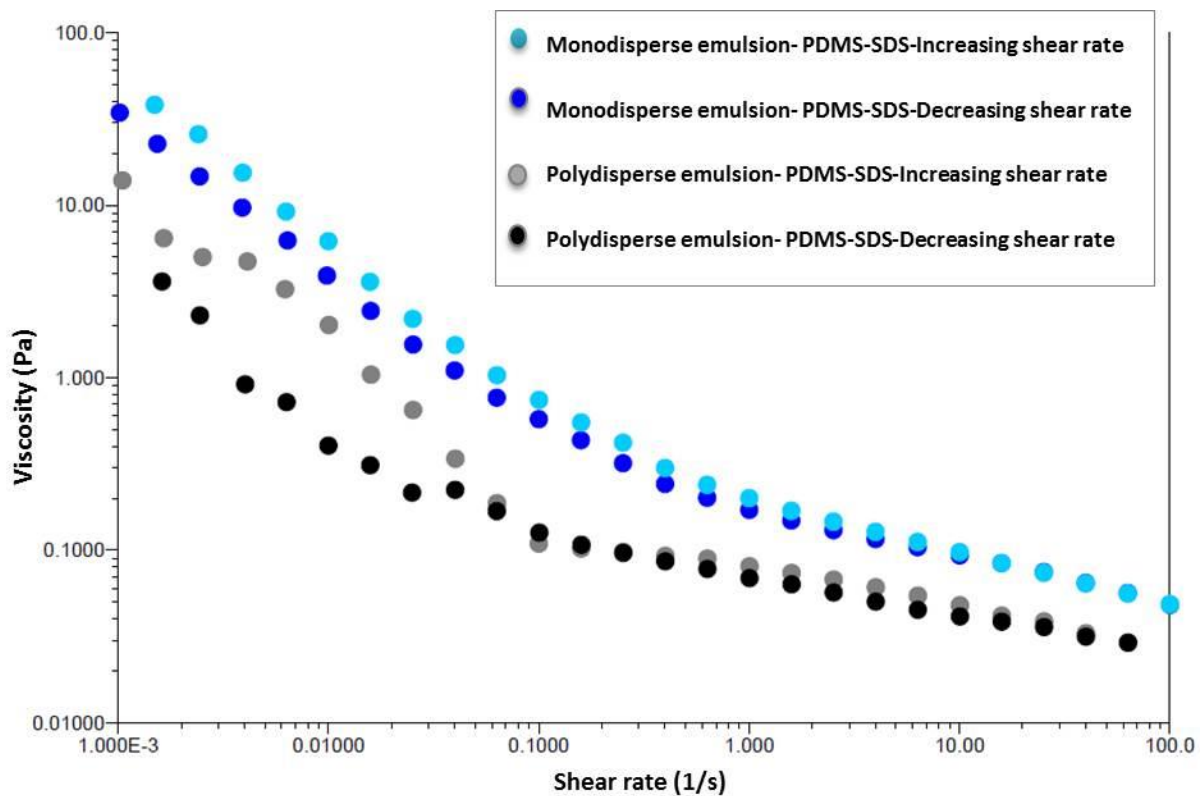
Fig. 5-39 Flow curves of monodisperse (top) and polydisperse (bottom) emulsions of PDMS/SDS.

As seen in Fig. 5-39 not only has the viscosity decreased, but also a hysteresis loop arises due to the introduction of polydispersity. This is because of different possible patterns of

packing as compared to a monodisperse system and consequently the greater dependency of the viscosity on the method of applying shear and its effect on the packing pattern. The same result is observed in the flow curves attributed to the emulsion system produced in the homogenizer but with a greater effect due to the higher polydispersity present in these emulsions (Fig. 5-40). This indicates that the more polydisperse the sample is, the more significant role the method of applying shear plays.
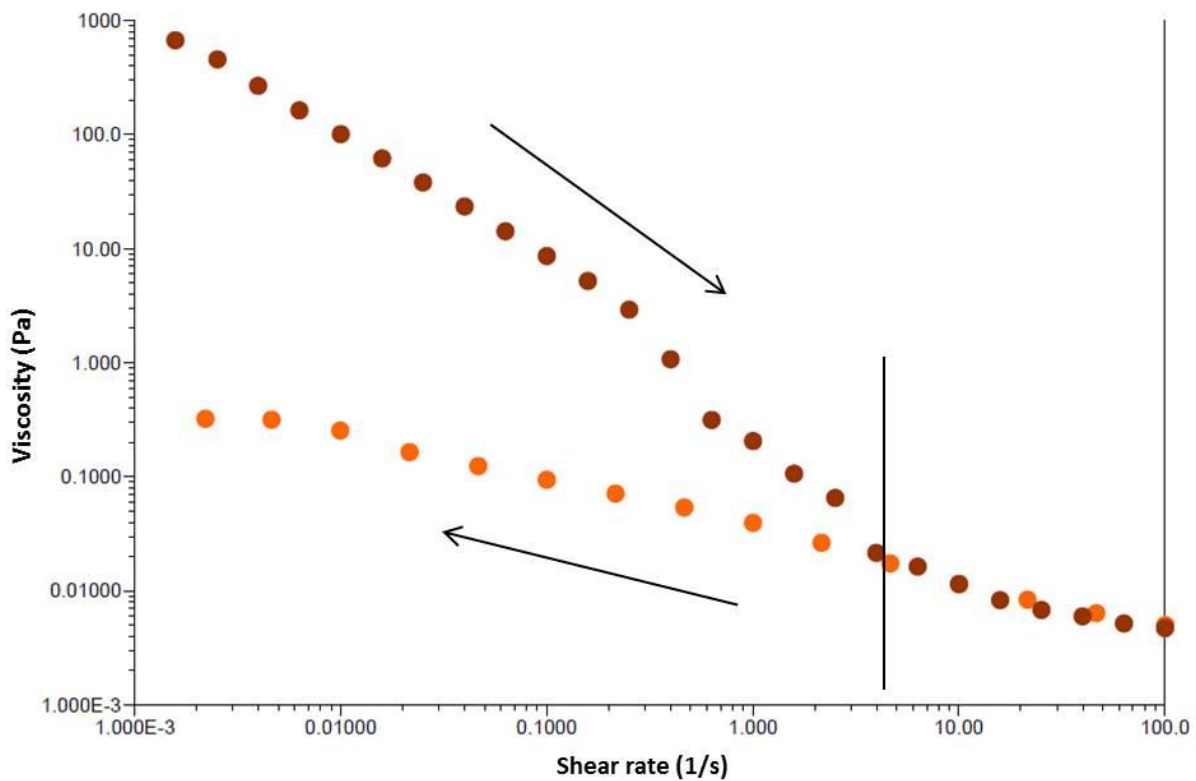
Fig. 5-40 Flow curve of a polydisperse dodecane/SDS emulsion generated in the homogenizer on increasing and decreasing shear rate.

As seen in Fig. 5-40, for shear rates higher than approximately 4/s the two curves match. This shear rate is the point at which the structure of the sample is changed and this change is irreversible for shear rates 4/s and above. Below this value the changed emulsion structure has different flow behaviours.

To further explore the effect of packing on the viscosity, we have mixed 50% of PDMS/SDS and 50% dodecane/SDS the droplet sizes are similar (30 and 32 μm). We then performed the steady state flow test. The data show that at low shear rates the PDMS-based system dominates the system. Upon increasing shear rate the response of the system begins to match that of the pure dodecane-based system. At very high shear rates however the

viscosity of the bimodal system falls below that of either of the individual systems (Fig. 5-41). This is the effect of introducing polydispersity to the system. At high shear rates ,where droplet interactions decrease, the external force, shear rate, makes the bimodal system flow easier than the monodisperse systems that make up the bimodal system.
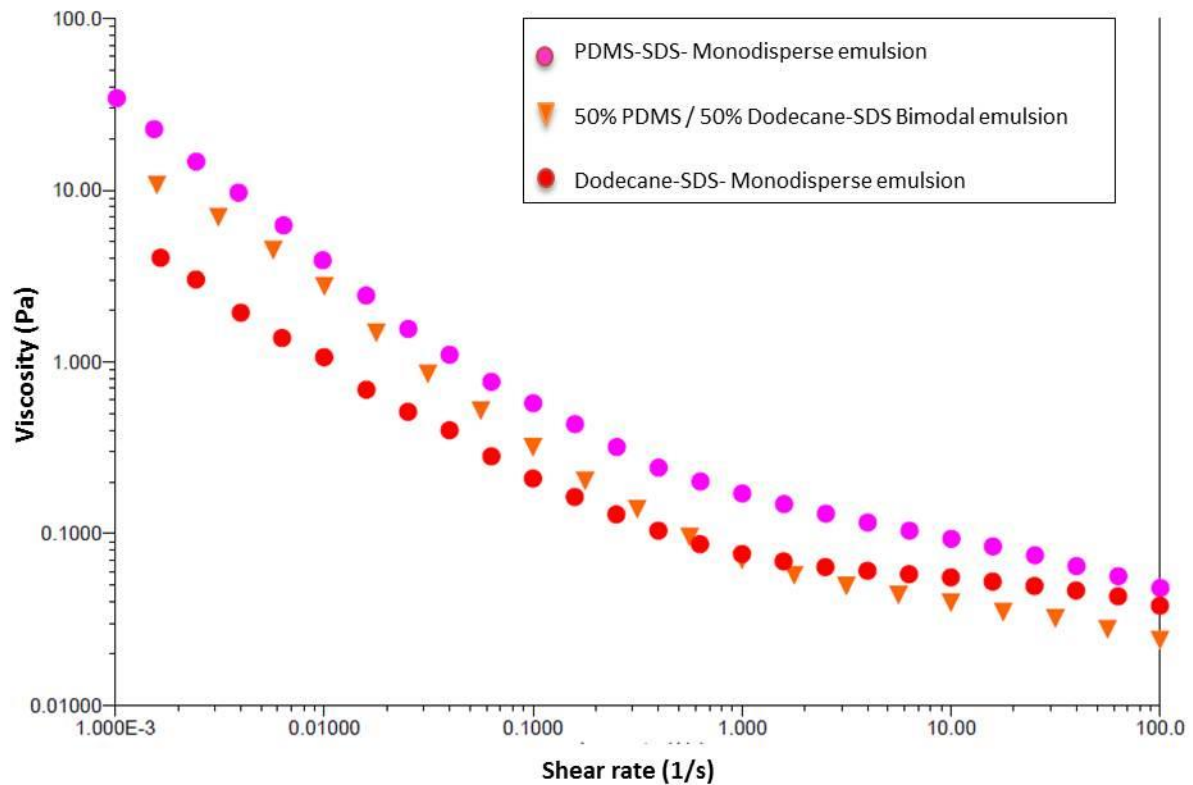
Fig. 5-41 Effect of the introduction of polydispersity on the flow behaviour of coarse emulsions.

5-3-4 Effect of surfactant

The interfacial layer plays an important role in emulsion rheology [105]. These days researchers explore this by investigating the interfacial rheology [106] which is out of the scope of this thesis. The correlation between the interfacial and bulk rheology is an interesting subject to study which might shed light on the contribution of the interface to the bulk rheology. In this research, monodisperse emulsions composed of two completely different surfactants in terms of structure and charge (F127 and SDS) have been generated. As a result the relevant flow curves are readily distinguishable based on the surfactant used no matter which oil has been used (dodecane or PDMS). Emulsions made with F127 always

have higher viscosity over the whole range of shear rates as compared to those made with SDS (Fig. 5-42).

The obvious differences based on surfactant alone is due to F127 having a larger polymeric structure compared with SDS. The interfacial layer comprised of F127 is thicker and has viscoelastic and deformability properties. These attributes give the system time dependency behaviour since the surfactant undergoes relaxation and deformation upon applying force.

The flow curve data can be fit using the Hershel-Bulkley relationship [107], to obtain the yield stress:

$$\tau = \tau_0 + b * \gamma^n \qquad\qquad Eq.\,5-27$$

where τ is shear stress, τ_0 is the yield stress and b and n are constant. The fit results are shown in Fig. 5-42.
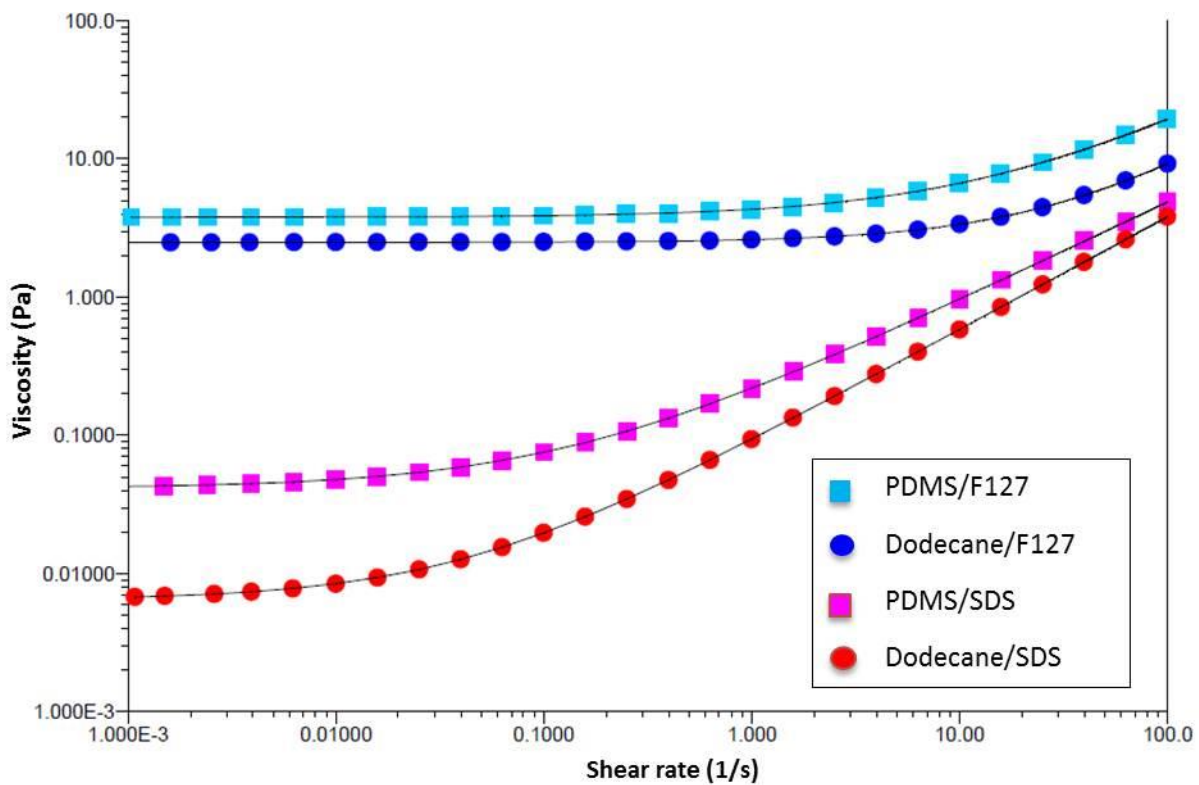
Fig. 5-42 Four monodisperse coarse emulsion flow curves fit to Hershl-Bulkey.

The estimated yield stresses are given in Table 5-13. These yield stresses highlight the surfactant differences. Yield stress is representative of the force needed to make a fluid flow

and therefore displays the resistance of the material against being flowed. As seen in Table 5-13 when the interfacial layer is comprised of large polymeric F127 the yield stress is orders of magnitude higher than when SDS is the surfactant. Also the data show that for a given surfactant (F127 or SDS) the yield stress of the system made with PDMS is higher than the dodecane-based system. This is due to higher viscosity of PDMS compared with dodecane (5 and 1 cp respectively). It is noted that the effect of the oil on the yield stress accents when the surfactant is SDS (0.0068 and 0.041 for dodecane/SDS and PDMS/SDS respectively); while in F127 based coarse emulsions this effect is less significant (2.49 and 3.48 for dodecane/F127 and PDMS/F127 respectively). The reason for this is that when the interfacial layer is thick the oil is too shielded (i.e. hidden) to affect the flow properties drastically.

By performing a creep test, the time dependent behaviour of the four coarse emulsions can be investigated. The systems made with SDS do not display time dependency whereas those prepared using F127 do even at high torque, e.g. 100 μN.m (Fig. 5-43 and Fig. 5-44). Again this can be attributed to the size and structure of F127 and the interfacial layer thickness as compared to SDS resulting in time dependency. This time dependency is also seen in the flow curves of the F127 systems (Fig. 5-45). The SDS-emulsions show negligible hysteresis.

Table 5-13 Yield stress of the four monodisperse emulsions

System	Yield stress
PDMS/F127	$3.78. \pm 0.01$
Dodecane/F127	2.49 ± 0.01
PDMS/SDS	0.041 ± 0.001
Dodecane/SDS	0.0068 ± 0.0001
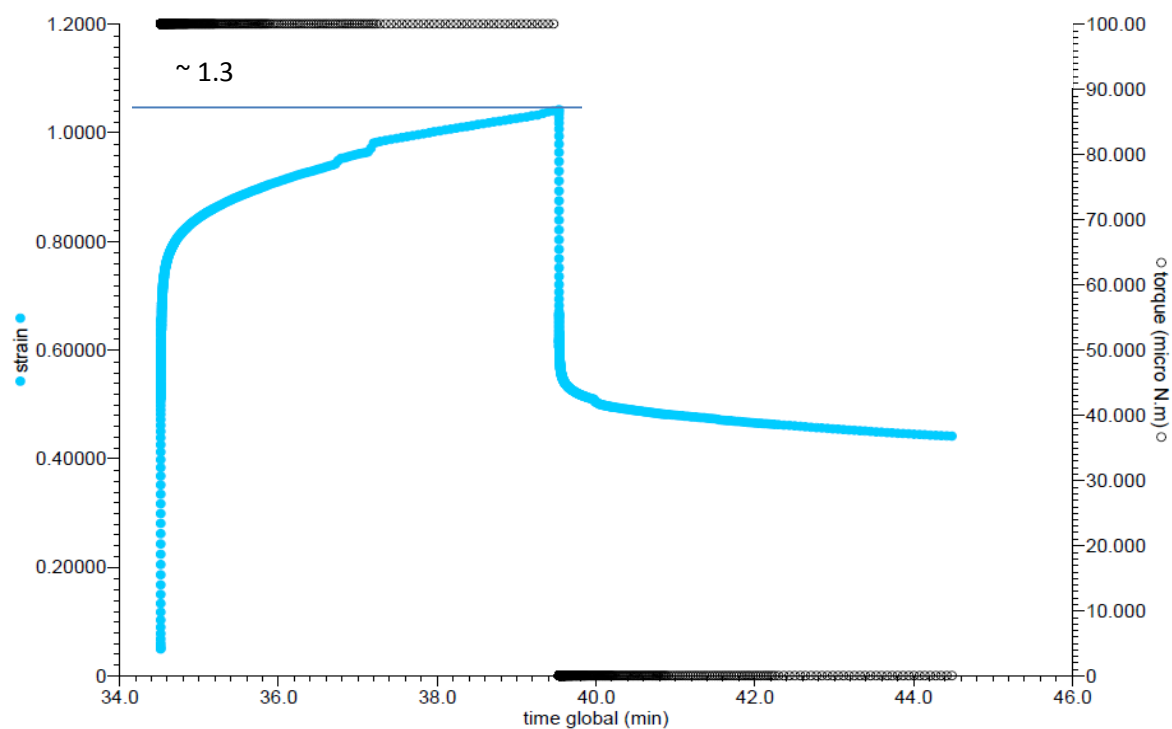
Fig. 5-43 Blue data points: Creep test data for the dodecane/F127/water monodisperse coarse emulsion. Black data points: Applied torque. Horizontal blue line: Maximum strain.
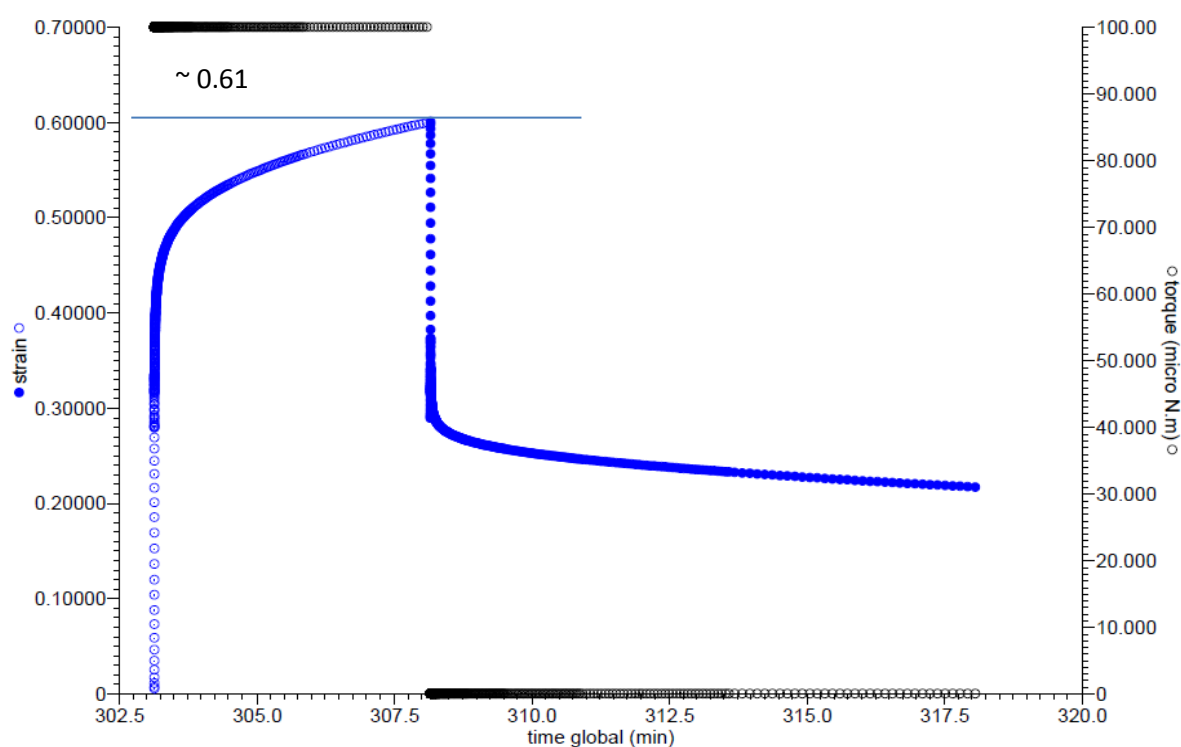
Fig. 5-44 Blue data points: Creep test data for the PDMS/F127/water monodisperse coarse emulsion. Black data points: Applied torque. Horizontal blue line: Maximum strain.
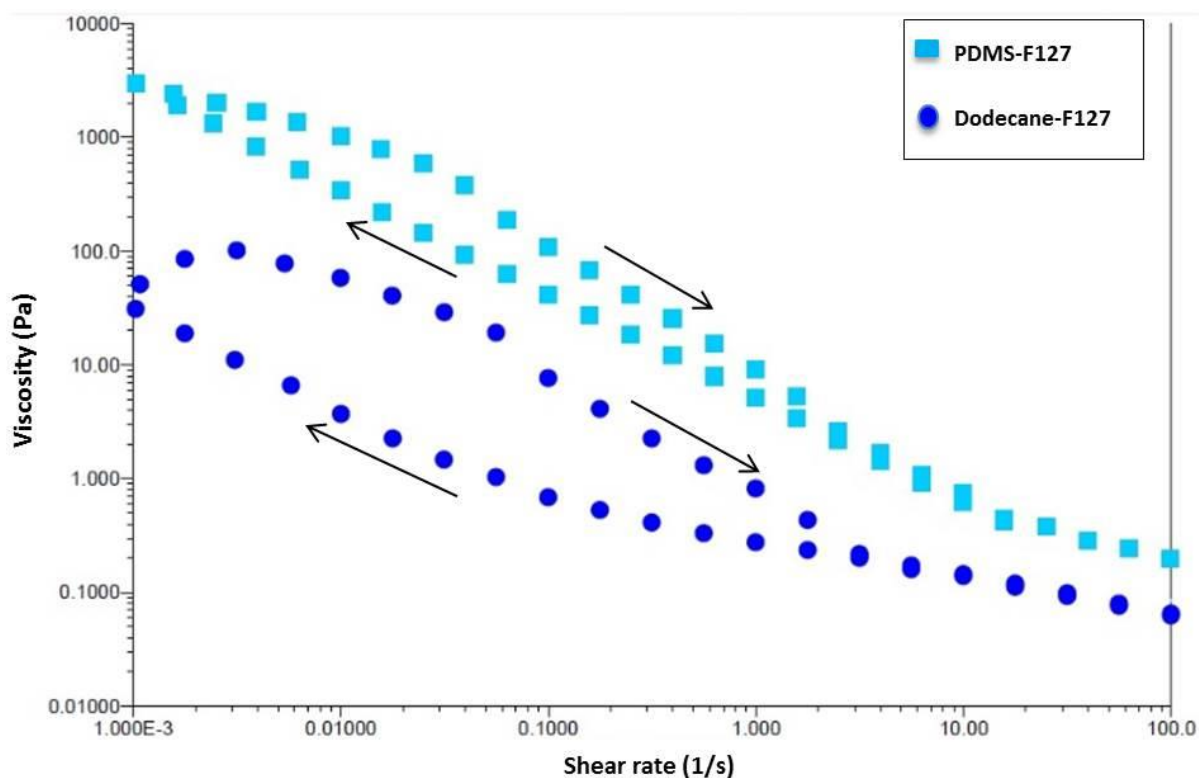
Fig. 5-45 Hysteresis loops observed in the flow curves of F127-based concentrated coarse emulsions.

As seen in Fig. 5-43 and Fig. 5-44 the maximum strain in the dodecane/F127 coarse emulsion system (~1.3) is about twice that of the PDMS/F127 coarse emulsion system (~0.61). This is because of the lower viscosity of dodecane (1 cp) as compared to PDMS (5 cp) allowing the droplets to deform more easily.

In another experiment we have made a system of PDMS and a mix of 50% F127 and 50% SDS. The flow curve of this system demonstrates a hysteresis loop that indicates time dependency in the system (Fig. 5-46). As discussed previously, the SDS/PDMS coarse emulsions do not show time dependant behaviour, however when 50% F127 is added to the interfacial layer the system shows time dependency.

This finding is confirmed in the creep test data (Fig. 5-47). The maximum strain that can be obtained in the mixed system (~0.27) is half of that of the pure F127/PDMS system (~0.60). The maximum is reached for the mixed system upon applying a very low torque (0.5 µN/m) while the pure PDMS/F127 system demonstrates time dependency up to high torque (100 µN.m) (Fig. 5-47).
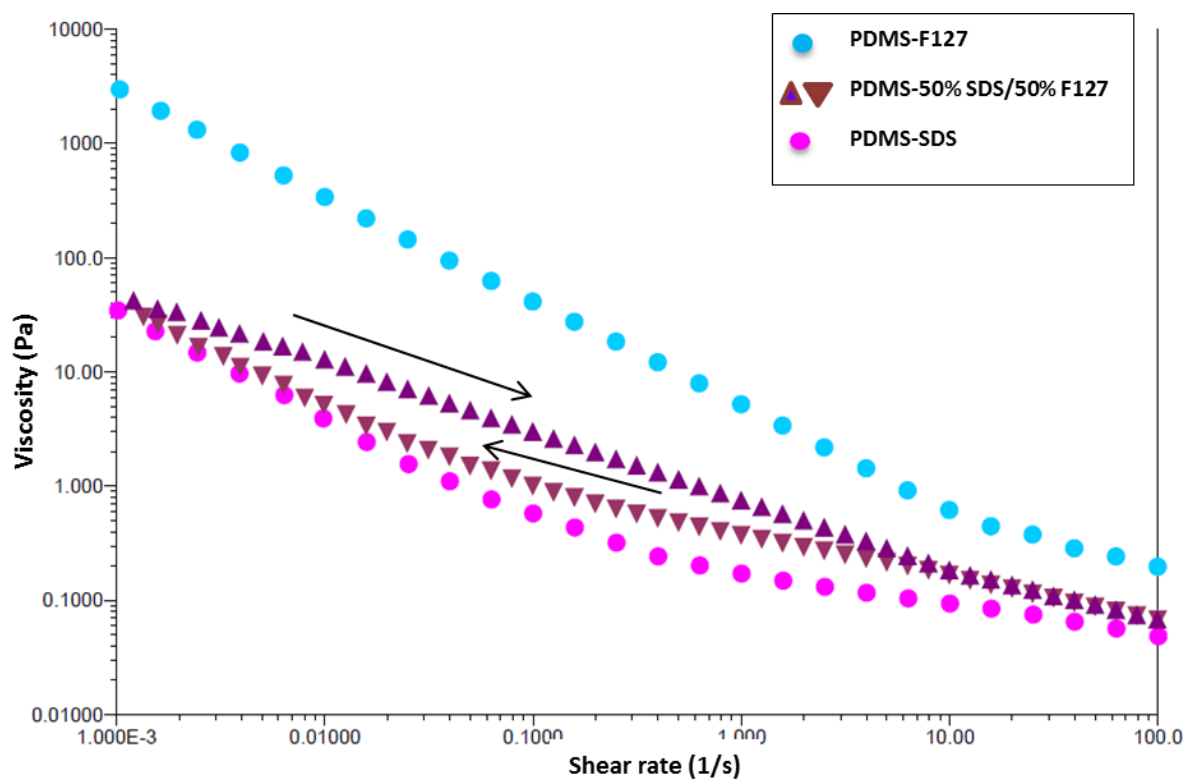
Fig. 5-46 Hysteresis loop in the flow curve of PDMS based emulsion with mixed surfactants of SDS and F127.
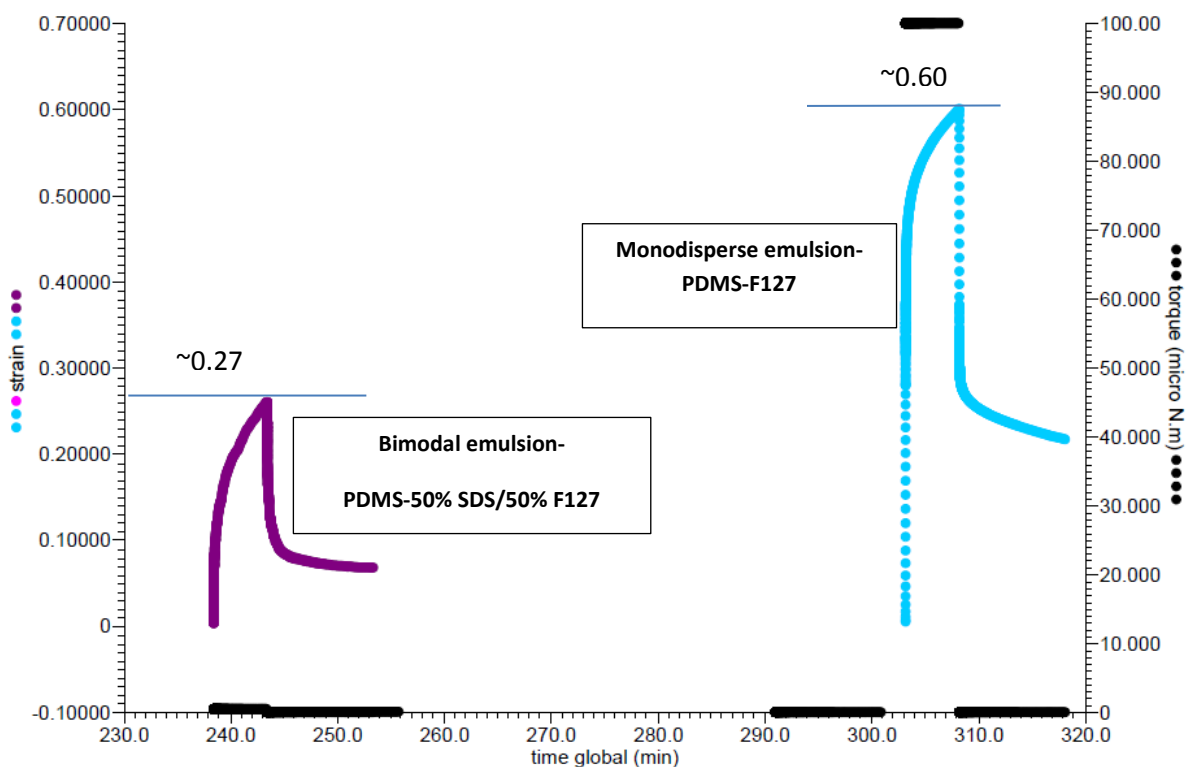
Fig. 5-47 Purple and blue data points: Creep tests for a PDMS based emulsion with mixed surfactants of SDS and F127 and a PDMS/F127 monodisperse emulsion respectively. Black data points: Applied torque. Horizontal blue lines: Maximum strain.

As explained previously the time dependency of the emulsion is highly affected by the interfacial layer properties. Comparing the time-dependent behaviour and the hysteresis loop in PDMS/F127 and the mixed F127/SDS system, demonstrates that these parameters are functions of the concentration of F127. As seen in Fig. 5-46 the value of the viscosity of the mixed system is not merely the average of the two individual systems that make up the final polydisperse system. This means that the relationship between the concentration of F127 and the flow properties is non-linear. The reason is that the interfacial layer is a mixture of F127 and SDS with its own physical and chemical properties that are not the average of the properties of each surfactant interfacial layer individually.

Other important factors that need to be taken into account are the inter-droplet forces. Such forces make the mixed system (especially upon applying decreasing shear rate) behave in a way similar to the PDMS/SDS coarse emulsion at low shear rate. As shear rate increases, droplet interactions become less important and the viscosity of the mixed system tends to the average value of the viscosities of the two systems.

It is worth noting that the droplet sizes of the PDMS/F127 and PDMS/SDS coarse emulsion droplets are similar to each other (30 and 32 μm respectively) which almost eliminates the effect of droplet size on the flow properties of these two systems and also the mixed system. This highlights the importance of the effect of interfacial layer properties (especially thickness) on the rheology of these systems.

Finally it should be noted that considering the maximum packing of PDMS/F127 system as compared to PDMS/SDS system (0.63 and 0.58 respectively), one would determine that the first system is more ordered. This significantly contributes to the high viscosity of this system. By mixing the two systems, the order is altered. This is why the viscosity of the mixed system is more similar to that of the PDMS/SDS system.

As explained above the interfacial layer affects the rheology. Determining a relationship between the viscosity of the sample and the frequency of oscillation provides a better understanding of the viscoelasticity due to interfacial film relaxation. Oldyard studied and developed the "similarity rule" which is valid for concentrated emulsions:

$$\eta^*(\omega) = \eta(\dot{\gamma}). \hspace{4cm} Eq. 5 - 28$$

$Eq. 5 - 28$ is actually the Cox-Merz rule [108] for viscoelastic polymer melts which relates the complex frequency-dependent viscosity to the apparent, strain-dependent viscosity.

Good agreement between experimental emulsion data and the similarity rule tells us that this rule expresses the elasticity of the system regardless of what components are included in the system.

This rule is expected to be applicable to our emulsions that are made out of F127 which is a polymeric surfactant, however it turns out that such a rule only holds for the PDMS/F127 system and not for the dodecane/F127 system (Fig. 5-48). By considering the static and dynamic rheological data of these two emulsions one would determine that the PDMS-based system is more robust than the dodecane-based one (due to the viscosity of PDMS being five times that of dodecane). It is concluded that not only is the interfacial layer of a higher mechanical strength for a system to follow Cox-Merz rule but also the droplets must be robust enough not to undergo significant deformation (Fig. 5-48 shows that the droplet deformation in PDMS/F127 system is very slight).
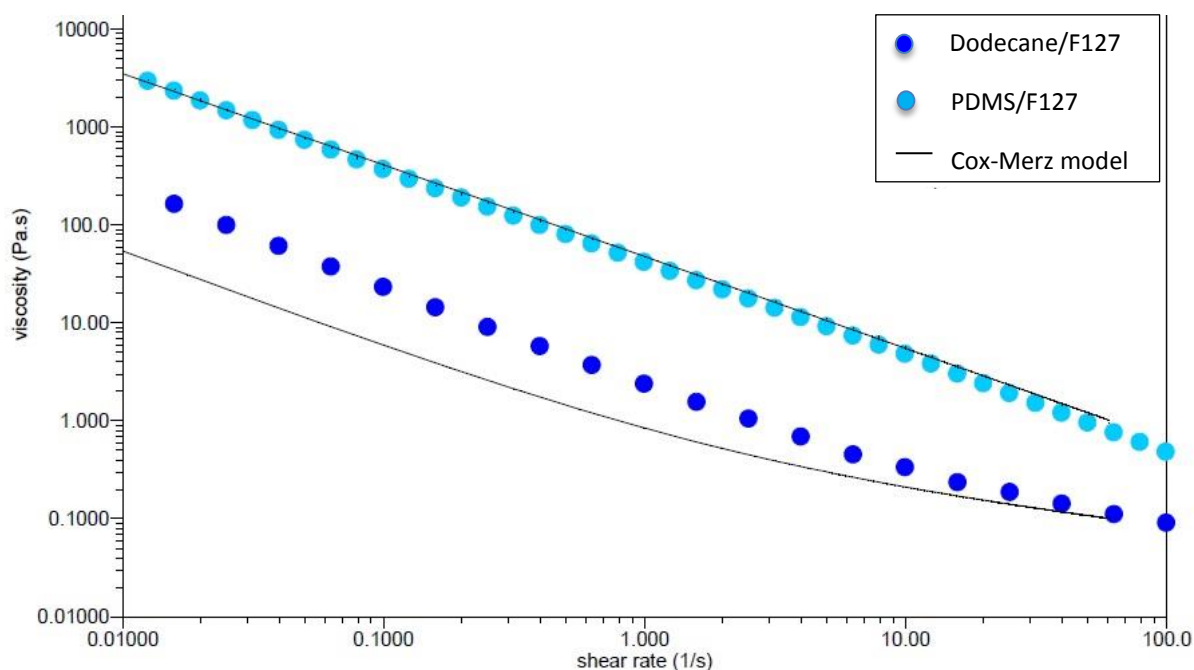
Fig. 5-48 Predicted flow curve from Cox-Merz rule as compared with experimental data.

5-3-5 Discussion

Rheological characterizations of coarse emulsions were undertaken. The most important factors affecting the rheological behaviour of these systems are droplet deformation and the characteristics of the interfacial layer. Importantly these factors are not accounted for in nearly all rheological models, where generally only volume fraction and/or viscosity ratio

between the continuous and dispersed phase are taken into account. However by applying the model proposed by Pal *et al.*, Eq. 1-4, that accounts for closest packing we have been able to fit our experimental data. The important modification to this relationship is that we consider the closest packing as a function of shear rate. This makes the relationship also include droplet deformation.

Droplet deformation was investigated individually by exploiting Eq. 5-24 that correlates the viscoelastic modulus and droplet size. Given the size is variable with the applied shear rate; droplet deformation vs. shear rate was attained.

A 2-D mathematical model was developed to calculate the viscoelastic modulus based on the interfacial tension. The gap size between the parallel plates of the rheometer needs to be adjusted and set to a comparable value to the droplet size to allow the model to be used. Using this model the linear viscoelastic modulus is able to be predicted.

The effect of polydispersity was also found to be significant with regard to both the viscosity and yield stress of the system. Both of these parameters decrease upon introducing droplets of different size into the system. The greater the size difference, the lower the viscosity of the mixed system and the yield stress.

According to the above discussion the proposed model for monodisperse macroemulsions is:

$$\eta = \eta_0 \qquad\qquad \dot{\gamma} < \dot{\gamma}_1 \qquad\qquad Eq.\,3-4\ (Recalled)$$

$$\eta = \eta_\infty + \frac{A}{\dot{\gamma}^n} \qquad\qquad \dot{\gamma}_1 < \dot{\gamma} \qquad\qquad Eq.\,5-17\ (Recalled)$$

where η_0 is defined by the surfactant properties and also the polydispersity of the system. It should be mentioned that the shear rate pattern, increasing or decreasing, is important and as explained previously usually the pattern should be increasing in order for one to be able to observe the initial solid-like behaviour, η_0.

The factor η_∞ is determined by the nature of the system. For example, as seen in Fig. 5-24 the infinite constant viscosity is likely to be reached sooner in SDS-based systems as compared to F127-based ones. This is due to the interfacial layer being comprised of large polymeric F127 that shows viscoelastic features upon applying higher shear rates as

compared with SDS. The parameters *A* and *n* are defined by droplet deformation and the rate of droplet deformation. The values of *A* and *n* are given in Table 5-10. *A* is a representative of the time scale in the system. As seen in Table 5-10 this factor is 4.7 s and 2.5 s for F127-based emulsions as compared to 0.08 s and 0.03 s for SDS-based emulsions. This is in line with F127-based systems being time dependant. This is all due to the increased thickness of the F127 interfacial layer that takes time to deform and relax back increasing the time scale of the system. *n* is the slope of the flow curve in a log-log plot. Hence the greater this factor, the more significant the decrease in the flow curve upon applying shear rate. This means the transformation from shear-thinning to Newtonian behaviour has a direct relationship with *n*.

It should be mentioned that for dilute emulsions the droplet size and size distribution can be neglected as many researchers suggest, however the reference viscosity used in relative viscosity calculations should be that of the surfactant solution. For such systems with a narrow size distribution, the above proposed model can be applied. For lower concentrations (below 1 wt. %) the model proposed for microemulsions, as previously proposed in Chapter 3, can be used. It should be mentioned that, as expressed above, the introduction of polydispersity to the system results in complicated flow behaviour and makes it very difficult to propose a model for the system. In this case experimental models need to be applied. It is worth mentioning that if a dilute emulsion is generated from a coarse monodisperse emulsion, due to its ordered structure, the applicability of the microemulsion models is evident up to high oil concentrations (see Fig. 5-25).

5-4 Conclusion

In this section a range of normal emulsions and coarse emulsions with length scales ranging from 0.5 to 40 µm where investigated.

Coarse emulsions, droplet size between 30 and 40 µm, are not stable due to their large droplet size. These systems were prepared using a microfluidic device. This devise generates monodisperse systems, therefore the effect of polydispersity can be omitted and deformation and packing within the system can be studied straightforwardly. These factors are the most significant parameters affecting the flow properties of concentrated emulsions. To investigate these parameters one needs to consider the droplet volume

fraction as well as maximum packing. The latter reflects how dense the system is and is itself affected by droplet size and volume fraction. It should be taken into account that droplet size changes when the system is under shear. In this Chapter we demonstrated how maximum packing is dependent on shear rate in our concentrated monodisperse coarse emulsions. As the droplet concentration in emulsions decreases, the flow behaviour is less dependent on droplet size. Therefore, Newtonian regions can be seen in flow curves, (see for example Fig. 5-20 & 21). According to the above discussion, the majority of rheological models proposed for dilute emulsions only include the oil volume fraction and they give a single number as the system viscosity which is the relevant Newtonian viscosity. In this research we applied shear rate dependant models, e.g. Sisko, and developed the model to be applicable to a range of droplet sizes and elaborated the physical meaning of the experimental parameters.

Dilute normal emulsions were fabricated with droplet sizes between 1 and 20 μm and with narrow size distributions. For these emulsions a simple rheological model, a combination of shear-thinning and Newtonian, can be used. However as polydispersity increases the behaviour becomes unpredictable.

An homogenizer was also used to prepare normal emulsions with a vast size distribution from 0.5 to 30 μm to explore the effect of polydispersity. As explained above there is no theoretical model to describe such systems as droplet interactions within the system are greatly complex. However, these polydisperse systems were generated to be compared with monodisperse systems and also explore the effect of polydispersity. Polydispersity in emulsions introduces time dependency to the system due to different possible packing patterns.

Finally, the value of this research is using techniques to decrease polydispersity in emulsions ranging from 0.5 to 40 μm with different concentrations, dilute and concentrated emulsions, in order to propose appropriate and relatively simple models for their flow properties. The results then were compared with polydisperse emulsion data to elaborate how polydispersity introduces time dependant behaviour and significantly complicated flow behaviour.

Conclusion

Nanoemulsions, microemulsions, normal emulsions and concentrated coarse emulsions were investigated in order to correlate their length scale to their flow properties. This has long been the subject of many researches however, the following detailed motivations for this PhD programme of research, and the corresponding findings, have not been the focus of much of the published work:

1- To study different types of emulsion behaviour over five orders of magnitude within a single base chemical system, in particular allowing investigation of the effect of length scale on flow behaviour.

In this research complex fluids with length scales varying from 1 nm to 40 µm were studied.

For concentrated coarse monodisperse emulsions, the existence of an inverse relationship between the droplet size and the Newtonian viscosity was confirmed and furthermore it was proposed that such a relationship has as its fundamental basis the maximum packing of the system, which has been shown here to be a function of droplet deformation.

For dilute emulsions the independency of the Newtonian viscosity on length scale was confirmed. The flow behaviour was observed to be significantly affected however by the introduction of polydispersity into the system.

For microemulsions, the inverse relationship between the Newtonian viscosity and length scale was confirmed and also it was found that the shape of the droplets determines the flow behaviour and in particular the Newtonian viscosity.

2- To account for the size distribution of the system.

Existing methods of emulsification, e.g. blending and homogenising, generate highly polydisperse systems. The normal emulsions prepared through such methods have complicated flow behaviour that is affected by packing and polydispersity. In this research it is proposed that by preparing monodisperse systems with narrow size distribution the system behaviour can be significantly simplified.

The size distribution in microemulsions and nanoemulsions prepared and investigated here have narrow size distributions due to the specific degree of curvature that is required to prepare such systems, which does not support a broad size distribution. In the case of microemulsions in particular the thermodynamic stability of the system also plays a role, because the more polydisperse the system, the more free energy and less stability is delivered to the system. This is why for the microemulsions that undergo microemulsion-nanoemulsion transition, the sample polydispersity is slightly increased.

It is also worth noting that the data obtained in this study showed that polydispersity can provide time-dependency to emulsion systems.

3- To study the effect of surfactant charge and size on the flow properties.

In general it was found that the HLB of the surfactant defines its capacity to solubilise oil. The lower the HLB the more oil can be solubilised.

The large polymeric structure of F127 imposes a high viscosity on all systems in comparison with the equivalent systems prepared using SDS, CTAB or Triton X-100.

Ionic surfactants have a significant effect on the shape changes that occur in microemulsion systems. This effect is particularly evident when the binary surfactant solution is compared to the corresponding ethanol/surfactant/water ternary aggregate, in which the added ethanol increases the charge density in the systems made with ionic surfactants giving rise to a spherical to rod-like transition in micelles.

4- To suggest a model that is applicable to fit and describe the flow behaviour for different types of emulsions.

In this research we used the following relationship for all systems having a narrow size distribution.

$$\eta = \acute{B} * \eta_0 + \frac{A}{\dot{\gamma}^n} + C * \eta_\infty \qquad\qquad Eq.\,6-1$$

where n is the slope of the shear-thinning region, which is between 0.3 and 1.14 for all systems investigated here. $\acute{B}$ is the coefficient of the zero-shear viscosity which is 1 or 0 depending on whether the applied shear rate sequence is low to high and high to low, respectively. It is noted that outside the solid-like region this coefficient is always zero. A is

the time scale of the system which is below 0.1 s for non-time-dependant systems. For the time dependant systems investigated here the time constant was found to be 4.7 ± 0.1 and 2.5 ± 0.1 s for PDMS/F127 and dodecane/F127 coarse monodisperse emulsions, respectively, these were the only two pure systems showing time-dependency in this study. The value of A within the Newtonian region or within the initial solid-like viscosity is zero. C is the coefficient of the infinite viscosity that is 1 for the systems that have a Newtonian region or 0 for the systems that do not have a Newtonian region (outside the Newtonian region A is always zero).

This model could be used to fit all systems investigated. Using a single model for all systems enables us to explore the most important factors that determine the flow behaviour at each length scale. The observed flow behaviours help us to gain information on such things as the stability of the system, microstructure, charge density at the interface, concentration, and fraction of the cosurfactant in the phases. In order to design a product for a specific need, it is necessary to know how the above parameters, can be controlled by for example controlling the flow behaviour.

Once polydispersity is introduced into a system the above model may not be able to be applicable due to the enhanced complexity of such a system.

5- To propose a relationship between the stability of the system and its flow behaviour.

The microemulsions investigated here all display a Newtonian region however, the corresponding nanoemulsions, prepared through the low energy method do not. These observations combined with the size distribution information shows that the observation of a Newtonian region in a system under shear can provide information on its stability; i.e. the higher polydispersity observed in the nanoemulsions as compared to their mother microemulsions is due to the transition from thermodynamic stability, the lowest Gibbs energy, in microemulsions to a higher energy state, kinetic stability, in nanoemulsions.

One of the reasons that microemulsions, nanoemulsions and macroemulsions are usually considered individually in an investigation and not alongside each other, as has been done in this work, is that there is a huge difference between the flow properties of microemulsions and normal emulsions which makes it difficult to use a single model to study both systems. The research undertaken here clearly shows that there are two key

reasons for the observed differences; polydispersity and interfacial tension. The enhanced polydispersity in normal emulsions and the higher interfacial tension, affecting the curvature and consequently the microstructure of the system work together to make emulsion systems significantly more complex than their seemingly very similar shorter length scale microemulsion cousins.

In this work, insight is provided that fills this gap between microemulsion rheology and emulsion rheology. This was achieved by investigating monodisperse coarse emulsions using a microfluidic device and near monodisperse normal emulsions using an added short-chain alcohol to reduce the effects of polydispersity and deliver systems with similar microstructures differing primarily only in length scale. Eq. 6-1 could then be used to fit the rheology data for microemulsions to coarse emulsions. This has not been done previously.

Finally, it should be mentioned that, to probe the Newtonian viscosity of microemulsion systems, the viscosity of the ternary oil/surfactant/alcohol aggregate was used as the reference viscosity. If this was not used as the reference viscosity and rather the viscosity of water was used, as assumed by many researchers, the predicted viscosities based on the existing models do not agree with the experimental data. It was also determined that there is a direct relationship between the ratio of the Newtonian viscosities of the ternary system and its corresponding microemulsion and their droplet sizes.

6-1 Future work

There is a need to further explore the relationship between the droplet dynamics in different types of emulsion systems with different length scales and polydispersity under shear and their flow behaviours; i.e. the effect of changing microstructure on flow behaviour upon applying shear and the phenomena that will occur due to this microstructure change such as mass transfer etc. For this purpose the following developments are suggested:

1- It would be very interesting to use coupled methods such as Rheo-microscopy, Rheo-NMR and Rheo-SAXS to follow the flow properties while shear is being applied to the system, this allows information on in-process deformation and structural change to be obtained.

2- By using other surfactants with different chemical functionality and charge the finding of this work can be broadened and modified.

3- Computer simulation can be used to provide information on the structure of the system and predict the effect of the packing pattern on the flow properties upon applying shear.

4- The model provided in this research, to calculate the viscoelastic modulus of a coarse monodisperse emulsion, is a 2-D model, a 3-D model is required to be developed, potentially including computer modelling.

5- There is a need to develop a Rheo-DLS machine that determines the viscosity of the initial solid-like state of the material and then uses this value to be applied in size calculations.

6- The interfacial tension in the system has a significant effect on the curvature and structure. It would be very interesting for this work to be continued by taking interfacial tension into account during the process in the microfluidic device and also while shear is being applied to the systems. This also requires computer modelling.

Appendixes

Appendix A-SAXS data

Small angle x-ray scattering (SAXS) was used to probe the size of the three surfactant solutions:
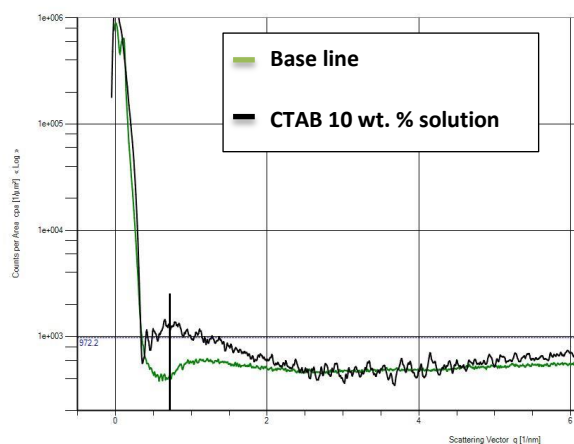
Fig. A-1 SAXS data obtained for CTAB surfactant solution.
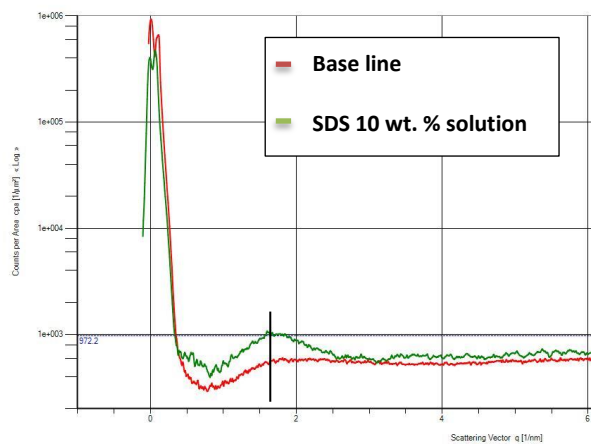
Fig. A-2 SAXS data obtained for SDS surfactant solution.
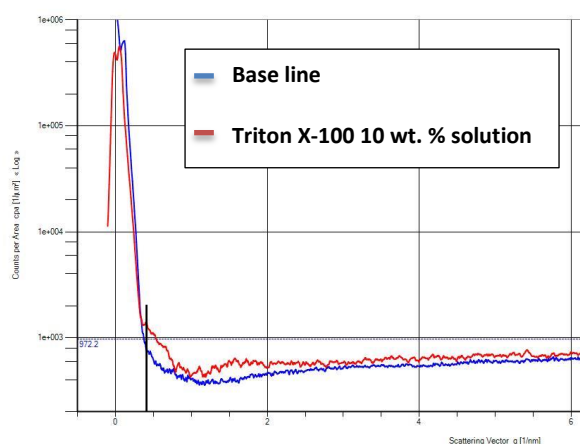
Fig. A-1 SAXS data obtained for CTAB surfactant solution.

The above graphs were considered to calculate the maximum amount of *q*. The relationship between *q* and the droplet size is:

$$Droplet\ size = \frac{2\pi}{q}$$

The values of q and the relevant droplet sizes are given in Table A-1.

Table A-1 *q* and droplet sizes of the surfactant solutions measured by SAXS

10 wt. % surfactant solution	*q*	Droplet size (nm)
SDS/water	1.70	3.7$\pm$0.5
CTAB/water	0.72	8.7$\pm$0.5
Triton X-100/water	0.38	16.5$\pm$0.5

## Appendix B-Interfacial tension measurement

To estimate the interfacial tension of the different emulsion systems prepared using the microchip system a tensiometer apparatus was used to measure the interacial tension at the oil/water interface. In this method a droplet of water which contains some emulsifier is pushed out of a needle which is attached to a syringe and kept hanging in the oil environment. The interfacial tension is calculated according to the change of the droplet shape over time. For each system in Table 5-3, the interfacial tension curve is plotted versus time for 150 s (Fig. A-1) and then extrapolated to determine the interfacial tension at

equilibrium (except for dodecane/SDS system, which requires more time to reach the equilibrium, see inset). The interfacial tension values reported in Table A-1 are steady state (equilibrium) values.
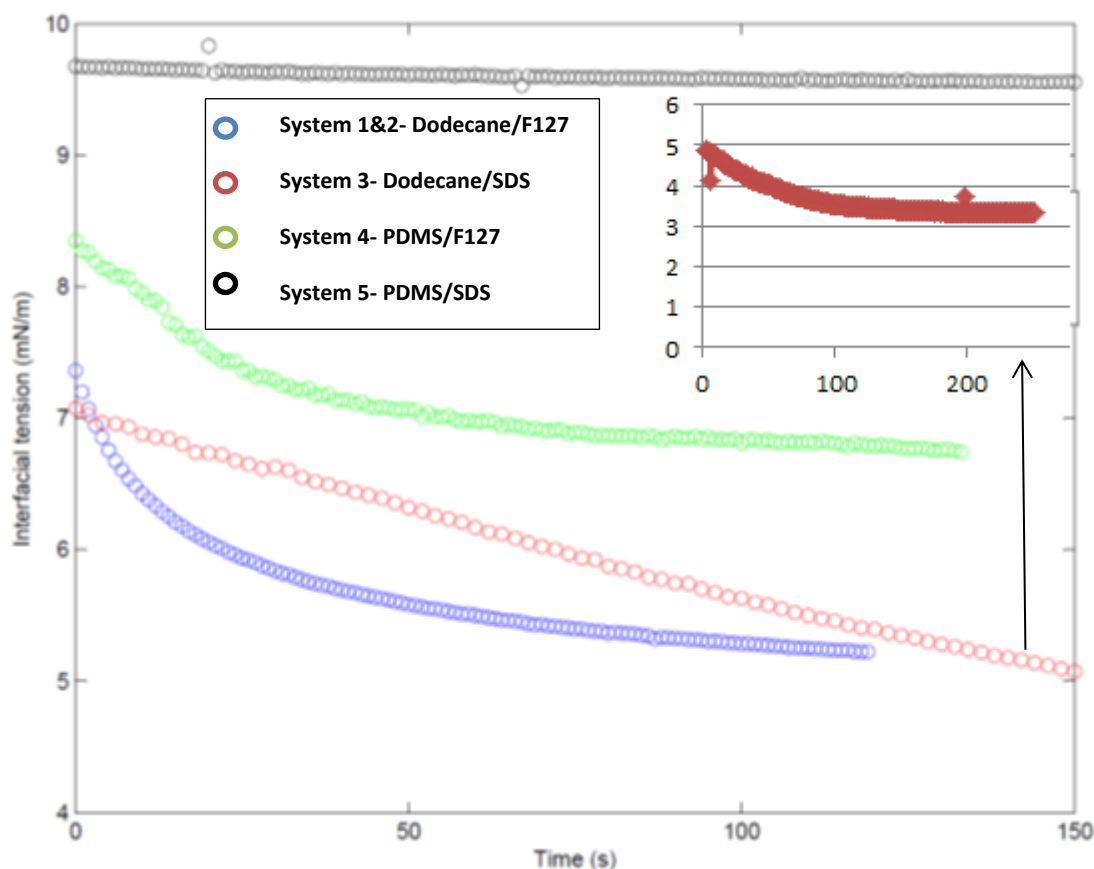
Fig. A-1 Interfacial tension for Systems 1 to 5 as listed in Table 5-3.

As seen in Fig A-1 System 5 (PDMS/SDS) and System 3 (Dodecane/SDS) are linear functions of time whereas System 4 (PDMS/F127) and Systems 1 and 2 (Dodecane/F127) are exponential. The difference in behaviour can be related to the change in emulsifier used to generate the system.

System 5 adsorbs the surfactant (F127) very gradually and its interfacial tension can be considered constant over time. System 3 adsorbs the surfactant (F127) linearly over time and obviously does not reach equilibrium in 150 seconds. Since 150 s is the maximum time that the droplets formed with 1 wt. % surfactant could be held within the system in order to run the experiment and measure the interfacial tension, it was not possible to extend the time for this experiment. However, this experiment with a longer time scale (250 s) and higher surfactant concentration (2 wt. % instead of 1 wt. %) was found to be able to provide

the equilibrium plateau. The relevant data are shown as an inset to the Fig. A-1. Systems 1, 2 and 4 are SDS-based and reach equilibrium exponentially in about 100 s (Fig. A-1). Based on the above data the interfacial tensions for the different Systems are given in Table A-2.

Table A-2 Measured equilibrium interfacial tension values

System	Materials	σ (mN/m)
1	Dodecane/F127	4.8 ± 0.2
2	Dodecane/F127	4.8 ± 0.2
3	Dodecane/SDS	3.2 ± 0.2
4	PDMS/F127	6.5 ± 0.2
5	PDMS/SDS	9.6 ± 0.2

References:

1. Kékicheff, P., *Phase diagram of sodium dodecyl sulfate-water system: 2. Complementary isoplethal and isothermal phase studies.* Journal of Colloid and Interface Science, 1989. **131**(1): p. 133-152.
2. Kékicheff, P., C. Grabielle-Madelmont, and M. Ollivon, *Phase diagram of sodium dodecyl sulfate-water system: 1. A calorimetric study.* Journal of Colloid and Interface Science, 1989. **131**(1): p. 112-132.
3. Galatanu, A.N., et al., *Ternary Phase Diagram of the Triton X-100/Poly(acrylic acid)/Water System†.* Langmuir, 2000. **16**(11): p. 4922-4928.
4. Lin, Z., et al., *Spherical-to-Wormlike Micelle Transition in CTAB Solutions.* The Journal of Physical Chemistry, 1994. **98**(23): p. 5984-5993.
5. Kim, T.-H., et al., *SANS study on self-assembled structures of Pluronic F127 triblock copolymer induced by additives and temperature.* Journal of Applied Crystallography, 2014. **47**(1): p. 53-59.
6. Derkach, S.R., *Rheology of emulsions.* Advances in Colloid and Interface Science, 2009. **151**(1-2): p. 1-23.
7. Mason, T.G., *New fundamental concepts in emulsion rheology.* Current Opinion in Colloid & Interface Science, 1999. **4**(3): p. 231-238.
8. McClements, D.J., *Nanoemulsions versus microemulsions: terminology, differences, and similarities.* Soft Matter, 2012. **8**(6): p. 1719-1729.
9. Gonnella, G. and M. Ruggieri, *Rheological behavior of microemulsions.* Physical review.E, Statistical, nonlinear, and soft matter physics, 2002. **66**(3 Pt 1): p. 031506.
10. Morris, J., *A review of microstructure in concentrated suspensions and its implications for rheology and bulk flow.* Rheologica Acta, 2009. **48**(8): p. 909-923.
11. Wang, L., et al., *Oil-in-water nanoemulsions for pesticide formulations.* Journal of Colloid and Interface Science, 2007. **314**(1): p. 230-235.
12. Foudazi, R., *Models for Structure-Rheology of Highly Concentrated Emulsions* in *Faculty of Engineering*2009, Cape Peninsula University of Technology: Cape Town. p. 165.
13. Lopez-Gonzalez, M.d.R., *Rheo-NMR of Wormlike Micelles*, in *School of Chemical and Physical sciences*2004, Victoria University of Wellington: Wellington. p. 188.
14. Silva, J.P.d., et al., *RheoSAXS studies of anisotropic complex fluids under shear.* Journal of Physics: Conference Series, 2010. **247**(1): p. 012052.
15. Woodward, A., et al., *Monodisperse emulsions from a microfluidic device, characterised by diffusion NMR.* Soft Matter, 2007. **3**(5): p. 627-633.
16. Hughes, E., et al., *Microfluidic preparation and self diffusion PFG-NMR analysis of monodisperse water-in-oil-in-water double emulsions.* Journal of Colloid and Interface Science, 2013. **389**(1): p. 147-156.
17. Matsumoto, S. and P. Sherman, *The viscosity of microemulsions.* Journal of Colloid and Interface Science, 1969. **30**(4): p. 525-536.
18. Kumar, C. and D. Balasubramanian, *Studies on the triton X-100: Alcohol: Water reverse micelles in cyclohexane.* Journal of Colloid and Interface Science, 1979. **69**(2): p. 271-279.
19. Shui, L., A. van den Berg, and J.C.T. Eijkel, *Interfacial tension controlled W/O and O/W 2-phase flows in microchannel.* Lab on a Chip, 2009. **9**(6): p. 795-801.
20. Skurtys, O. and J.M. Aguilera, *Applications of microfluidic devices in food engineering.* Food Biophysics, 2008. **3**(1): p. 1-15.
21. Brody, J.P., Yager, P., Goldstein, R. E. and R.H. Austin, *Biotechnology at low Reynolds numbers.* Biophysical Journal, 1996. **71**(6): p. 3430-3441.
22. Christopher, G.F. and S.L. Anna, *Microfluidic methods for generating continuous droplet streams.* Journal of Physics D: Applied Physics, 2007. **40**(19): p. R319.

23.   Flanagan, J., et al., *Solubilisation of soybean oil in microemulsions using various surfactants.* Food Hydrocolloids, 2006. **20**(2–3): p. 253-260.

24.   Wu, S.-H., Y. Hung, and C.-Y. Mou, *Compartmentalized Hollow Silica Nanospheres Templated from Nanoemulsions.* Chemistry of Materials, 2013. **25**(3): p. 352-364.

25.   Brummer, R., *Rheology Essential of Cosmetic and Food Emulsions*2006, Hamburg: Springer.

26.   Stejskal, E.O. and J.E. Tanner, *Spin diffusion measurements: spin echoes in the presence of a time-dependent field gradient.* The Journal of Chemical Physics, 1965: p. 288–292.

27.   Tanner, J.E. and E.O. Stejskal, *Restricted self-diffusion of protons in colloidal systems by the pulsed-gradient, spin-echo method.* The Journal of Chemical Physics, 1968: p. 1768–1777.

28.   Abragam, A., *The principles of nuclear magnetism*1961: Oxford university press.

29.   Paul.T, C., *Principles of Nuclear Magnetic Resonance Microscopy*1991, New York: Oxford University Press Inc.

30.   Pena, A.A. and G.J. Hirasaki, *NMR Characterization of Emulsions*, in *Emulsions and Emulsion Stability*2006, Taylor & Francis. p. 283-309.

31.   Tanner, J.E., *Use of the Stimulated Echo in NMR Diffusion Studies.* The Journal of Chemical Physics, 1970. **52**(5): p. 2523-2526.

32.   Murday, J.S. and R.M. Cotts, *SELF-DIFFUSION COEFFCIENT OF LIQUID LITHIUM.* Journal of Chemical Physics, 1968. **48**(11): p. 4938-&.

33.   Denkova, P.S., Tcholakova, S., Denkov, N. D., Danov, K. D., Campbell, B., Shawl, C. and D. Kim, *Evaluation of the precision of drop-size determination in oil/water emulsions by low-resolution NMR spectroscopy.* Langmuir, 2004. **20**(26): p. 11402-11413.

34.   Balinov, B., O. Soderman, and T. Warnheim, *DETERMINATION OF WATER DROPLET SIZE IN MARGARINES AND LOW-CALORIE SPREADS BY NUCLEAR-MAGNETIC-RESONANCE SELF-DIFFUSION.* Journal of the American Oil Chemists Society, 1994. **71**(5): p. 513-518.

35.   Mitra, P.P., Sen, P. N., Schwartz, L. M. and P. Ledoussal, *DIFFUSION PROPAGATOR AS A PROBE OF THE STRUCTURE OF POROUS-MEDIA.* Physical Review Letters, 1992. **68**(24): p. 3555-3558.

36.   Callaghan, P.T., Coy, A., Macgowan, D., Packer, K. J. and F.O. Zelaya, *DIFFRACTION-LIKE EFFECTS IN NMR DIFFUSION STUDIES OF FLUIDS IN POROUS SOLIDS.* Nature, 1991. **351**(6326): p. 467-469.

37.   Ageno, M., *On the Nature of the Hydrogen Bond and the Structure of Water.* Proceedings of the National Academy of Sciences of the United States of America, 1967. **57**(3): p. 567-572.

38.   Ageno, M. and C. Frontali, *Viscosity Measurements of Alcohol-Water Mixtures and the Structure of Water.* Proceedings of the National Academy of Sciences of the United States of America, 1967. **57**(4): p. 856-860.

39.   Briceno.M.I, *Rheology of Suspensions and emulsions*, in *Pharmaceutical emulsions and suspensions*2000, Mrcel Dekker: New York-Basel.

40.   Rojas, M.R., A.J. Müller, and A.E. Sáez, *Shear rheology and porous media flow of wormlike micelle solutions formed by mixtures of surfactants of opposite charge.* Journal of Colloid and Interface Science, 2008. **326**(1): p. 221-226.

41.   Walker, L.M., *Rheology and structure of worm-like micelles.* Current Opinion in Colloid & Interface Science, 2001. **6**(5–6): p. 451-456.

42.   Ezrahi, S., E. Tuval, and A. Aserin, *Properties, main applications and perspectives of worm micelles.* Advances in Colloid and Interface Science, 2006. **128–130**(0): p. 77-102.

43.   Magid, L.J., Z. Li, and P.D. Butler, *Flexibility of Elongated Sodium Dodecyl Sulfate Micelles in Aqueous Sodium Chloride: A Small-Angle Neutron Scattering Study.* Langmuir, 2000. **16**(26): p. 10028-10036.

44.   Frisch, H.L. and R. Simha, *the viscosity of colloidal suspensions and macromolecular solutions*, in *Rheology, Theory and Applications*1956, New York Press: New York.

45.   Inoue, T., Y. Inoue, and H. Watanabe, *Nonlinear Rheology of CTAB/NaSal Aqueous Solutions: Finite Extensibility of a Network of Wormlike Micelles.* Langmuir, 2005. **21**(4): p. 1201-1208.

46.   Chu, Z., C.A. Dreiss, and Y. Feng, *Smart wormlike micelles.* Chemical Society Reviews, 2013. **42**(17): p. 7174-7203.

47.   Baglioni, P. and L. Kevan, *Structural effects of alcohol addition to sodium dodecyl sulfate micelles studied by electron spin-echo modulation of 5-doxylstearic acid spin probe.* The Journal of Physical Chemistry, 1987. **91**(6): p. 1516-1518.

48.   Dharaiya, N., et al., *Light scattering and NMR studies of Triton X-100 micelles in the presence of short chain alcohols and ethoxylates.* Colloids and Surfaces A: Physicochemical and Engineering Aspects, 2013. **436**(0): p. 252-259.

49.   Leung, R. and D.O. Shah, *Dynamic properties of micellar solutions: I. Effects of short-chain alcohols and polymers on micellar stability.* Journal of Colloid and Interface Science, 1986. **113**(2): p. 484-499.

50.   Zana, R., *Aqueous surfactant-alcohol systems: A review.* Advances in Colloid and Interface Science, 1995. **57**(0): p. 1-64.

51.   Førland, G.M., et al., *Influence of Alcohol on the Behavior of Sodium Dodecylsulfate Micelles.* Journal of Colloid and Interface Science, 1998. **203**(2): p. 328-334.

52.   Aramaki, K., S. Hoshida, and S. Arima, *Effect of carbon chain length of cosurfactant on the rheological properties of nonionic wormlike micellar solutions formed by a sugar surfactant and monohydroxy alcohols.* Colloids and Surfaces A: Physicochemical and Engineering Aspects, 2010. **366**(1–3): p. 58-62.

53.   Oda, R., L. Bourdieu, and M. Schmutz, *Micelle to Vesicle Transition Induced by Cosurfactant: Rheological Study and Direct Observations.* The Journal of Physical Chemistry B, 1997. **101**(31): p. 5913-5916.

54.   Porte, G., et al., *Morphological transformations of the primary surfactant structures in brine-rich mixtures of ternary systems (surfactant/alcohol/brine).* The Journal of Physical Chemistry, 1986. **90**(22): p. 5746-5751.

55.   Hu, Y.T., P. Boltenhagen, and D.J. Pine, *Shear thickening in low-concentration solutions of wormlike micelles. I. Direct visualization of transient behavior and phase transitions.* Journal of Rheology (1978-present), 1998. **42**(5): p. 1185-1208.

56.   Israelachvili, J.N., D.J. Mitchell, and B.W. Ninham, *Theory of self-assembly of hydrocarbon amphiphiles into micelles and bilayers.* Journal of the Chemical Society, Faraday Transactions 2: Molecular and Chemical Physics, 1976. **72**(0): p. 1525-1568.

57.   *Physical chemistry of macromolecules. Charles Tanford, John Wiley & Sons, Inc., 440 Park Ave. South, New York 16, N. Y., 1961. xiv + 710 pp. 15 × 23 cm. Price $18.* Journal of Pharmaceutical Sciences, 1962. **51**(2): p. 190-190.

58.   Goyal, P.S., et al., *Shapes and sizes of micelles in CTAB solutions.* Physica B: Condensed Matter, 1991. **174**(1–4): p. 196-199.

59.   Tolbert, S.H., et al., *Phase Transitions in Mesostructured Silica/Surfactant Composites: Surfactant Packing and the Role of Charge Density Matching†.* Chemistry of Materials, 2001. **13**(7): p. 2247-2256.

60.   E., K. and M. J., *Calculation of Alkoxide and Hydroxide Ion Activity Ratios in the Water—Ethanol System.* Chemical Papers, 1993. **47**(3): p. 156-159.

61.   Guo, L., et al., *Micellar structure changes in aqueous mixtures of nonionic surfactants.* Journal of Rheology (1978-present), 2001. **45**(5): p. 1223-1243.

62.   Tchakalova, V., C. Bailly, and W. Fieber, *Food-grade bicontinuous microemulsions.* Flavour and Fragrance Journal, 2014. **29**(1): p. 67-74.

63.   Attwood, D., L.R.J. Currie, and P.H. Elworthy, *Studies of solubilized micellar solutions. III. The viscosity of solutions formed with nonionic surfactants.* Journal of Colloid and Interface Science, 1974. **46**(2): p. 261-265.

64.   Chen, C.M. and G.G. Warr, *Rheology of ternary microemulsions.* The Journal of Physical Chemistry, 1992. **96**(23): p. 9492-9497.

65.   Warr, G.G., *Shear and elongational rheology of ternary microemulsions.* Colloids and Surfaces A: Physicochemical and Engineering Aspects, 1995. **103**(3): p. 273-279.

66.   Li, G., et al., *Cationic microgel emulsion with a high solid content by a multistep addition method in inverse microemulsion polymerization.* Journal of Applied Polymer Science, 2014. **131**(15): p. n/a-n/a.

67.   Bidyut, K.P. and P.M. Satya, *The viscosity bahaviours of microemulsions: An overview.* PINSA, 2000. **66, A**(5): p. 499-519.

68.   Abdel-Rahem, R.A., et al., *Rheology of Aqueous Solutions Containing SLES, CAPB, and Microemulsion: Influence of Cosurfactant and Salt.* Journal of Dispersion Science and Technology, 2013. **35**(1): p. 64-75.

69.   Mueller, S., E.W. Llewellin, and H.M. Mader, *The rheology of suspensions of solid particles.* Proceedings: Mathematical, Physical and Engineering Sciences, 2010. **466**(2116): p. 1201-1228.

70.   Gupta, R.K. and S.G. Seshadri, *Maximum Loading Levels in Filled Liquid Systems.* Journal of rheology, 1986. **30**: p. 503-508.

71.   OWUSU, M., *Statistical Characterization of Performance of Biopolymer Drill-In Fluid for Different Rheological Models*, 2013.

72.   Pons, R., et al., *Formation and properties of miniemulsions formed by microemulsions dilution.* Advances in Colloid and Interface Science, 2003. **106**(1–3): p. 129-146.

73.   Solans, C. and I. Solé, *Nano-emulsions: Formation by low-energy methods.* Current Opinion in Colloid & Interface Science, 2012. **17**(5): p. 246-254.

74.   Wulff-Pérez, M., et al., *The effect of polymeric surfactants on the rheological properties of nanoemulsions.* Colloid and Polymer Science, 2013. **291**(3): p. 709-716.

75.   Anna, S.L. and H.C. Mayer, *Microscale tipstreaming in a microfluidic flow focusing device.* Physics of Fluids, 2006. **18**(12): p. 121512.

76.   Xu, Q. and M. Nakajima, *The generation of highly monodisperse droplets through the breakup of hydrodynamically focused microthread in a microfluidic device.* Applied Physics Letters, 2004. **85**(17): p. 3726-3728.

77.   Monahan.N, *Master thesis:Structure and rheology of monodisperse and bimodal emulsions*, 2010, Victoria University of Wellington.

78.   Taylor, G.I., *The Formation of Emulsions in Definable Fields of Flow.* Proceedings of the Royal Society of London. Series A, Containing Papers of a Mathematical and Physical Character, 1934. **146**(858): p. 501-523.

79.   De Bruijn, R.A., *Tipstreaming of drops in simple shear flows.* Chemical Engineering Science, 1993. **48**(2): p. 277-284.

80.   Hu, Y.T., D.J. Pine, and L.G. Leal, *Drop deformation, breakup, and coalescence with compatibilizer.* Physics of Fluids, 2000. **12**(3): p. 484-489.

81.   Guido, S., *Shear-induced droplet deformation: Effects of confined geometry and viscoelasticity.* Current Opinion in Colloid & Interface Science, 2011. **16**(1): p. 61-70.

82.   Romoscanu, A.I., Fenollosa, A., Acquistapace, S., Gunes, D., Martins-Deuchande, T., Clausen, P., Mezzenga, R., Nyden, M., Zick, K. and E. Hughes, *Structure, Diffusion, and Permeability of Protein-Stabilized Monodispersed Oil in Water Emulsions and Their Gels: A Self-Diffusion NMR Study.* Langmuir, 2010. **26**(9): p. 6184-6192.

83.   Lequeux, F., *Emulsion rheology.* Current Opinion in Colloid & Interface Science, 1998. **3**(4): p. 408-411.

84.   Hughes, A.J., *The Einstein Relation between Relative Viscosity and Volume Concentration of Suspensions of Spheres.* Nature, 1954. **173**(4414): p. 1089-1090.

85.   Mason, T.G., J. Bibette, and D.A. Weitz, *Yielding and Flow of Monodisperse Emulsions.* Journal of Colloid and Interface Science, 1996. **179**(2): p. 439-448.

86.   Ladd, A.J.C., *Hydrodynamic transport coefficients of random dispersions of hard spheres*. Vol. 93. 1990: AIP. 3484-3494.

87.   Howe, A.M., A. Clarke, and T.H. Whitesides, *Viscosity of Emulsions of Polydisperse Droplets with a Thick Adsorbed Layer.* Langmuir, 1997. **13**(10): p. 2617-2626.

88.   Batchelor, G.K., *The effect of Brownian motion on the bulk stress in a suspension of spherical particles.* Journal of Fluid Mechanics, 1977. **83**(01): p. 97-117.

89.   Yaron, I. and B. Gal-Or, *On viscous flow and effective viscosity of concentrated suspensions and emulsions - Effect of particle concentration and surfactant impurities.* Rheologica Acta, 1972. **11**(3-4): p. 241-252.

90.   Choi, S.J. and W.R. Schowalter, *Rheological properties of nondilute suspensions of deformable particles.* Physics of Fluids (1958-1988), 1975. **18**(4): p. 420-427.

91.   Pal, R., *Shear viscosity behavior of emulsions of two immiscible liquids.* Journal of Colloid and Interface Science, 2000. **225**(2): p. 359-366.

92.   Pal, R., *Novel viscosity equations for emulsions of two immiscible liquids.* J Rheol, 2001: p. 509.

93.   Lapasin. in *AERC,*. Sep.2003. Portugal.

94.   Delaney, G., et al., *Random packing of elliptical disks.* Philosophical Magazine Letters, 2005. **85**(2): p. 89-96.

95.   Coussot, P., Tabuteau, H., Chateau, X., Tocquer, L. and G. Ovarlez, *Aging and solid or liquid behavior in pastes.* Journal of Rheology, 2006. **50**(6): p. 975-994.

96.   Oldroyd, J.G., *The Elastic and Viscous Properties of Emulsions and Suspensions.* Proceedings of the Royal Society of London. Series A. Mathematical and Physical Sciences, 1953. **218**(1132): p. 122-132.

97.   LI, X. and C. POZRIKIDIS, *The effect of surfactants on drop deformation and on the rheology of dilute emulsions in Stokes flow.* Journal of Fluid Mechanics, 1997. **341**: p. 165-194.

98.   Princen, H.M. and A.D. Kiss, *Rheology of foams and highly concentrated emulsions : III. Static shear modulus.* Journal of Colloid and Interface Science, 1986. **112**(2): p. 427-437.

99.   Princen, H.M., *Rheology of foams and highly concentrated emulsions : I. Elastic properties and yield stress of a cylindrical model system.* Journal of Colloid and Interface Science, 1983. **91**(1): p. 160-175.

100.   Pal, R., *Effect of droplet size on the rheology of emulsions.* AIChE Journal, 1996. **42**(11): p. 3181-3190.

101.   Farris, R.J., *Prediction of the viscosity of multimodal suspensions from unimodal viscosity data.* Trans. Soc. Rheol., 1968: p. 281-301.

102.   Hoffman, R., *Factors affecting the viscosity of unimodal and multimodal colloidal dispersions.* J. Rheol., 1992: p. 947-965.

103.   Lequeux, F., *Emulsion rheology.* Curr. Opin. Colloid Interface Sci., 1998: p. 408-411.

104.   Saiki, Y., R.G. Horn, and C.A. Prestidge, *Droplet structure instability in concentrated emulsions.* Journal of Colloid and Interface Science, 2008. **320**(2): p. 569-574.

105.   Wilde, P.J., *Interfaces: their role in foam and emulsion behaviour.* Current Opinion in Colloid & Interface Science, 2000. **5**(3–4): p. 176-181.

106.   Mendoza, A.J., et al., *Particle laden fluid interfaces: Dynamics and interfacial rheology.* Advances in Colloid and Interface Science, 2014. **206**(0): p. 303-319.

107.   Herschel, W. and R. Bulkley, *Konsistenzmessungen von Gummi-Benzollösungen.* Kolloid-Zeitschrift, 1926. **39**(4): p. 291-300.

108.   Cox, W.P. and E.H. Merz, *Correlation of dynamic and steady flow viscosities.* Journal of Polymer Science, 1958. **28**(118): p. 619-622.